NASA TECHNICAL NOTE

NASA TN D-4527

NASA TN D-4527

THE GEOMAGNETIC SECULAR VARIATION 1900 - 1965

by Joseph C. Cain and Shirley J. Hendricks

Goddard Space Flight Center
Greenbelt, Md.

NATIONAL AERONAUTICS AND SPACE ADMINISTRATION • WASHINGTON, D. C. • APRIL 1968

THE GEOMAGNETIC SECULAR VARIATION

1900 - 1965

By Joseph C. Cain and Shirley J. Hendricks

Goddard Space Flight Center
Greenbelt, Md.

NATIONAL AERONAUTICS AND SPACE ADMINISTRATION

For sale by the Clearinghouse for Federal Scientific and Technical Information
Springfield, Virginia 22151 – CFSTI price $3.00

ABSTRACT

The GSFC (12/66) model of the main geomagnetic field uses linear and parabolic terms in time, to represent secular change over the interval 1900-1965. The predicted field is compared with observatory annual means to investigate systematic residuals. Deviations of the order of 100γ occur for short spans of years and only in limited regions. Otherwise, the trends of the computed field parallel the observations. Secular-change charts agree well with those drawn by earlier analyses.

The westward drift is generally apparent in the vector representation of the harmonic coefficients, except that a few terms predominantly undergo an amplitude change. The components below $\left(g_6{}^6,\ h_6{}^6\right)$ that show a recognizable eastward drift are the (3,2), (5,1), and (5,2) terms.

Both dipole poles move smoothly northwestward over the interval, whereas the dipole position initially drifts eastward, reverses direction near 1920, and then moves westward at a rate up to about 0.07 degrees per year. Its 1965 position is found to be 78.8°N, 70.0°W.

CONTENTS

Abstract ii

INTRODUCTION 1

COMPARISON WITH OBSERVATORY ANNUAL MEANS 2

COMPARISON WITH EARLIER ISOPORIC CHARTS 5

THE GEOMAGNETIC SECULAR VARIATION FIELD IN 1965 5

DRIFT OF HARMONIC COMPONENTS 6

CHANGES IN SURFACE FEATURES 7

POSITION OF POLES 8

DECREASE IN MAGNETIC MOMENT OF DIPOLE 8

CONCLUSIONS 9

References 10

Appendix A—Comparison of Observatory Annual Mean Values 1900-1965 With Elements Computed From GSFC (12/66) 13

Appendix B—Comparison of Isoporic Charts (1912-1942) From GSFC (12/66) With Those From Vestine et al. (1947). . . 157

Appendix C—Main Field Component and Isoporic Charts Computed From GSFC (12/66) for 1965.0 at the Earth's Surface . . 207

THE GEOMAGNETIC SECULAR VARIATION 1900 - 1965*

by
Joseph C. Cain and Shirley J. Hendricks
Goddard Space Flight Center

INTRODUCTION

In the last few centuries over a hundred papers have been written concerning the main geomagnetic field and its secular variation. These research efforts have followed two main lines of approach: (1) the data from fixed observatories or relocatable positions (repeat stations) are compared quantitatively over a year or two and the differences by components contoured on charts. These secular-change, or isoporic, charts can be compared at intervals (e.g., decades) to attempt to learn how the patterns are changing with time. (2) Magnetic charts for given epochs are constructed, using survey observations reduced to the epoch of the chart. These charts are subjected to spherical-harmonic analysis and the results compared for several epochs (Mauersberger, 1952; McDonald and Gunst, 1967).

Recently we have chosen a different approach making a numerical fitting to all of the *observational* data available through the Magnetic Division of the United States Coast and Geodetic Survey for the period 1900-1964 plus some recent global satellite data acquired by the OGO-2 satellite. The result of this work, designated the GSFC(12/66) field model (Cain et al., 1967), is intended for use as an initial tool in evaluating time variations in the field observed by OGO-2. A set of 120 spherical harmonics of the internal potential were obtained, including their first and second time derivatives.

The accuracy of this expansion in matching the observational data was expressed in terms of the residuals of fit by type of data, component, and epoch. It was shown that the non-satellite data was scattered about the fit with a Gaussian distribution ($\sigma \sim 120\gamma$), apart from some higher-than-Gaussian tails. Over half the data of a given component lay within 100γ, 75 percent within 200γ and 95 percent within 500γ of the fit. The distribution by component varied slightly, with the Gaussian "core" of the ΔZ distribution being the widest at 210γ, whereas the total field distribution (with a 100γ core) was the narrowest. Inspection of the data makes it clear that the large non-Gaussian excursions of the survey data about the fitting surface are due to crustal anomalies.

*This paper was presented at the International Union of Geodesy and Geophysics 14th General Assembly St. Gall, Switzerland, September 30, 1967.

(Considering the fact that the distributions were obtained *without* our making any selection of the observations, and no corrections were made for short period variations, it is remarkable that only 5 percent of the data fall outside the 500γ limit.)

The satellite data are free from the influence of these crustal anomalies and depart by much less from the fitting surface. The OGO-2 total field data used were taken from a magnetically quiet period (October 29-November 15, 1965) and deviated with an almost Gaussian distribution whose constant was 12γ. The root-mean-square residuals of the survey data (those differing by more than 2000γ were rejected) were of the order of 180-260γ for individual years over the interval 1906-1964, after decreasing from a peak of 320γ in 1900. It was suggested in the previous paper that there may thus be systematic deviations of the secular change estimates from the fitting surface.

In creating the GSFC(12/66) field model, a deviation was made from previous practice. No special heavy weighting was given to the observatory data included in the fit. As explained in the discussion of the GSFC(12/66) derivation, the earlier evaluations (Cain et al., 1965; Hendricks and Cain, 1966; and Cain, 1966) used very heavy relative weights for the observatory data because these are more accurate than the field survey data. However, these analyses showed that the scatter of the observatory data was not appreciably different from that of the rest of the observations; the main disturbing factor is the presence of crustal anomalies and not measurement inaccuracies. The observatory annual means were thus entered into the fit with the same relative weights as the other surface data.

In past work on secular change, displays of comparisons between the observational data and the results of analysis have been surprisingly few. This paper shows how the parabolic series for the spherical harmonic coefficients matches the field variations measured at selected magnetic observatories, and points out how some features of secular change compare with those reported in past papers.

COMPARISON WITH OBSERVATORY ANNUAL MEANS

Appendix A, consisting of a map (Figure A1) and 212 graphs (Figures A2 through A213) shows the results of comparing the field components computed from the GSFC(12/66) model with annual means observed at a selection of magnetic observatories. (Figure A1 shows the location of most of the observatories.) The graphs (plotted automatically) are arranged alphabetically by observatory name. An observatory is omitted only if it offers less than five annual means. Under each observatory's name is its latest location, given by geodetic longitude and latitude in decimal degrees (positive east and north) and its altitude in kilometers, if known and above 100 meters. The vertical scales, arranged from left to right, show H and Z in gammas with 1000γ between abscissa (Z positive down), and D in degrees (positive eastward) at 2-degree intervals. The computed values are traced by the solid lines and are labeled on the right side according as they are H, D, or Z. There is a break in the computed curves if the observatory was moved. The calculations are made as appropriate to the site of observation.

The observed annual means are plotted as ⊕ for H, ⊙ for D, and □ for Z. In reproduction, these symbols are not always clear but may appear as filled circles or squares. (The symbols H, D, or Z also appear before the first hourly mean for each graph, as appropriate.) The computed values are fed to the cathode-ray-tube plotter for each year for which there are observations of a component. The plotter beam is left on between points and traces out a straight line. The continuous curves thus appear lighter for those years for which observed means are missing, since the beam moves more quickly; and, whereas a continuous set of points seems to give a smooth curve, large gaps in the data (e.g., Chelyuskin, Hel) result in a straight line connecting the points.

One feature of the plots is that the observed data occasionally disappear from the top or bottom of the plots. This problem arose in imperfections in the computer algorithm which was computed in order to give a scale that would suit all graphs. Since only a few plots were affected and the algorithm was already quite complex, it was decided to omit the worst offenders and keep the rest. Thus in a few instances (e.g., Dombas Z before 1928) there are more observed data than appear on the graphs. The fact that observed and measured data often parallel each other with up to a few hundred gammas displacement (e.g., Alibag) suggests that the absolute differences are due to crustal anomalies. This view is supported by such examples as Honolulu, where the observed values hopped from one side of the computed D and H curves when the station was moved, around 1947. The question then arises: does the total observed secular change represent that of the main field, or does it include a contribution from crustal matter with a "soft" permeability? Here we assume that the changes with time in the anomaly field are unimportant; they are probably of the order of the percentage secular change multiplied by the size of the anomaly. Thus, for the 95 percent of the data within 500γ, variations of the anomaly field due to a change of the main field by a few percent would represent only a few gammas. The graphs indicate that the oscillation of the data from the fitting surface is more often of the order of 100γ.

Eleman (1966) has pointed out another factor regarding the influence of anomalies. If a constant anomaly causes the observed annual means H and D to deviate from the normal field H_N and D_N, then a representation of secular change in terms of $\dot{H}$ and $\dot{D}$ can be erroneous. If $\delta = D_N - D$, the secular change of the normal field is given by

$$\dot{D}_N \approx (H/H_N)\dot{D} - (\dot{H}/H_N)\delta ,$$

$$\dot{H}_N = \dot{H} + H\dot{D}\delta ,$$

provided that δ is sufficiently small, so that $\cos\delta \approx 1$ and $\sin\delta \approx \delta$. Eleman showed that for Kiruna (1954-1955) the second terms amount to about 1 minute per year for $\dot{D}$ and 4γ per year for $\dot{H}$. A plot of the data in the orthogonal components X, Y, and Z should eliminate any concern over this geometric interaction. We have chosen to make the comparison here in terms of the observed values, since at this stage such refinements are not essential.

If the displacement due to crustal anomalies is taken into account, curve trends can be profitably compared with the observations. Considering that the fit was made to a selection of all data without any corrections for storm variations or other transient effects such as the diurnal variations, the agreement is, in general, fairly good. For most observatories, the computed and measured H component trends not only are very nearly parallel but also show little absolute displacement. Declination trends agree somewhat less well. The vertical intensity curves show the largest displacements and the poorest agreement of the curves as a whole, and the largest scatter of individual points.

Significant discrepancies between predicted and observed data occur at the western edge of the Indian Ocean. Mauritius vertical-intensity and Tananarive declination curves have a smooth parabolic shape that differs considerably from the computed curves. Alibag vertical intensity, after tracking very well for the first 40 years, now shows an increasing deviation from computed values.

For most of the other graphs, the deviations from the computed curves must be real because they exceed any possible errors of measurement; but generally they can be regarded as second-order perturbations from the main trend of secular change. These deviations can matter seriously when the field model is used to compute a reference field, particularly when extrapolating beyond 1965.

A relationship may exist between the earth rotation rate and secular change (Dicke, 1966). In the period 1900-1920, for example, there may have been a short-lived reversal of the slowing of the earth's rotation rate that has otherwise appeared to be almost constant from 1800 through 1950 (Munk and MacDonald, 1960). The high residuals of fit from 1900 to 1910 noted in the previous paper (Cain et al., 1967) may have been related to this phenomena. In the absence of 18th-century survey data, it is uncertain that such an increase was not due to the numerical process of least squares, where the residuals are sometimes largest near the fringes of the data set—particularly when the data distribution is relatively thin (as it is for 1900-1910).

However, the graphs in Appendix A do show a definite trend away from the parabolic curves for 1900-1910 for some components and stations. The curves for all English and European observatories (e.g., Bochum, Stonyhurst, Kew, DeBilt, Greenwich, etc.) show that the measured secular change in H is significantly more positive than that computed. Likewise, for the same area the secular change in declination is more negative than that predicted. The boundaries of this phenomenon are somewhat vague but it is clearly not present in the Pacific, South America, and Asia (e.g., Melbourne, Hong Kong, Kakioka, Christchurch, Kodaikanal, Huancayo, Santiago, Colaba, etc.). In the United States (Cheltenham, Baldwin, Sitka) and central Russia (Sverdlovsk) the higher observed secular change in H is evident, but not the corresponding disparity in declination. It is undoubtedly such irregularities that have led investigators (e.g., Chapman and Bartels, 1940, p. 130) to conclude that secular variation is a regional phenomenon. Although the deviations seem to correlate for observing stations in a given region so that a very accurate mathematical model would require their inclusion in some way, it is apparent that the general character of secular change is well enough represented by this model.

COMPARISON WITH EARLIER ISOPORIC CHARTS

Using the GSFC(12/66) coefficients it is possible to compute the secular change of the components at any epoch. This is a simple process for the orthogonal components (differentiating the expressions for those components and evaluating $-\nabla\dot{V}$), but the representation of $\dot{H}$, $\dot{D}$, and $\dot{I}$ requires special expansions. It is therefore simpler to compute the field for a small increment of time (e.g., 0.5 year) on either side of an epoch and take the difference. This procedure was carried out for the epochs 1912.5, 1922.5, 1932.5, and 1942.5 for the components H, I, X, Y, Z, and F and isoporic charts drawn by means of an automatic contouring procedure similar to that described by Cain and Neilon (1963). These charts appear in Appendix B along with reproductions of the corresponding ones from Vestine et al. (1947). These charts may also be compared with those for 1922 by Fisk (Chapman and Bartels, 1940, p. 115-119).

Comparison with the earlier charts shows in all instances the same basic cell structure. The GSFC-map extreme values for the force components differ by a few tens of gammas per year from the values given by Vestine et al. and generally have a smaller absolute magnitude. For the inclination charts, the agreement with Vestine is within a few minutes per year for the center cells. Comparison with the diagrams by Fisk for 1922 also leads to the conclusion that the GSFC extreme values are of smaller absolute value than those on the earlier works. This suggests that the analysis using only 120 spherical harmonics may give too smooth a picture of the secular change patterns.

THE GEOMAGNETIC SECULAR VARIATION FIELD IN 1965

For those wishing to use the GSFC(12/66) model as a reference at current epochs, Appendix C presents a set of surface charts for 1965.0 (Figures C1 through C13). These closely agree with the U. S. World Magnetic Charts for the same epoch; although, as previously noted in the comparison with the earlier isoporic charts, the GSFC(12/66) patterns are slightly broader and less intense.

Comparing the computed rate of change since 1960 with that observed at various observatories shows some systematic deviations over certain areas of the earth. For example, the observed rate of change in the vertical component over South America is of the order of 40 gammas per year greater than the computed rate. Increasing the computed rate for the area by this amount would sharpen the low cell pattern to the northeast and bring the GSFC(12/66) model into closer agreement with the U. S. Charts. Also, for the region around the Caspian Sea, the observed change in the horizontal intensity is about 30γ per year *less* than that computed. Changing the computed rate by this amount would again result in better agreement with the U. S. Charts. Other regional deviations since 1960 were noted. In Europe and North America, the observed change in Z is about 15γ per year less than that computed; in Europe and South America, the variation in H is about 15γ per year greater than that computed; in Central America, the variation in H is about 30γ per year less than that computed. The secular change in declination appears to be 1 to 2 minutes per year less than that computed in Europe and most of Russia, 2 to 4 minutes per year less in South America, and up to 10 minutes per year less along the northern coast of Scandinavia and Russia.

Thus, the present model apparently produces patterns of secular change that may, in general, be smoother than the observed changes, but it would be hard to improve the representation realistically over the whole sphere, using the present sparse data set. However, these comparisons do suggest that the user of the GSFC(12/66) model as a reference beyond 1965 should be wary of possible deviations of the order of magnitude indicated above.

DRIFT OF HARMONIC COMPONENTS

Figure 1, a plot of g and h harmonic vectors, displays one aspect of secular change. The trace of the individual components is given from 1900 to 1970, with the arrow at the later date, for the components (g_1^1, h_1^1) through (g_6^6, h_6^6). The scale is in gammas and must be divided by 5 for the (g_5^1, h_5^1) through (g_6^6, h_6^6) traces. Also, the scale is broken for the large h_1^1 component. This figure is very similar to one that Cain and Hide (1966) show for the results of an earlier analysis. A single curved arrow is used for the whole interval without indicating the location of the points for the years between 1900 and 1970; however, a detailed inspection of the data revealed that the years fall almost uniformly along each path.

Consideration of the westward drift in terms of harmonic components was first discussed by Carlheim-Gyllensköld, who deduced that the harmonic components of the first few terms drifted westward at an increasing rate according to the degree of the expansion. Bartels disagreed with this deduction on the basis of his analysis of data from the period 1902-1920 (cf. Chapman and Bartels, 1940, p. 666). Phase changes for the spherical harmonics are also discussed in several later works (cf. Nagata, 1962) which conclude that all components up to (4, 4)* drift westward with the exception of (3, 2).

Figure 1 supports the general pattern of westward drift as indicated by the number of components moving clockwise about the origin. The components predominantly moving westward are (2, 1), (2, 2), (3, 3), (4, 1), (4, 2), (4, 3), (5, 4), (6, 1), (6, 2), (6, 3); those predominantly moving eastward are (3, 2), (5, 1) and (5, 2). The others tend to be special cases. For example, (3, 1) and (4, 4) and (6, 5) show a large amplitude change and move predominantly westward; (5, 3) and (6, 4) show a large amplitude change and move predominantly eastward. The dipole term (1, 1) is drawn with a bar across at the 1900 starting point. It traces out from 1900 to about 1920 in an increasing-amplitude, eastward direction and then suddenly reverses and overlays itself with a slight westward motion. As pointed out earlier, it would be unwise to infer too much from this reversal before a systematic analysis is performed that includes pre-1900 data.

*The notation (n, m) is used here to denote the components (g_n^m, h_n^m).

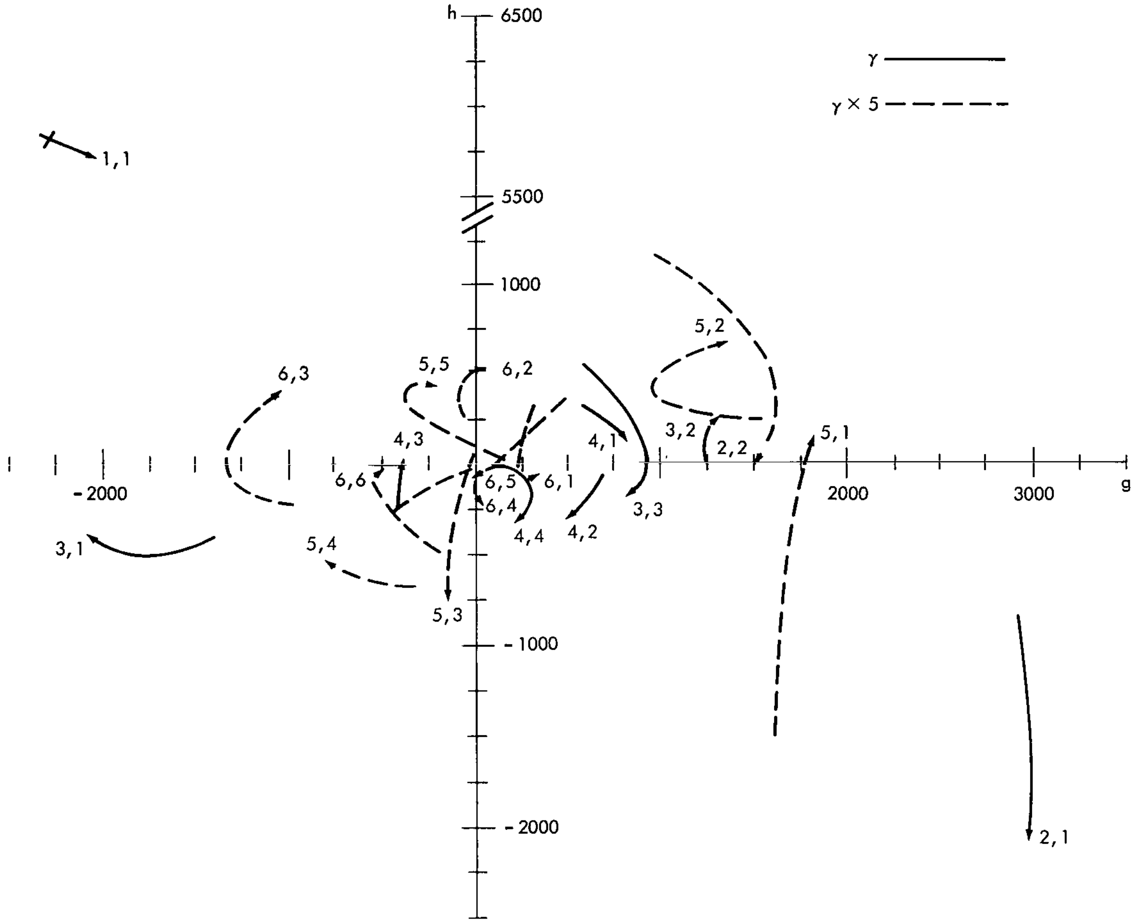

Figure 1—GSFC(12/66) coefficients 1900 to 1970.

The more constant and characteristic feature of this diagram, which was also discussed by Cain and Hide (1966), is that—with the exception of the (6, 1) and (5, 3) traces—both eastward- and westward-moving components have a clockwise curl.

CHANGES IN SURFACE FEATURES

Bullard et al. (1950) treated the question of westward drift by considering the "non-dipole" field. This they defined by vectorially subtracting the eccentric-dipole field from a real field. This subtraction is commonly performed because the dipole contribution is so much larger than the others, appears to change differently, and thus may have a different physical basis. However, the *absolute* change in the (1, 1) component is not disproportionate to that in the other harmonic terms (Figure 1). The small angular change in its phase is due to its relatively large amplitude and a reversal of trend. At this juncture we shall discuss features pertaining to the whole field.

A cursory inspection of some of the surface features confirms the general westerly motion of the field depicted by our model. The 0.23-degree-per-year drift of the Brazilian minimum in total field for this model has already been discussed (Cain, Langel, and Hendricks, 1967). The Siberian high in F at the surface is estimated by the model to be located at 61.8°N, 107.6°E in 1960 and moving at a rate of 0.03 degree per year north in latitude and 0.1 degree per year west in longitude. The Canadian high is also moving north from its 1960 position of 56.7°N, 98.0°W at a rate of 0.08 degree per year, but has an easterly drift of about 0.03 degree per year.

POSITION OF POLES

The GSFC(12/66) model shows both the north and south dip poles moving northwesterly. The change in position of these two points for the period of the data is shown in Table 1.

The 1965 latitude values agree exactly with those adopted for the U. S. (Hurwitz et al., 1966) and for the U. K. (Leaton, Malin, and evans, 1965) World Magnetic Charts but the longitude values differ by a few tenths of a degree.

Table 1

Drift of Dip Poles-GSFC(12/66) Model.

Date	North Dip Pole (degrees)		South Dip Pole (degrees)	
1900	71.2 N,	96.9 W	72.3 S,	153.2 E
1930	72.6 N,	99.0 W	68.8 S,	144.7 E
1960	75.1 N,	100.7 W	66.7 S,	140.7 E
1965	75.5 N,	101.0 W	65.5 S,	140.3 E

Although the positions of the computed dipoles varied smoothly over the period 1900-1965, the direction of motion of the dipole appeared to reverse, as already indicated in Figure 1. The positions of the boreal point are given in Table 2. After the reversal near 1920, the pole began to move westward at a current rate of about 0.07 degree per year.

Table 2

North Dipole Location - GSFC(12/66) Model.

Date	Latitude (degrees)	Longitude (degrees)	Westward Drift Rate (degrees/year)
1900	79.0 N	69.0 W	
			-0.03
1910	78.8 N	68.6 W	
			-0.01
1920	78.7 N	68.5 W	
			0.01
1930	78.7 N	68.6 W	
			0.02
1940	78.7 N	68.8 W	
			0.04
1950	78.7 N	69.2 W	
			0.05
1960	78.7 N	69.7 W	
			0.07
1965	78.8 N	70.0 W	

The 1965 location given here can be compared with the 78.6°N, 70.4°W position given by Leaton, Malin, and Evans (1965) and the 78.6°N, 70.0°W position given by Hurwitz et al. (1966).

DECREASE IN MAGNETIC MOMENT OF DIPOLE

The first three terms of the expansion can be used to compute an equivalent dipole moment and equatorial field (Chapman and

Bartels, 1940, p. 642). With a value of $a = 6.3712 \times 10^8$ cm for a mean radius, the value of M and H_0 are given in Table 3. Since field reversals are believed to have occurred in geological times (Cox et al., 1967), it has recently become popular (Leaton and Malin, 1967; McDonald and Gunst, 1967) to speculate on the demise of the main-field dipole (about 3700-4000 A.D.) by extrapolating a linear trend from such data as the above. Note, however, the tendency toward a reduction in the rate of decrease. Since our analysis included data for a time span during which there is only a 3-percent change in M, extrapolations to zero are most untrustworthy.

Table 3

Dipole Moment and Horizontal Field of Equivalent Dipole.

Date	$M \times 10^{-25}$ (cgs)	H_0 (Γ)	$\dot{H}_0$ (γ/year)
1900	8.298	0.3209	
			-20
1920	8.197	0.3170	
			-18
1940	8.105	0.3134	
			-16
1960	8.023	0.3102	

CONCLUSIONS

Since the GSFC(12/66) field analysis was performed on survey data without correcting them for short-period fluctuations such as Dst and Sq, it is remarkable that the main patterns of secular change represented agree so closely with earlier analyses in which the data were subjected to a careful screening and correction process. The main defects of the model result from the irregular regional changes superimposed on the general trends and the use of a parabolic representation over too long an interval. Therefore, extrapolation of the model to epochs beyond the last data used (1965.8) will be increasingly in error—by as much as a few tens of gammas per year, in some areas. This deviation may seem large, but better forecasts can hardly be made until recent satellite survey data are evaluated over a year or more, to allow for a more accurate *global* estimate of secular change. This work does indicate that there is no special need for fixed repeat stations for monitoring the secular change. Although data from such stations were indeed a valuable addition to the data set, the analysis ignored the fact that they remained in one location. It may later be possible to monitor the main field using only satellite data corrected for time variations as derived from the fluctuations observed at the surface observatories.

The westward motion of most of the spherical-harmonic vectors confirms earlier observations. The clockwise curvature pattern for almost all components is noted for the first time as a curious and unexplained fact. The sudden reversal of the eastward drift of the dipole poles near 1920 may be due to inaccuracies in the analysis resulting partly from the poor distribution of data. On the other hand, the change may be connected with the 1900-1920 anomalous increase of the earth's rate of rotation. The slight slowing of the rate of decrease of the moment of the earth's main dipole suggests that the field is not beginning a cycle of reversal. To check such suggestions requires subjecting a much longer span of magnetic-field observations to a consistent analysis.

Goddard Space Flight Center
National Aeronautics and Space Administration
Greenbelt, Maryland, November 22, 1967
841-12-02-06-51

REFERENCES

1. Bullard, E. C., C. Freedman, H. Gellman, and J. Nixon, "The Westward Drift of the Earth's Magnetic Field," *Phil. Trans. Roy. Soc., 243A,* 67-92, 1950.

2. Cain, J. C., and J. R. Neilon, "Automatic Mapping of the Geomagnetic Field," *J. Geophys. Res., 68,* 4689-4698, 1963.

3. Cain, J. C., W. E. Daniels, S. J. Hendricks, and D. C. Jensen, "An Evaluation of the Main Geomagnetic Field, 1940-1962," *J. Geophys. Res., 70,* 3647-3674, 1965.

4. Cain, J. C., and R. Hide, "The Secular Change of the Geomagnetic Field (abstract)," *Trans. Am. Geophys. Union, 47,* 57, 1966.

5. Cain, J. C., "Models of the Earth's Magnetic Field," in *Radiation Trapped in the Earth's Magnetic Field,* edited by D. Reidel, p. 1, 1966.

6. Cain, J. C., S. J. Hendricks, R. A. Langel, and W. V. Hudson, "A Proposed Model for the International Geomagnetic Reference Field," Goddard Space Flight Center Document X-612-67-173, 1967.

7. Cain, J. C., R. A. Langel, and S. J. Hendricks, "Magnetic Chart of the Brazilian Anomaly - A Verification," Goddard Space Flight Center Document, X-612-67-373, 1967.

8. Chapman, S., and J. Bartels, *Geomagnetism,* Oxford University Press, London, 1940.

9. Cox, A., G. B. Dalrymple, and R. R. Doell, "Reversals of the Earth's Magnetic Field," *Sci. Am., 216,* 44, 1967.

10. Dicke, R. H., "The Secular Acceleration of the Earth's Rotation and Cosmology," in *The Earth Moon System,* p. 141, Plenum Press, New York, 1966.

11. Eleman, F., "Time Variations of Geomagnetic H and D at Disturbed Stations," *Nature, 209,* 1120-1121, 1966.

12. Hendricks, S. J., and J. C. Cain, "Magnetic Field Data for Trapped Particle Evaluations," *J. Geophys. Res., 71,* 346, 1966.

13. Hide, R., "Free Hydromagnetic Oscillations of the Earth's Core and the Theory of the Geomagnetic Secular Variation," *Phil. Trans. Royal Soc., A259,* 615-647, 1966.

14. Hurwitz, L., D. G. Knapp, J. H. Nelson, and D. E. Watson, "Mathematical Model of the Geomagnetic Field," *J. Geophys. Res., 71,* 2373, 1966.

15. Leaton, B. R., S. R. C. Malin, and M. J. Evans, "An Analytical Representation of the Estimated Geomagnetic Field and Its Secular Change for the Epoch 1965.0," *J. Geomag. Geoelec., 17,* 187-194, 1965.

16. Leaton, B. R., and S. R. C. Malin, "Recent Changes in the Magnetic Dipole Moment of the Earth," *Nature, 213,* 1110, 1967.

17. Mauersberger, P., "A Discussion of the Variation with Time of the Parameters of the Geomagnetic Field Based on the Existing Potential Analysis, NASA TT-F-8443, 1963.

18. McDonald, K. L. and R. H. Gunst, "An Analysis of the Earth's Magnetic Field from 1835 to 1965," *ESSA Tech. Rept. IER 46-IES 1,* 1967.

19. Munk, W. H., and G. J. F. MacDonald, *The Rotation of the Earth,* University Press, Cambridge [England], 1960.

20. Nagata, T., "Two Main Aspects of Geomagnetic Secular Variation—Westward Drift and Non-Drifting Components," Benedum Earth's Magnetism Symposium, U. of Pittsburgh Press, 1962.

21. Vestine, E. H., I. Lange, L. Laporte, and W. E. Scott, "The Geomagnetic Field, Its Description and Analysis," Carnegie Institution of Washington, Publication 580, 1947.

Appendix A

Comparison of Observatory Annual Mean Values 1900 - 1965 With Elements Computed From GSFC (12/66)

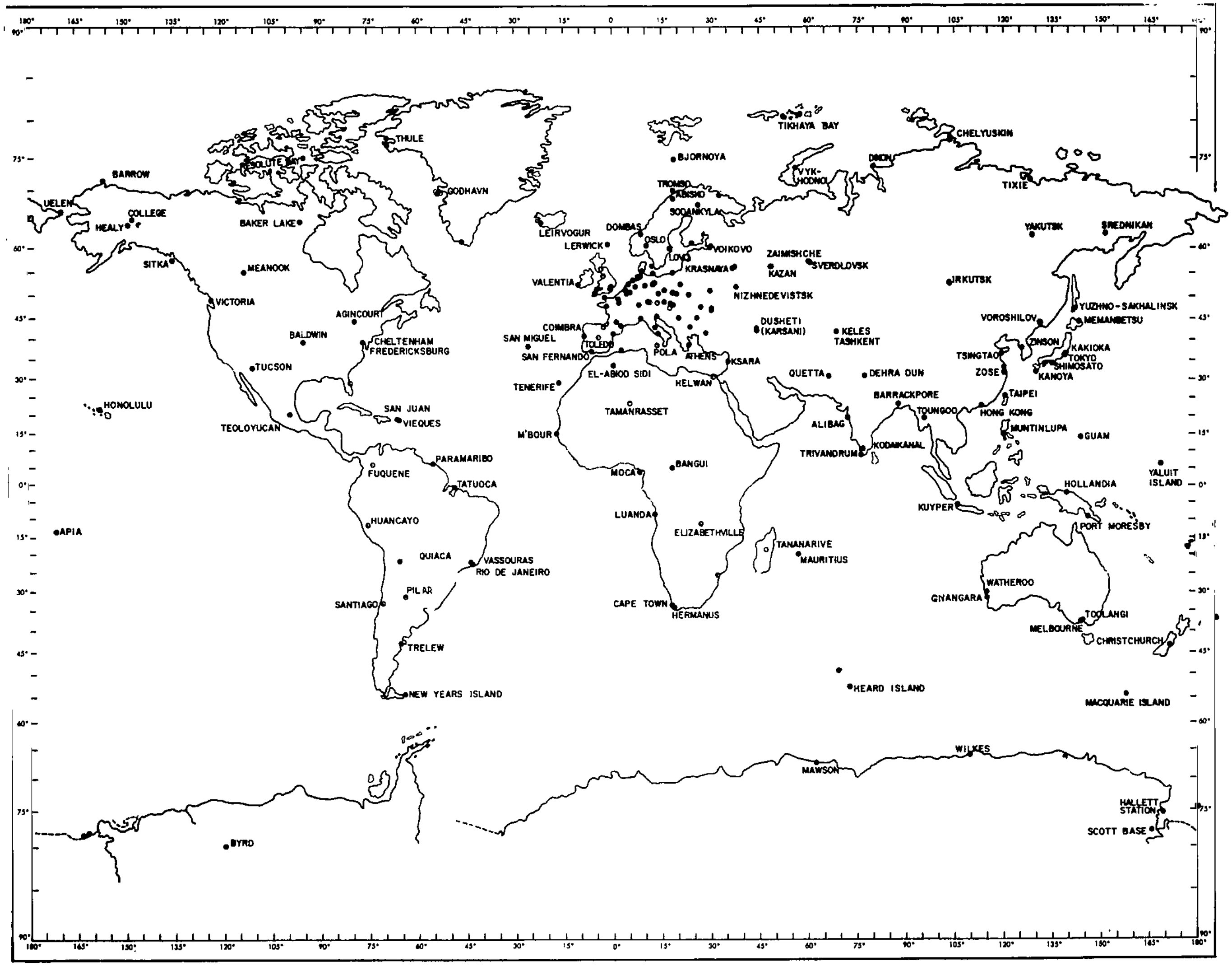

THULE
GODHAVN
BARROW
UELEN
COLLEGE
HEALY
BAKER LAKE
RESOLUTE BAY
SITKA
MEANOOK
VICTORIA
AGINCOURT
BALDWIN
CHELTENHAM
FREDERICKSBURG
TUCSON
HONOLULU
TEOLOYUCAN
SAN JUAN
VIEQUES
PARAMARIBO
FUQUENE
TATUOCA
HUANCAYO
APIA
QUIACA
VASSOURAS
RIO DE JANEIRO
PILAR
SANTIAGO
TRELEW
NEW YEARS ISLAND
BYRD
LEIRVOGUR
LERWICK
DOMBAS
OSLO
VALENTIA
COIMBRA
SAN MIGUEL
SAN FERNANDO
TOLEDO
TENERIFE
EL-ABIOD SIDI
M'BOUR
TAMANRASSET
BJORNOYA
TROMSO
ABISKO
SODANKYLA
LOVO
VOIKOVO
KRASNAYA
NIZHNEDEVISTSK
POLA
ATHENS
KSARA
HELWAN
BANGUI
MOCA
LUANDA
ELIZABETHVILLE
CAPE TOWN
HERMANUS
TANANARIVE
MAURITIUS
TIKHAYA BAY
VYK-HODNOI
DIKSON
ZAIMISHCHE
KAZAN
SVERDLOVSK
DUSHETI
(KARSANI)
KELES
TASHKENT
QUETTA
DEHRA DUN
ALIBAG
TRIVANDRUM
KODAIKANAL
BARRACKPORE
TOUNGOO
HEARD ISLAND
MAWSON
WILKES
CHELYUSKIN
TIXIE
YAKUTSK
SREDNIKAN
IRKUTSK
VOROSHILOV
YUZHNO-SAKHALINSK
MEMANBETSU
ONSON
KAKIOKA
TOKYO
SHIMOSATO
KANOYA
TSINGTAO
ZOSE
TAIPEI
HONG KONG
MUNTINLUPA
GUAM
YALUIT
ISLAND
HOLLANDIA
KUYPER
PORT MORESBY
WATHEROO
GNANGARA
TOOLANGI
MELBOURNE
CHRISTCHURCH
MACQUARIE ISLAND
HALLETT
STATION
SCOTT BASE

Figure A1

ABINGER
Lat 51.18 Long -0.38

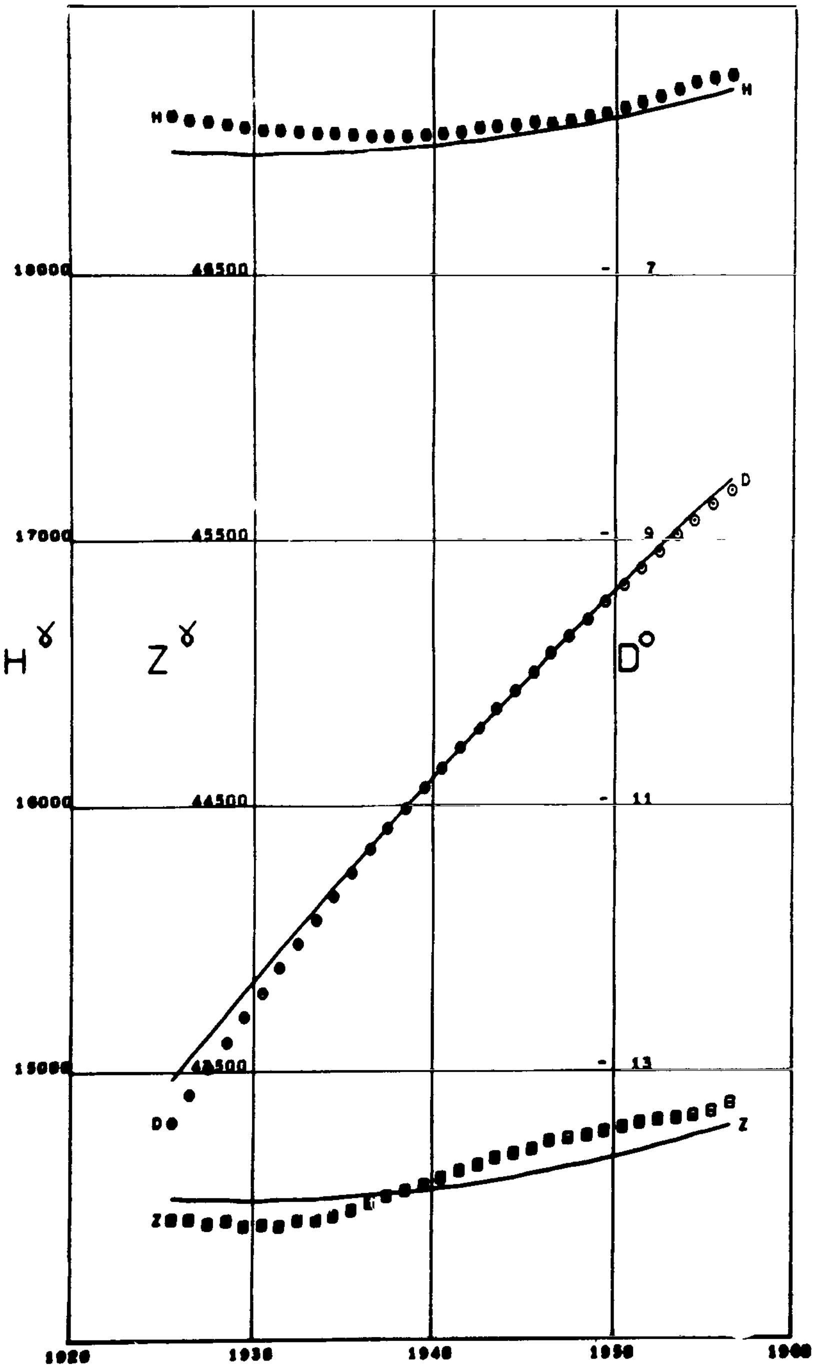

Figure A2

ABISKO
Lat 68.35 Long 18.82

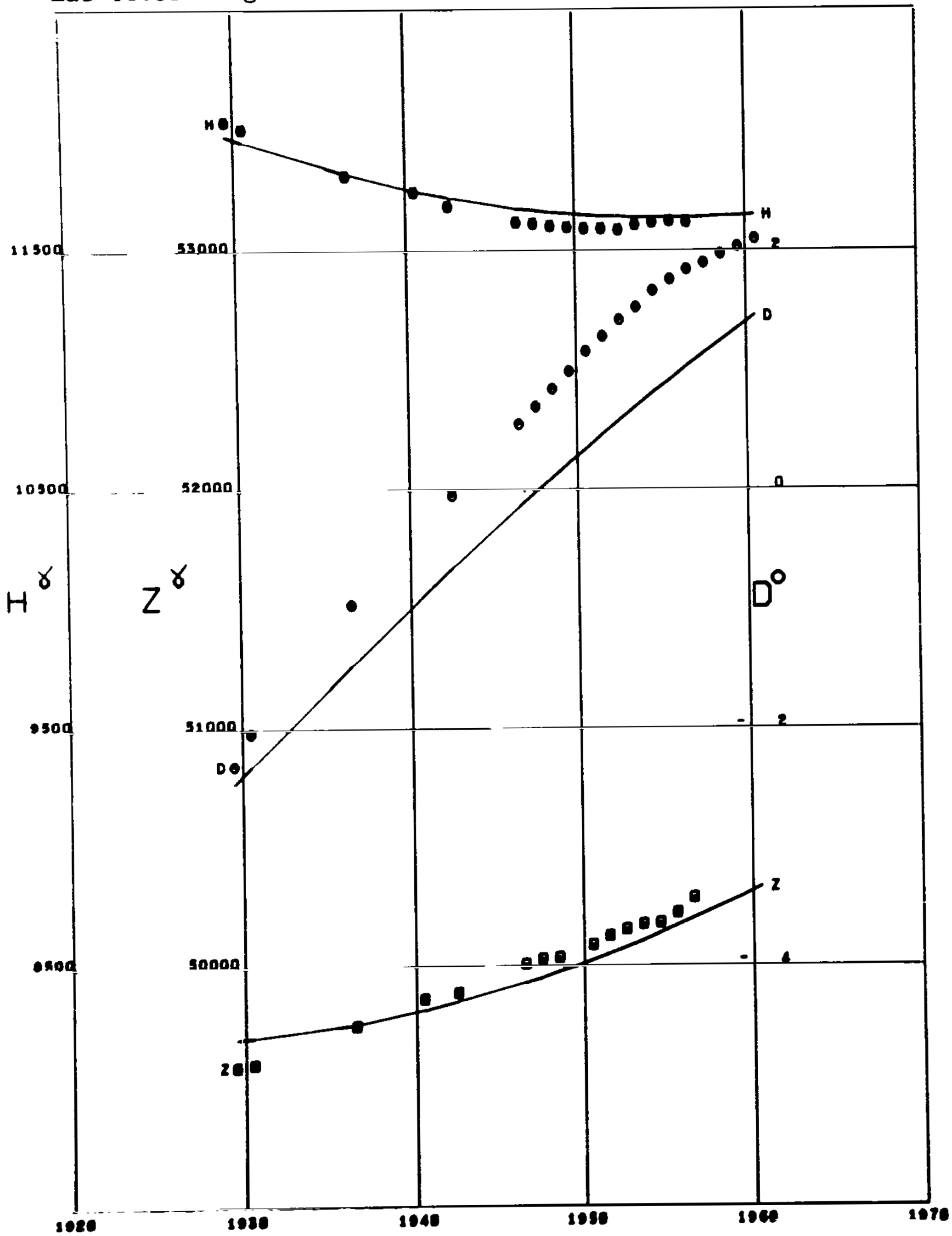

Figure A3

ADDIS ABABA
Lat 9.03 Long 38.76 Alt 2.44

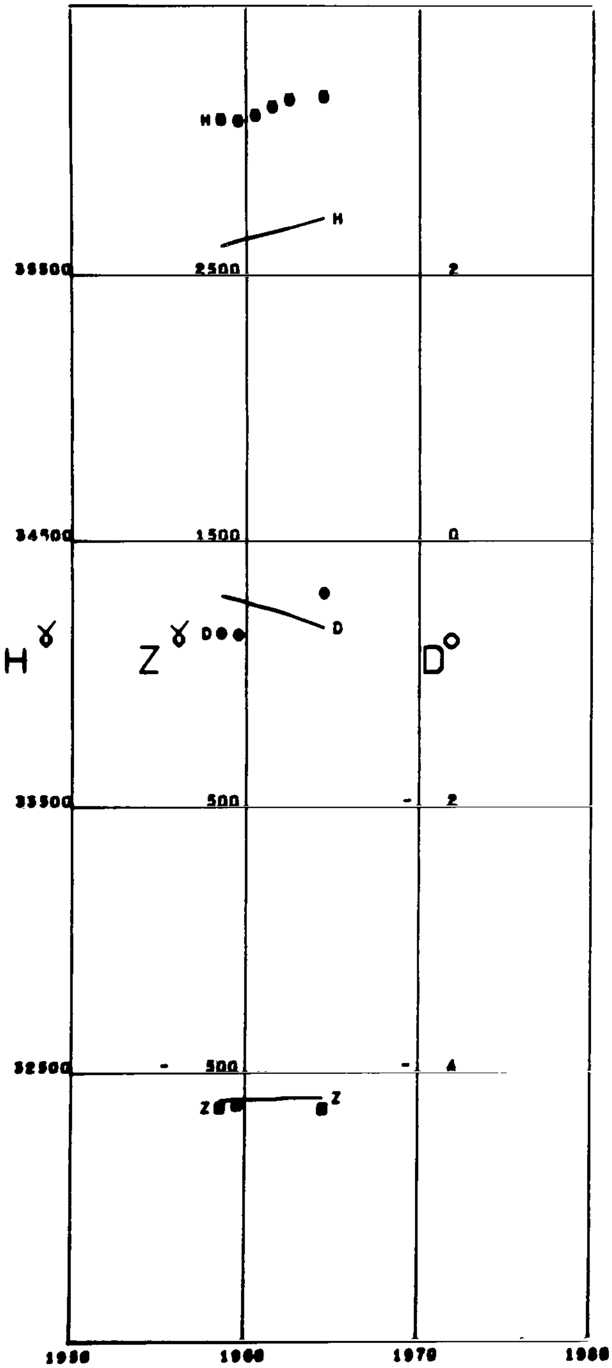

Figure A4

AGINCOURT
Lat 43.78 Long -79.26 Alt 0.18

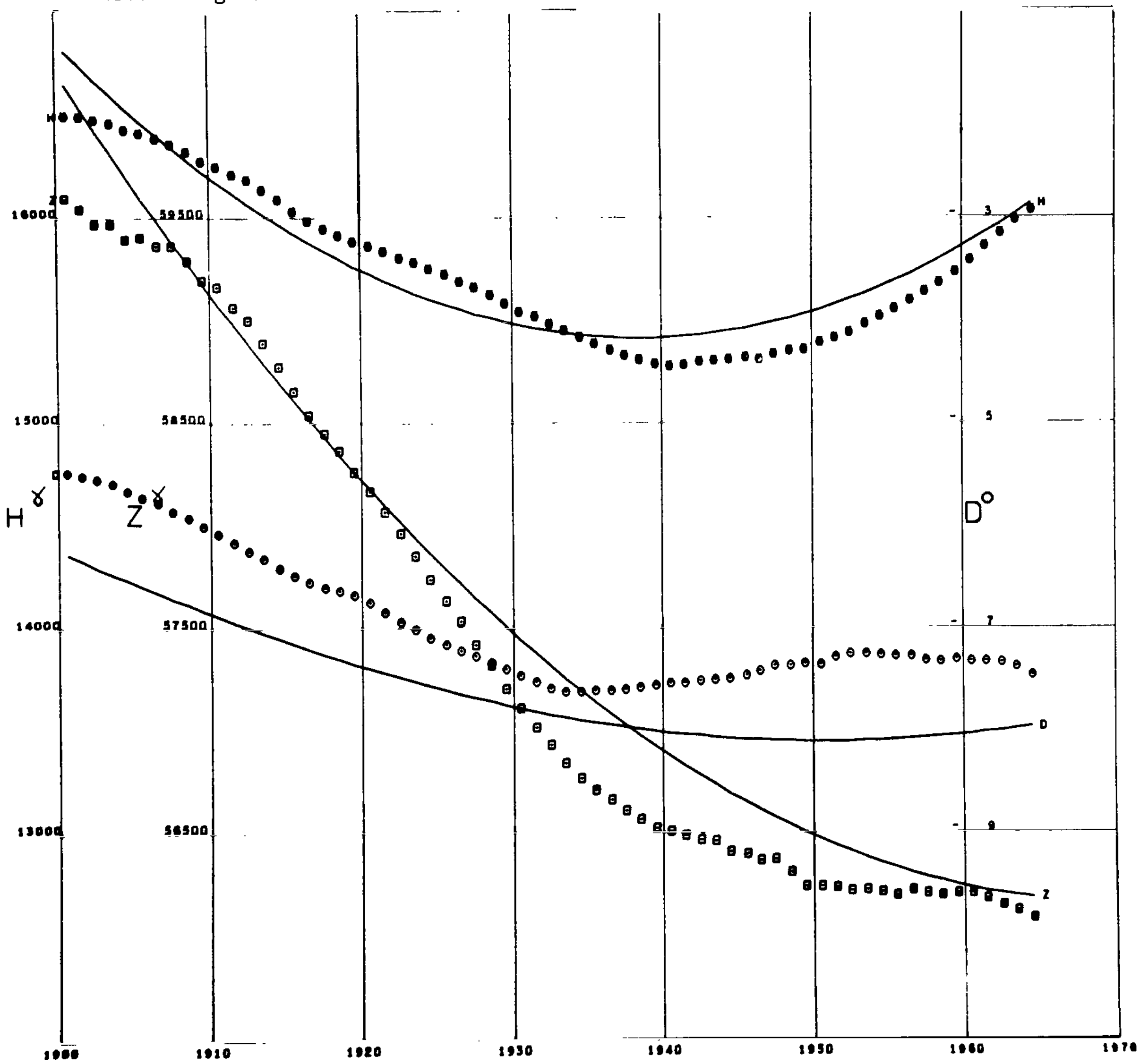

Figure A5

ALIBAG
Lat 18.63 Long 72.87 Alt 0.01

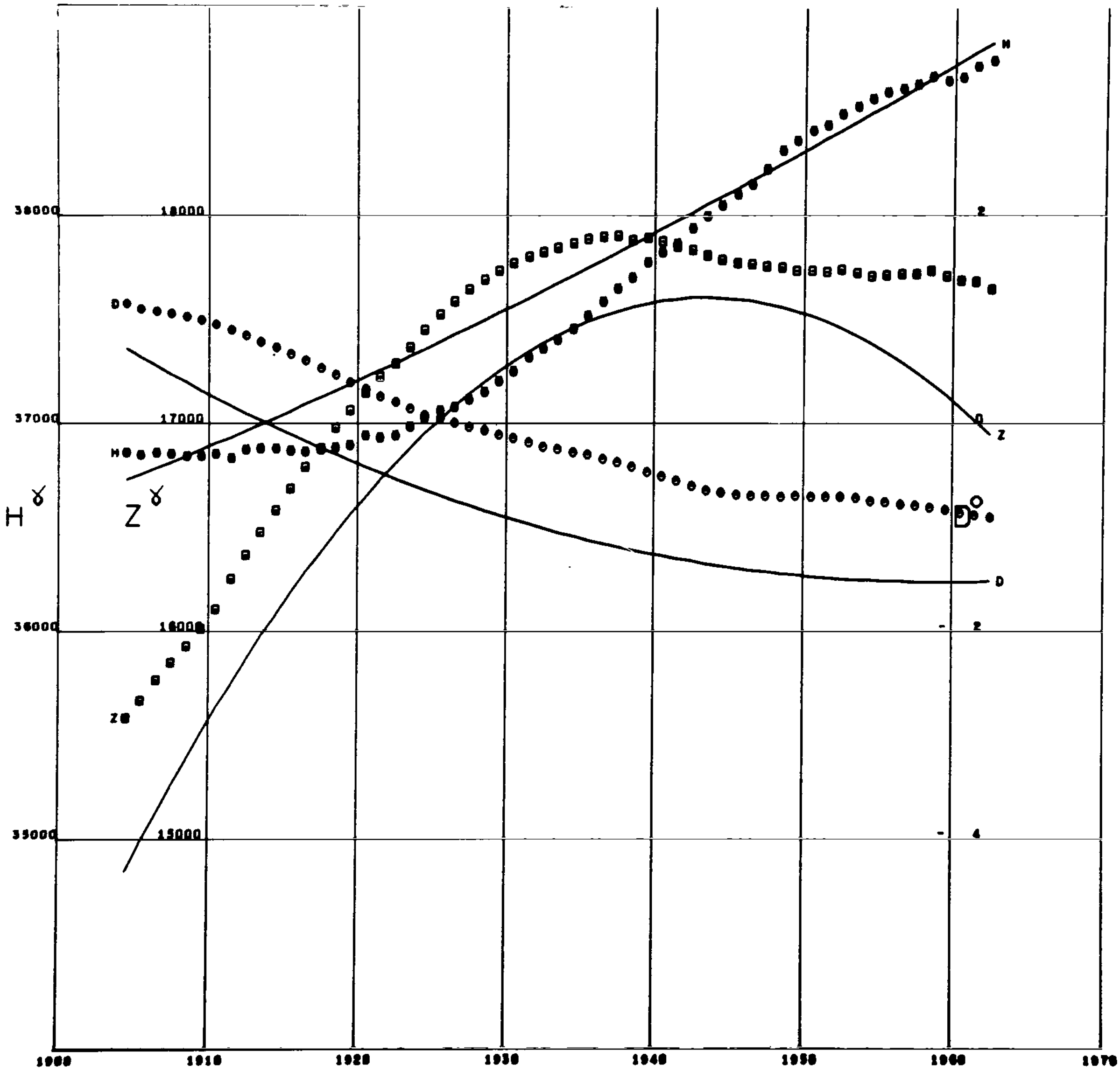

Figure A6

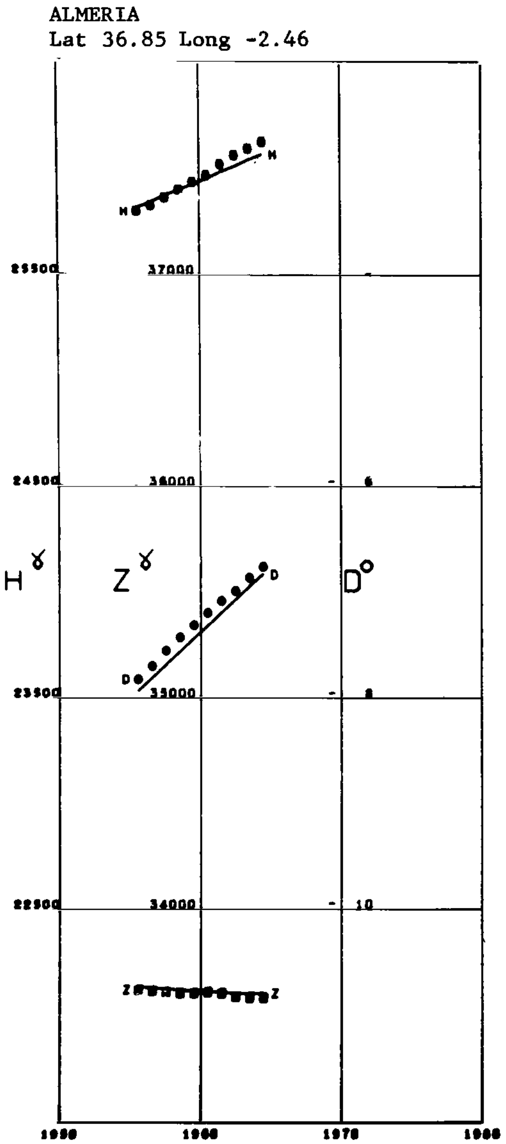

Figure A7

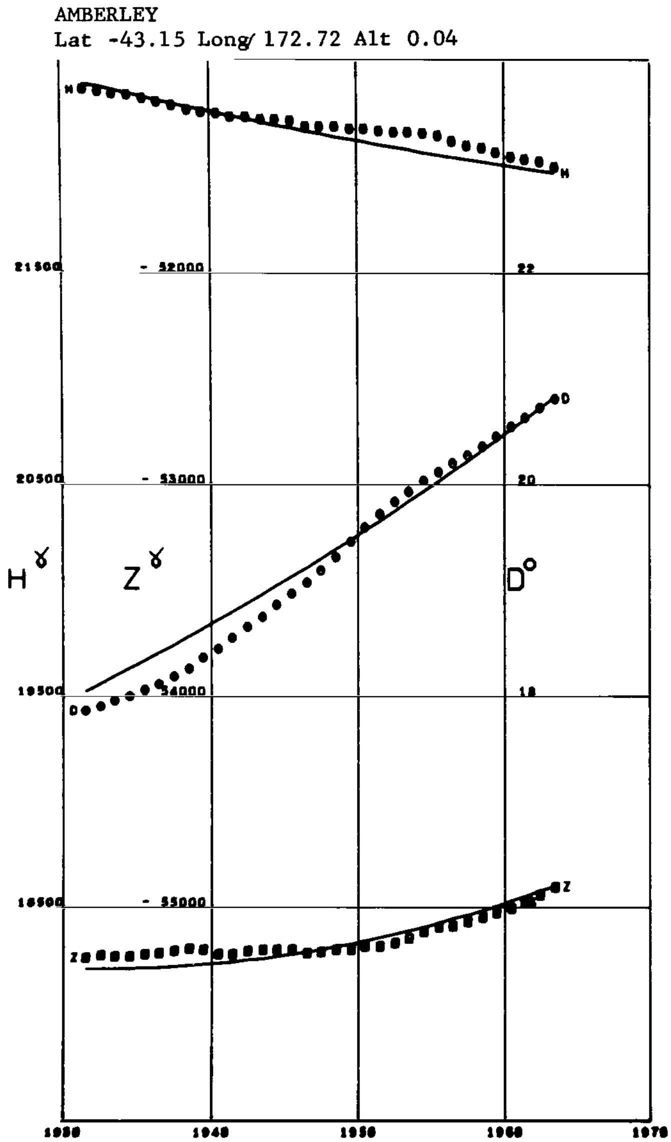

Figure A8

ANNAMALAINAGAR
Lat 11.40 Long 79.68

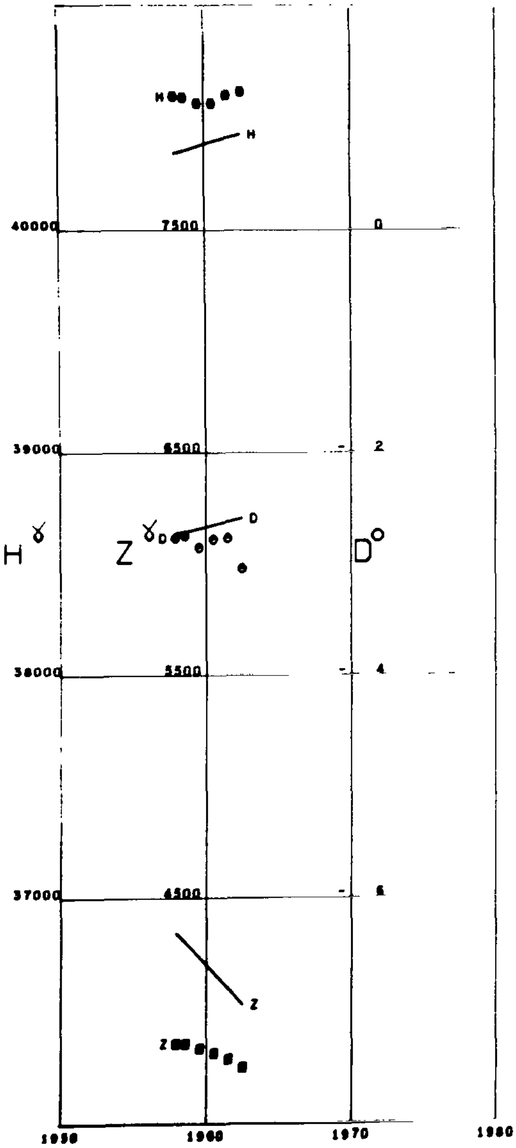

Figure A9

ANTIPOLO
Lat 14.60 Long 121.16

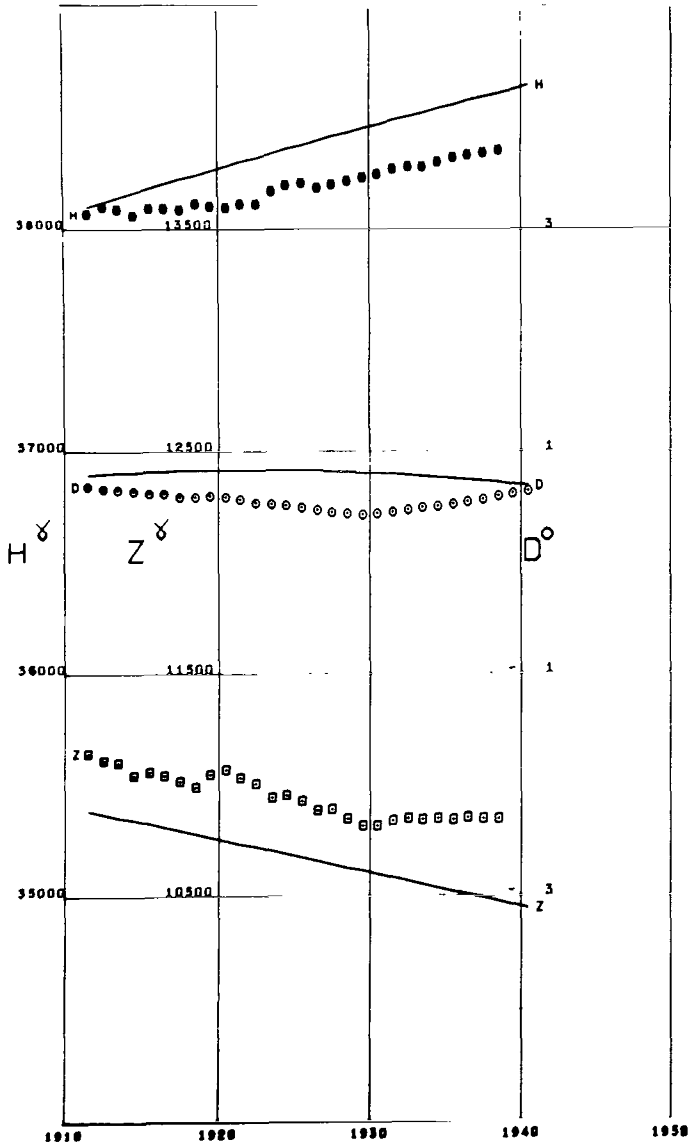

Figure A10

APIA
Lat -13.80 Long -171.77

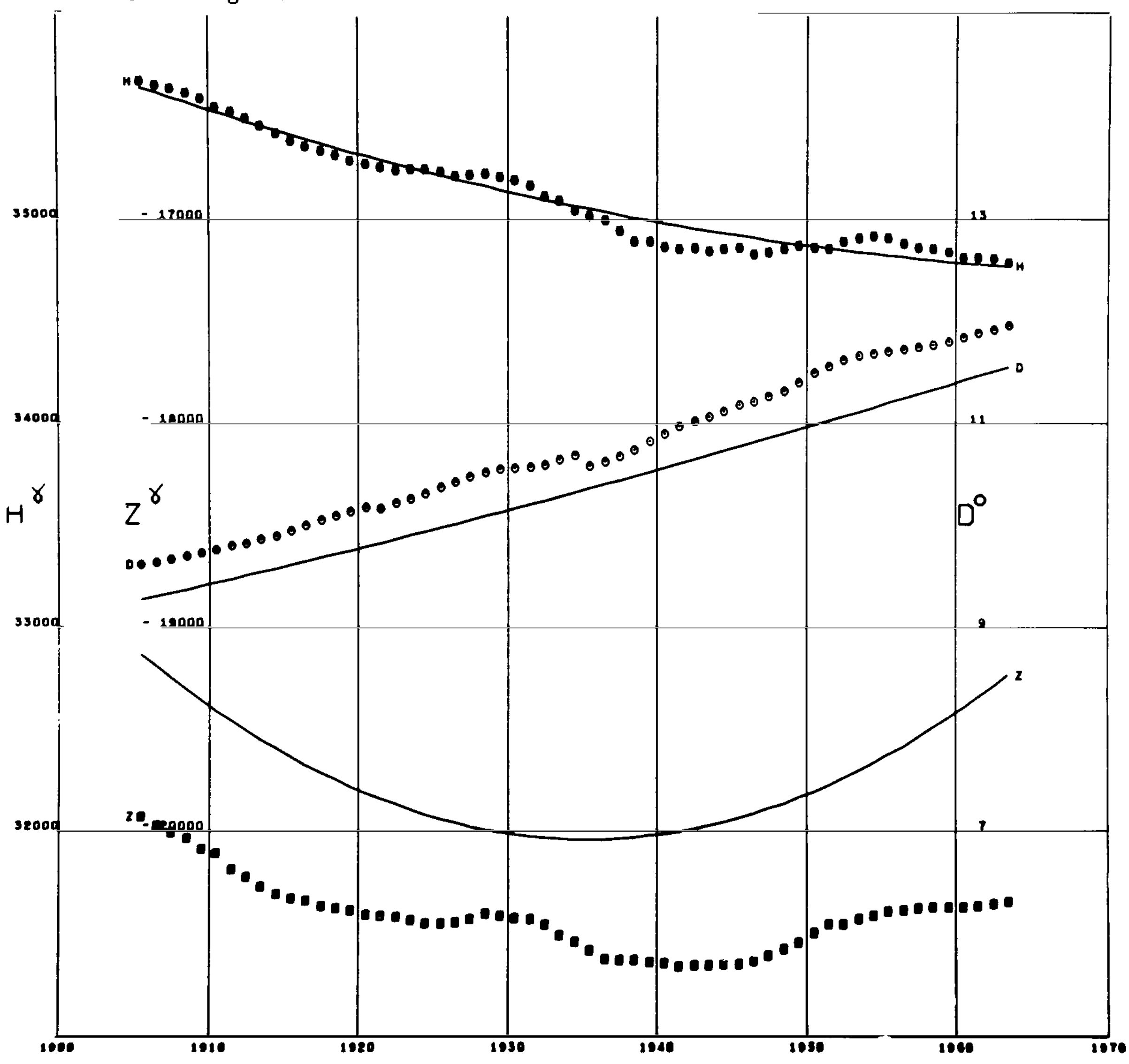

Figure A11

AQUILA
Lat 42.38 Long 13.31

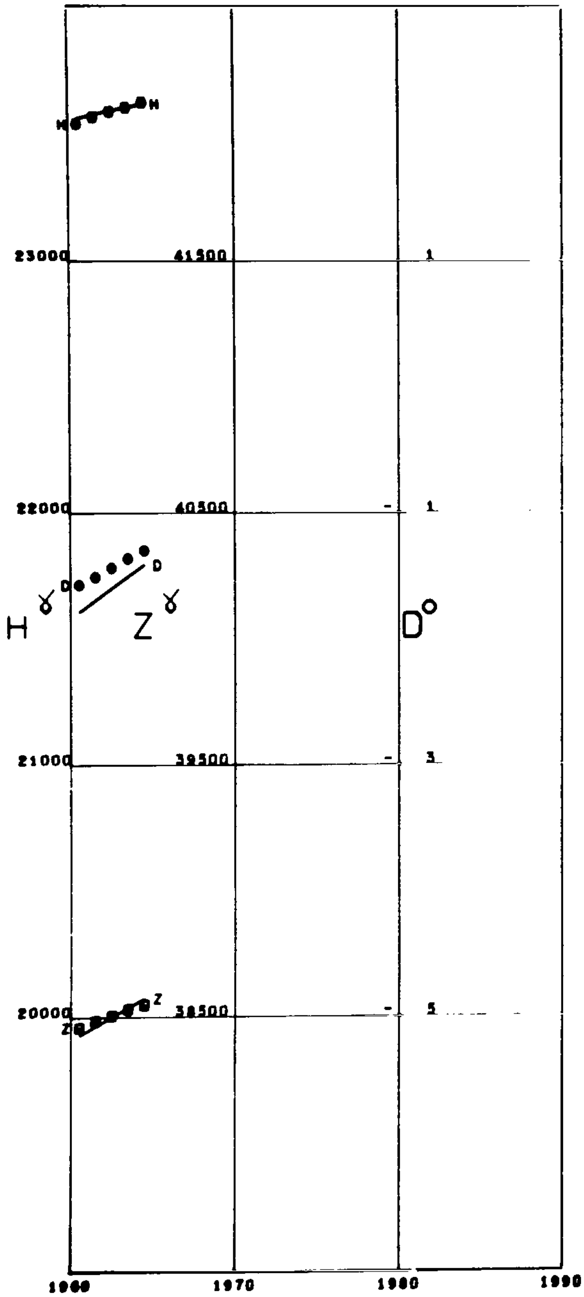

Figure A12

ARGENTINE ISLAND
Lat -65.24 Long -64.25

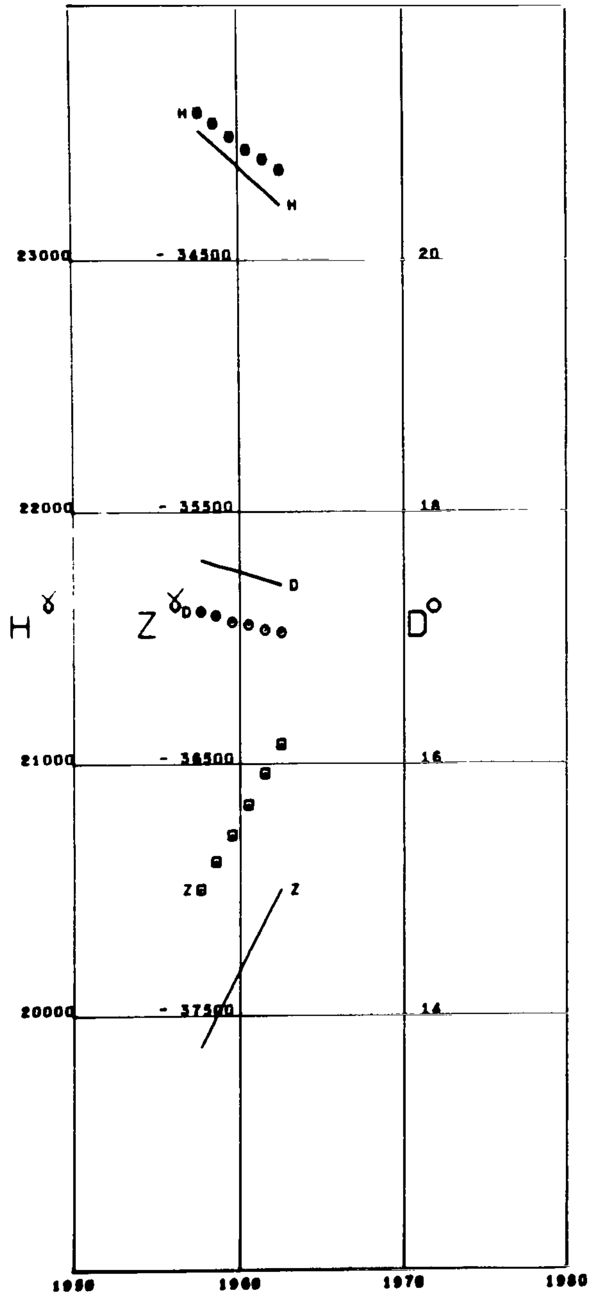

Figure A13

ATHENS
Lat 37.97 Long 23.72

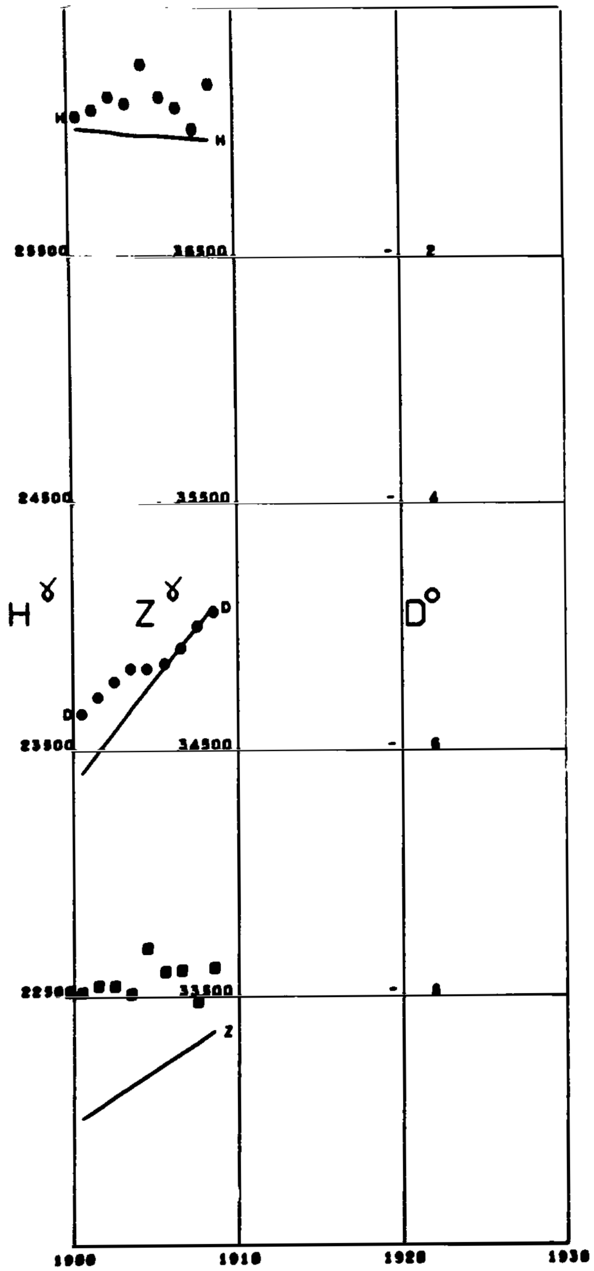

Figure A14

AU TAU
Lat 22.44 Long 114.04

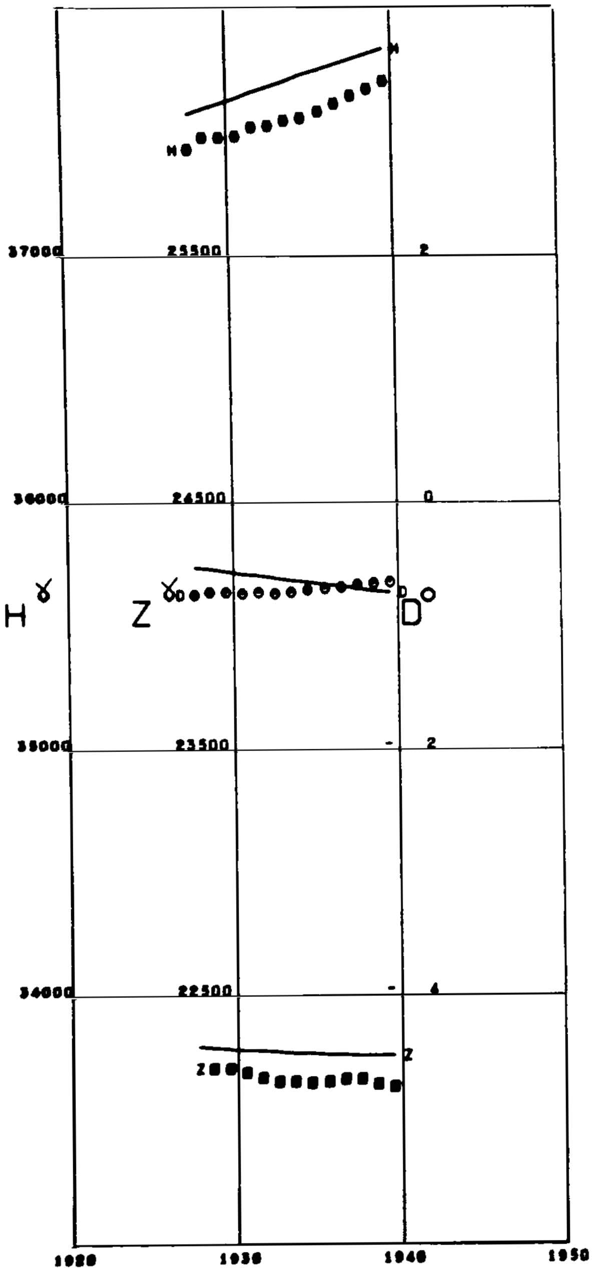

Figure A15

BAKER LAKE
Lat 64.33 Long -96.03 Alt 0.04

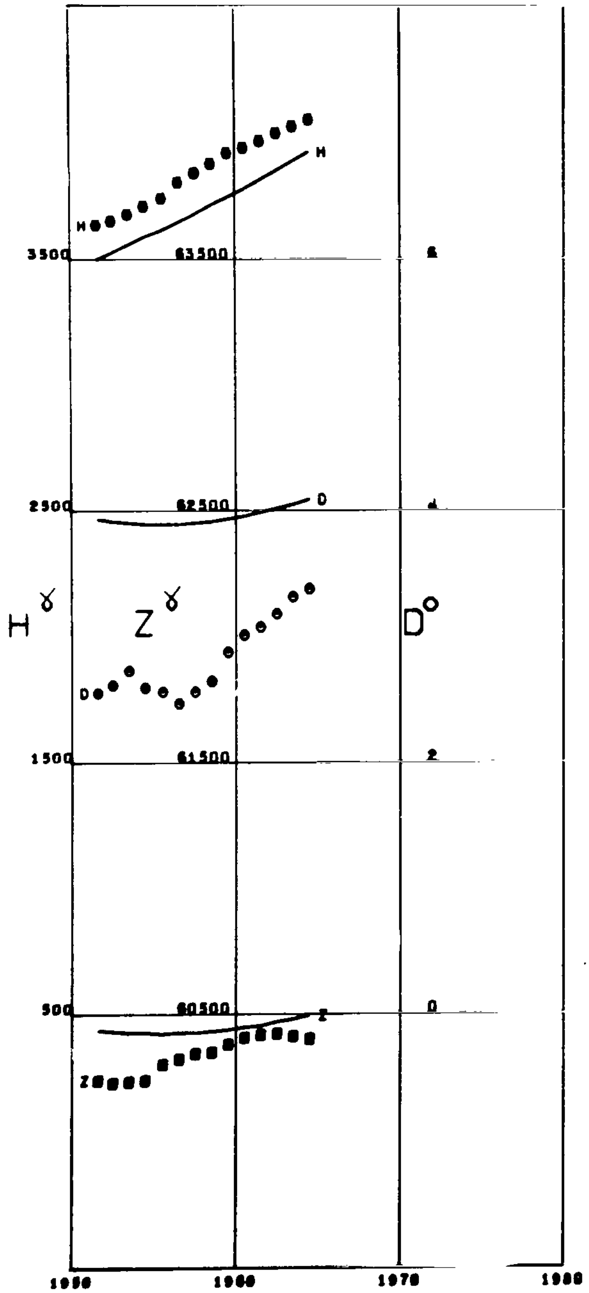

Figure A16

BALDWIN
Lat 38.78 Long -95.16

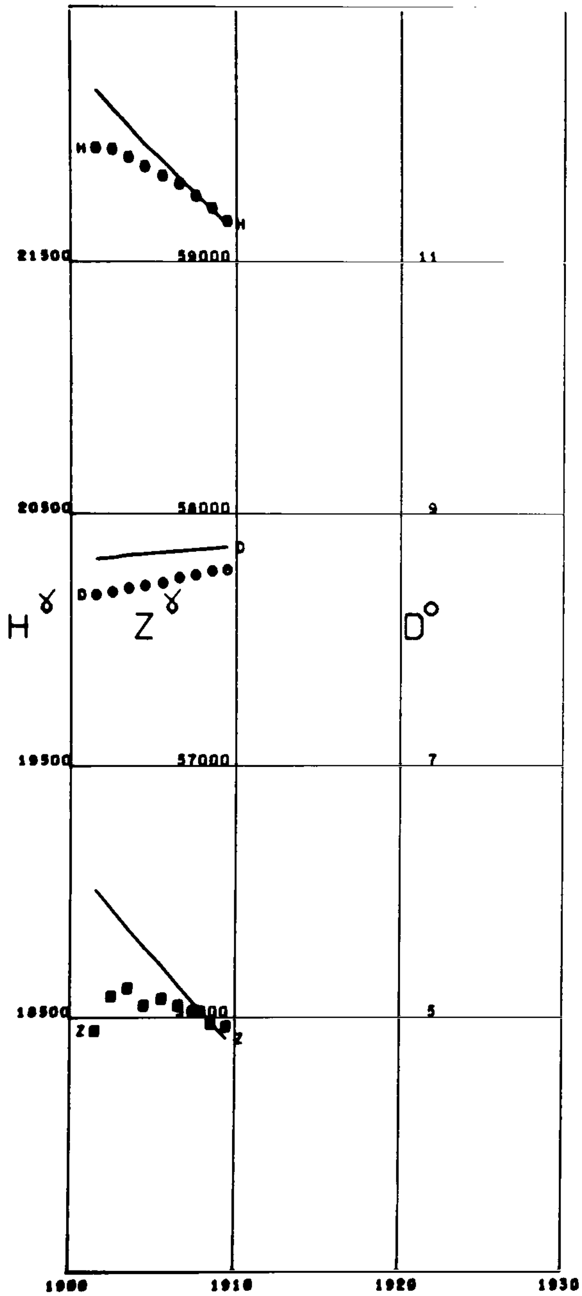

Figure A17

BANGUI
Lat 4.43 Long 18.56 Alt 0.44

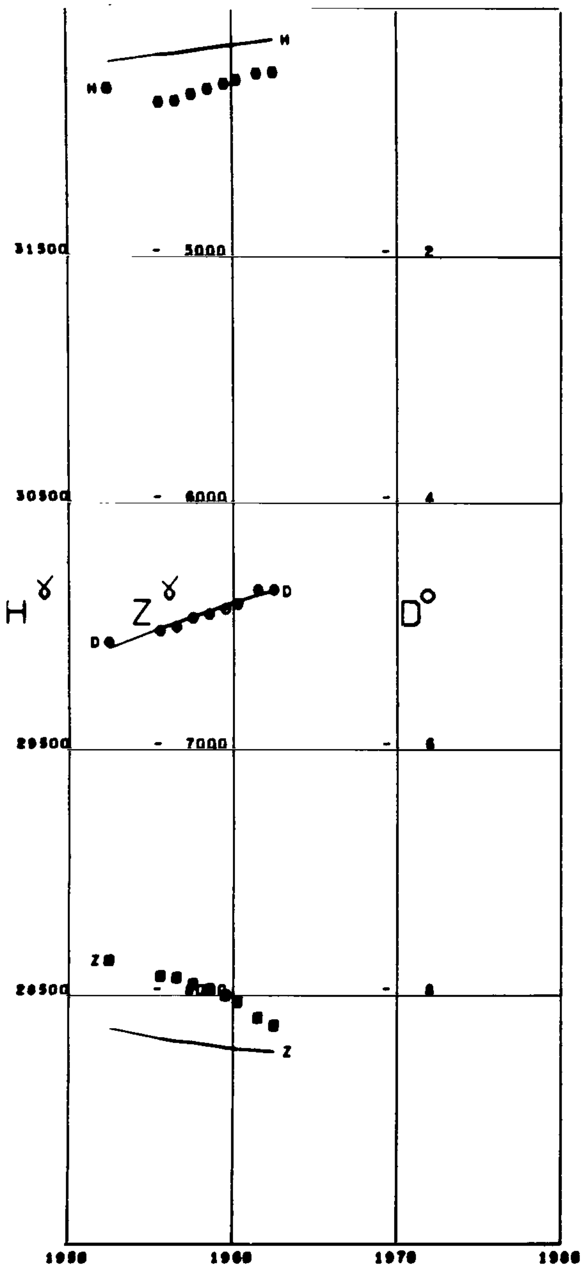

Figure A18

BARRACKPORE
Lat 22.77 Long 88.36

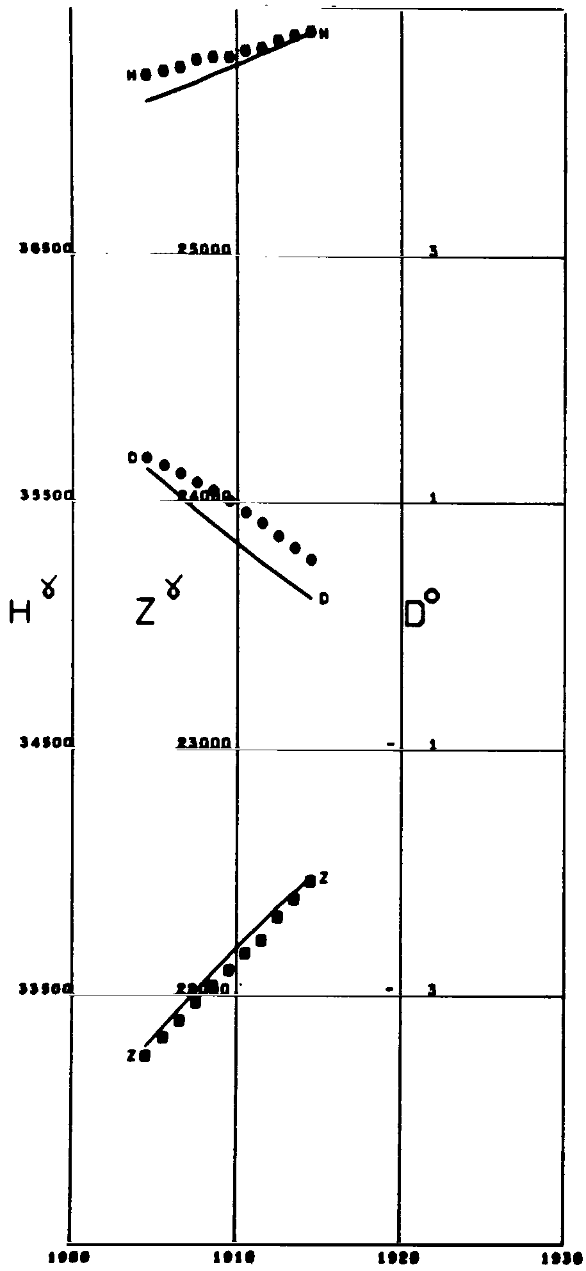

Figure A19

BARROW
Lat 71.30 Long -156.74

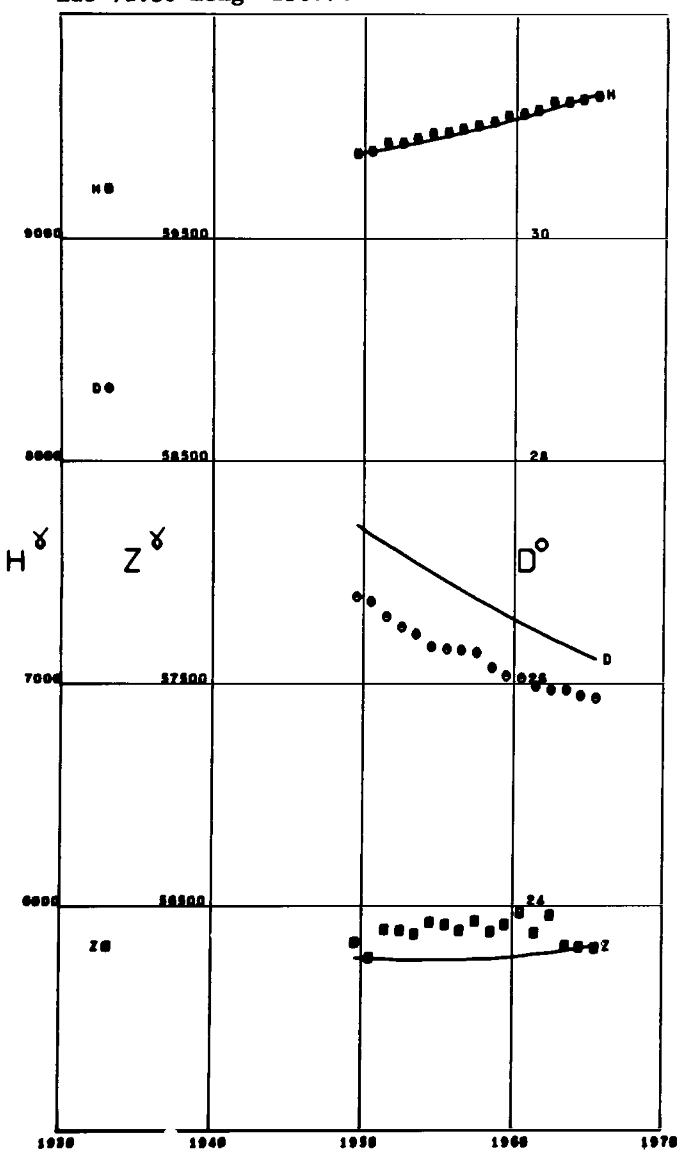

Figure A20

BATAVIA
Lat -6.18 Long 106.83

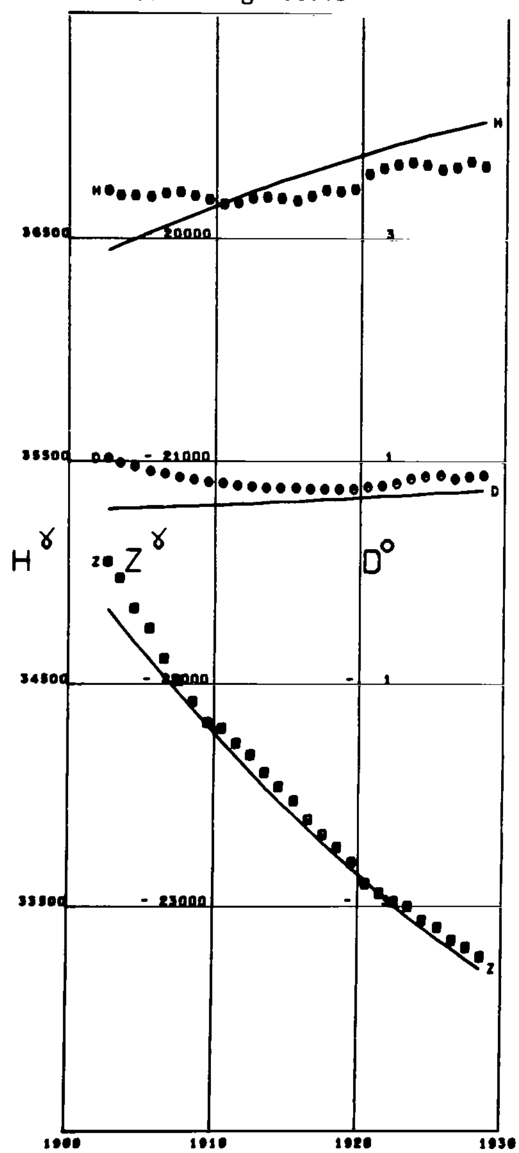

Figure A21

BEUTHEN
Lat 50.35 Long 18.92

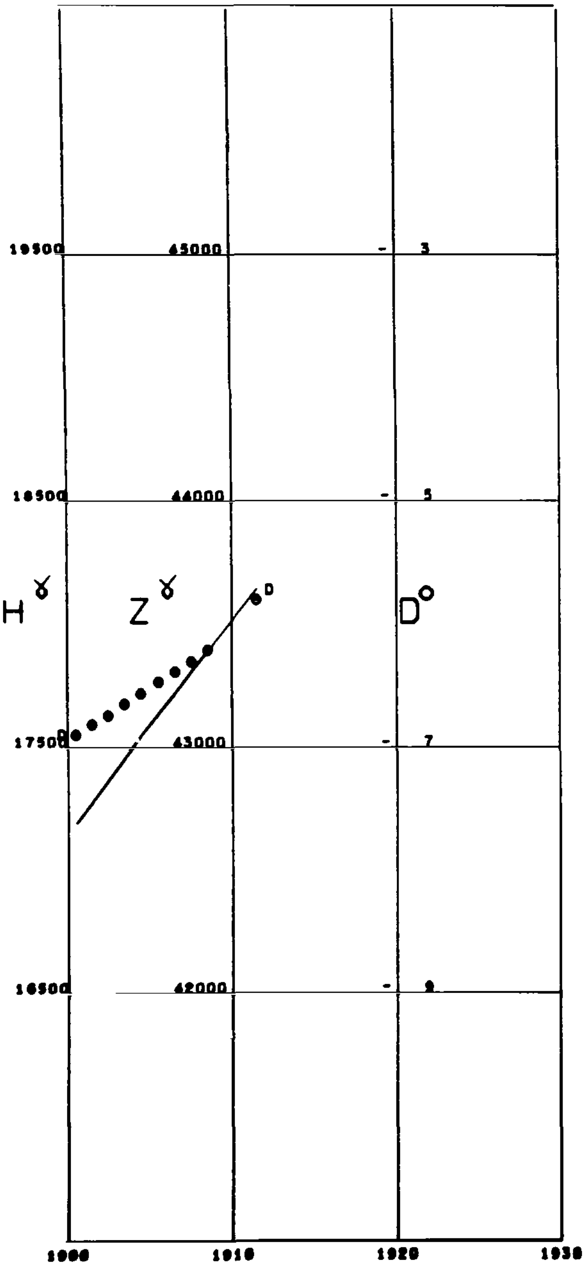

Figure A22

BEUTHEN MIKILOW
Lat 50.15 Long 18.90

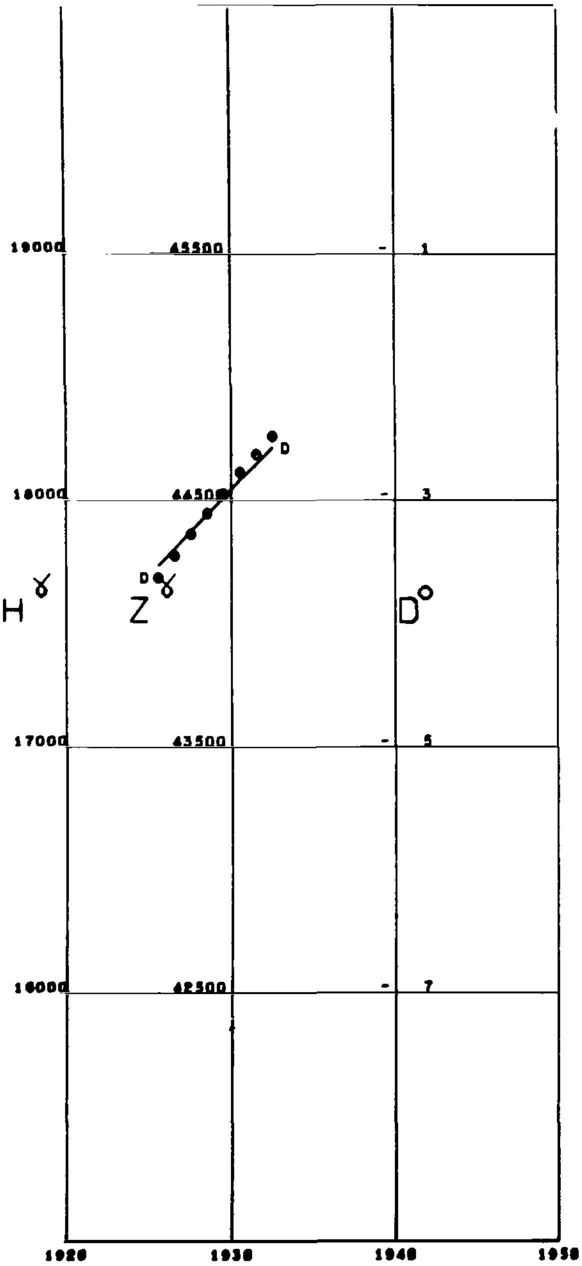

Figure A23

BJORNOYA
Lat 74.50 Long 19.20

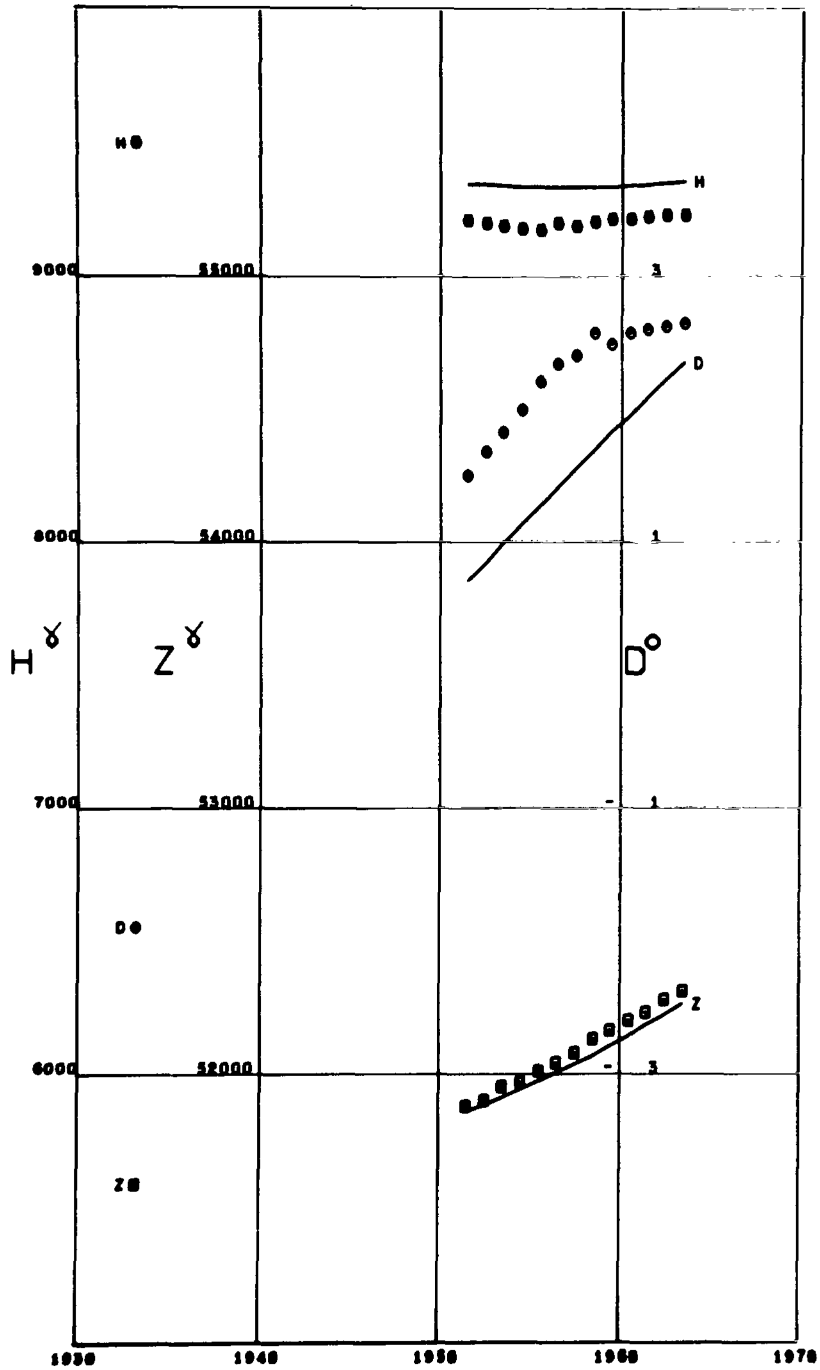

Figure A24

BOCHUM
Lat 51.49 Long 7.23

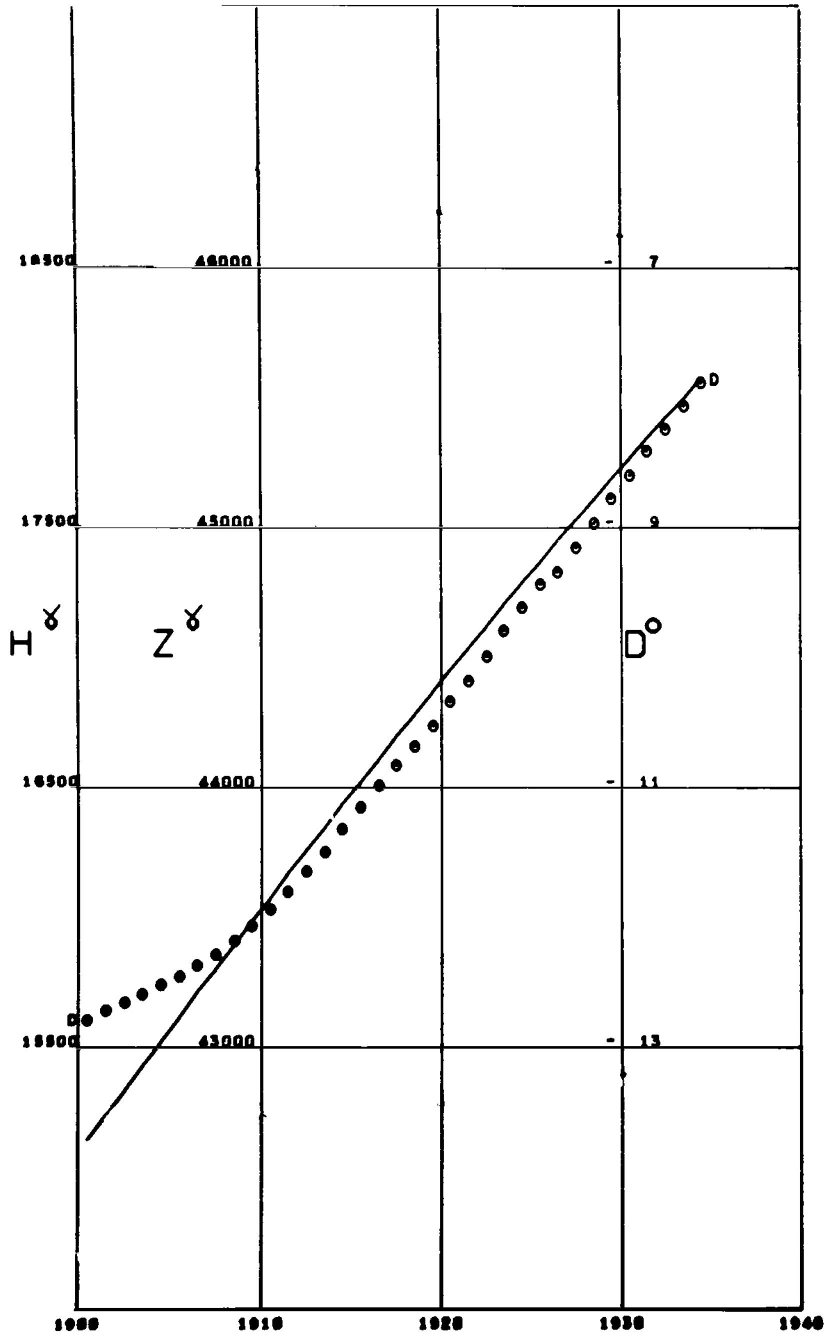

Figure A25

BOUZAREAH
Lat 36.80 Long 3.01

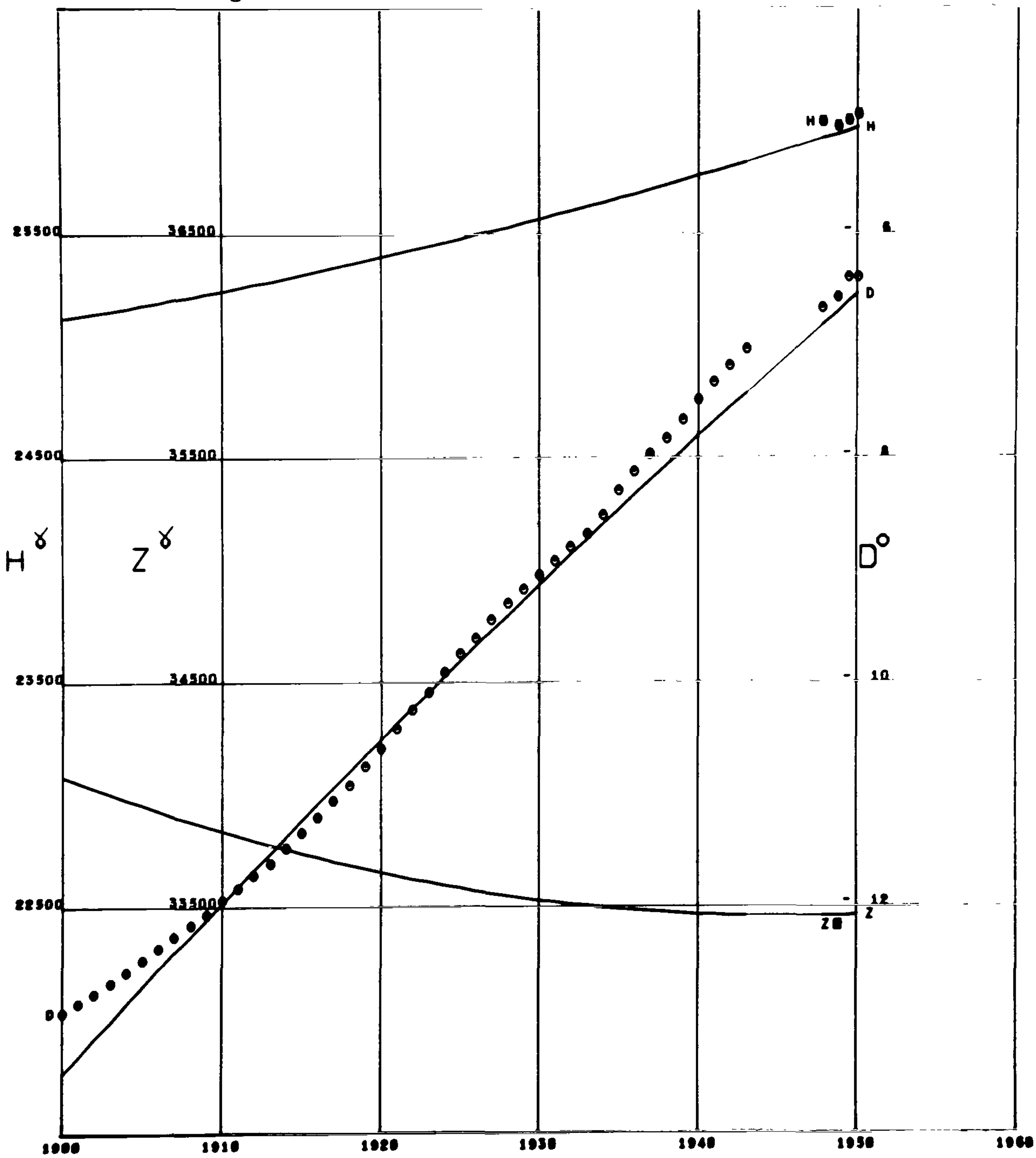

Figure A26

BUDAKESZI
Lat 47.52 Long 18.89

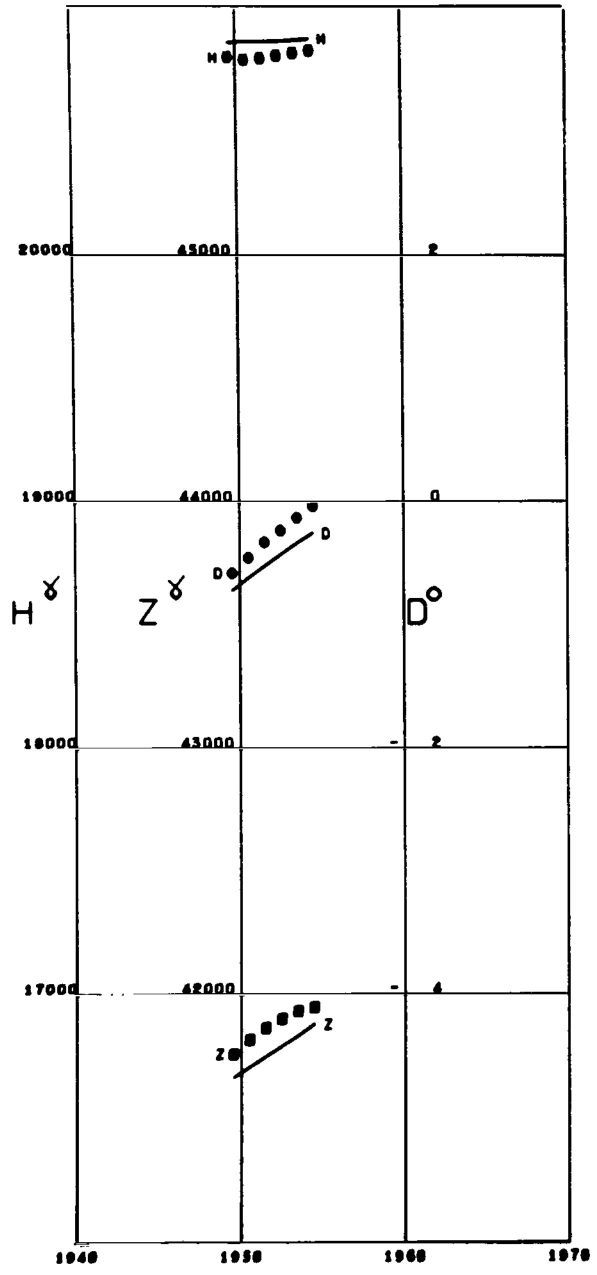

Figure A27

BYRD
Lat -80.01 Long -119.51 Alt 1.52

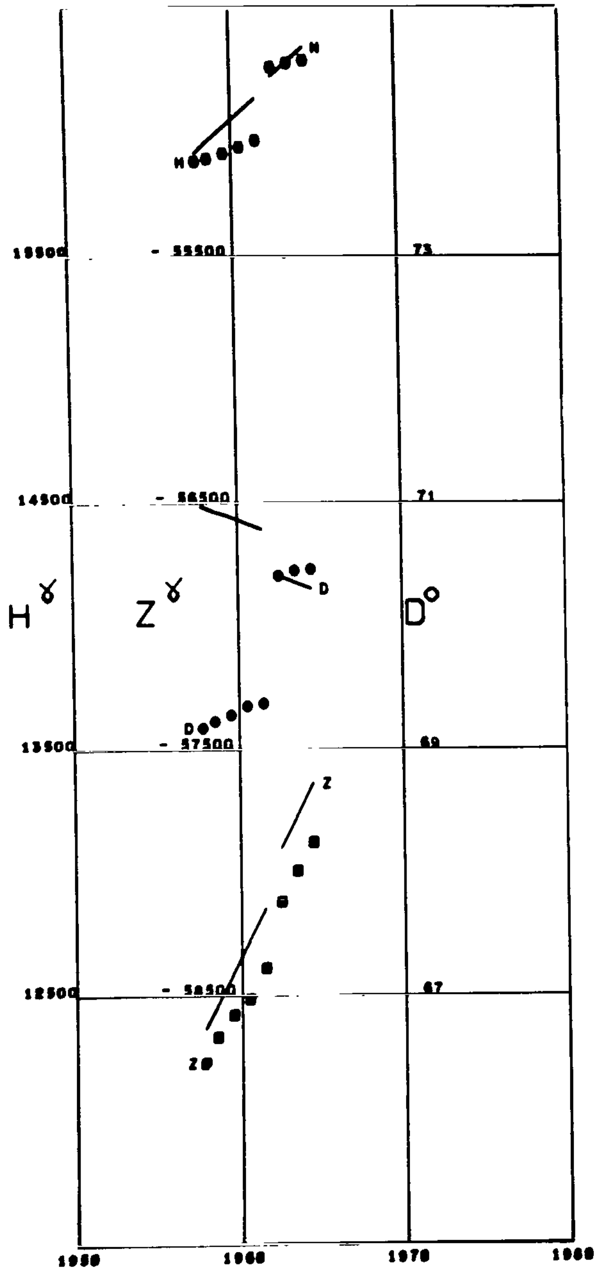

Figure A28

CAPETOWN
Lat -33.95 Long 18.46

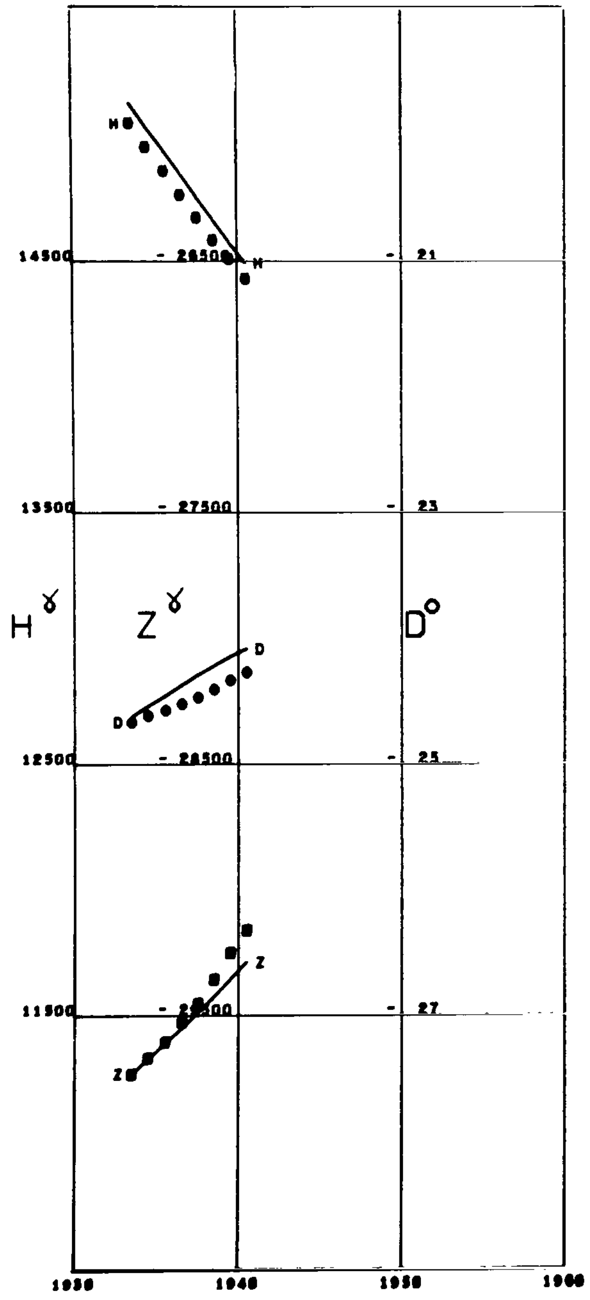

Figure A29

CAPODIMONTE
Lat 40.86 Long 14.25

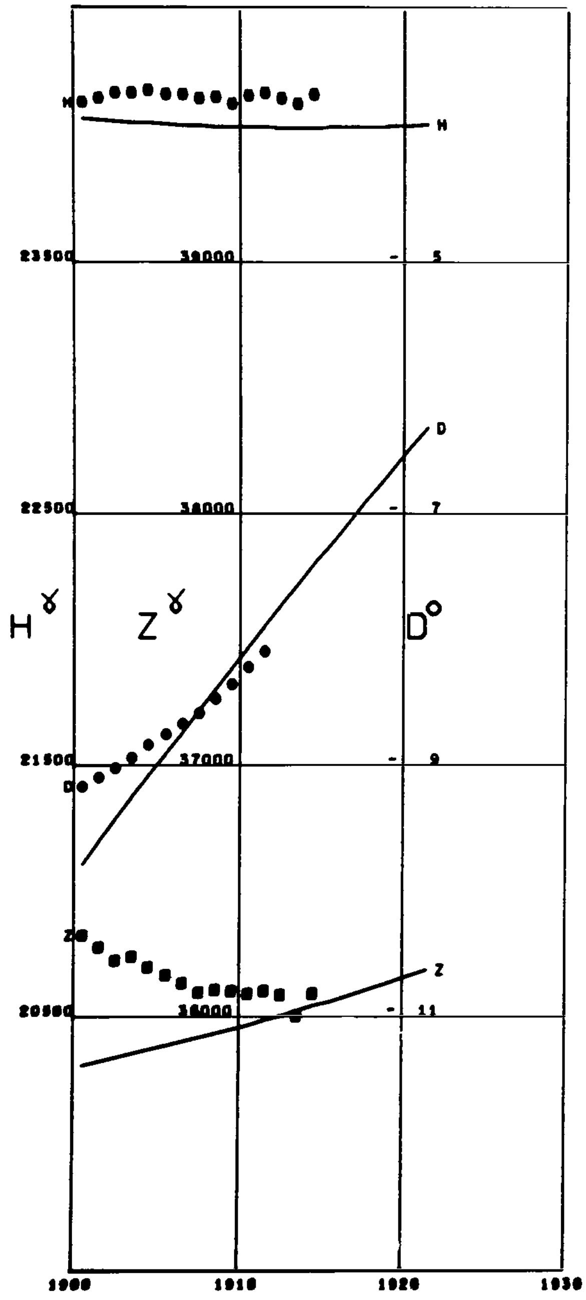

Figure A30

CASTELLACCIO
Lat 44.43 Long 8.93

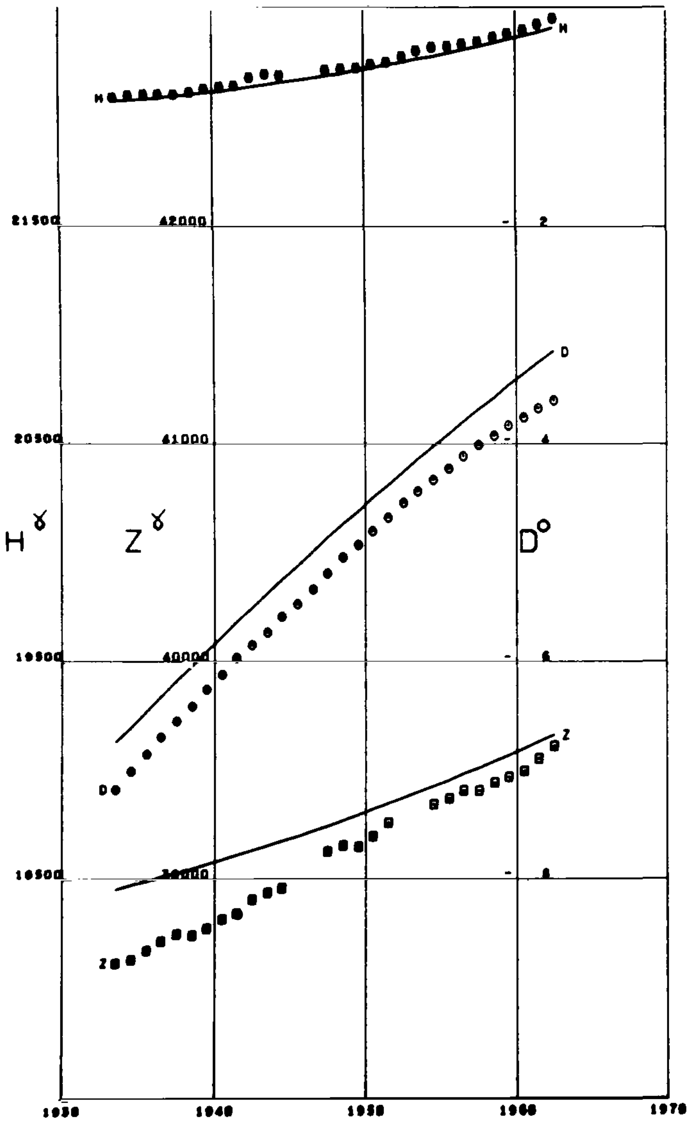

Figure A31

CHA PA
Lat 22.35 Long 103.83

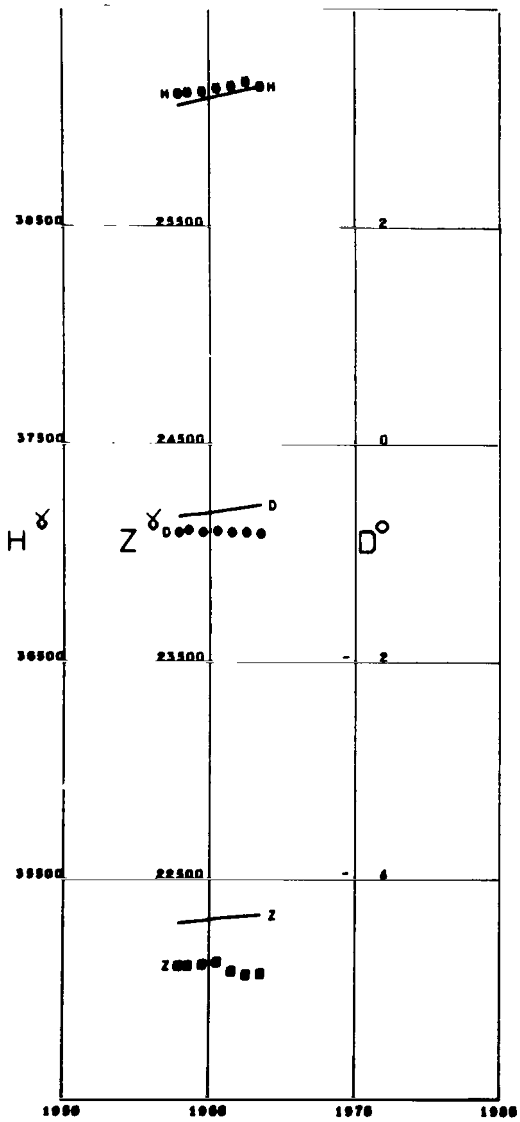

Figure A32

CHAMBON-LA-FORET
Lat 48.02 Long 2.26

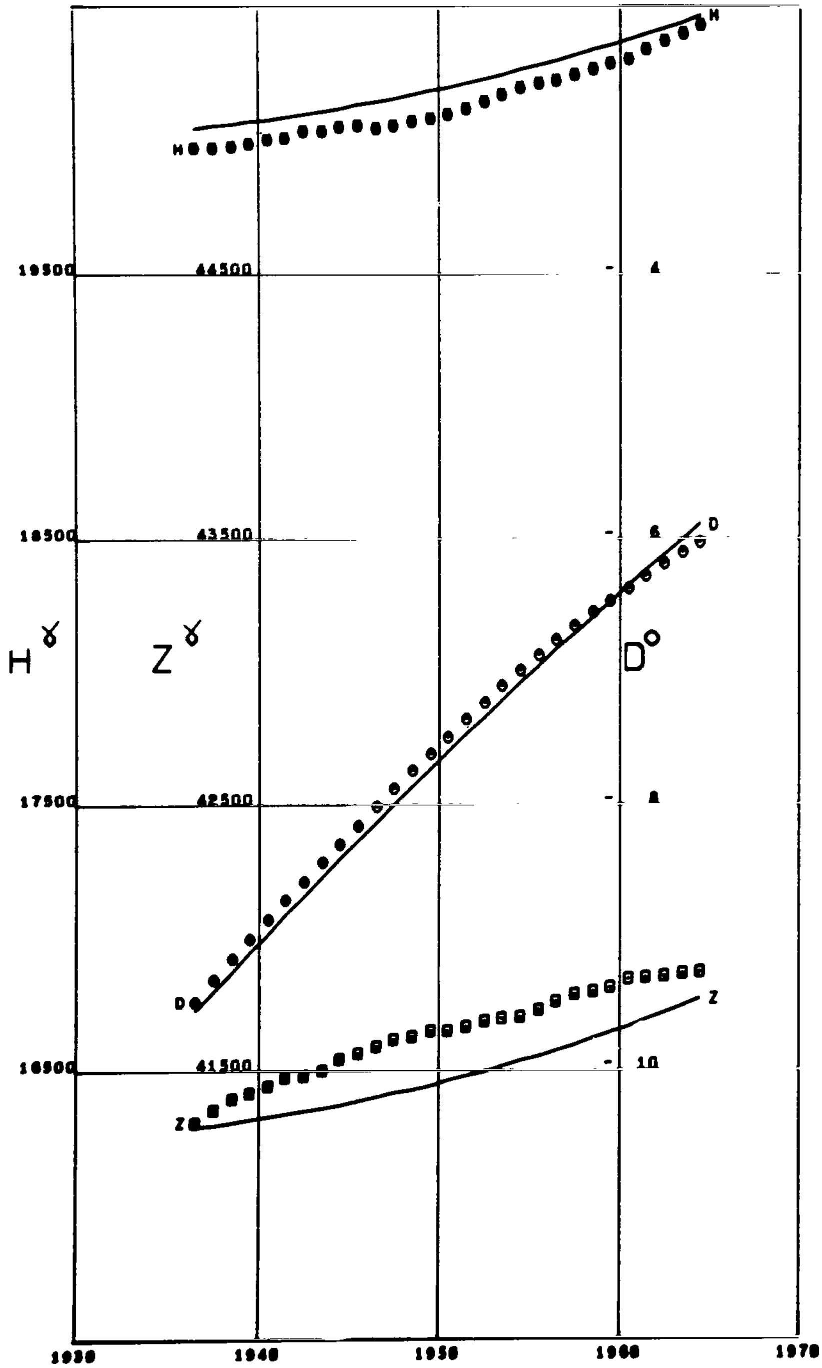

Figure A33

CHELTENHAM
Lat 38.73 Long -76.84

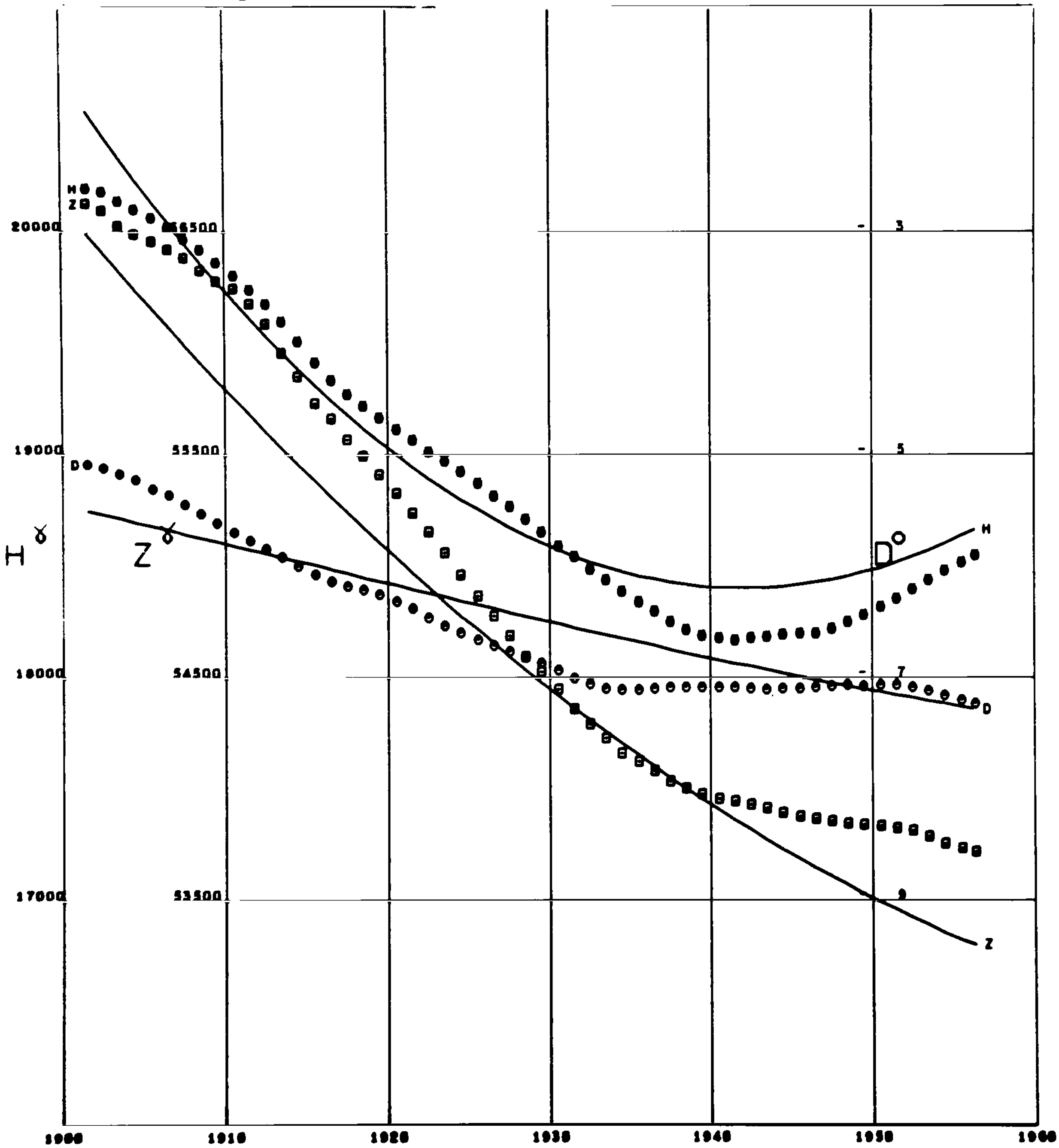

Figure A34

CHELYUSKIN
Lat 77.71 Long 104.28

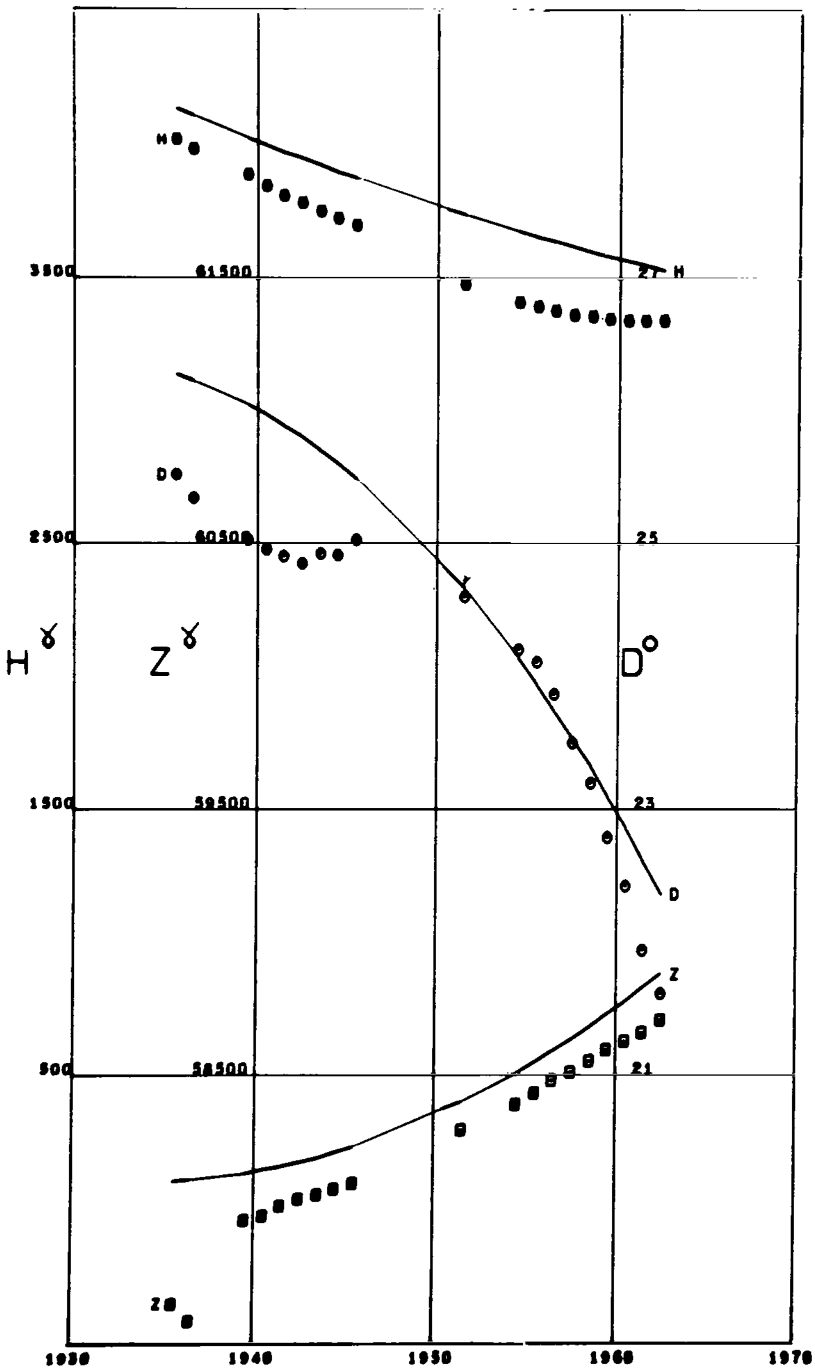

Figure A35

CHRISTCHURCH
Lat -43.53 Long 172.62

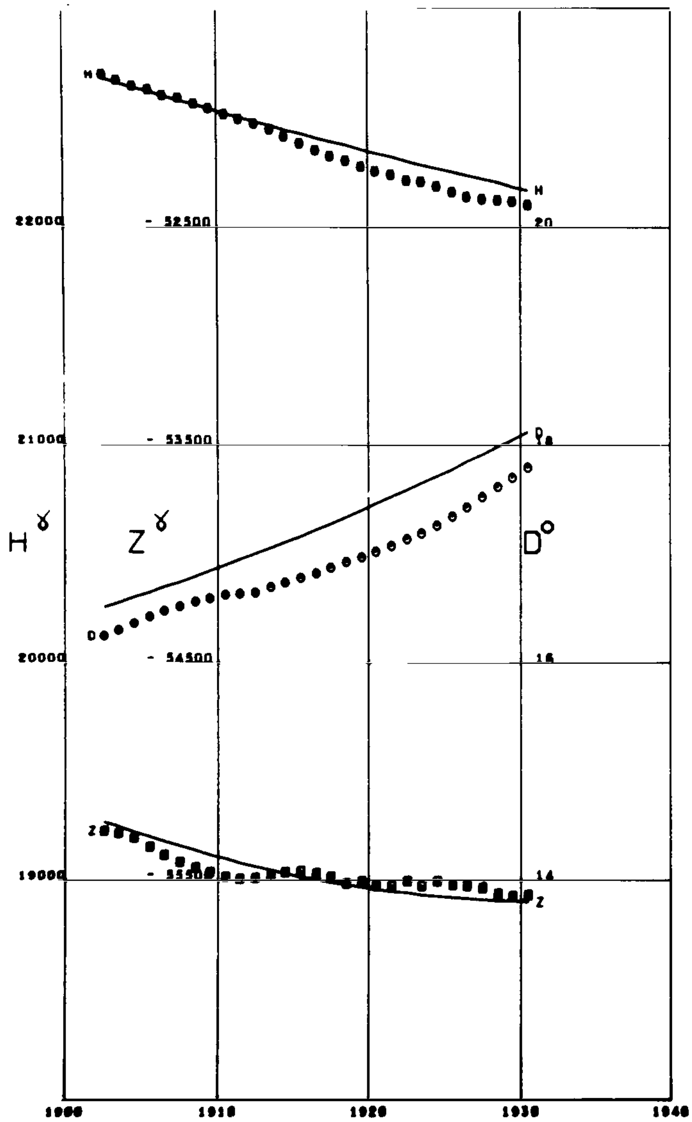

Figure A36

CLAUSTHAL
Lat 51.80 Long 10.33

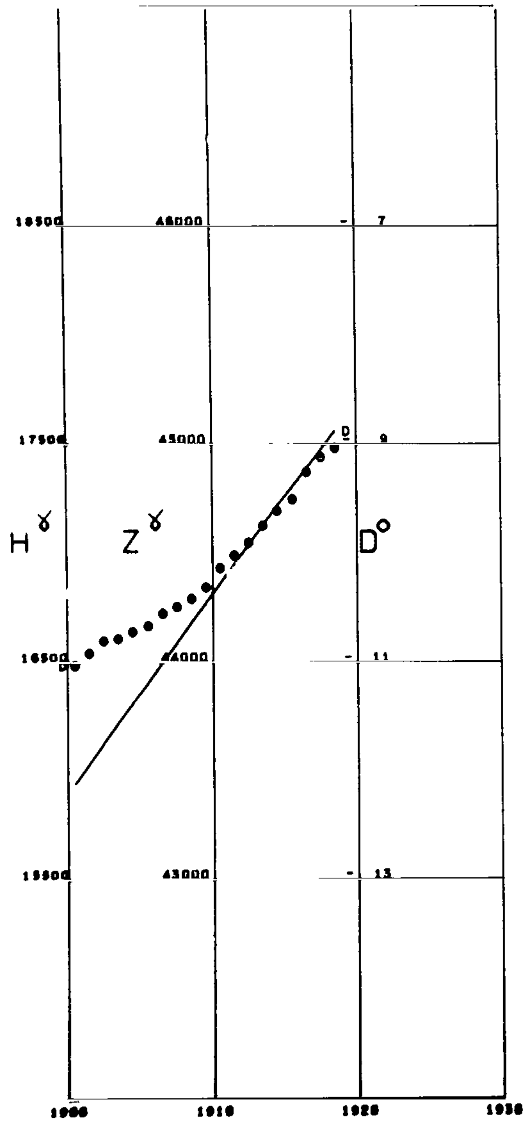

Figure A37

COIMBRA
Lat 40.22 Long -8.42

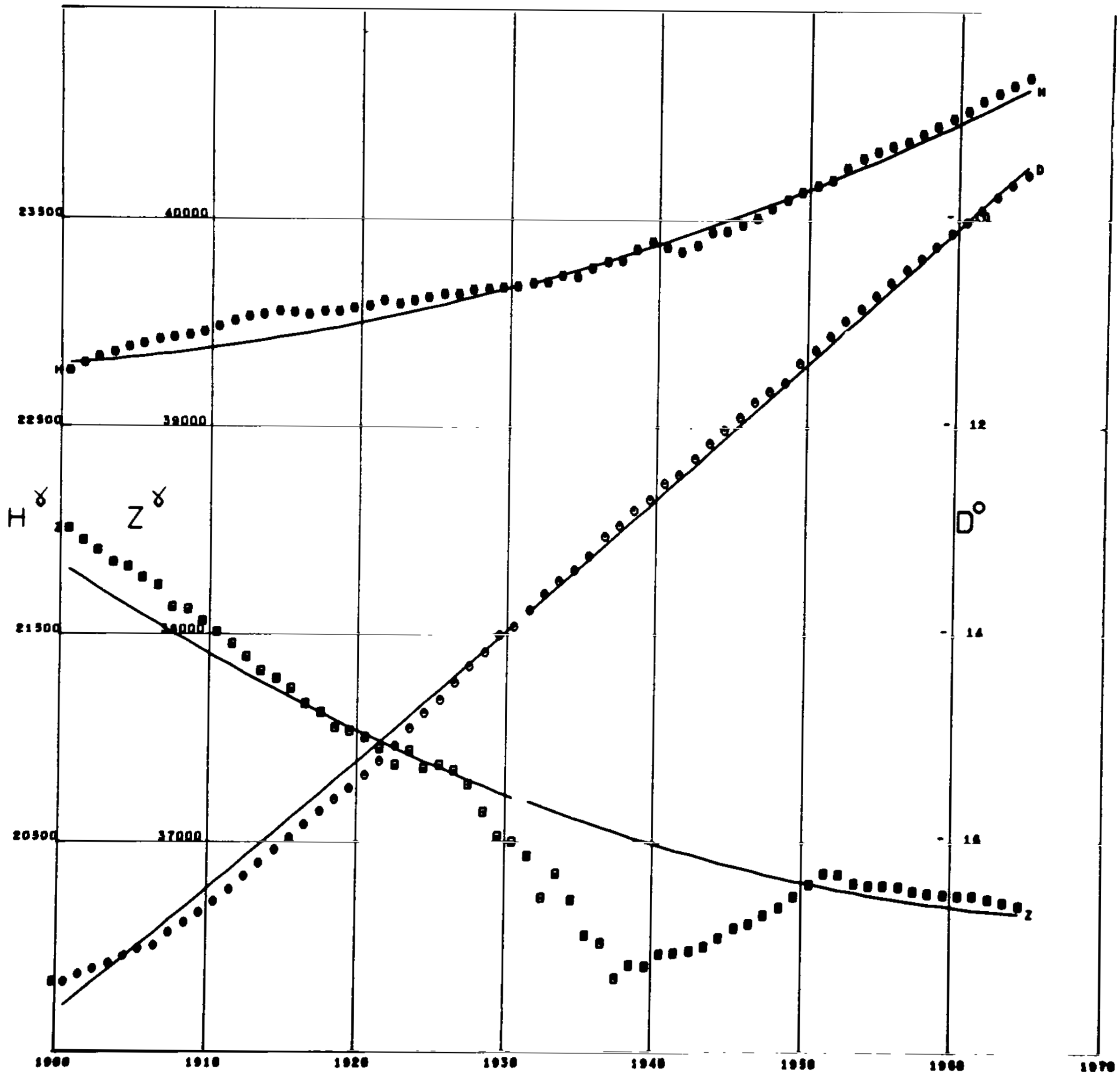

Figure A38

COLABA
Lat 18.89 Long 72.81

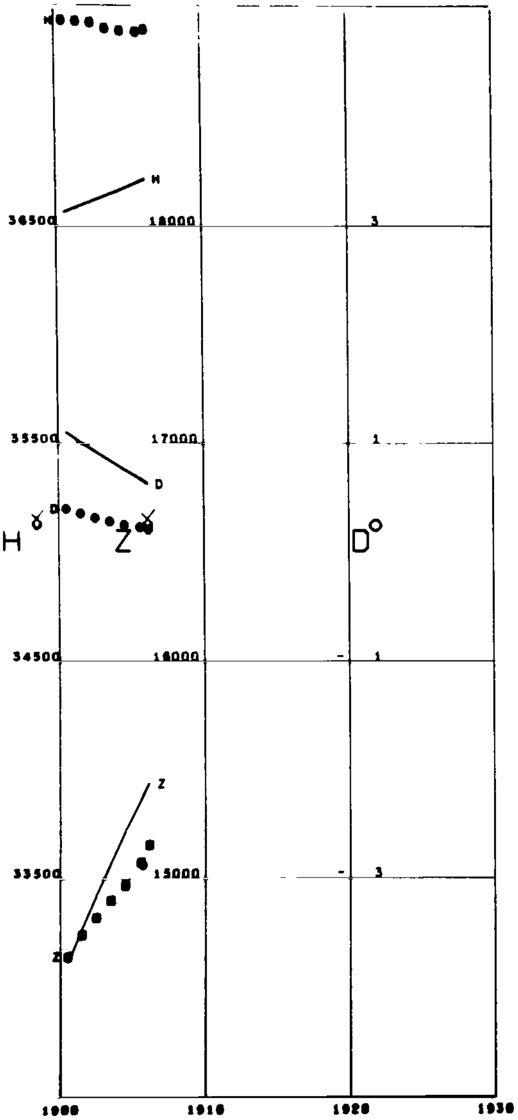

Figure A39

COLLEGE
Lat 64.86 Long -147.83 Alt 0.20

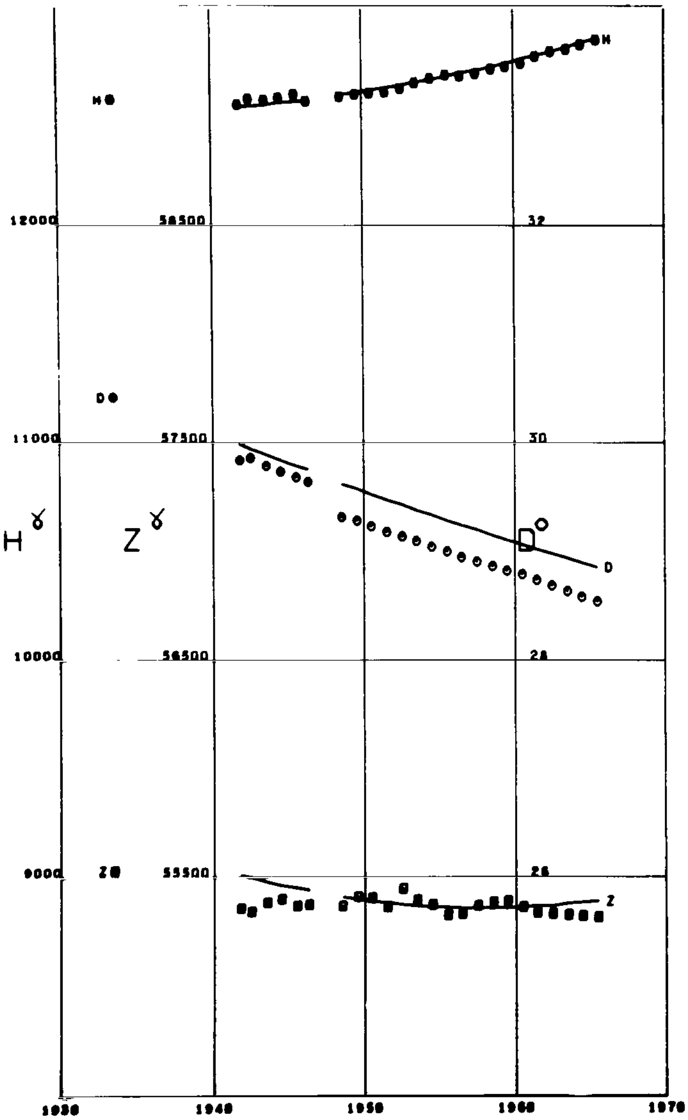

Figure A40

CRACOW
Lat 50.05 Long 19.95

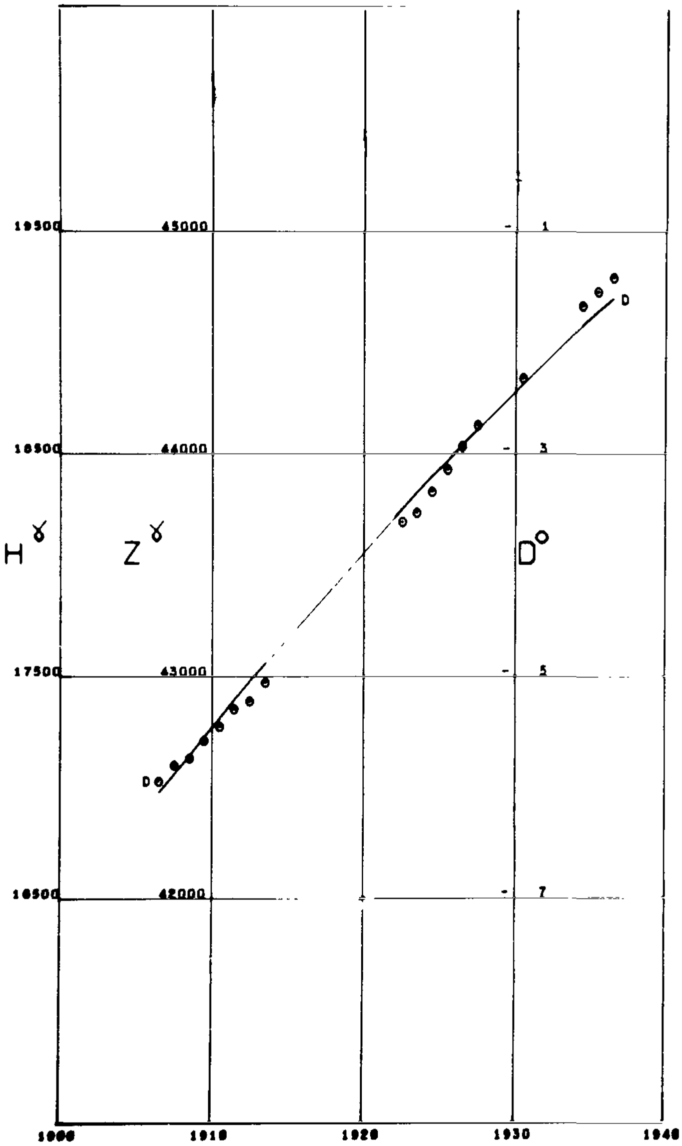

Figure A41

CUAJIMALPA
Lat 19.37 Long -99.28

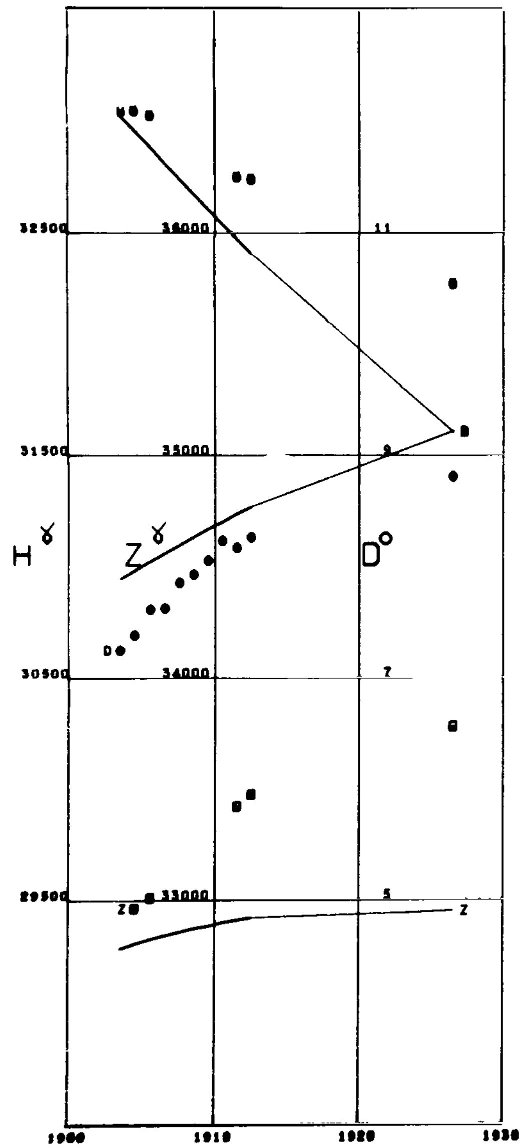

Figure A42

DE BILT
Lat 52.10 Long 5.17

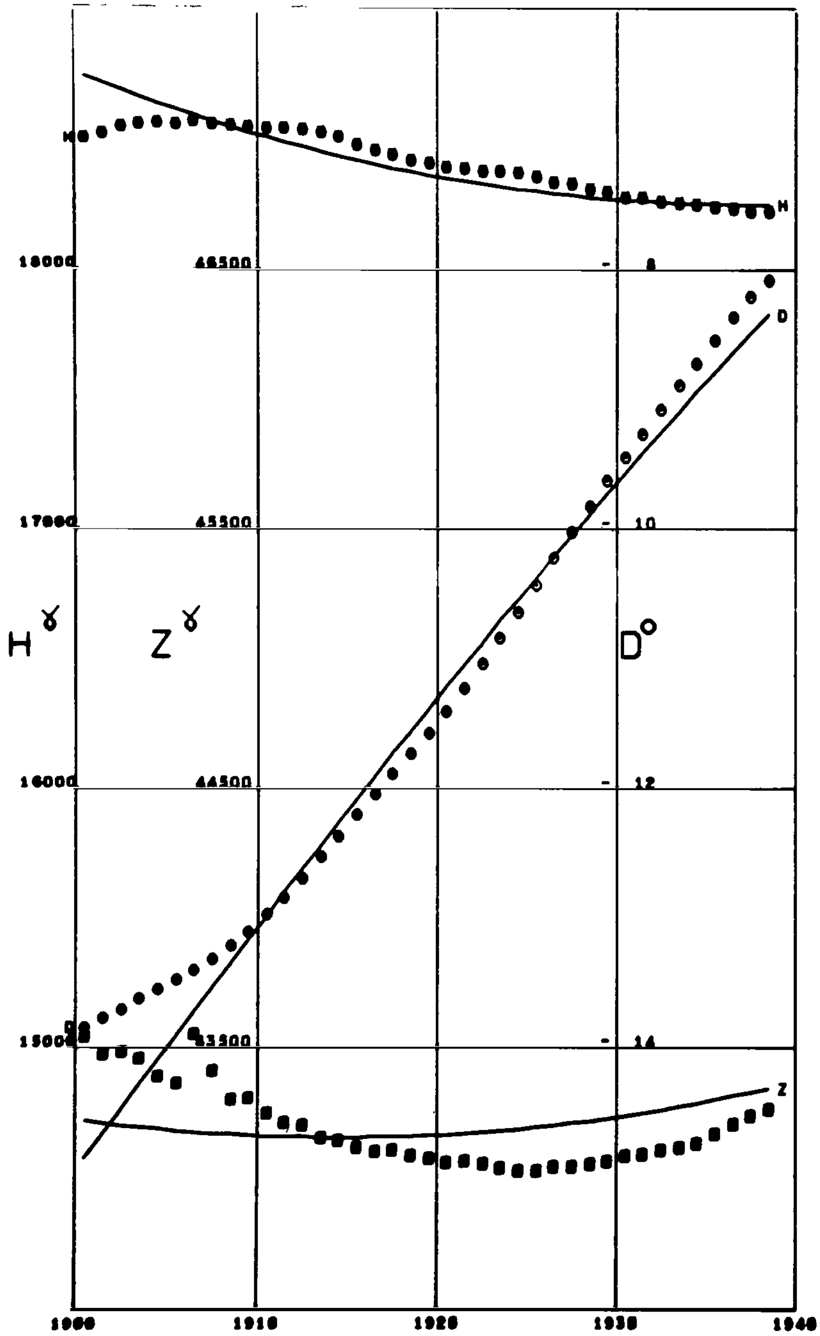

Figure A43

DEHRA DUN
Lat 30.32 Long 78.05

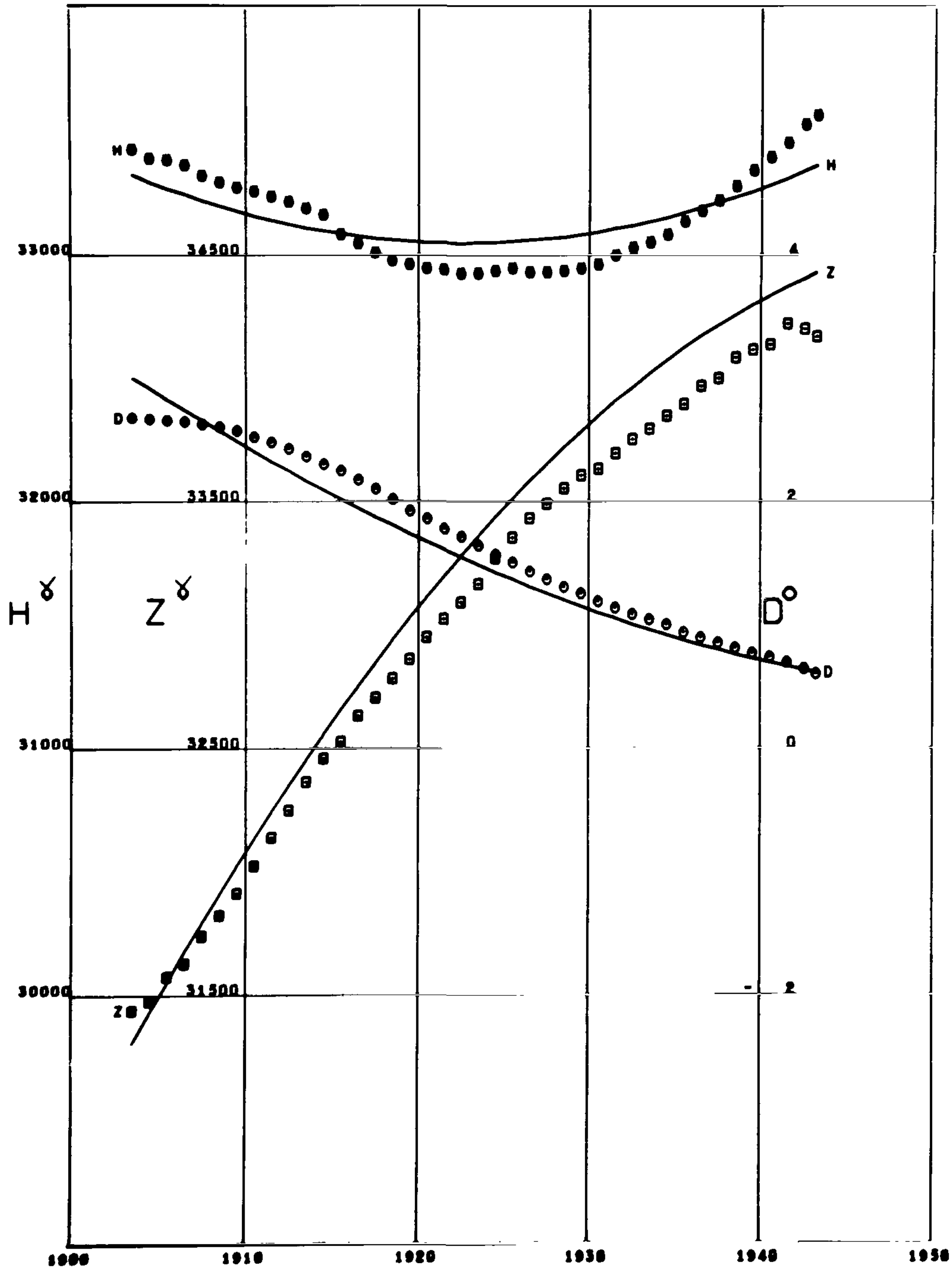

Figure A44

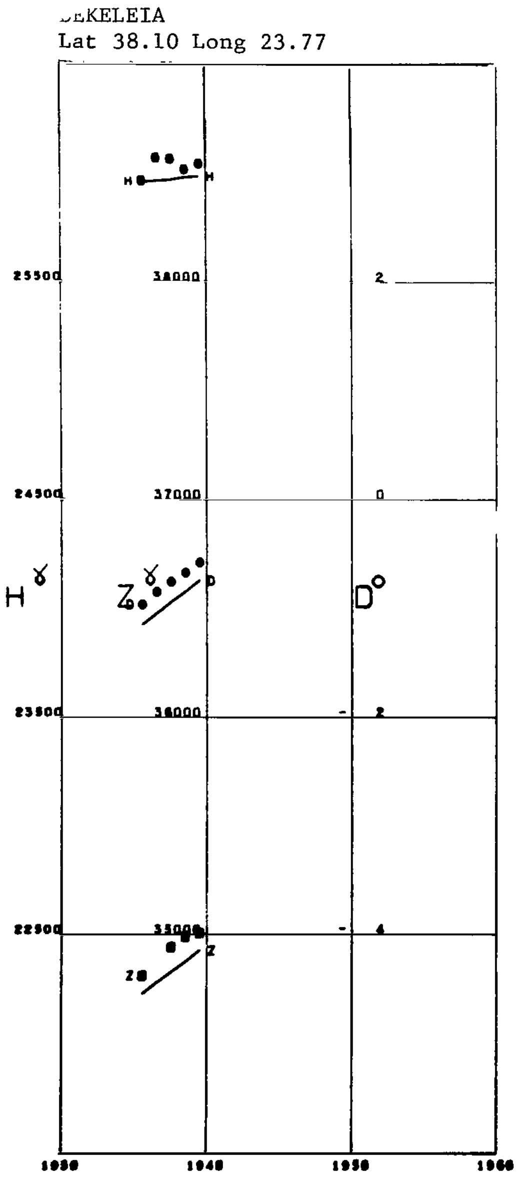

Figure A45

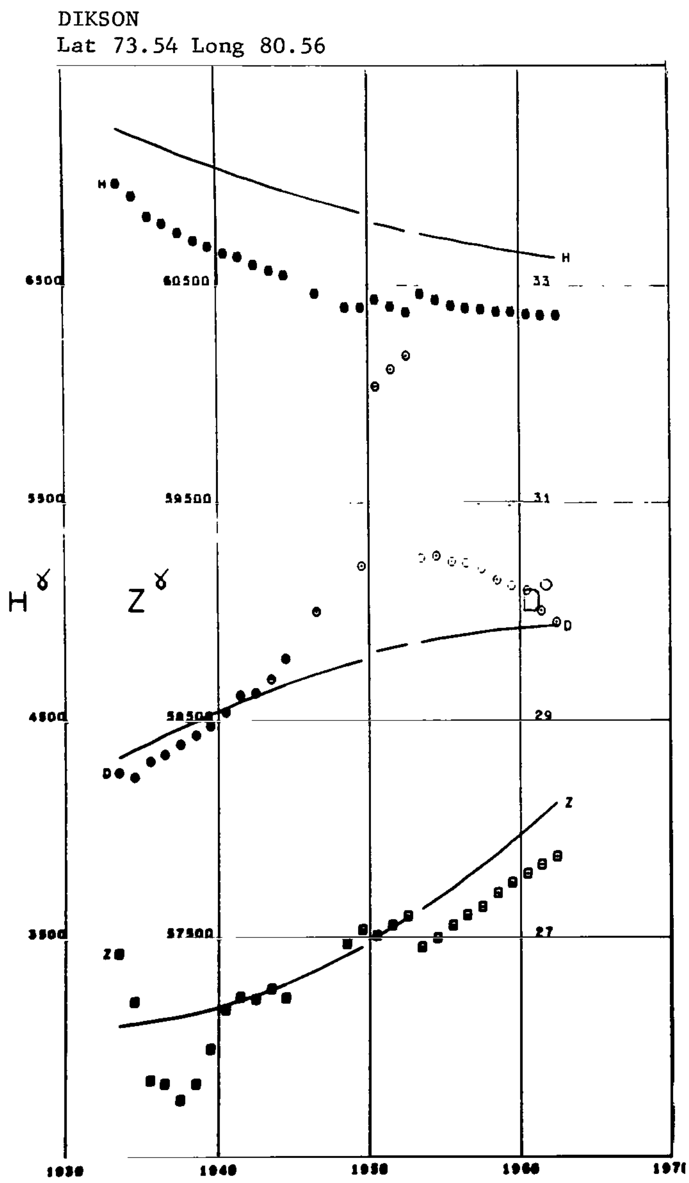

Figure A46

DOMBAS
Lat 62.07 Long 9.11

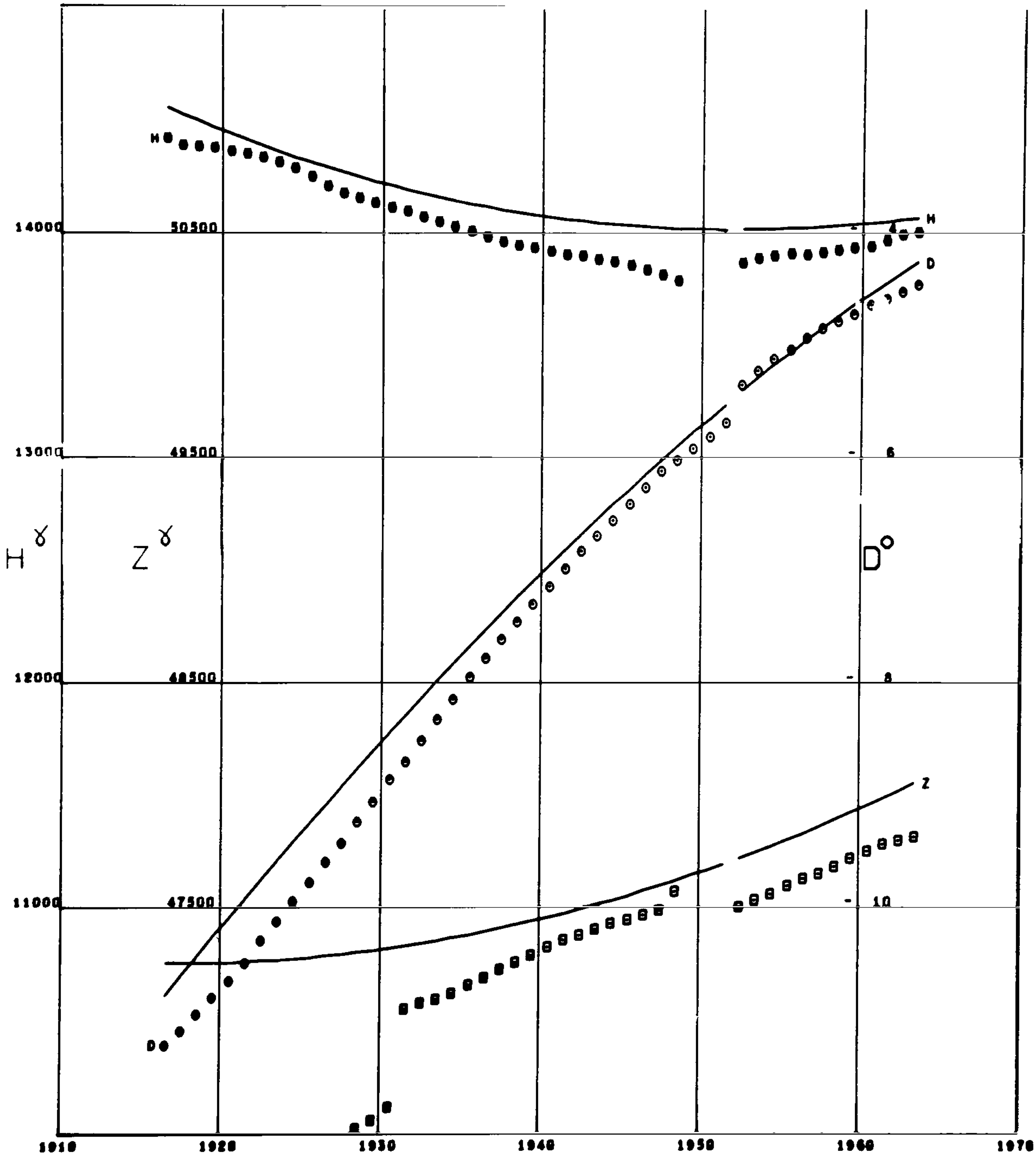

Figure A47

DOURBES
Lat 50.09 Long 4.59

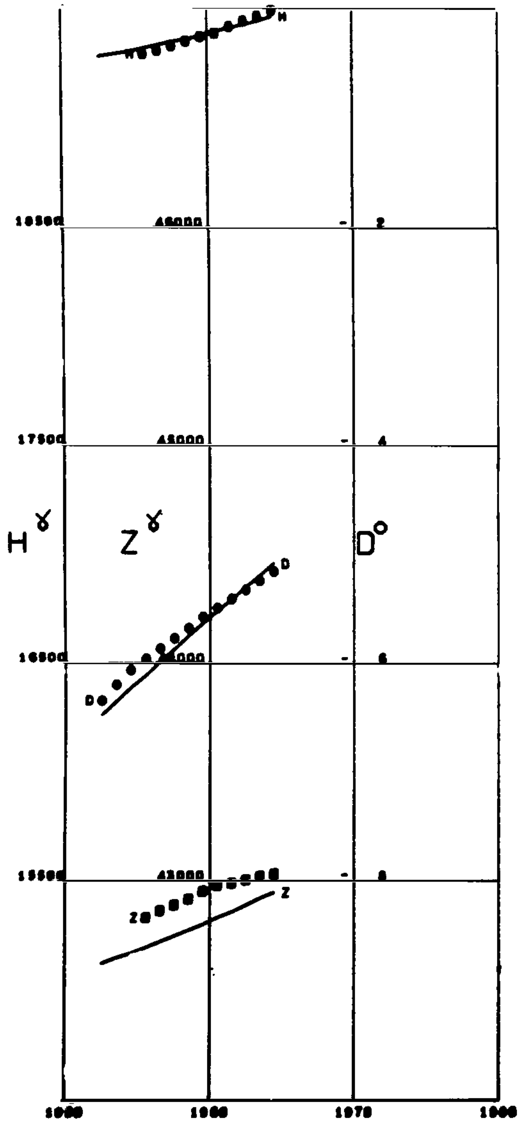

Figure A48

DUSHETI
Lat 42.09 Long 44.70

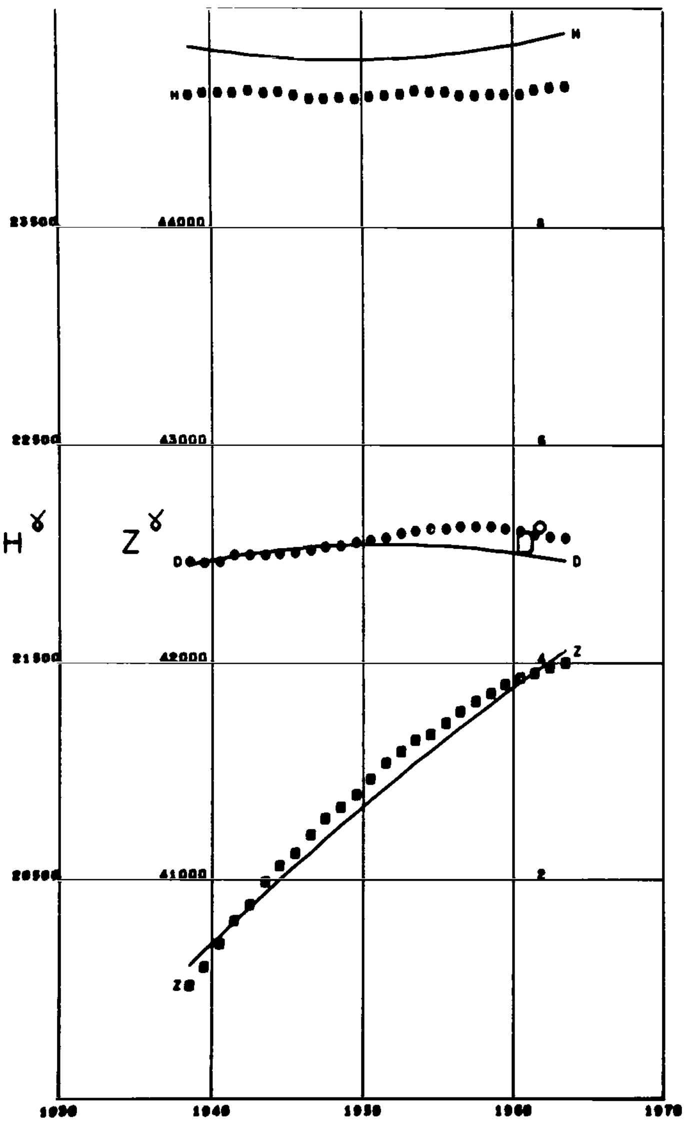

Figure A49

EBRO
Lat 40 [illegible]2 Long 0.49 Alt 0.05

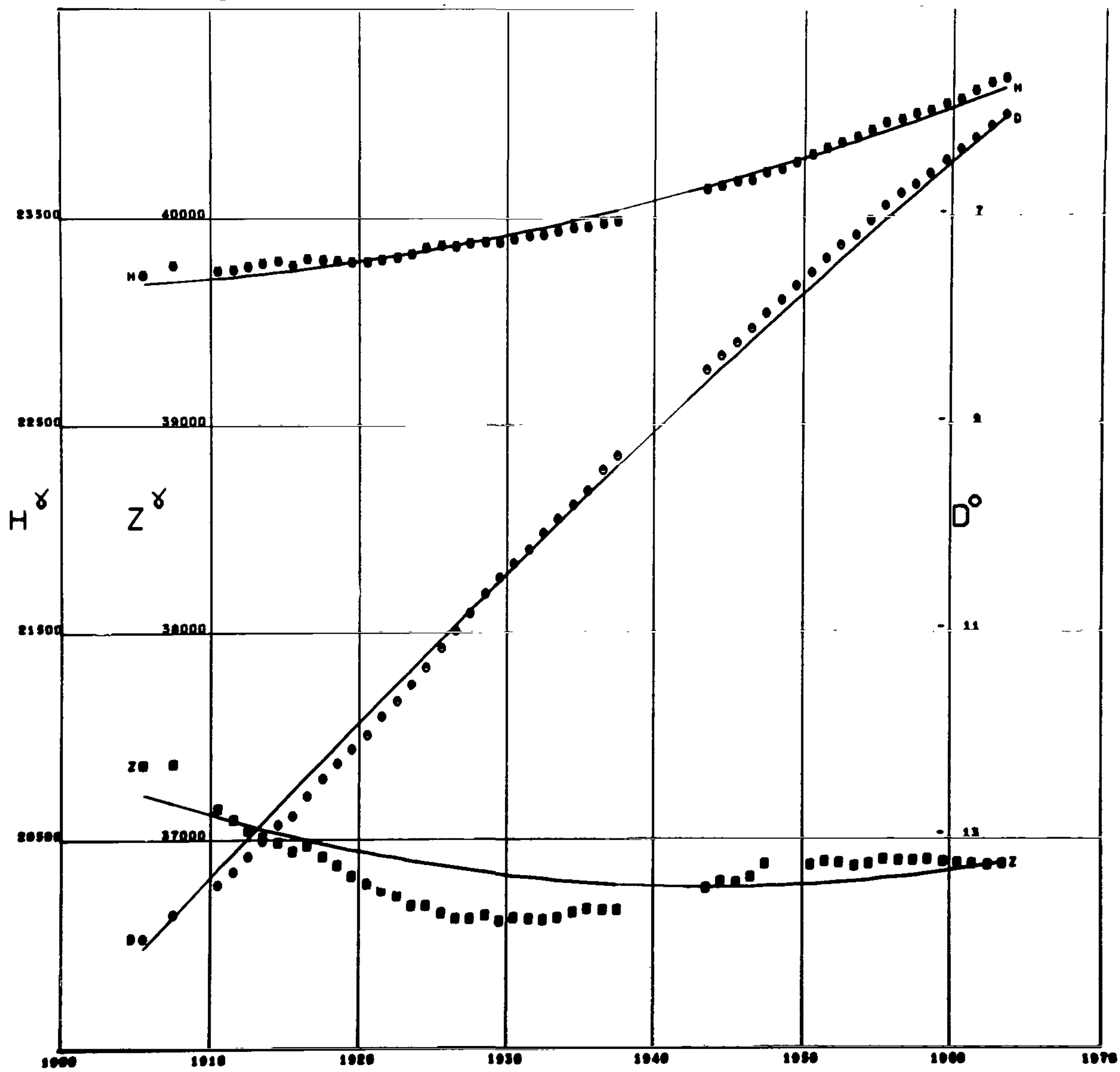

Figure A50

EL ABIOD SIDI
Lat 32.90 Long 0.55

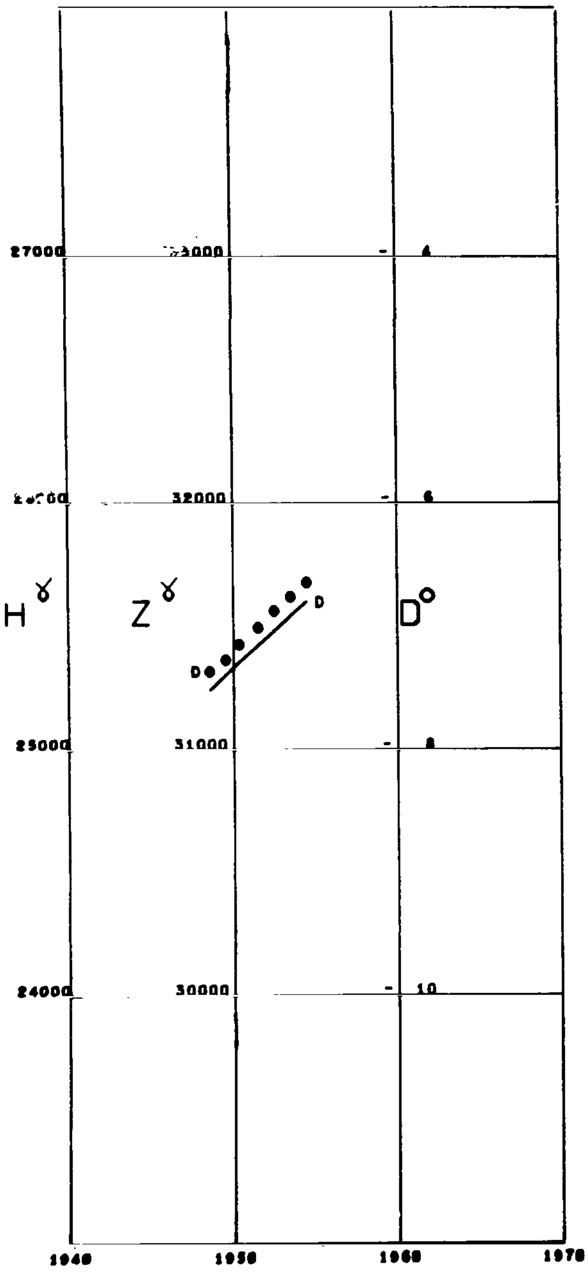

Figure A51

ELISABETHVILLE
Lat -11.65 Long 27.46

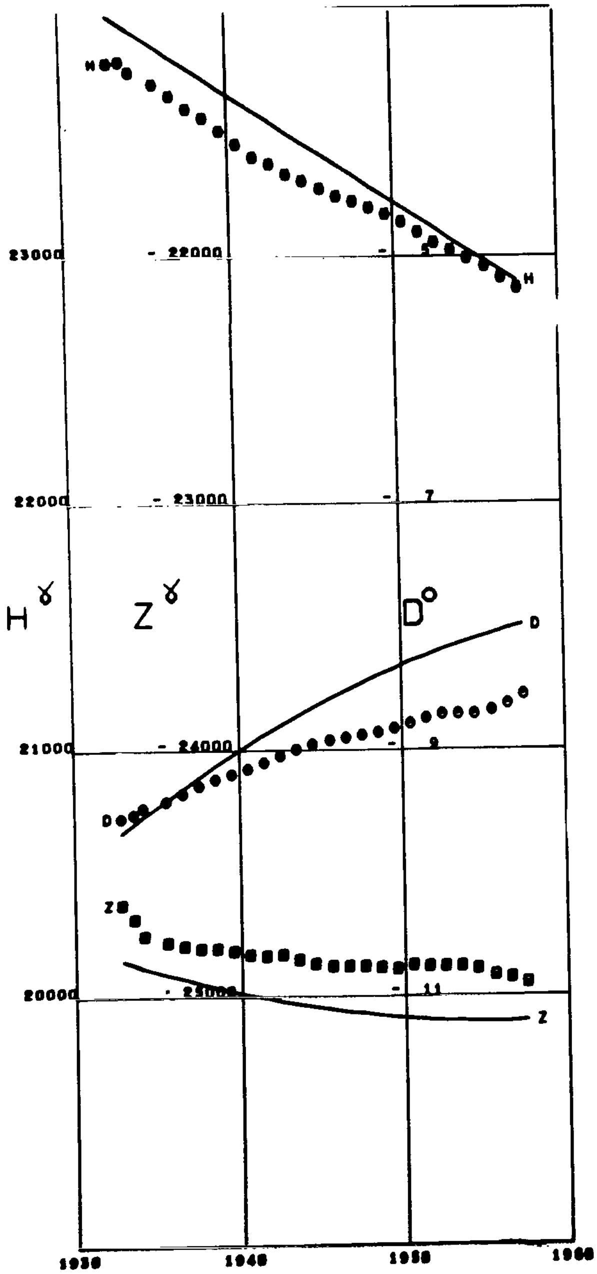

Figure A52

ESKDALEMUIR
Lat 55.31 Long -3.20

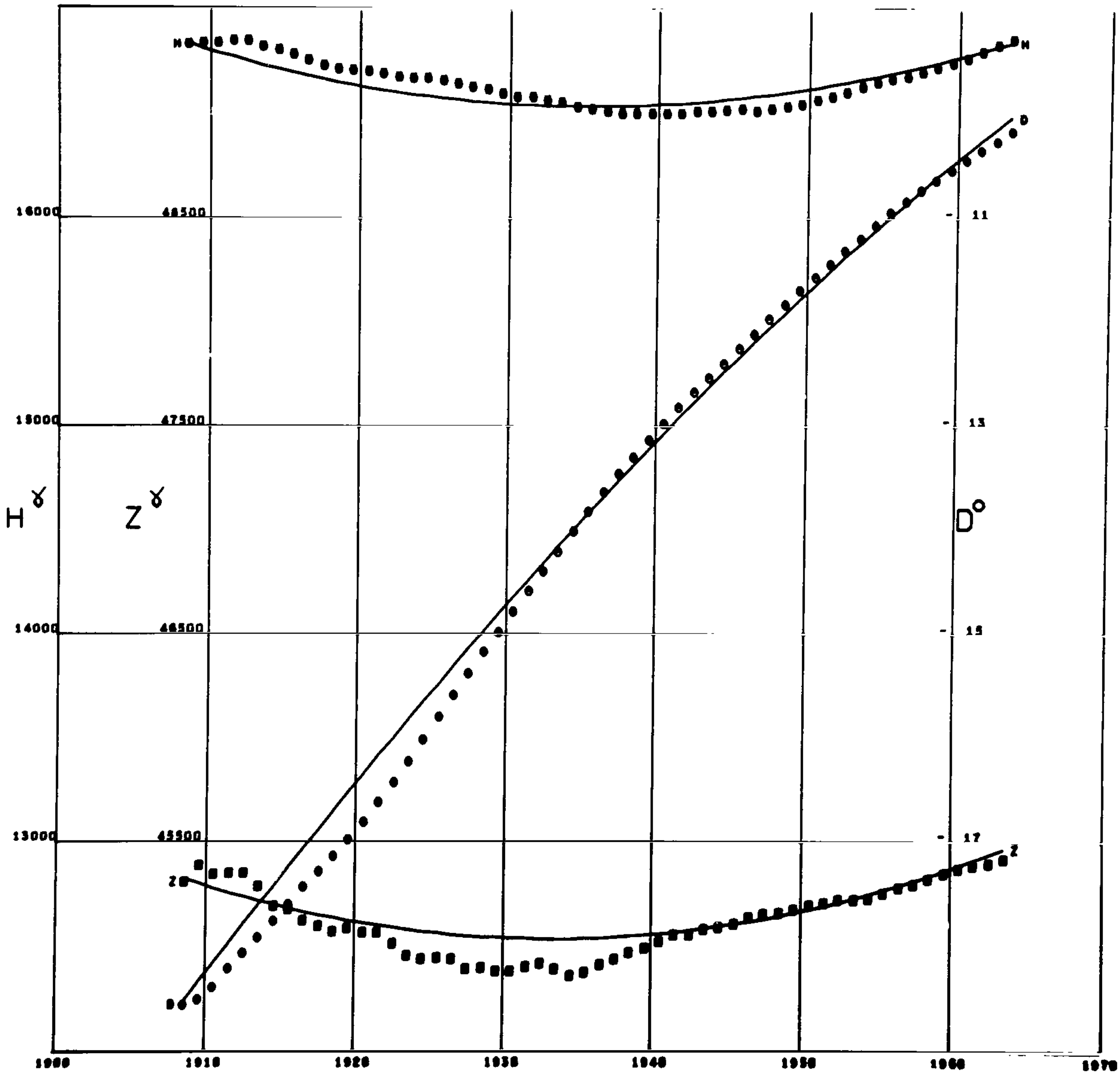

Figure A53

FALMOUTH
Lat 50.15 Long -5.07

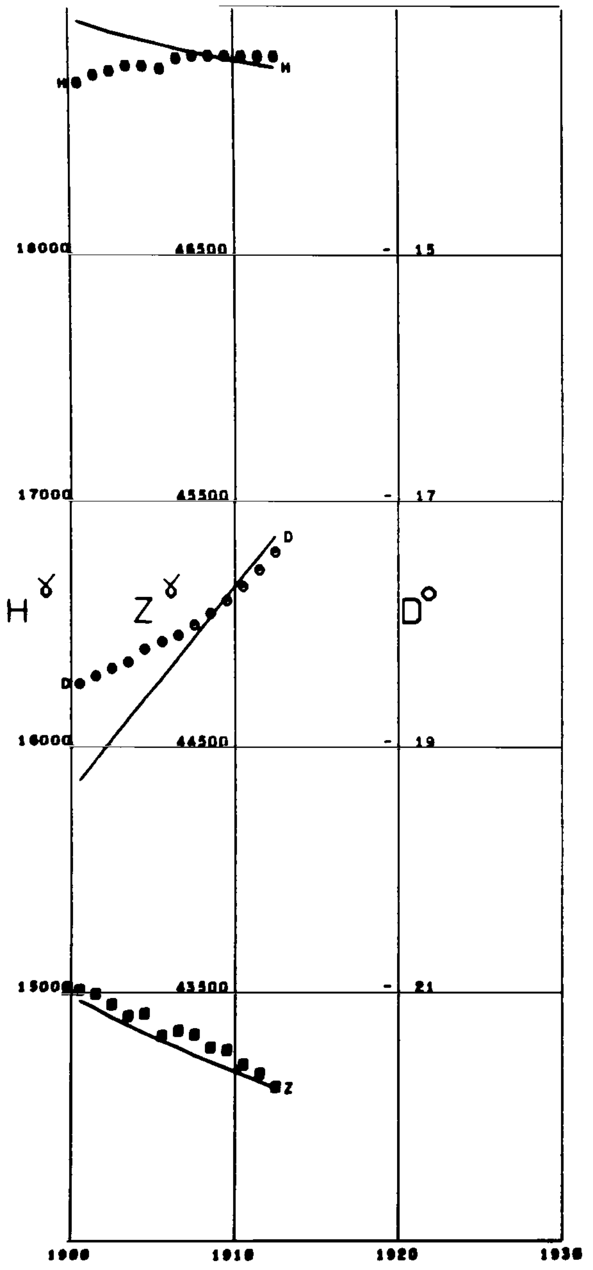

Figure A54

FREDERICKSBURG
Lat 38.20 Long -77.37 Alt 0.07

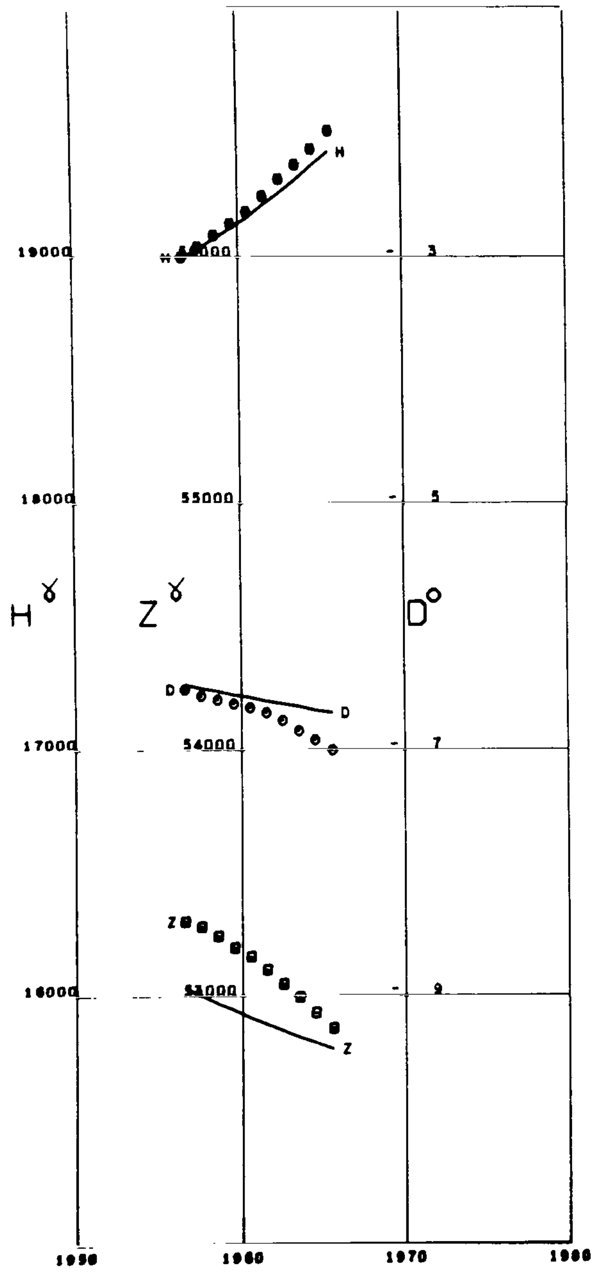

Figure A55

FUQUENE
Lat 5.47 Long -73.73 Alt 2.54

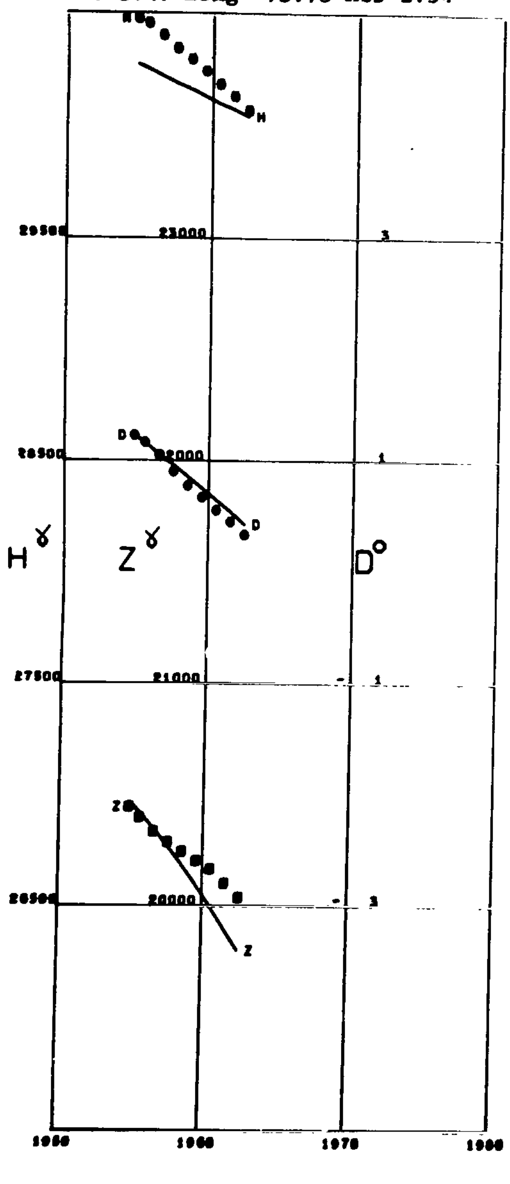

Figure A56

FURSTENFELDBRUCK
Lat 48.16 Long 11.27 Alt 0.57

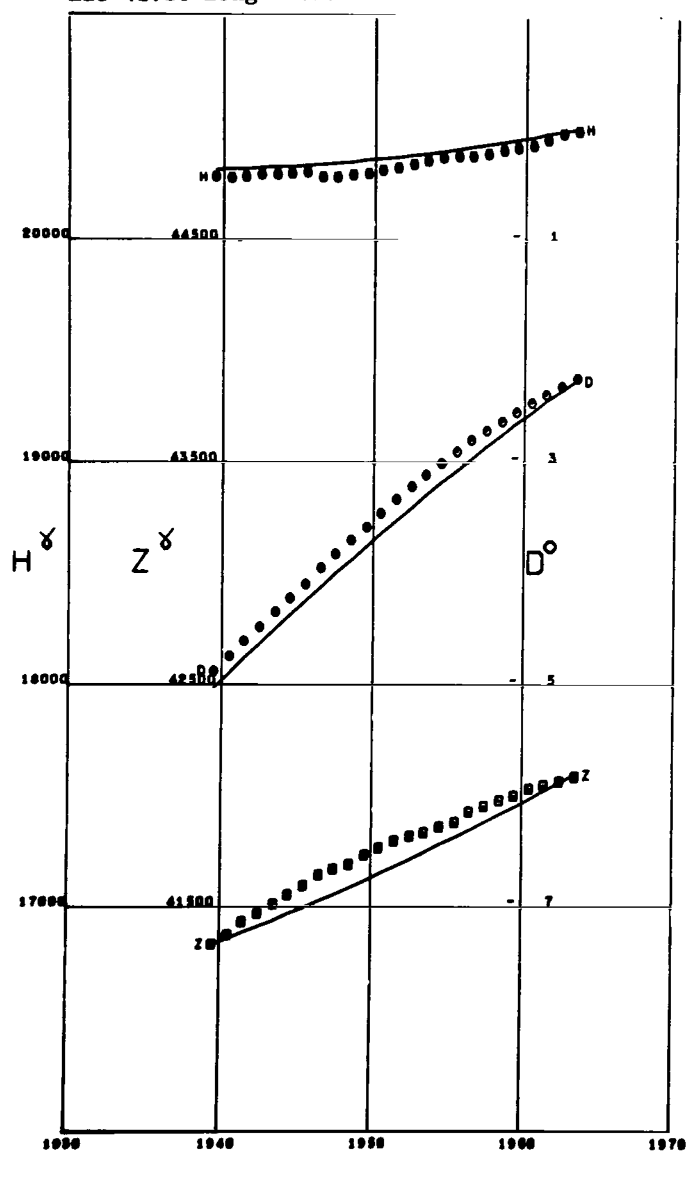

Figure A57

GNANGARA
Lat -31.78 Long 115.95 Alt 0.06

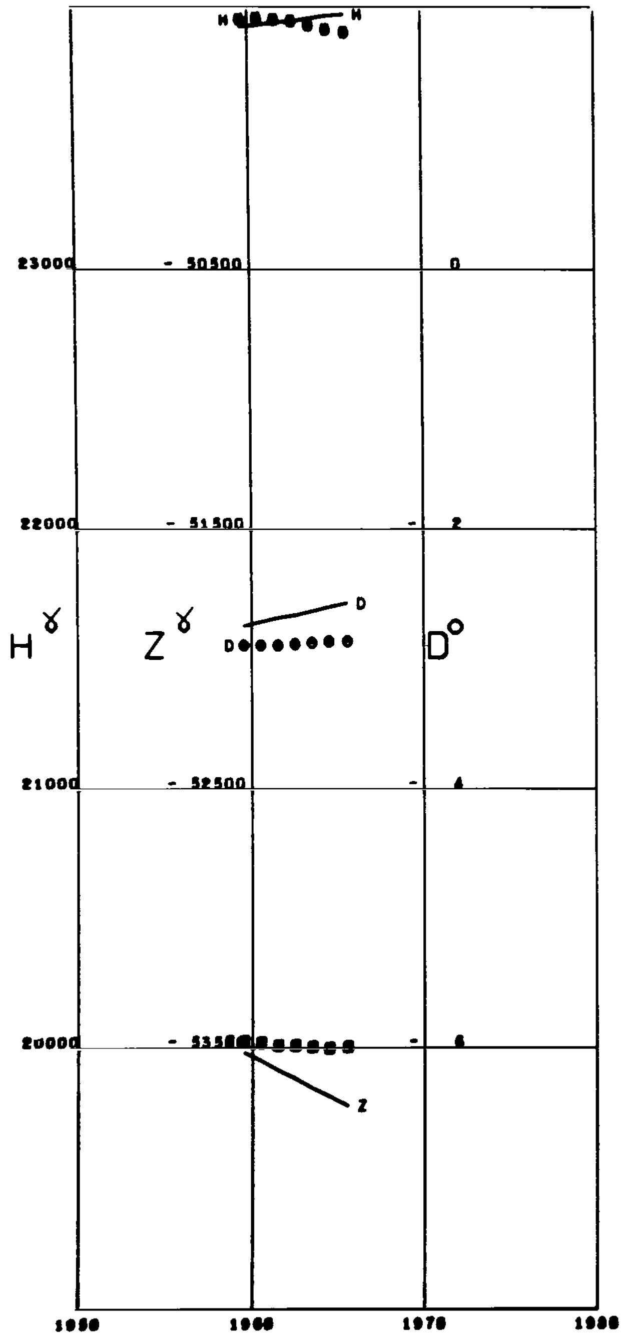

Figure A58

GODHAVN
Lat 69.24 Long -53.52 Alt 0.01

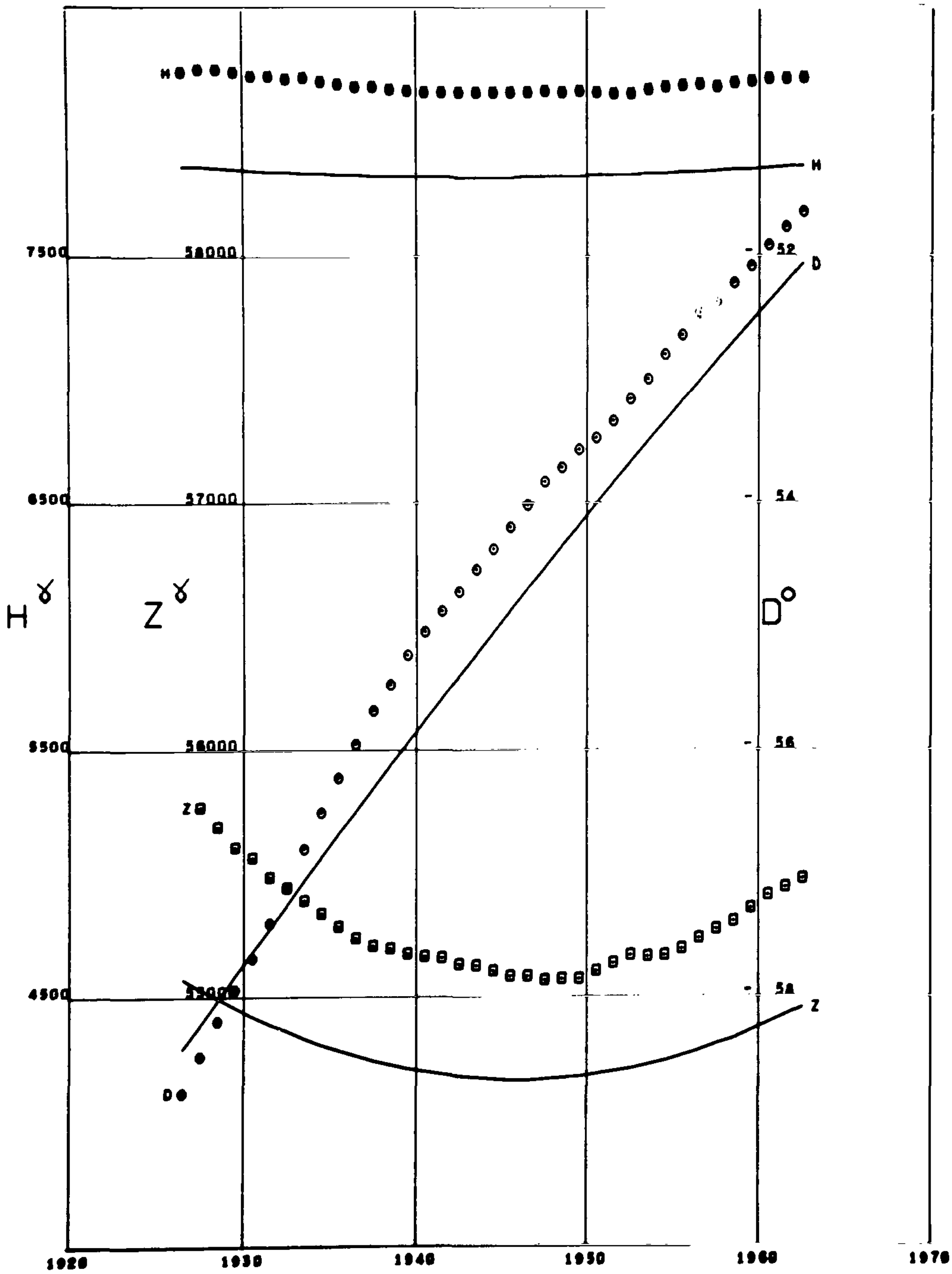

Figure A59

GORNOTAYEZHNAYA
Lat 43.68 Long 132.16

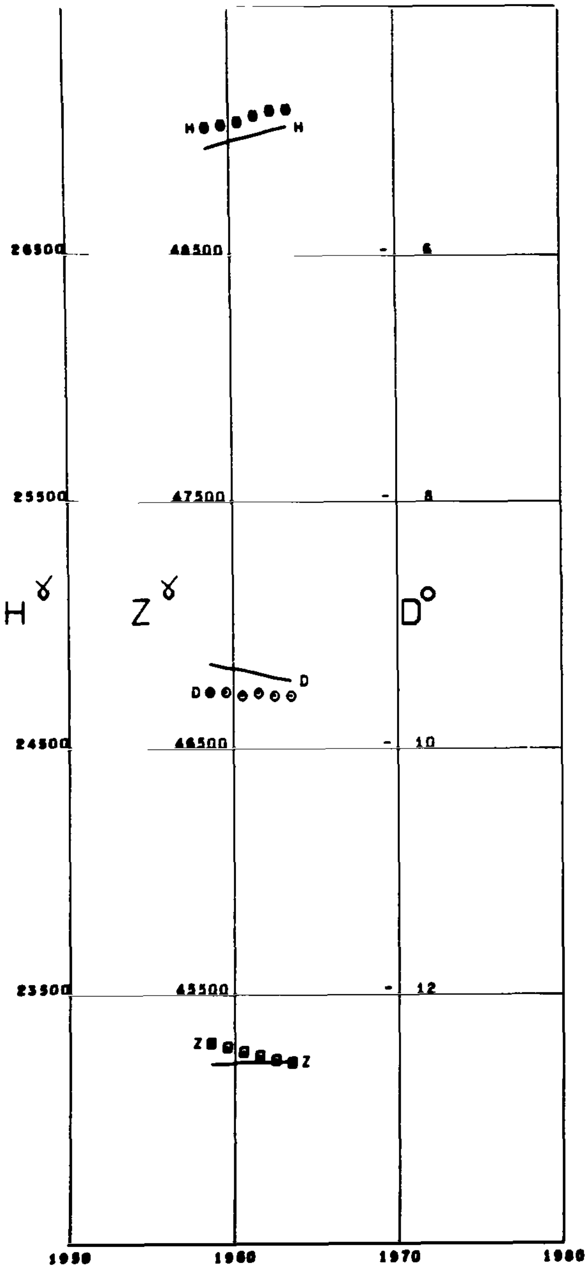

Figure A60

GREENWICH
Lat 51.47 Long 0.00

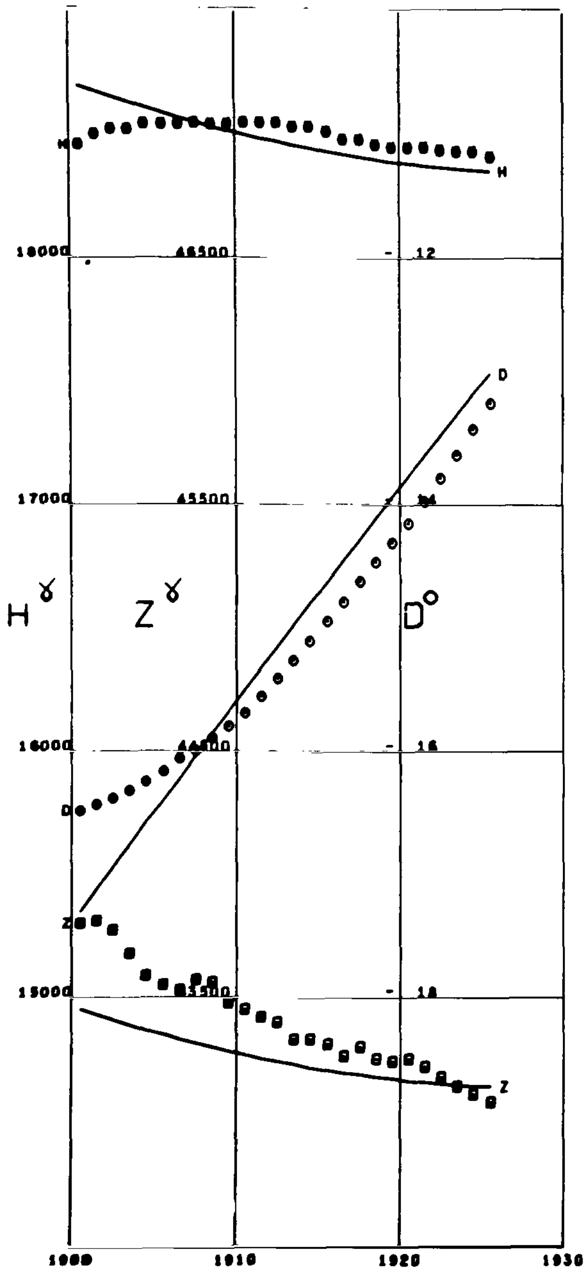

Figure A61

GROCKA
Lat 44.63 Long 20.76

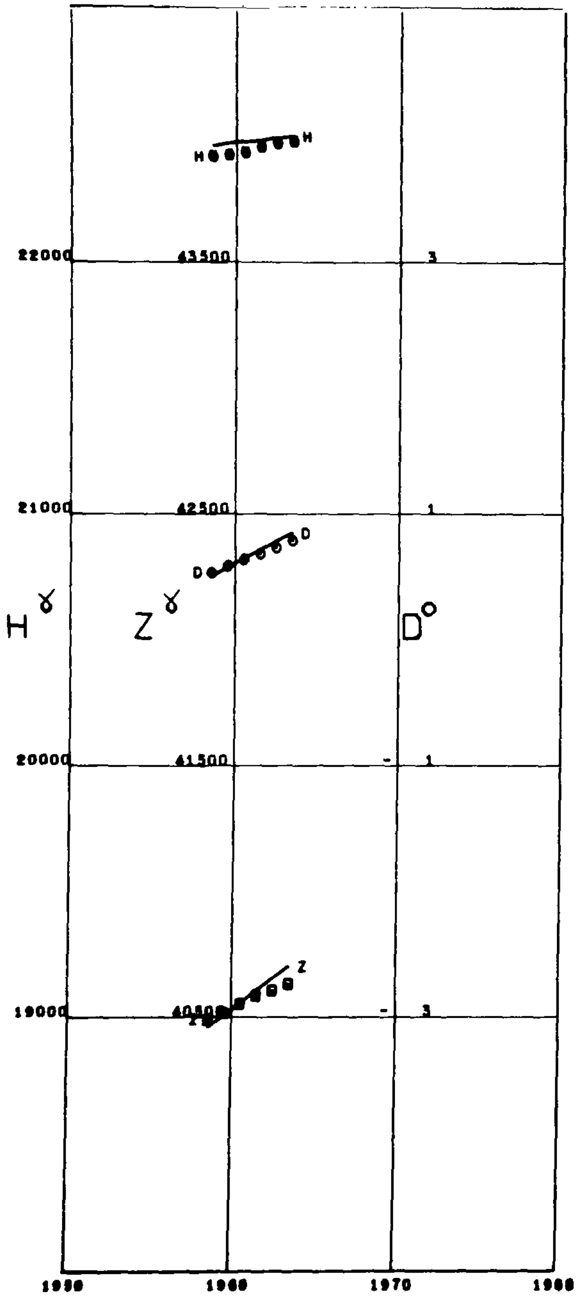

Figure A62

GUAM
Lat 13.58 Long 144.87 Alt 0.15

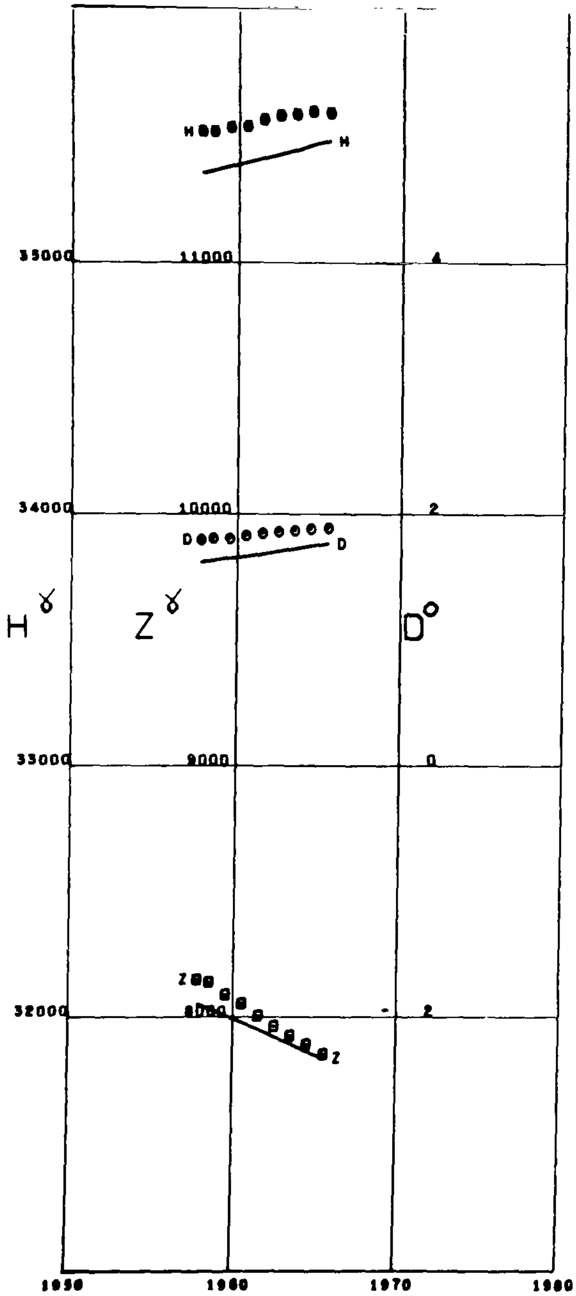

Figure A63

HALLETT STATION
Lat -72.31 Long 170.21

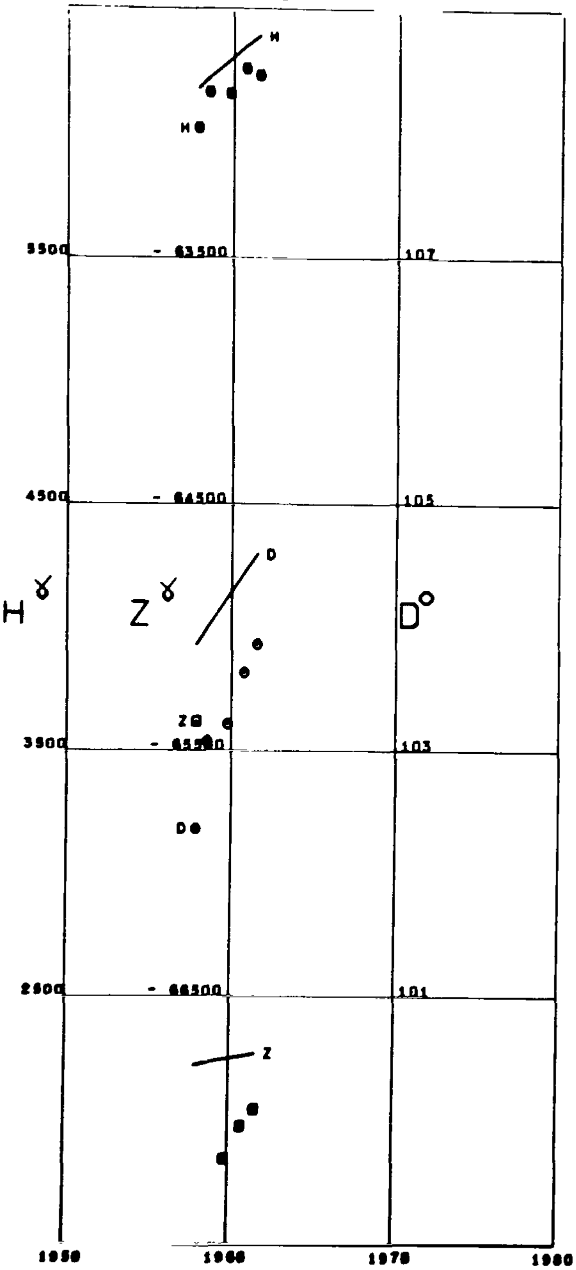

Figure A64

HARTLAND
Lat 50.99 Long -4.48 Alt 0.09

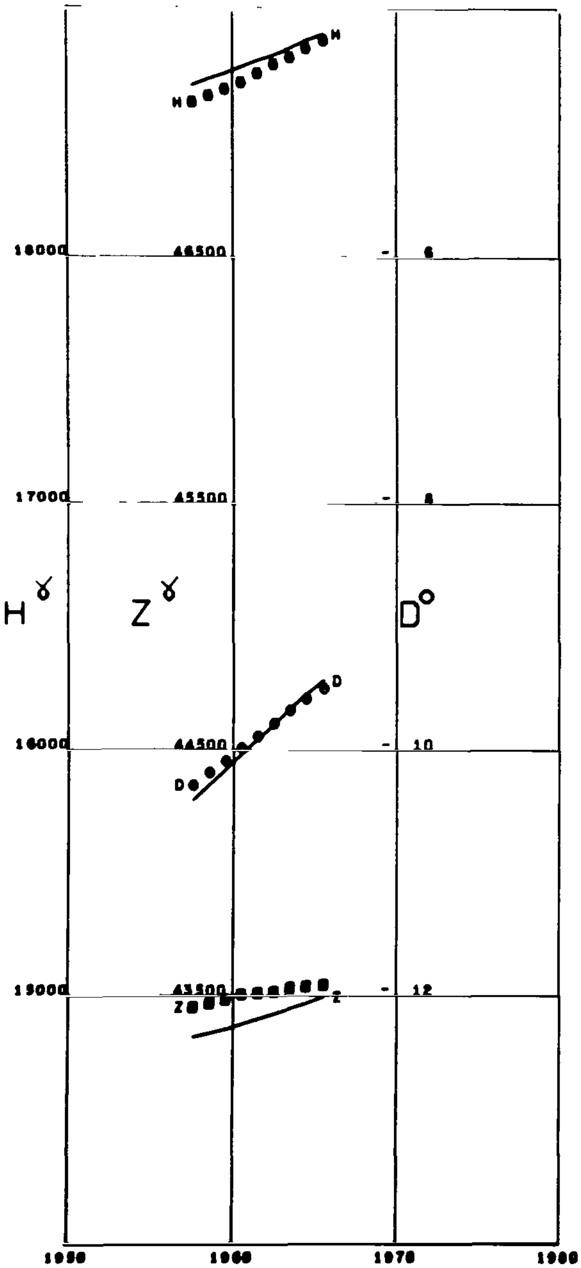

Figure A65

HEARD ISLAND
Lat -53.03 Long 73.36

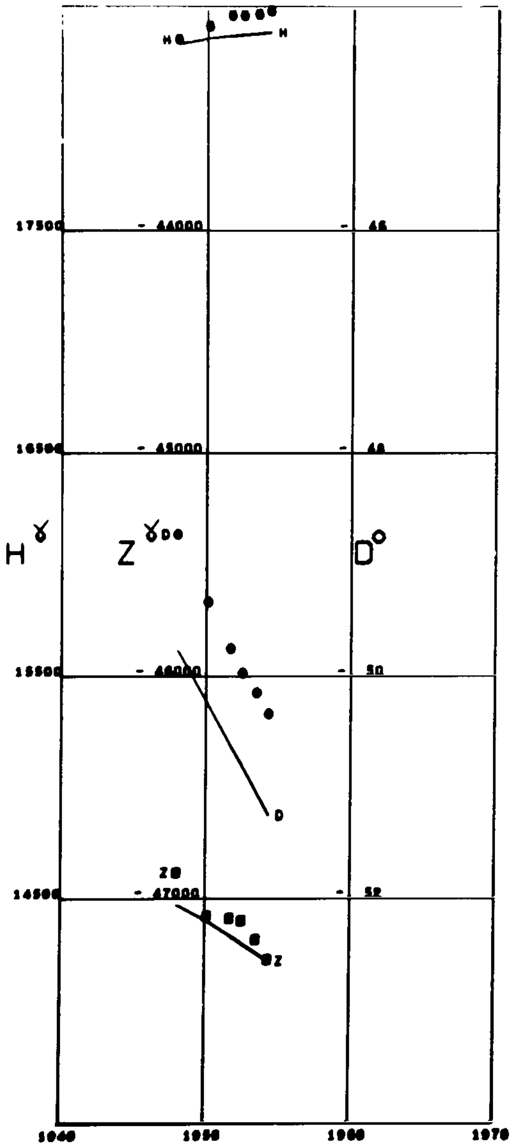

Figure A66

HEL
Lat 54.60 Long 18.81

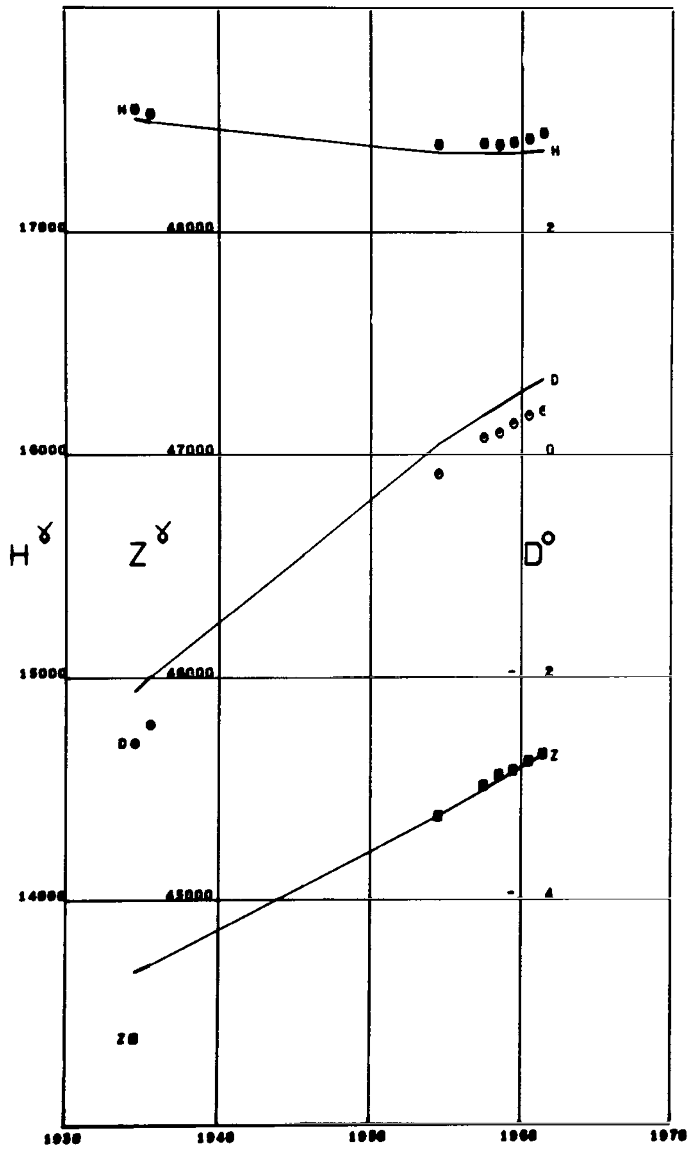

Figure A67

HELWAN
Lat 29.85 Long 31.34

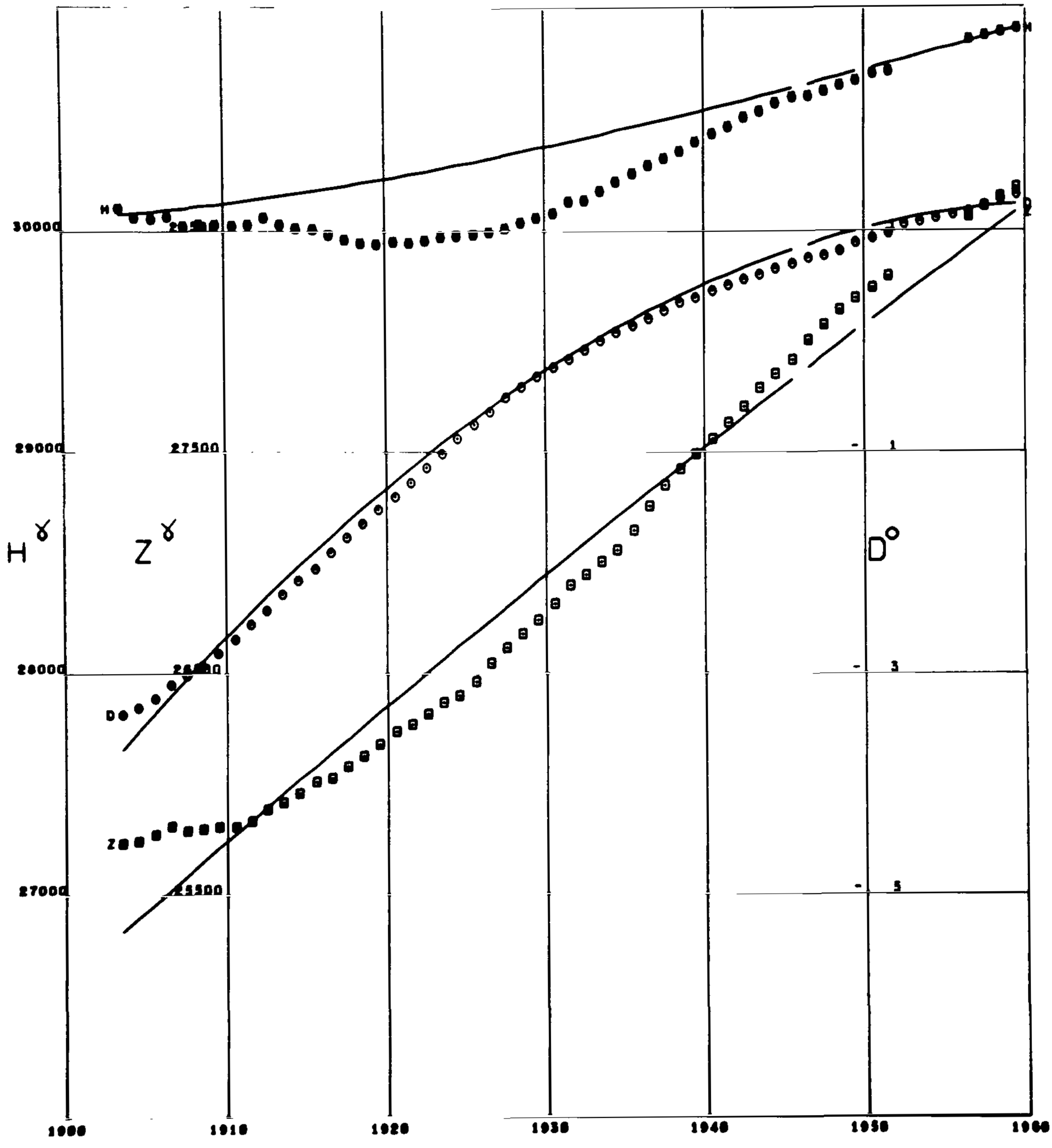

Figure A68

HERMANUS
Lat -34.42 Long 19.22 Alt 0.02

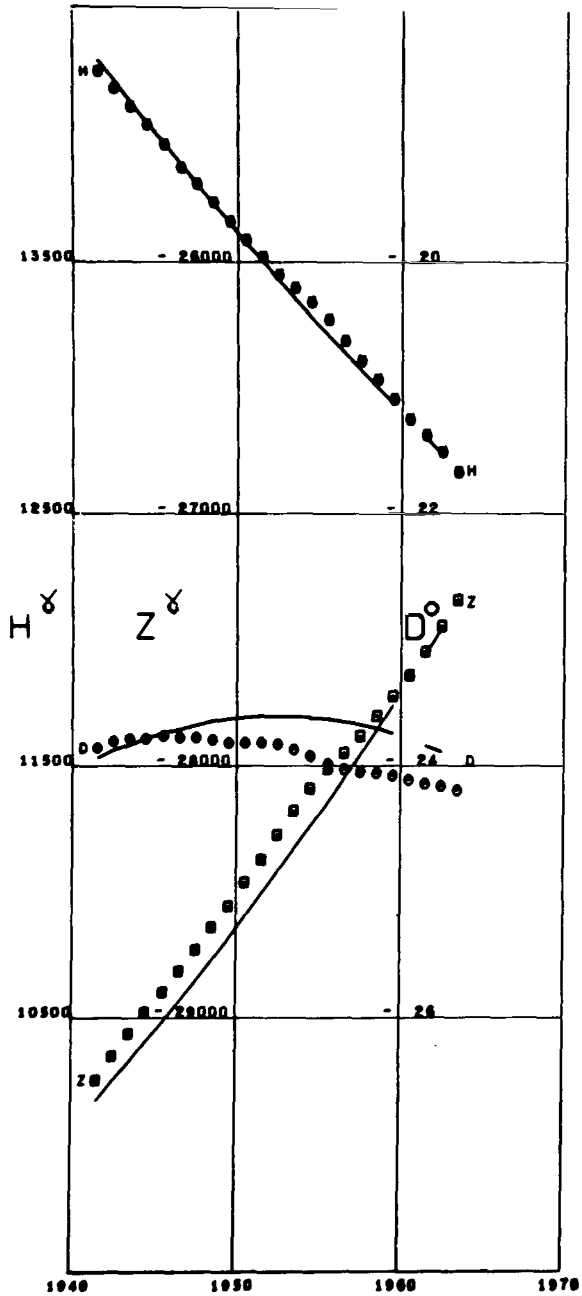

Figure A69

HERMSDORF
Lat 50.76 Long 16.23

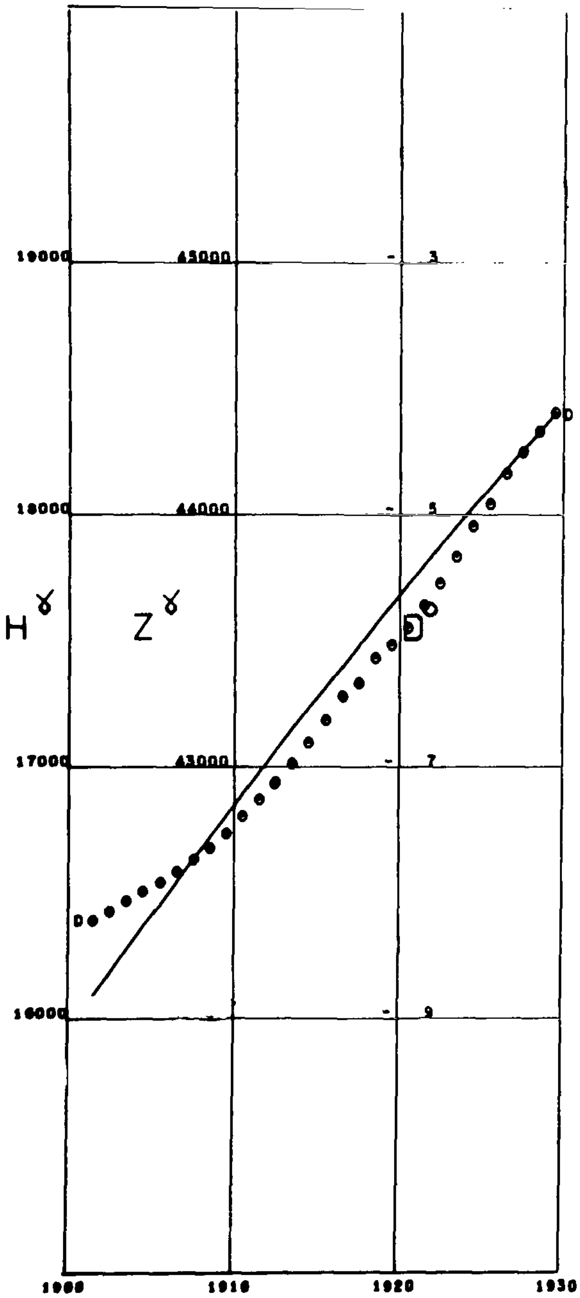

Figure A70

HOLLANDIA
Lat -2.57 Long 140.51

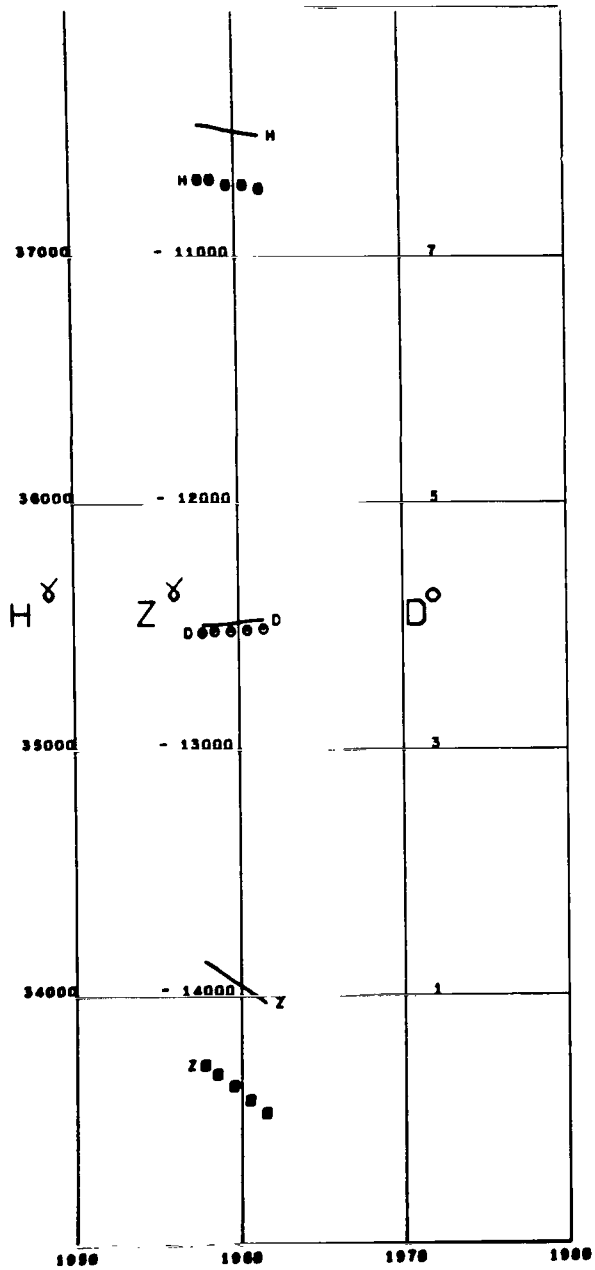

Figure A71

HONGKONG
Lat 22.30 Long 114.17

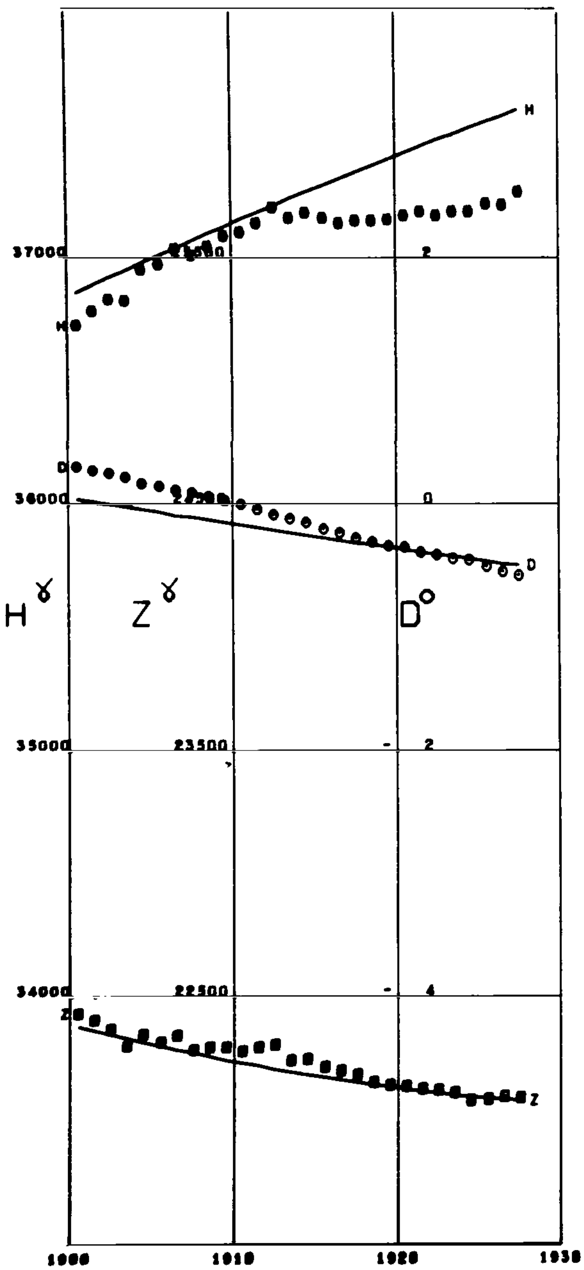

Figure A72

HONOLULU
Lat 21.32 Long -158.00

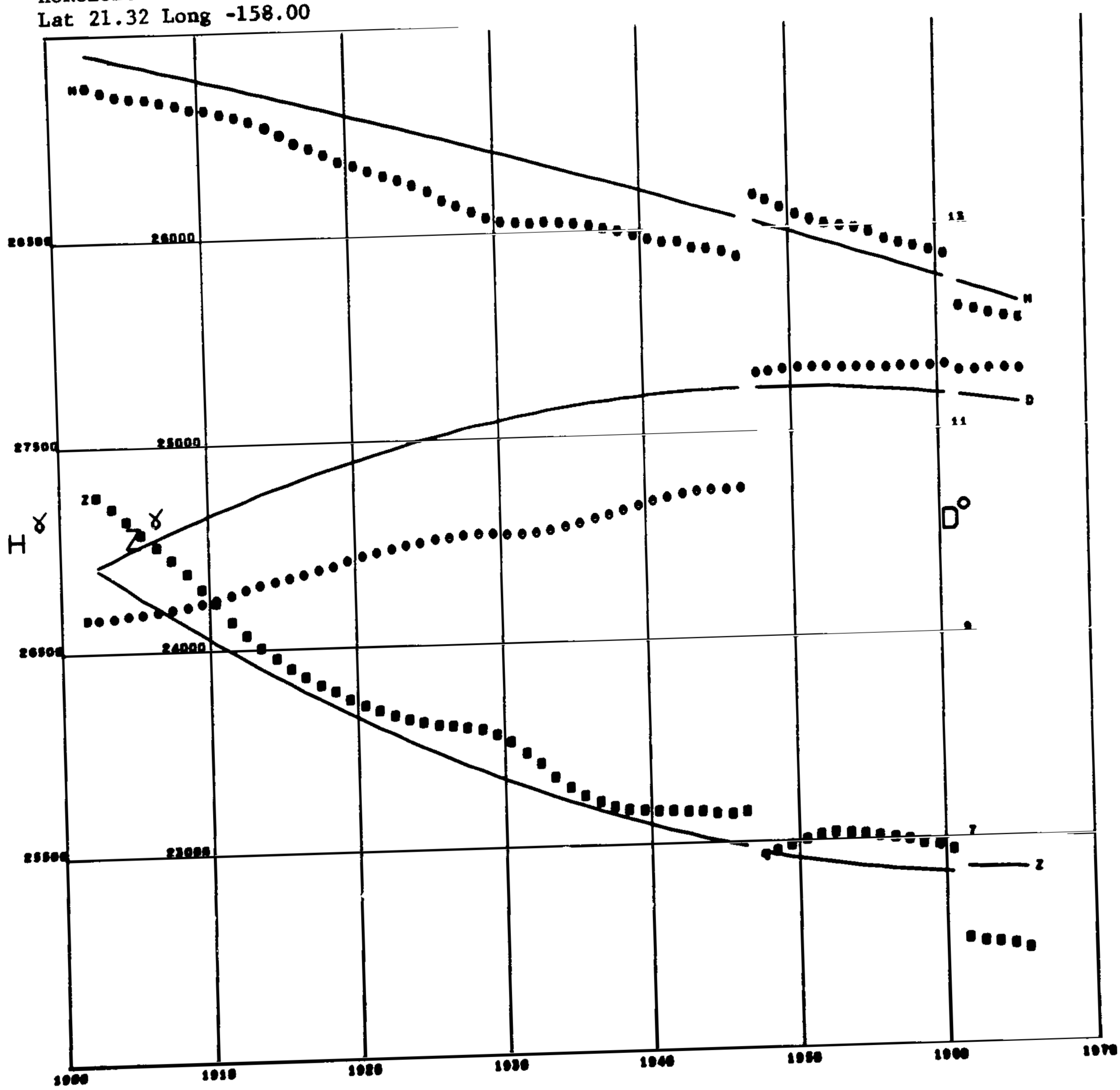

Figure A73

HUANCAYO
Lat -12.04 Long -75.34 Alt 3.35

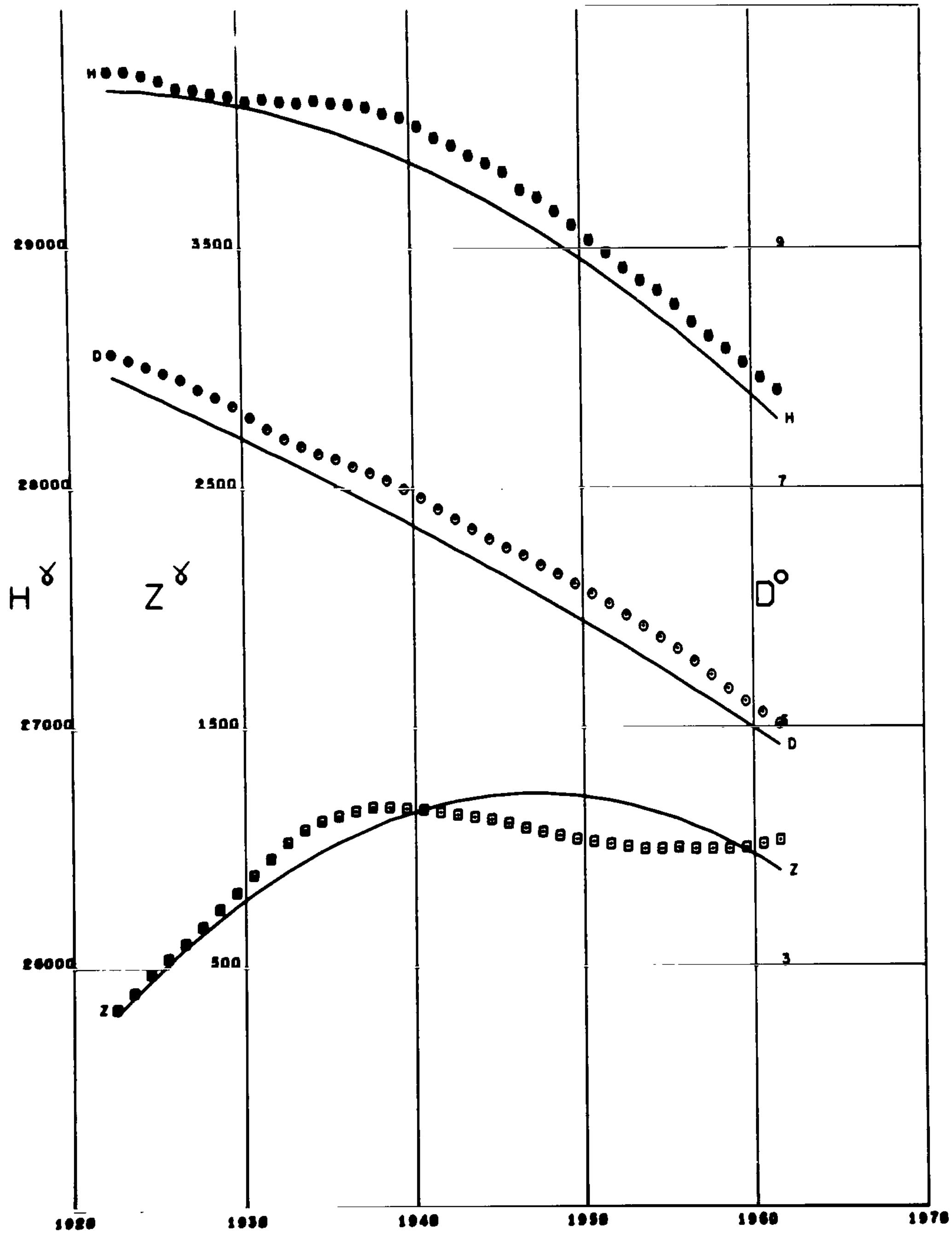

Figure A74

HURBANOVO
Lat 47.87 Long 18.19

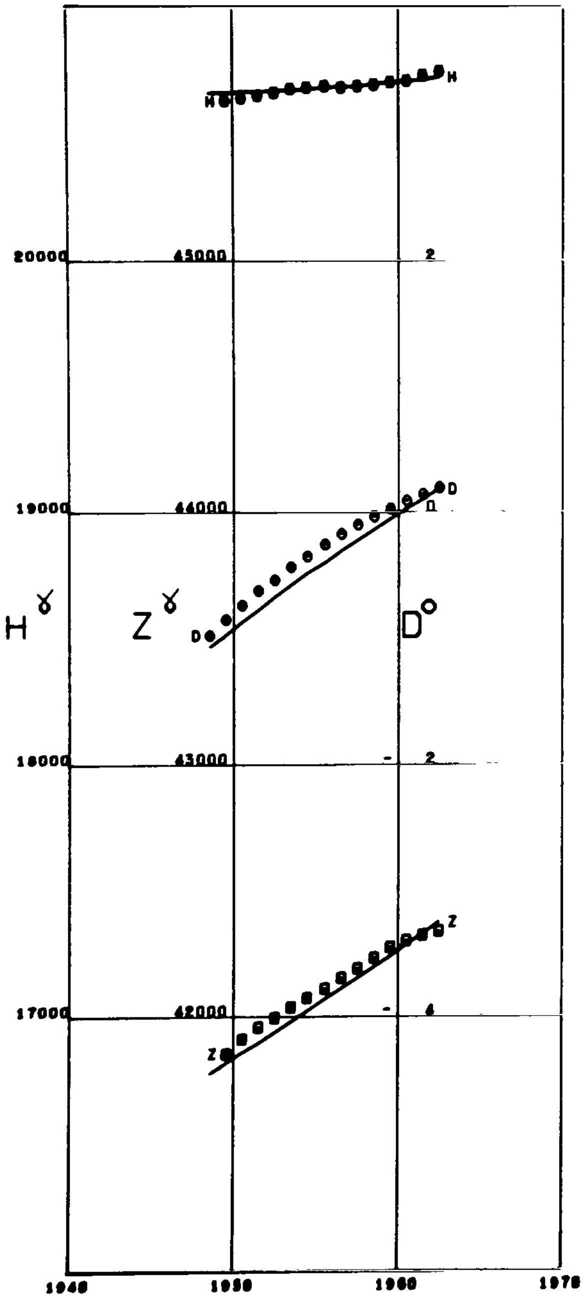

Figure A75

IBADAN
Lat 7.43 Long 3.90

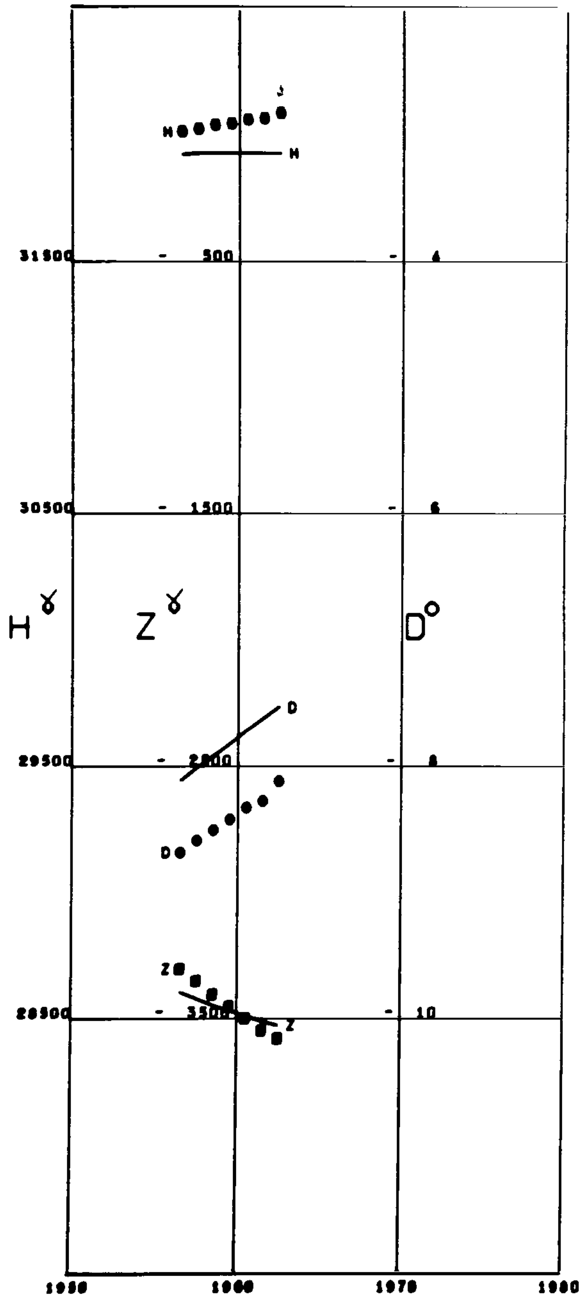

Figure A76

IRKUTSK
Lat 52.26 Long 104.26

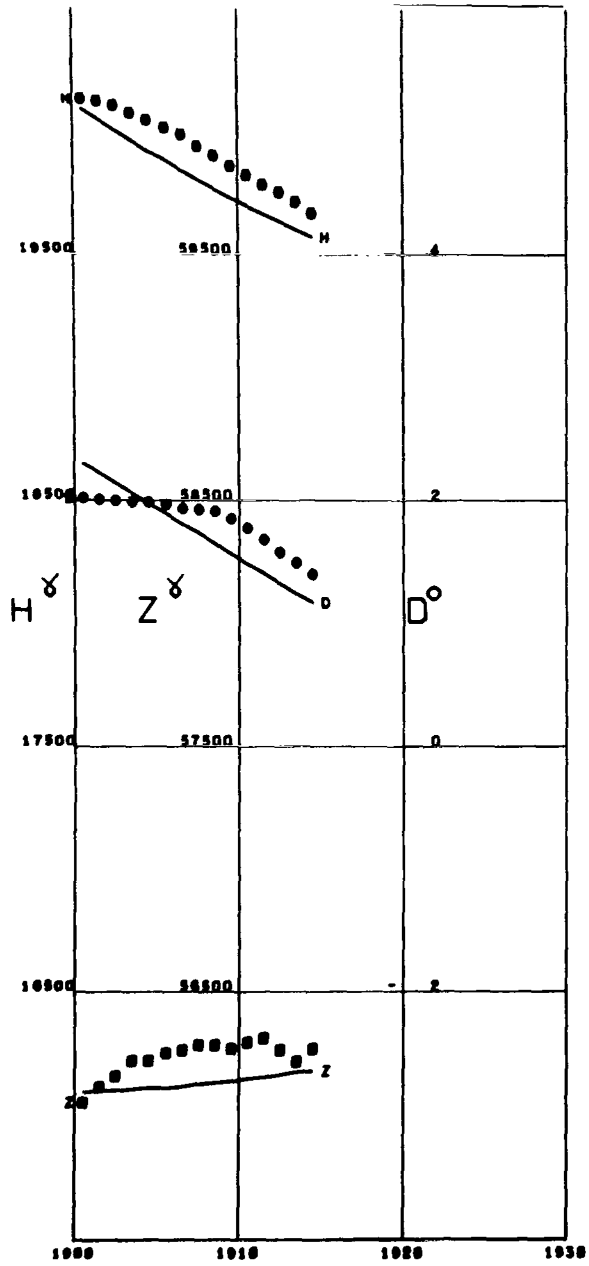

Figure A77

ISTANBUL KANDILLI
Lat 41.06 Long 29.06

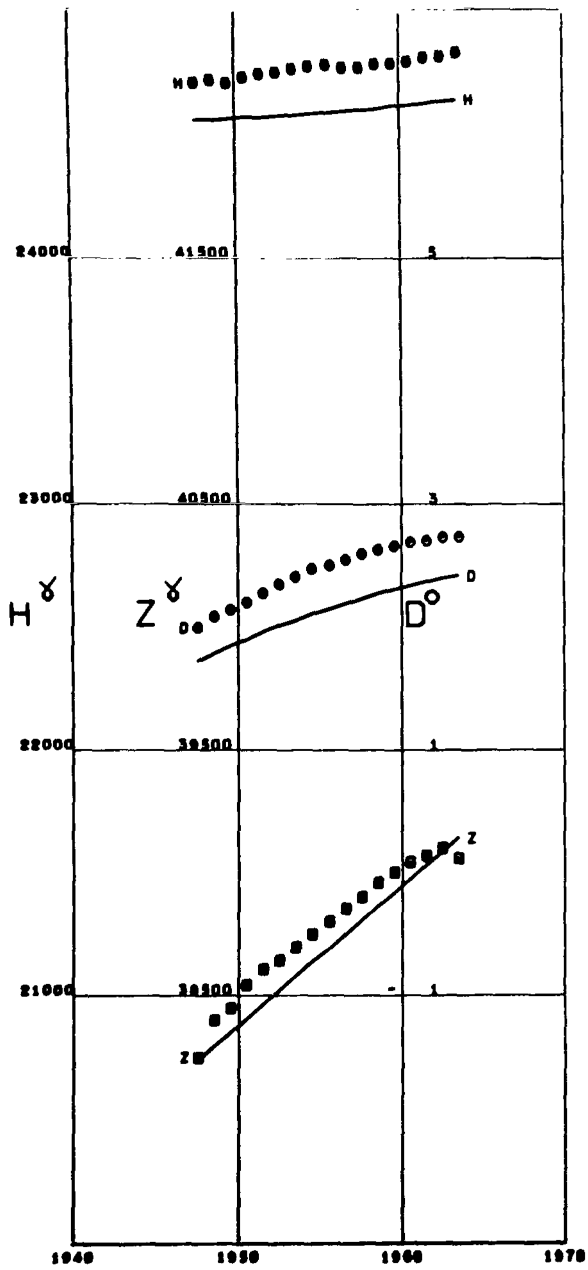

Figure A78

JALUIT
Lat 5.91 Long 169.65

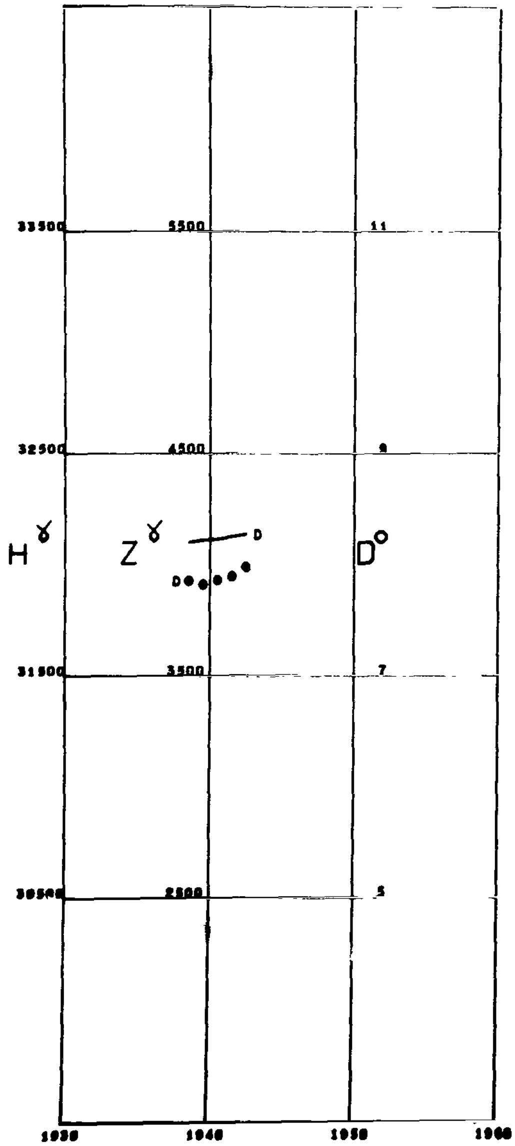

Figure A79

JASSY
Lat 47.18 Long 27.53

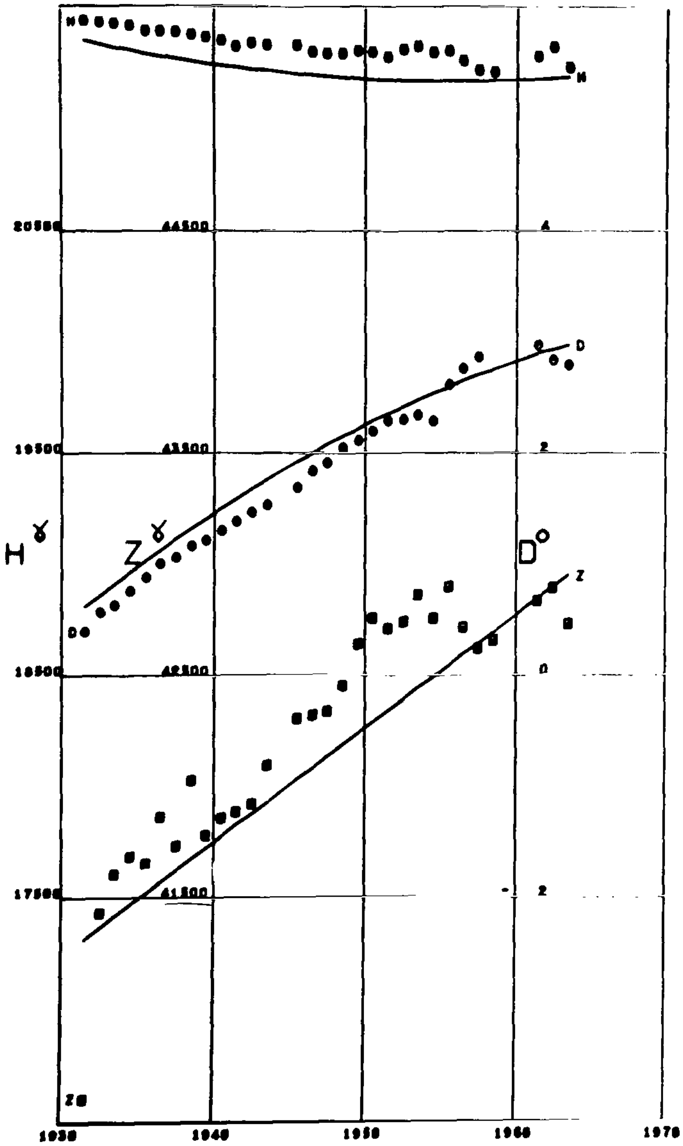

Figure A80

KAKIOKA
Lat 36.23 Long 140.19 Alt 0.03

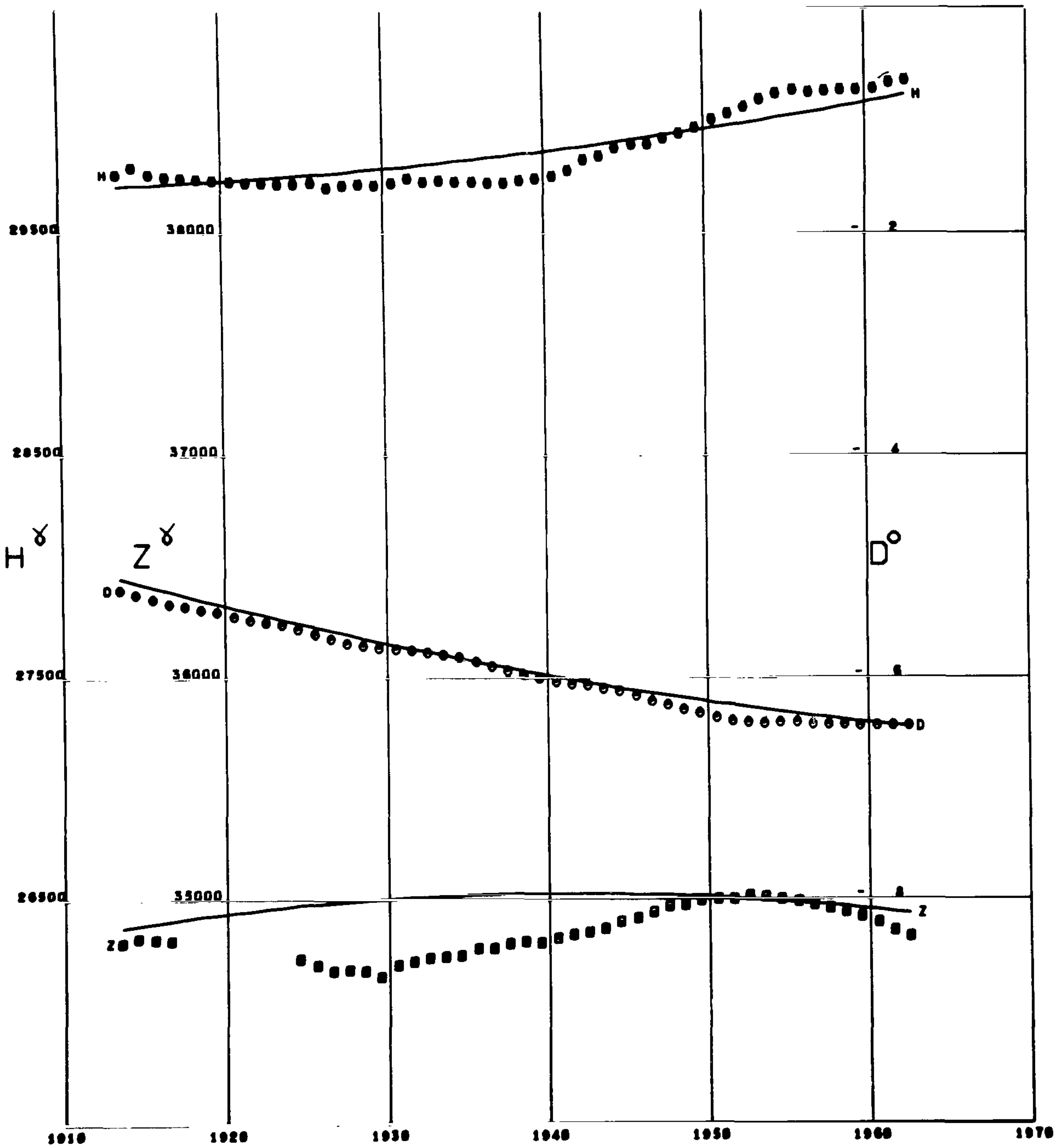

Figure A81

KANOYA
Lat 31.42 Long 130.88

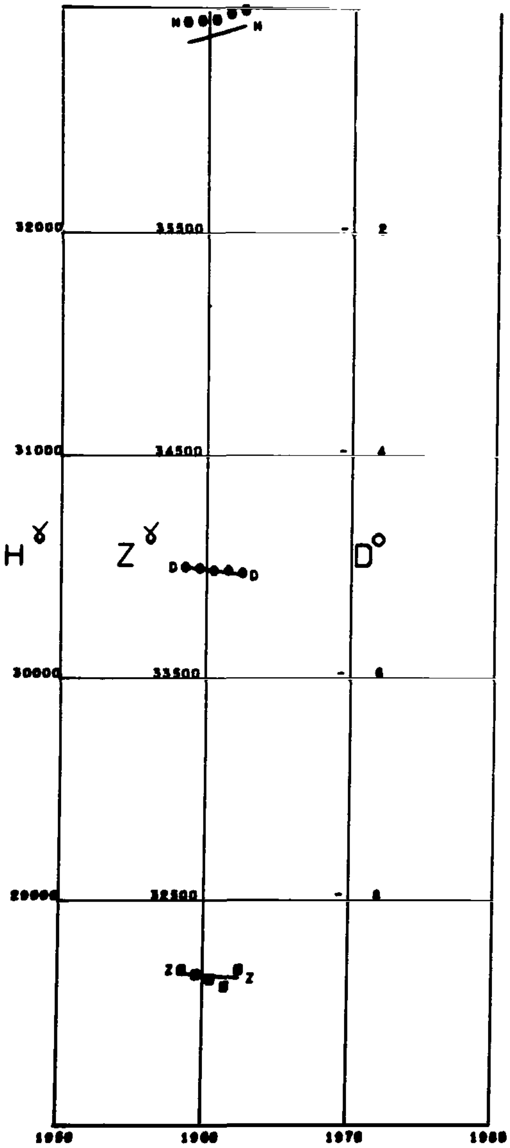

Figure A82

KARSANI
Lat 41.83 Long 44.70

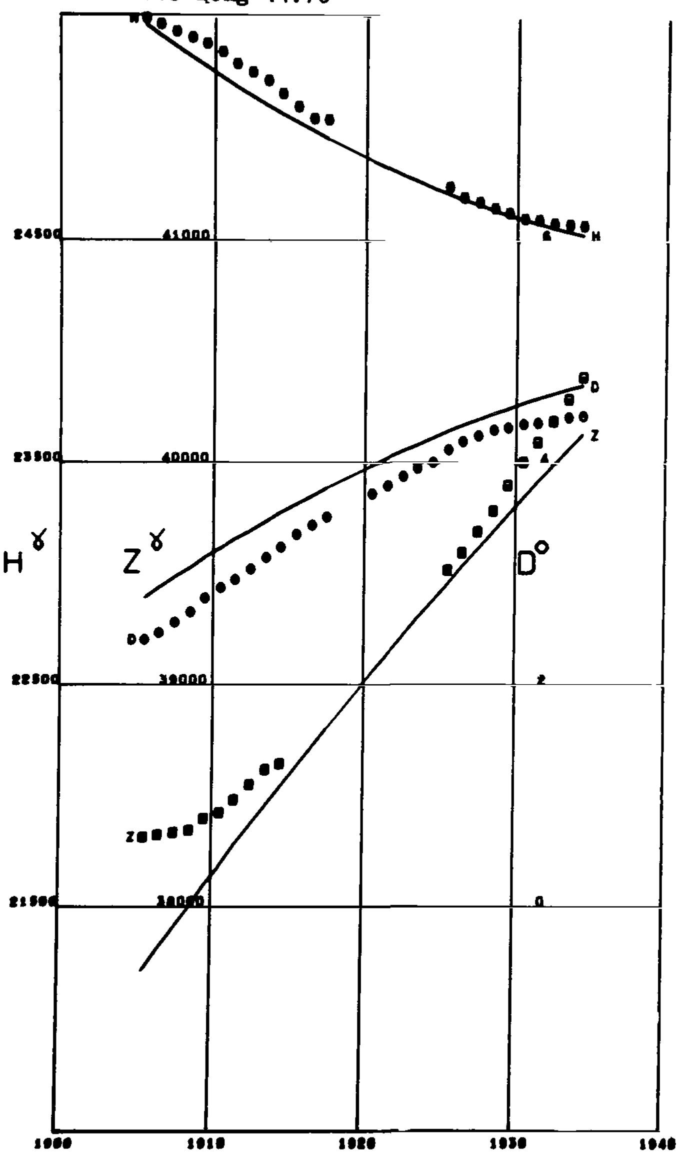

Figure A83

KATUURA
Lat 33.63 Long 135.94

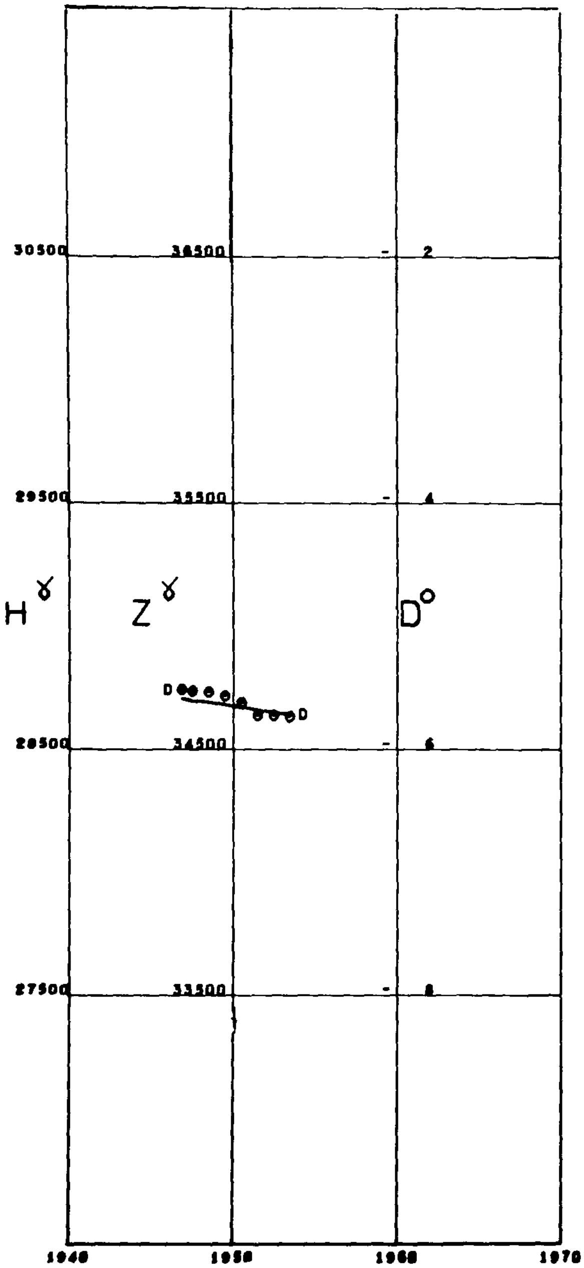

Figure A84

KAZAN
Lat 55.78 Long 49.13

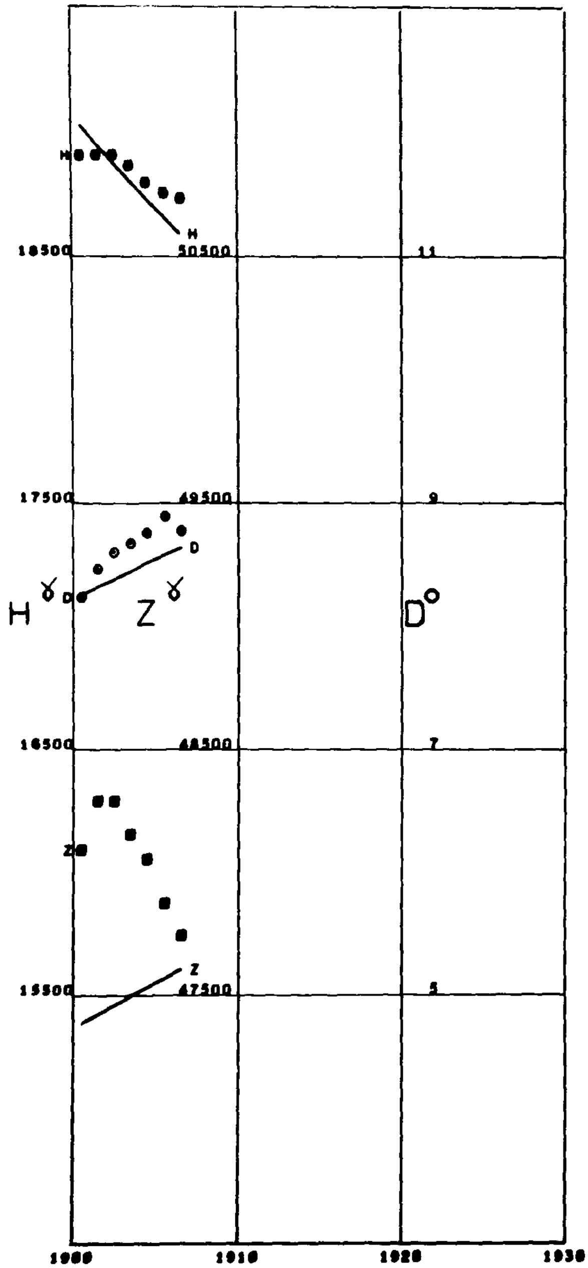

Figure A85

KELES
Lat 41.42 Long 69.20

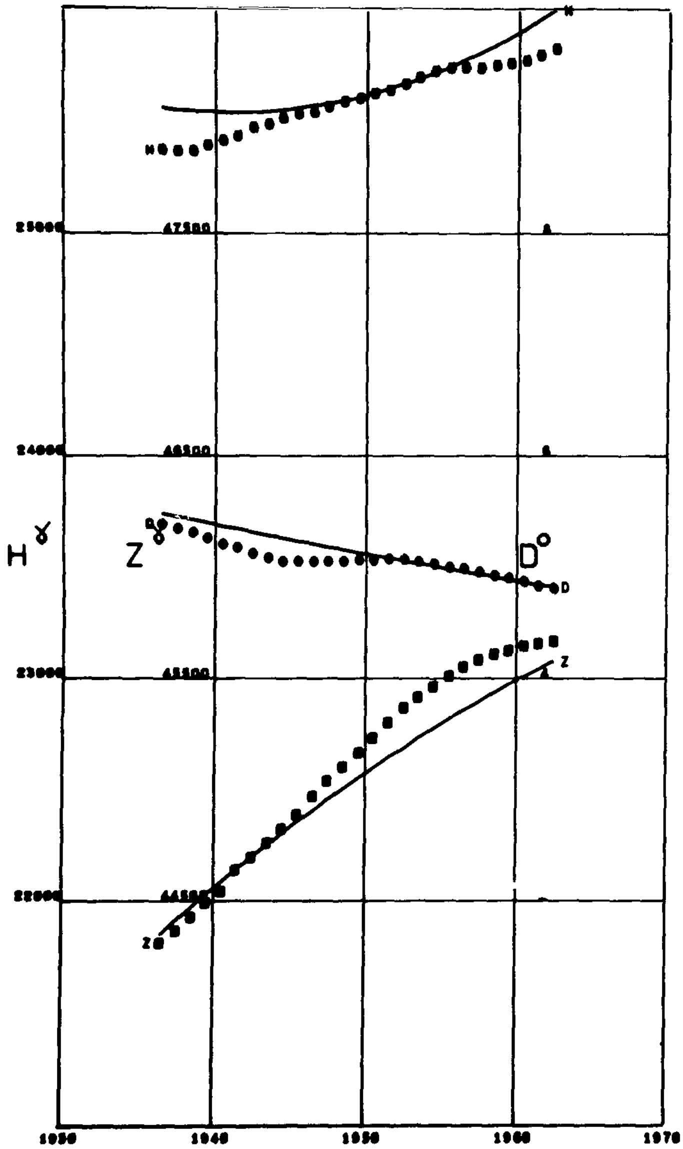

Figure A86

KERGUELEN
Lat -49.35 Long 70.20

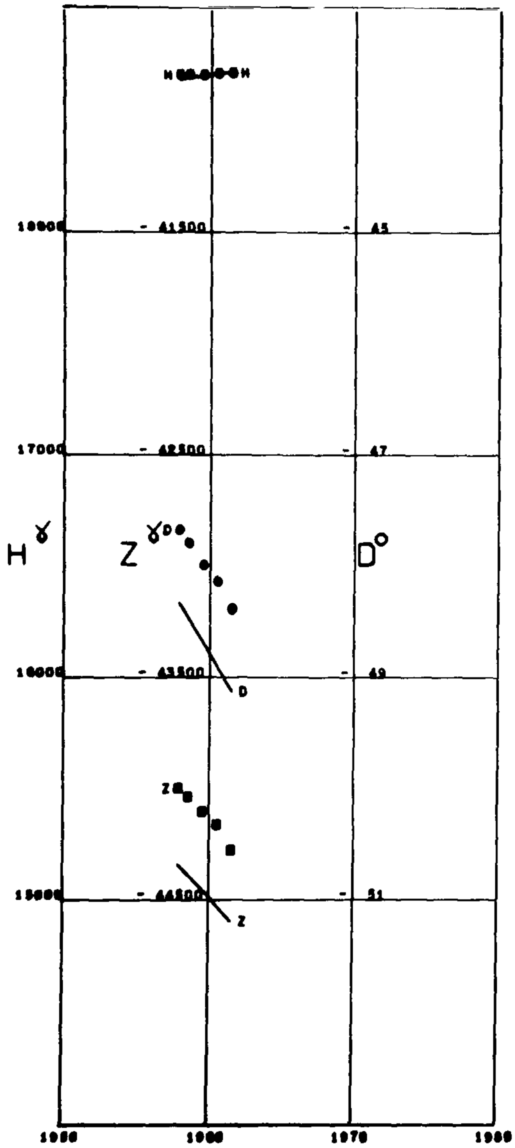

Figure A87

KEW
Lat 51.46 Long -0.31

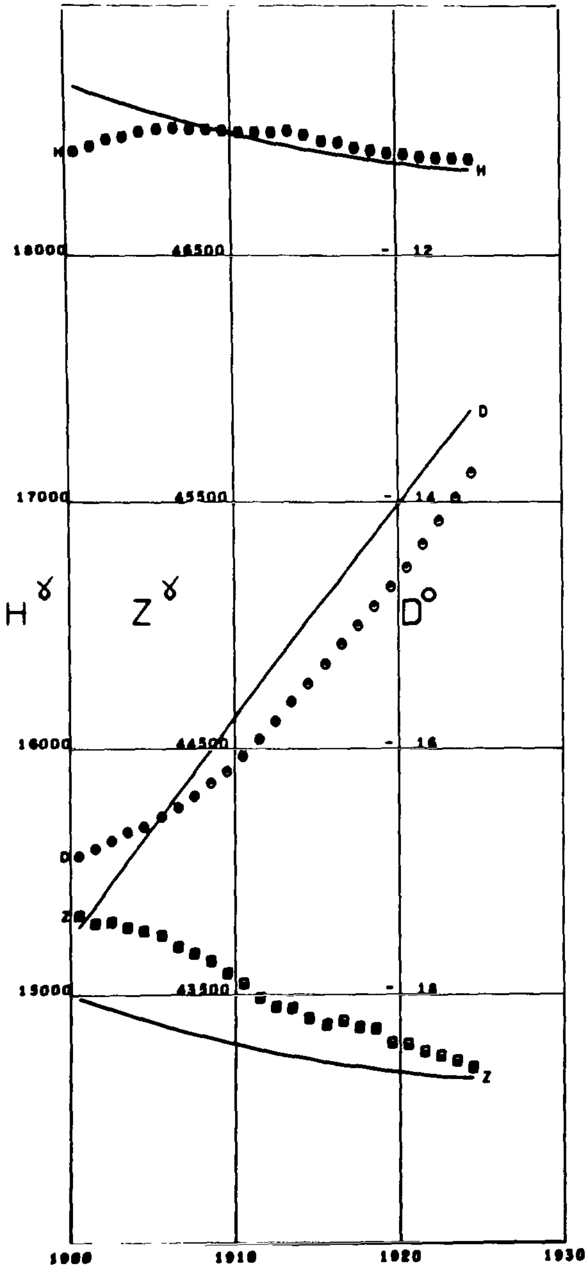

Figure A88

KIEV
Lat 50.71 Long 30.30

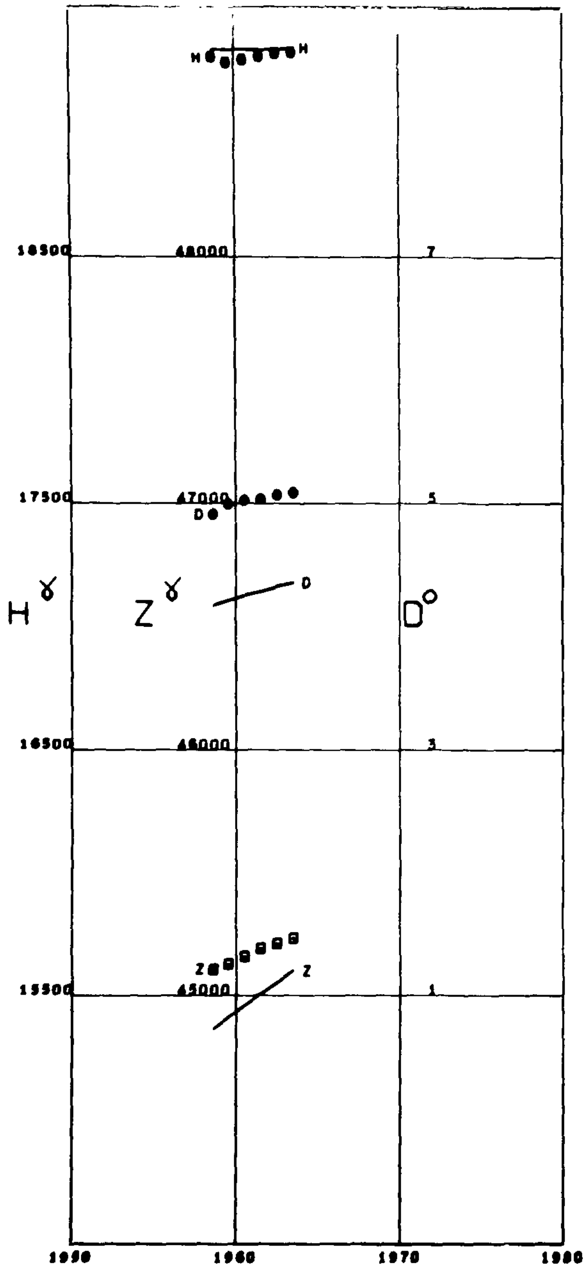

Figure A89

KODAIKANAL
Lat 10.23 Long 77.46

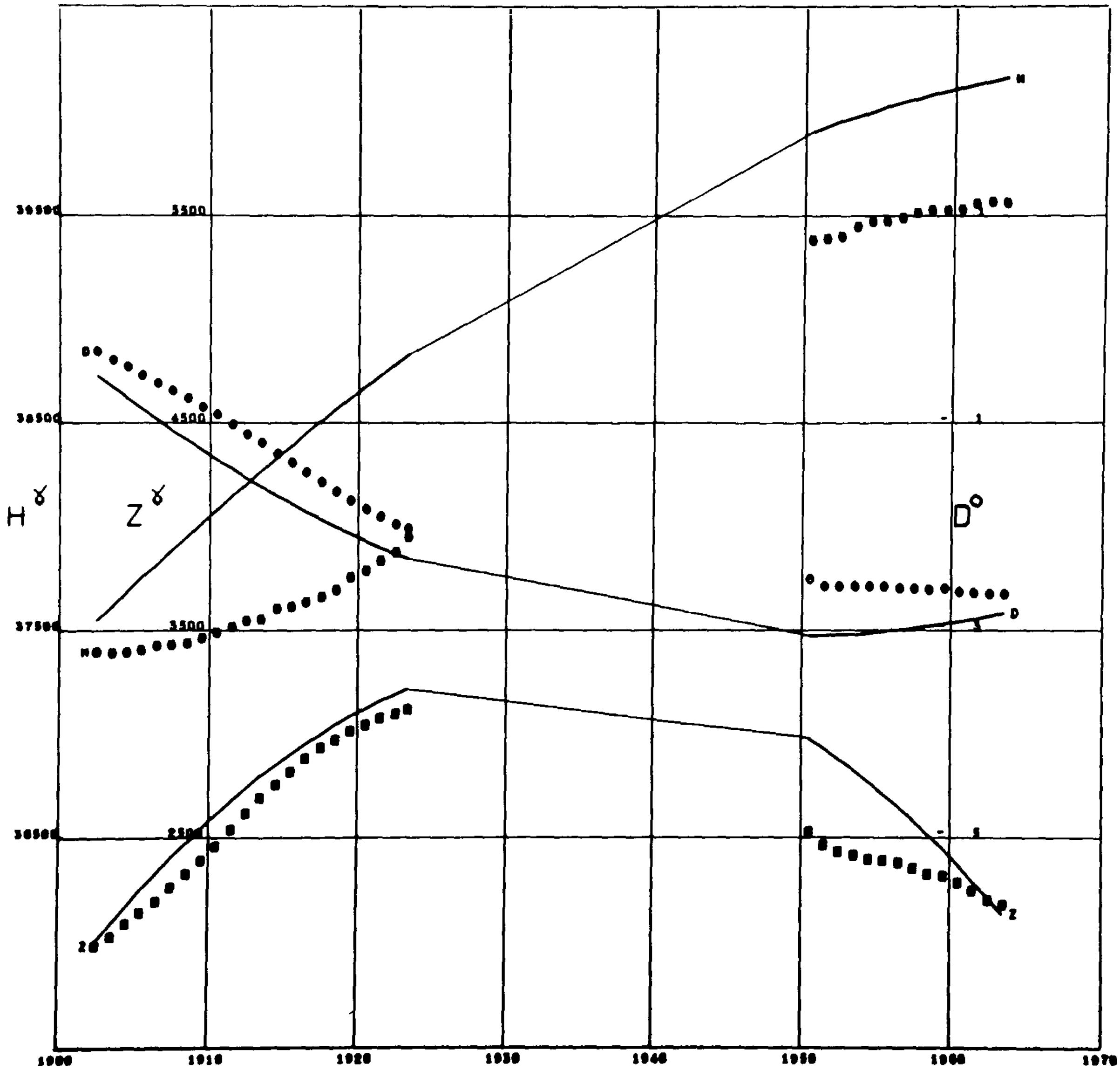

Figure A90

KRASNAYA PAKHRA
Lat 55.47 Long 37.31

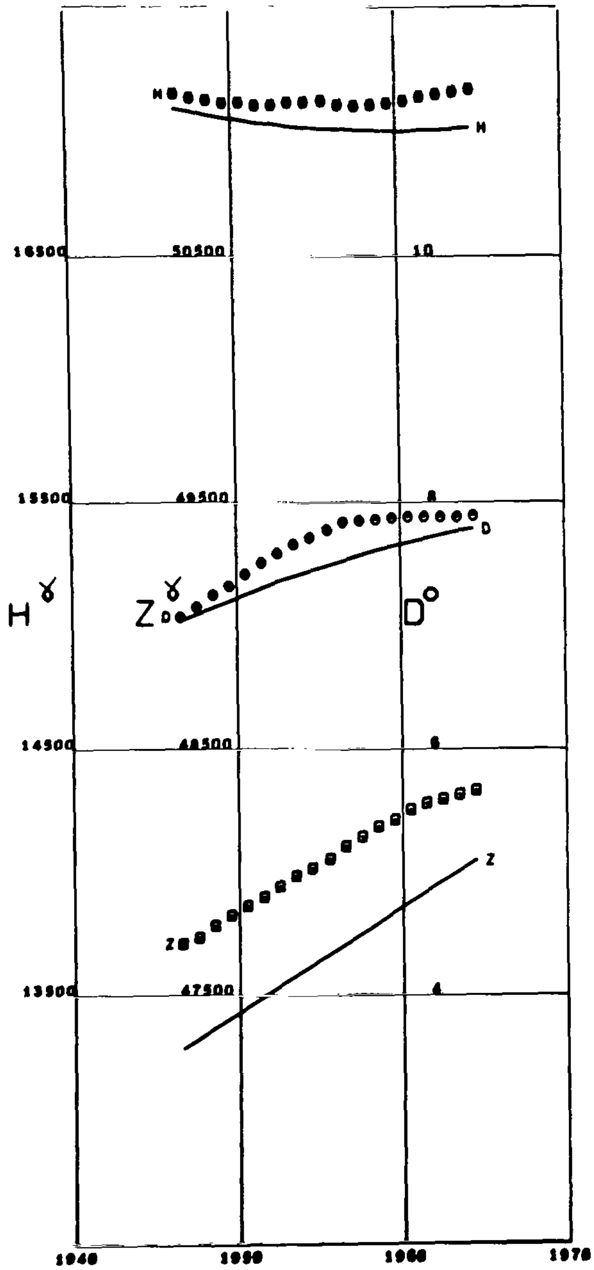

Figure A91

KREMSMUNSTER
Lat 48.05 Long 14.13

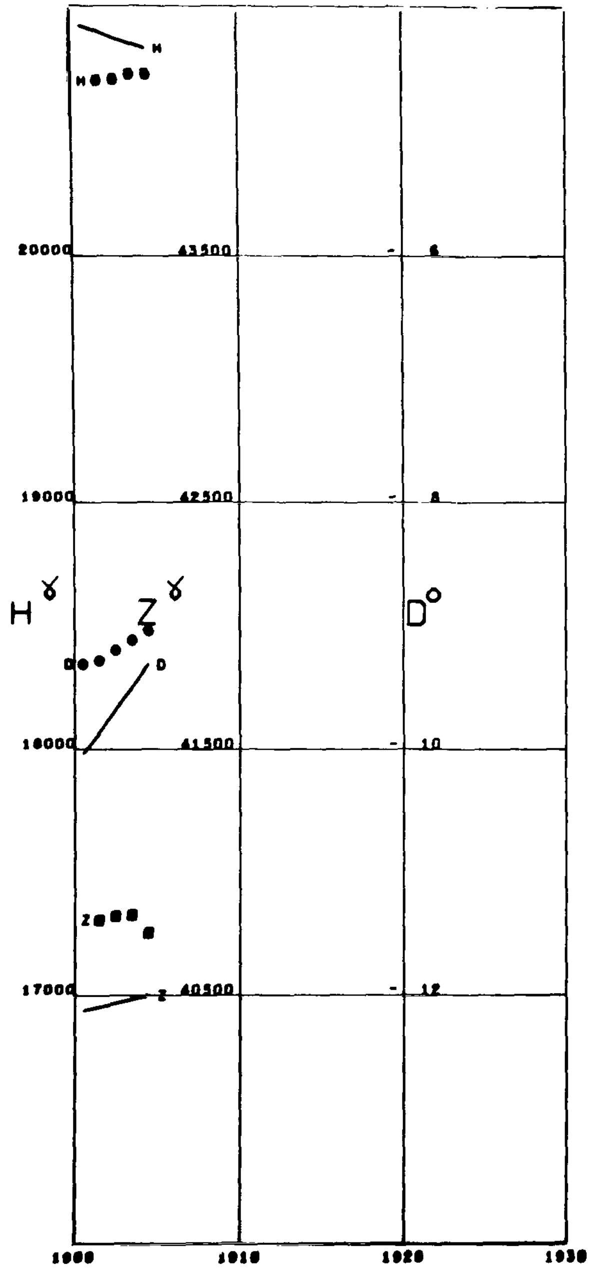

Figure A92

KSARA
Lat 33.82 Long 35.88

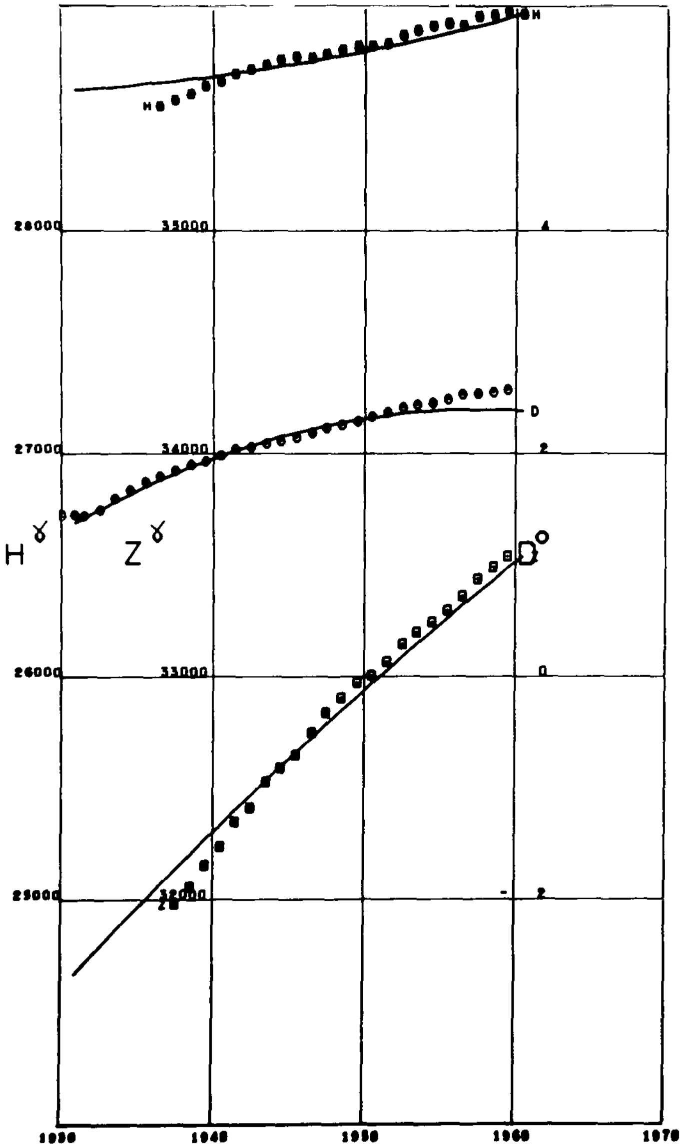

Figure A93

KUTSCHINO
Lat 55.76 Long 37.96

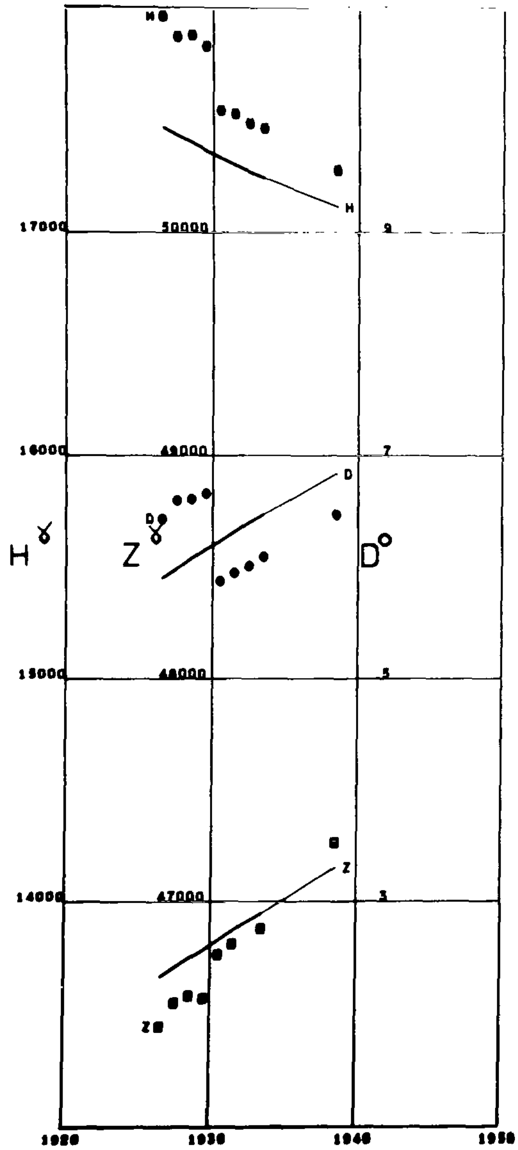

Figure A94

KUYPER
Lat -6.03 Long 106.73

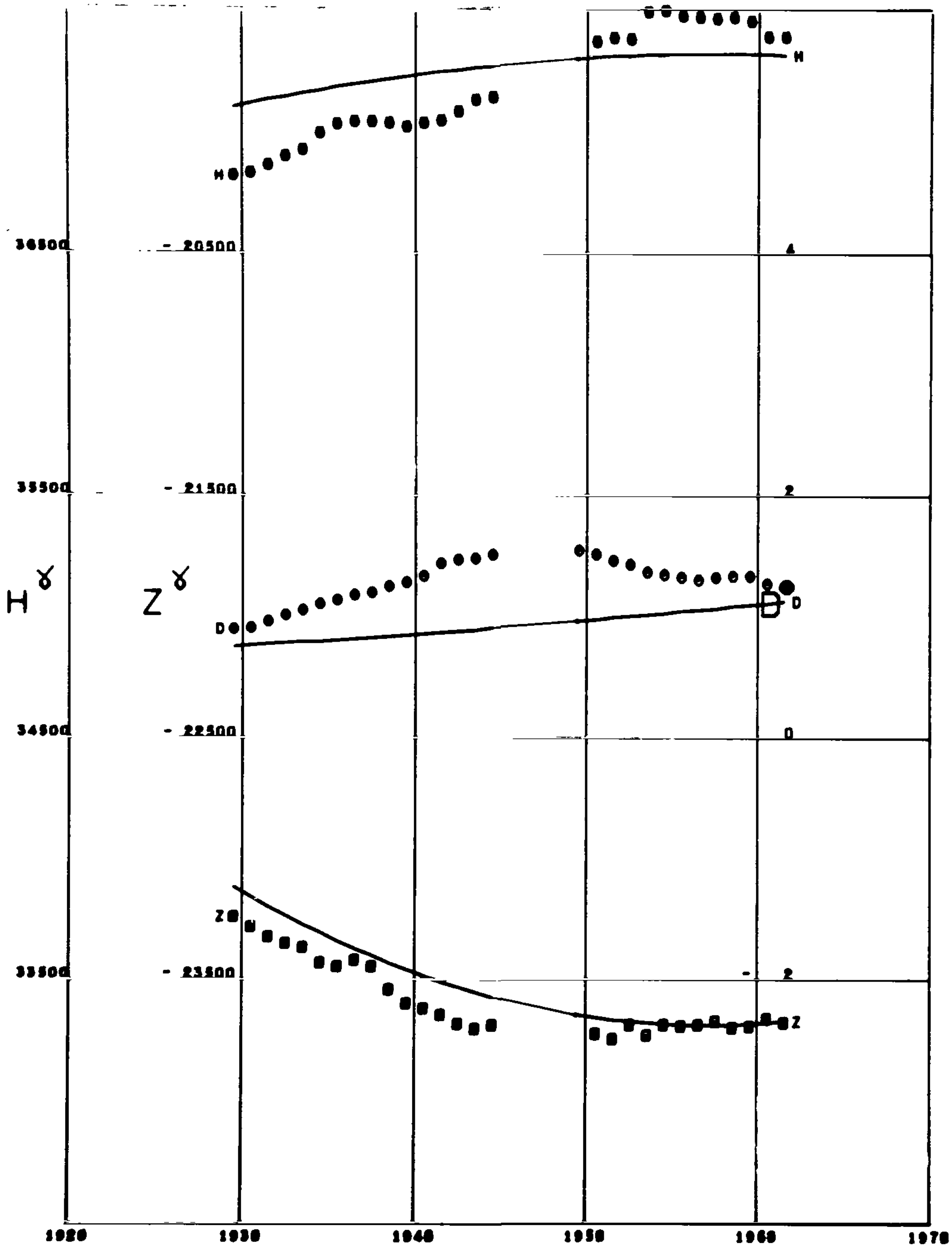

Figure A95

LEIRVOGUR
Lat 64.18 Long -21.70 Alt 0.01

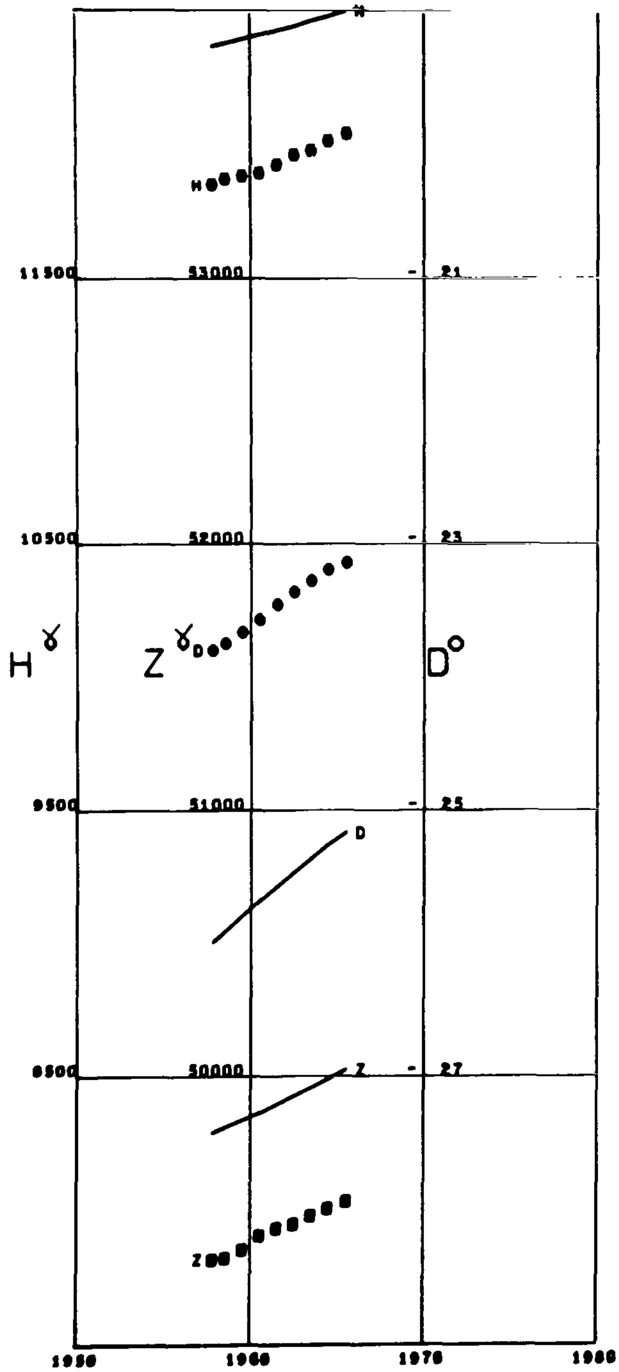

Figure A96

LERWICK
Lat 60.13 Long -1.18

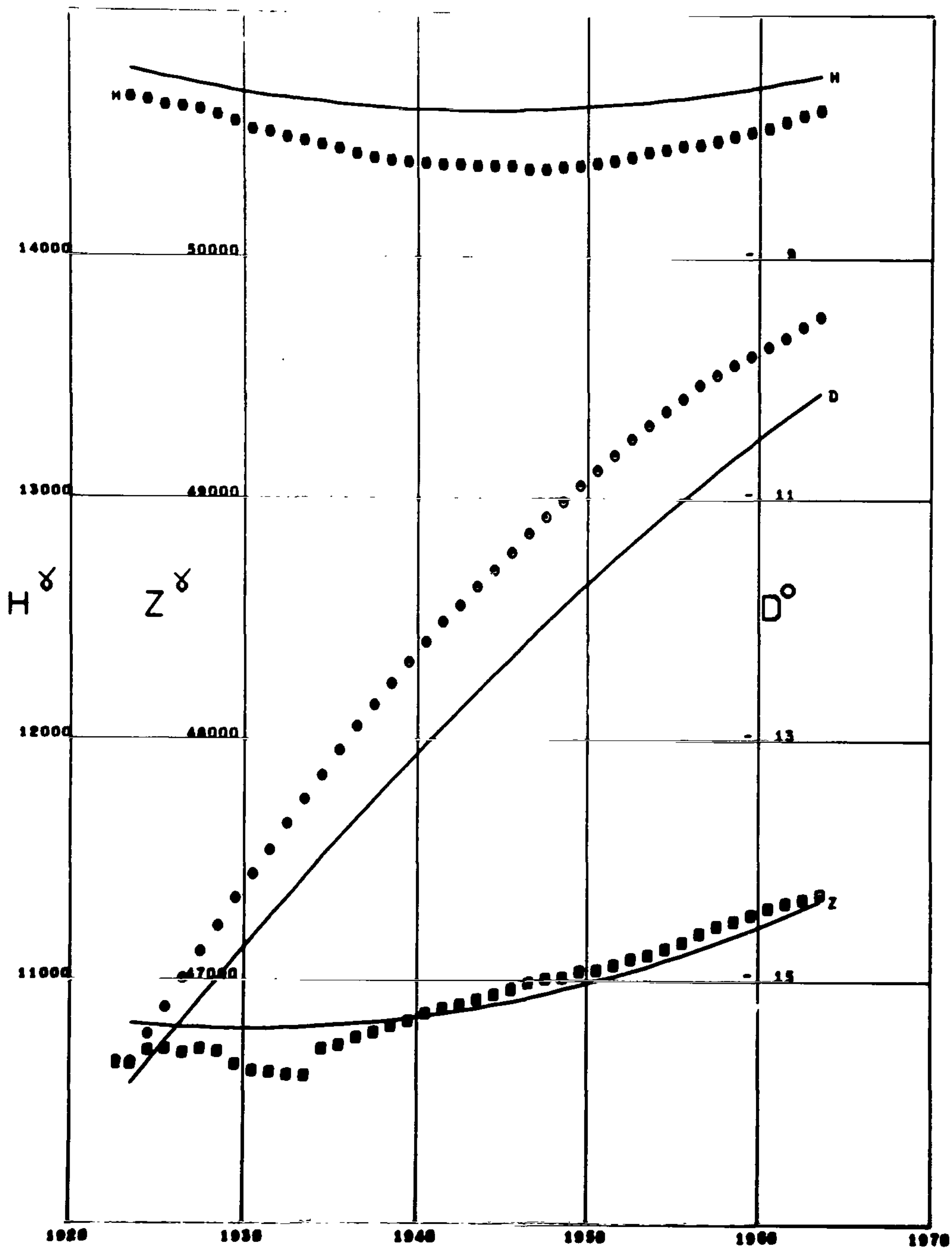

Figure A97

LOGRONO
Lat 42.45 Long -2.50

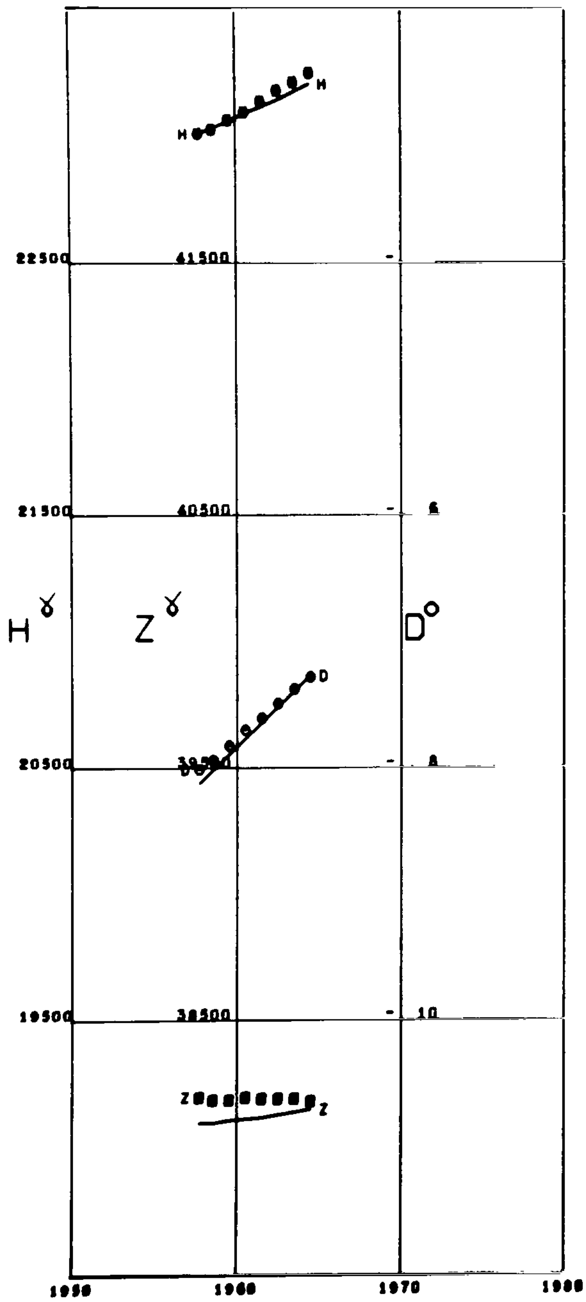

Figure A98

LOURENCO MARQUES
Lat -25.91 Long 32.58

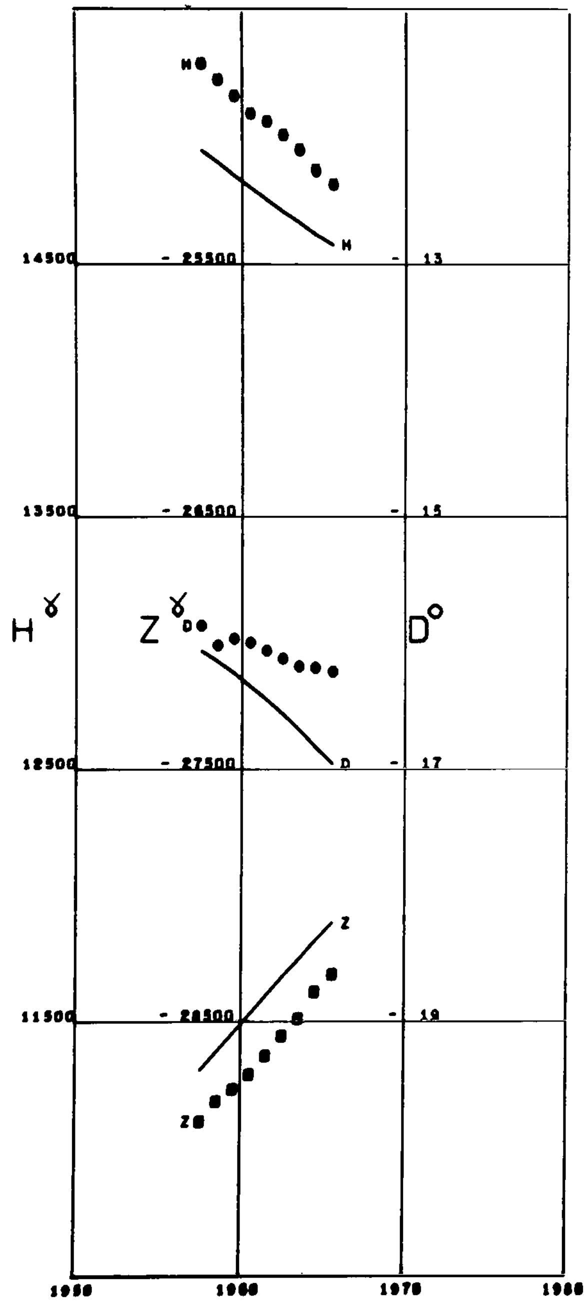

Figure A99

LOVO
Lat 59.34 Long 17.82 Alt 0.02

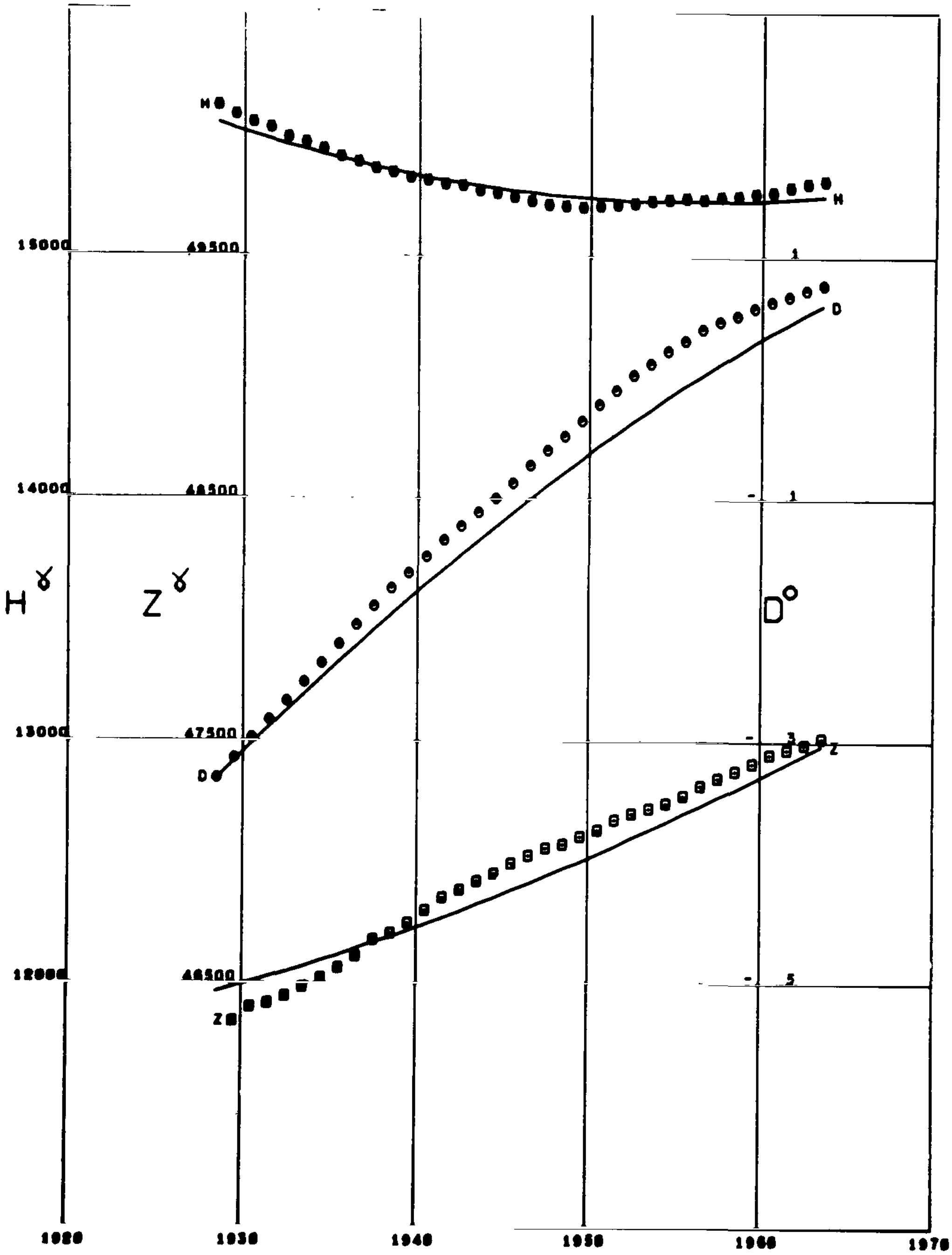

Figure A100

LUANDA BELAS
Lat -8.91 Long 13.16

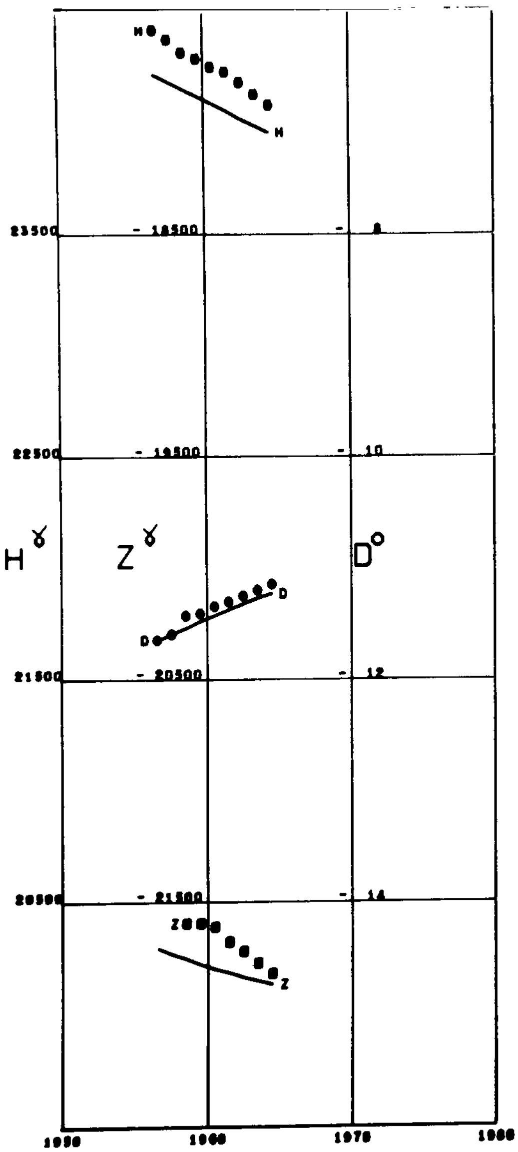

Figure A101

LUKIAPANG
Lat 31.31 Long 121.04

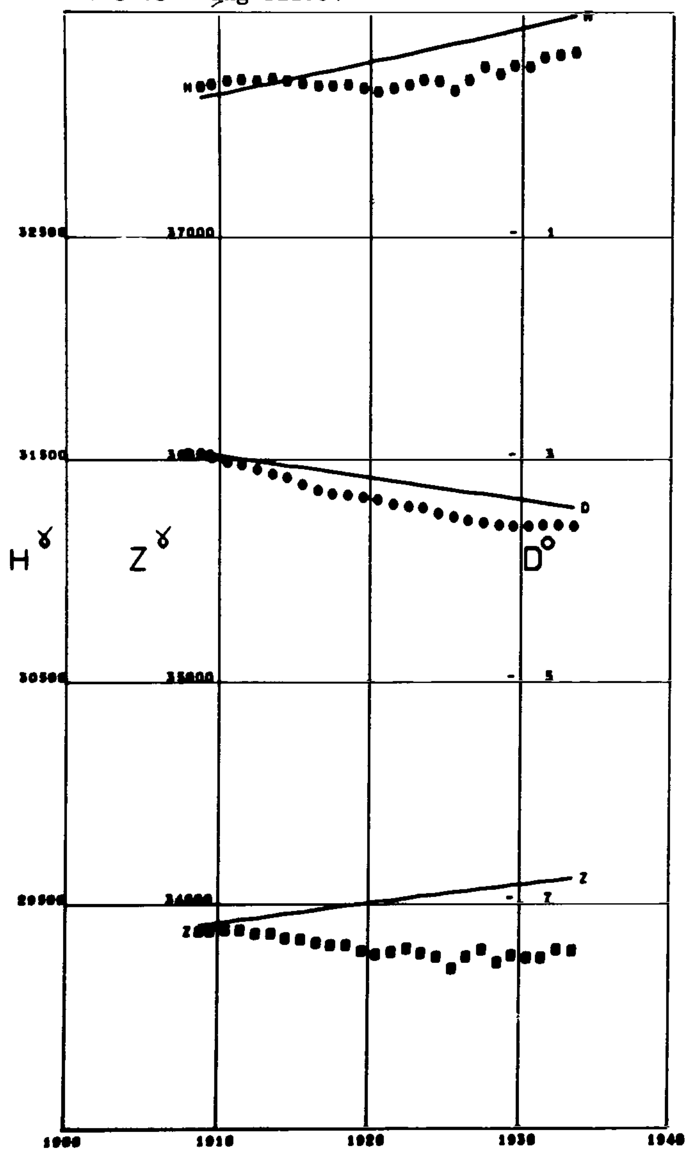

Figure A102

LVOV
Lat 49.90 Long 23.75

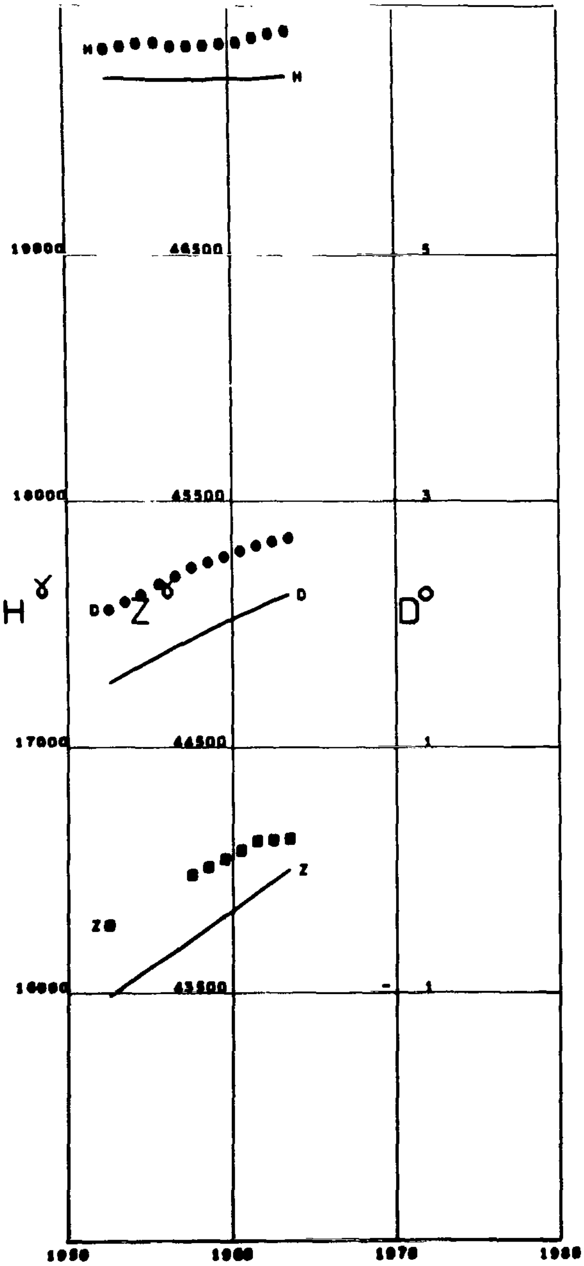

Figure A103

M'BOUR
Lat 14.39 Long ->16.95 Alt 0.01

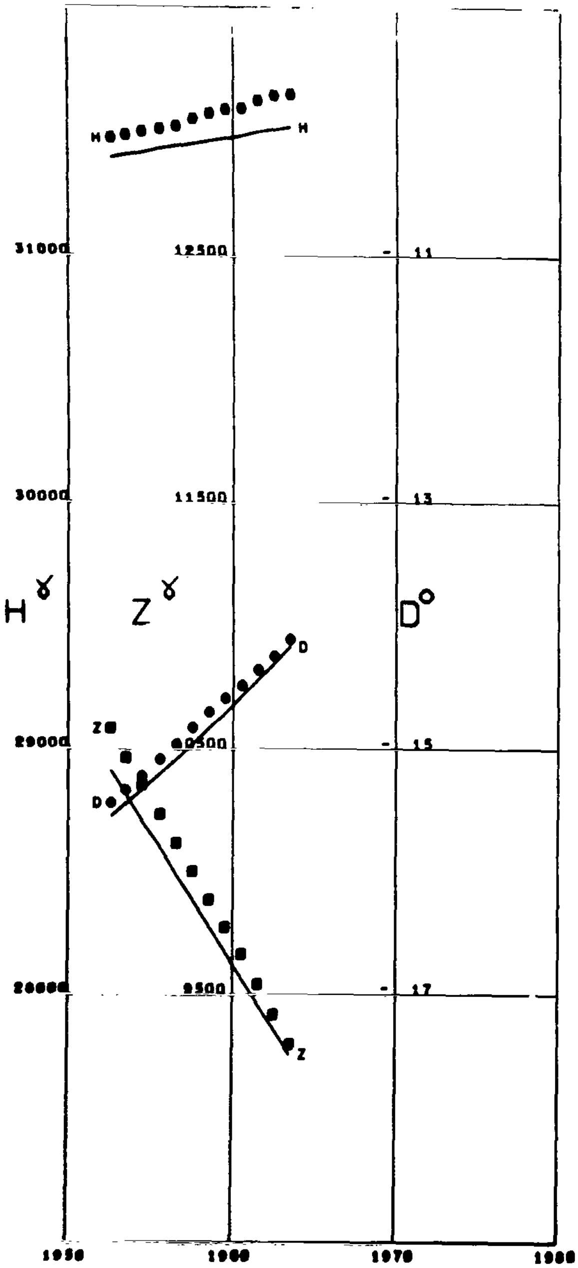

Figure A104

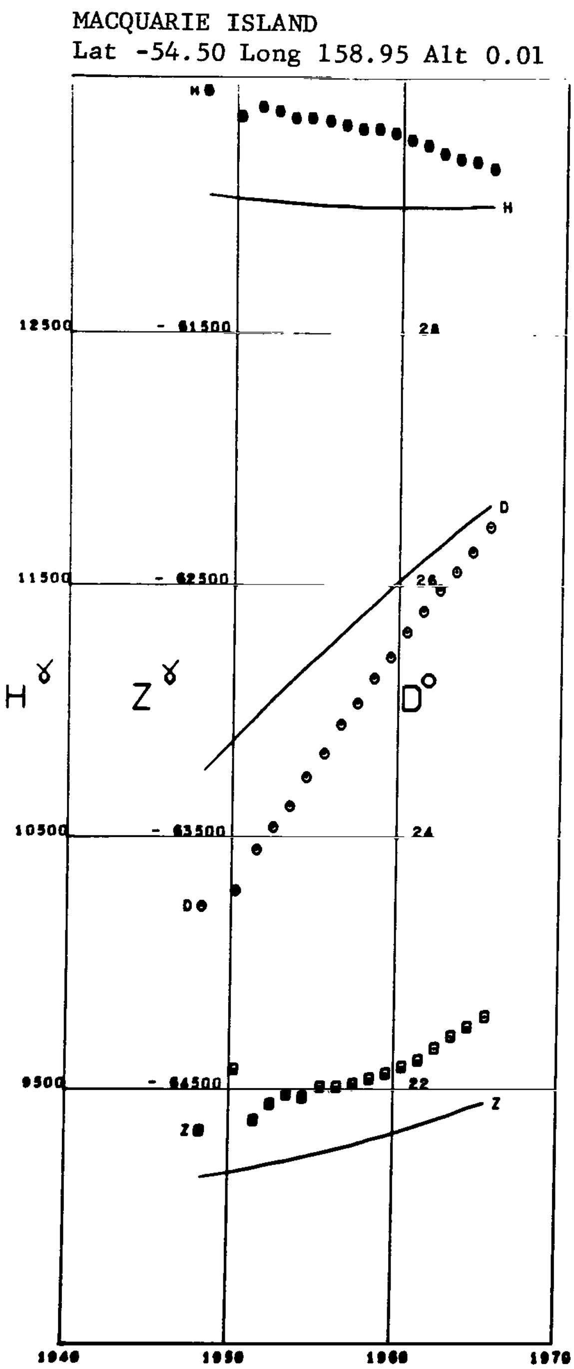

Figure A105

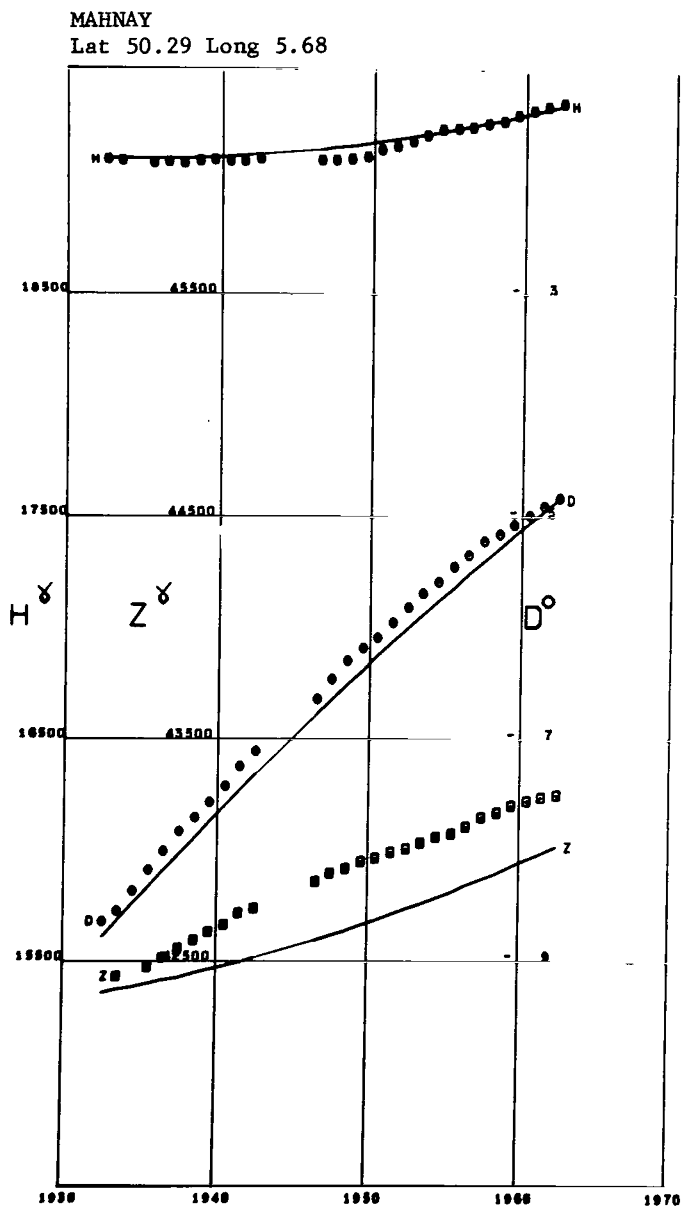

Figure A106

MAISACH
Lat 48.20 Long 11.26 Alt 0.57

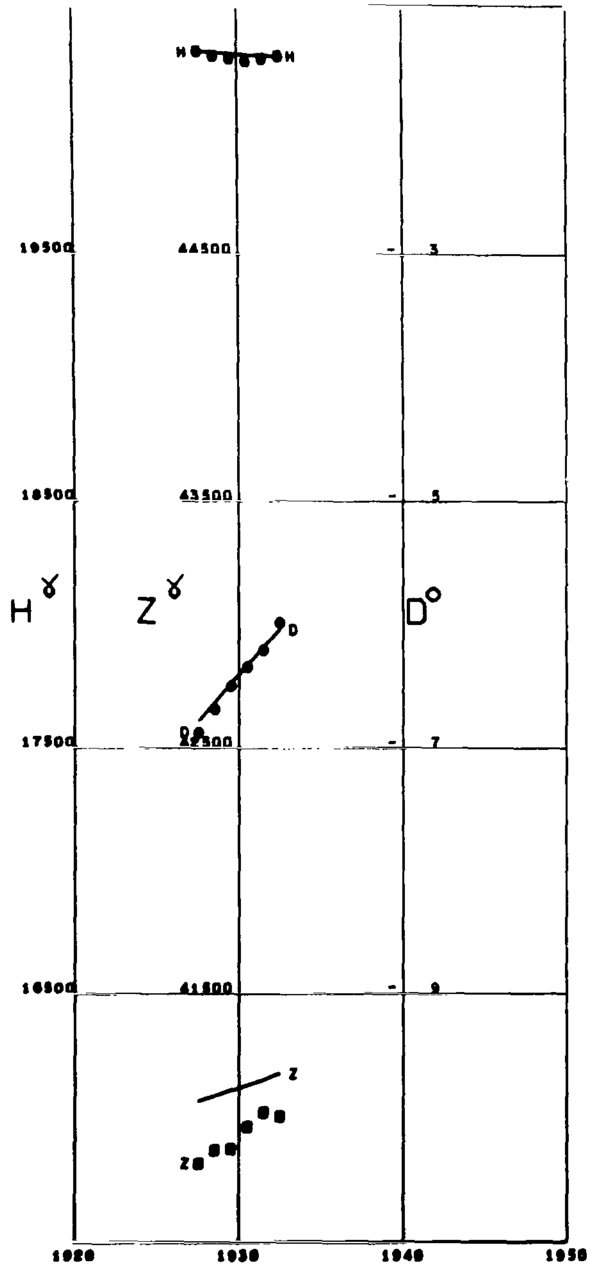

Figure A107

MAITUN
Lat 43.25 Long 132.33

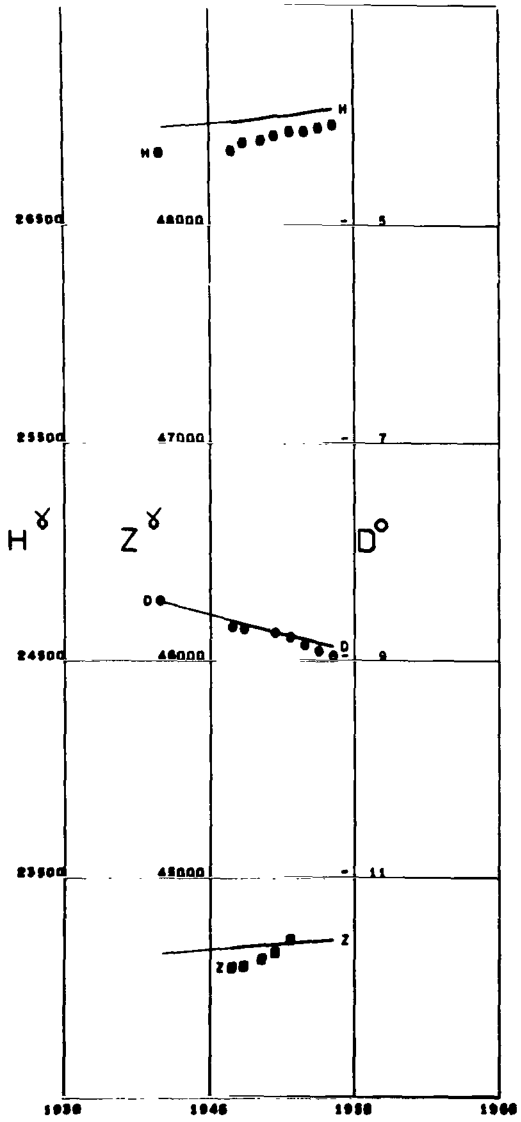

Figure A108

MANILA
Lat 14.57 Long 120.97

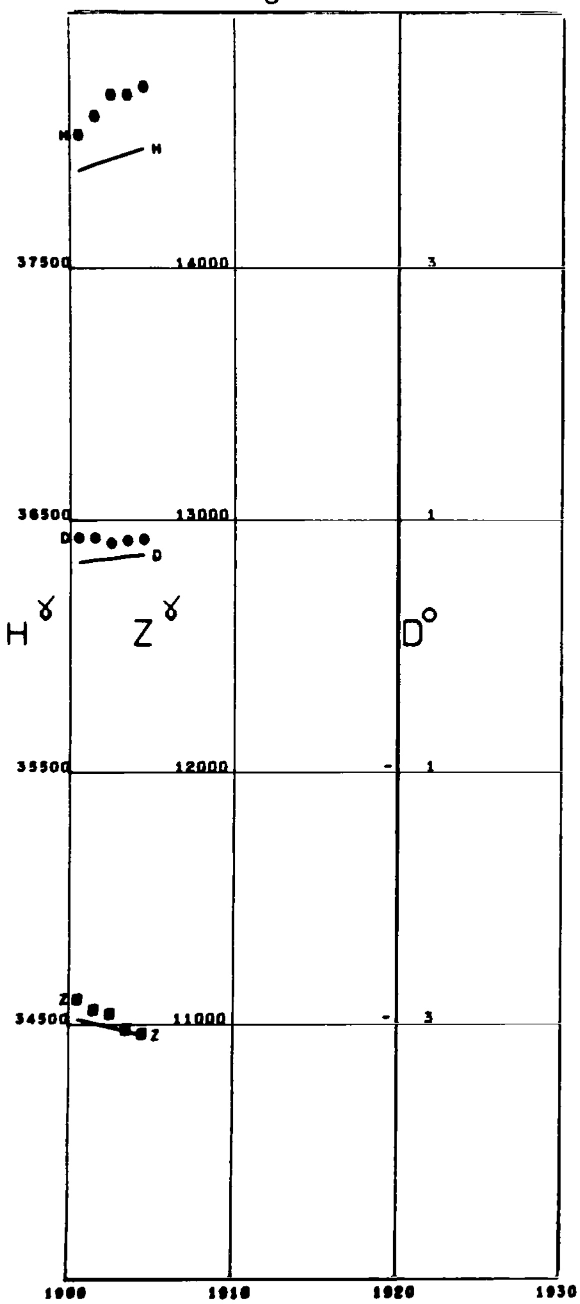

Figure A109

MATOCHKIN SHAR
Lat 73.26 Long 56.39

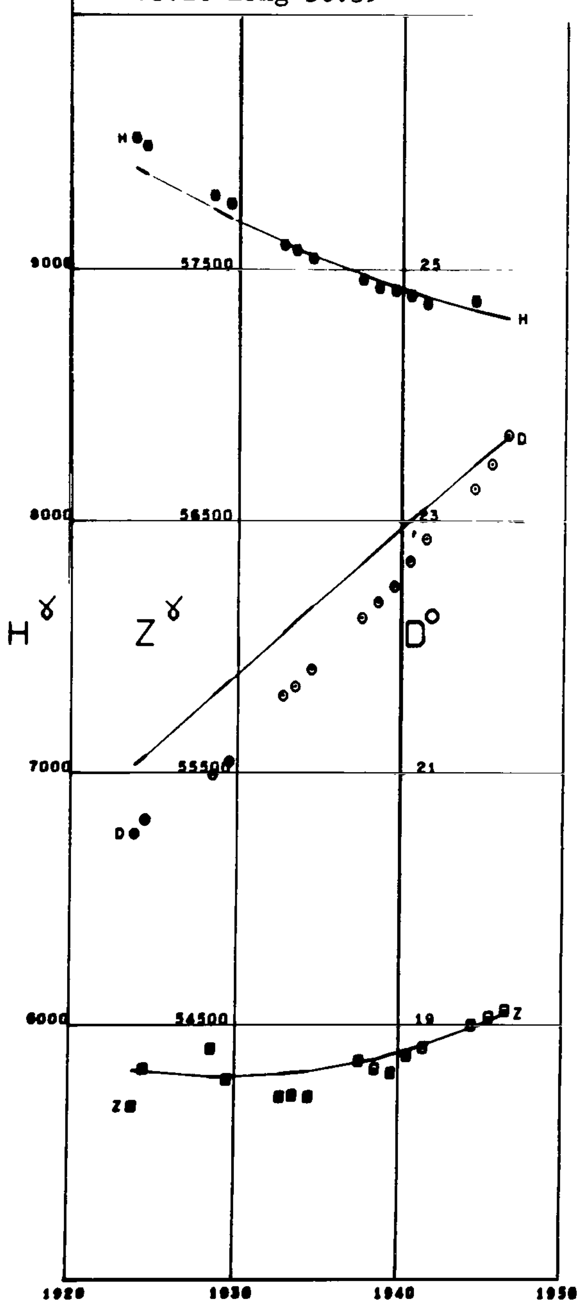

Figure A110

MAURITIUS
Lat -20.09 Long 57.55

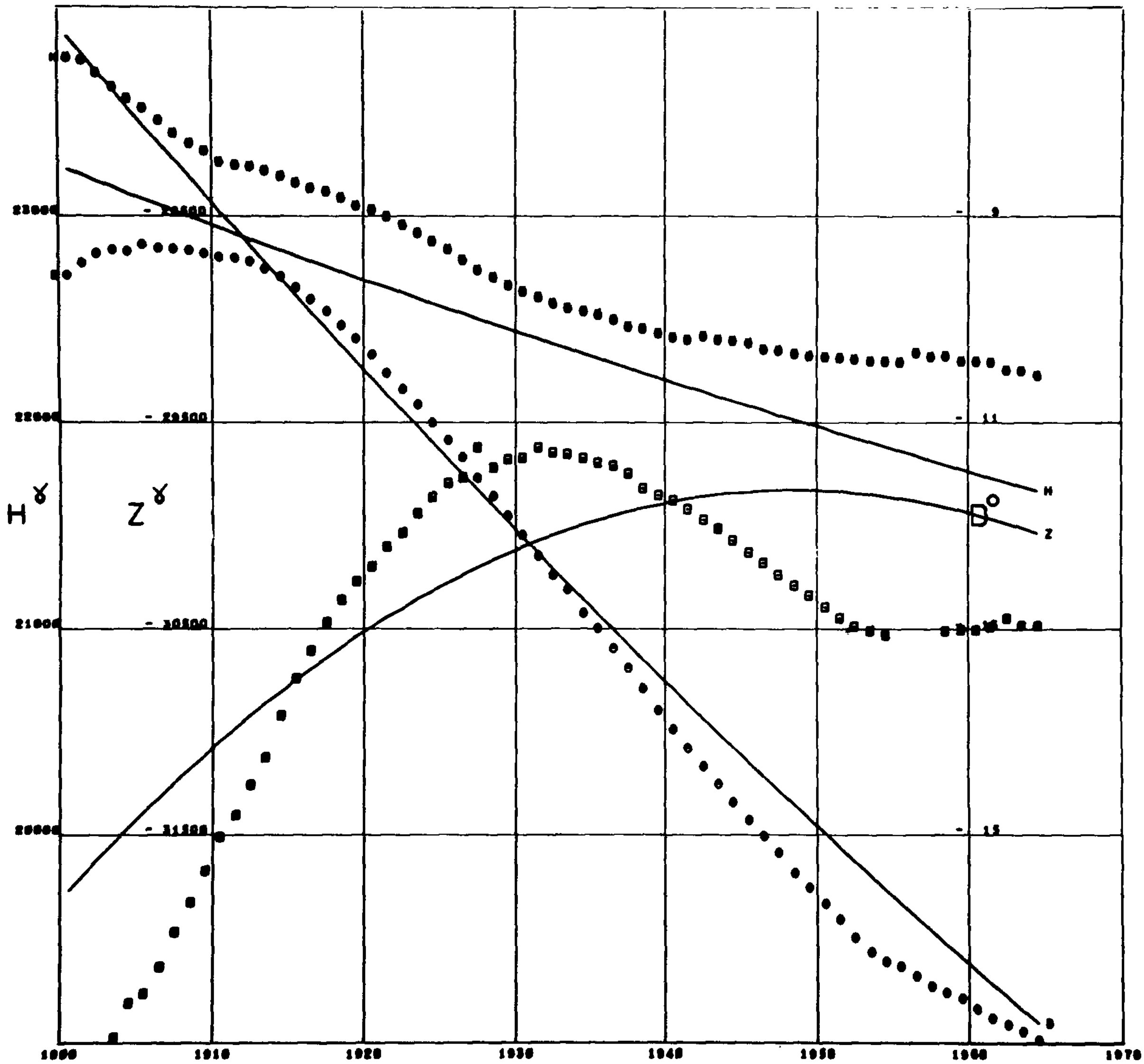

Figure A111

MAWSON
Lat -67.60 Long 62.88

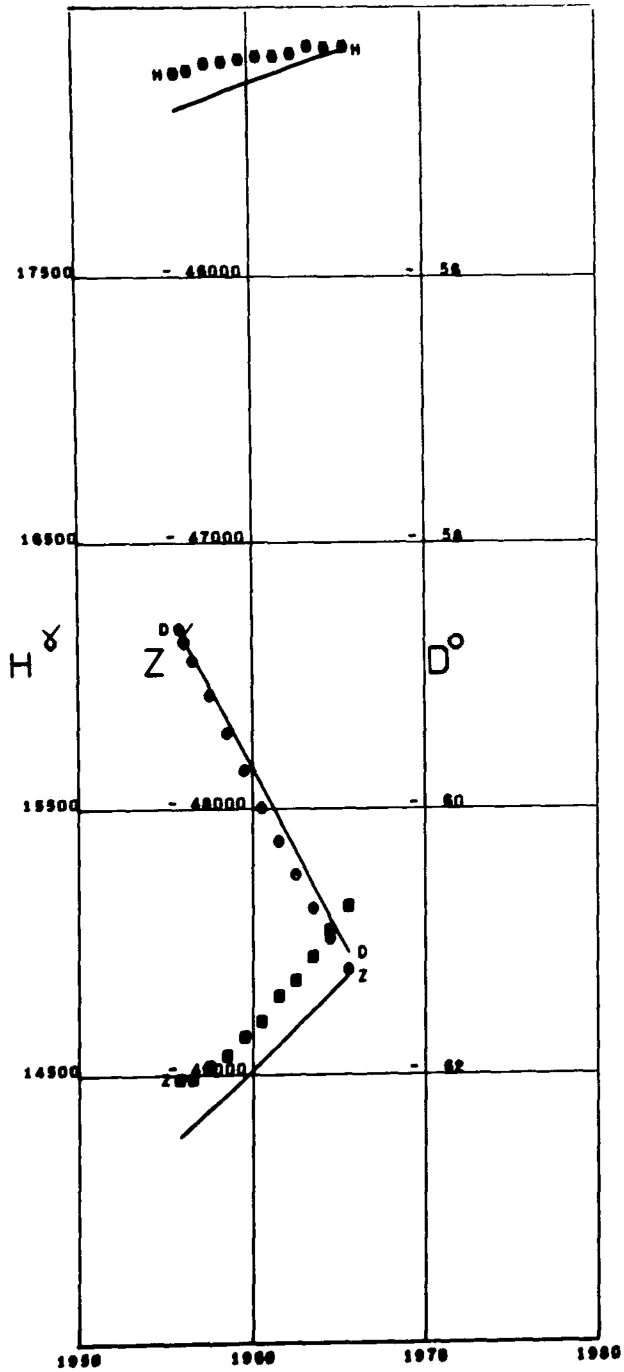

Figure A112

MEANOOK
Lat 54.61 Long -113.33 Alt 0.68

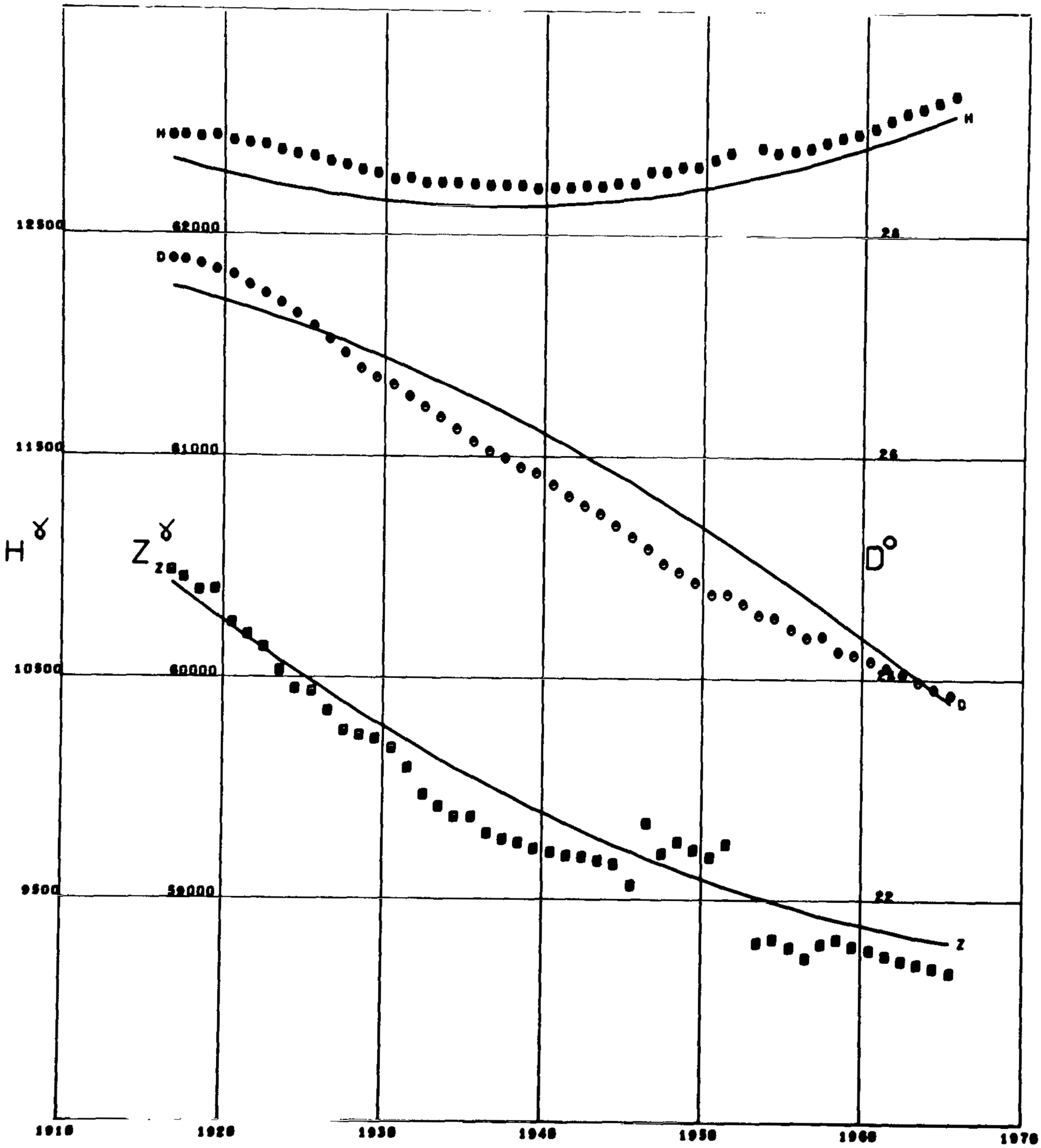

Figure A113

MELBOURNE
Lat -37.83 Long 144.97

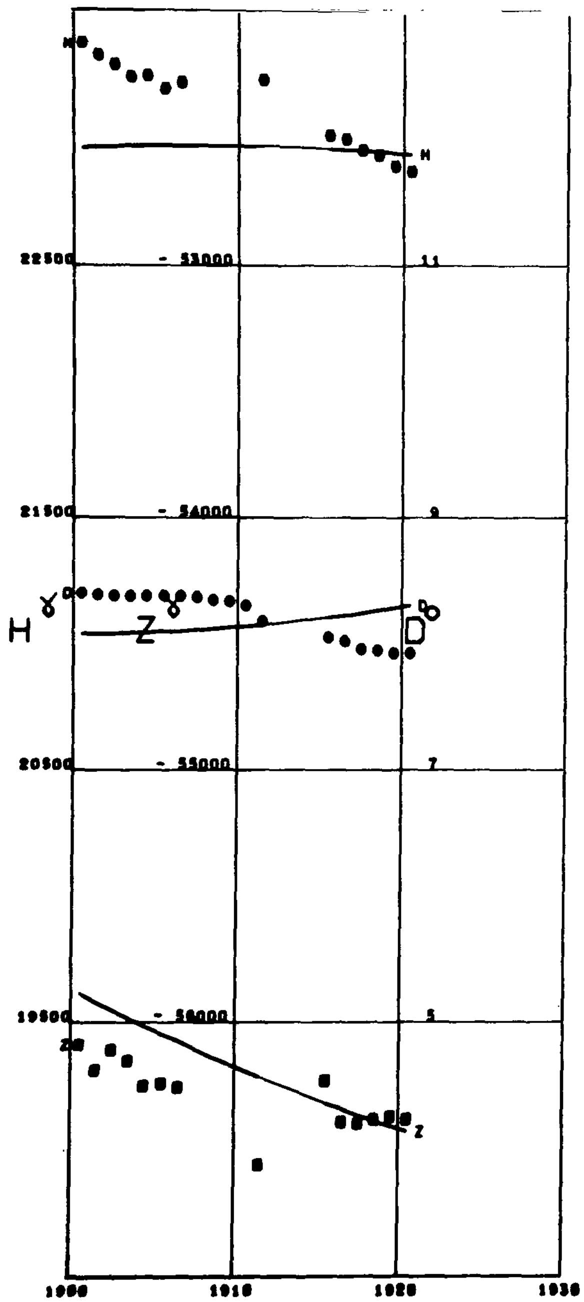

Figure A114

MEMAMBETSU
Lat 43.90 Long 144.19 Alt 0.04

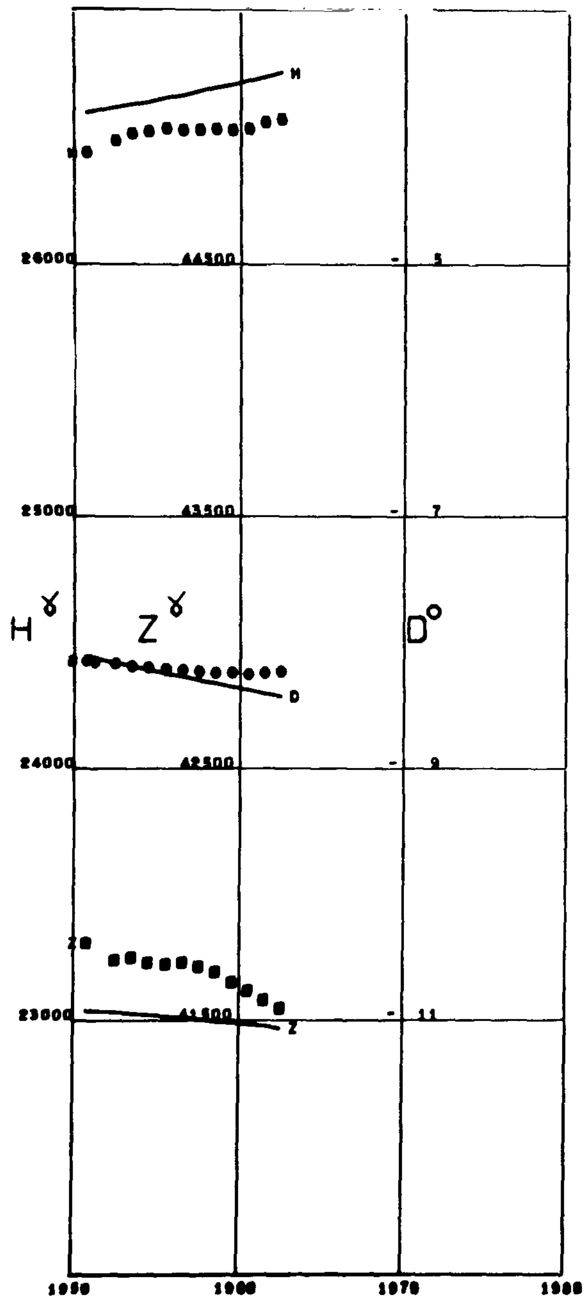

Figure A115

MIRNYY
Lat -66.55 Long 93.01

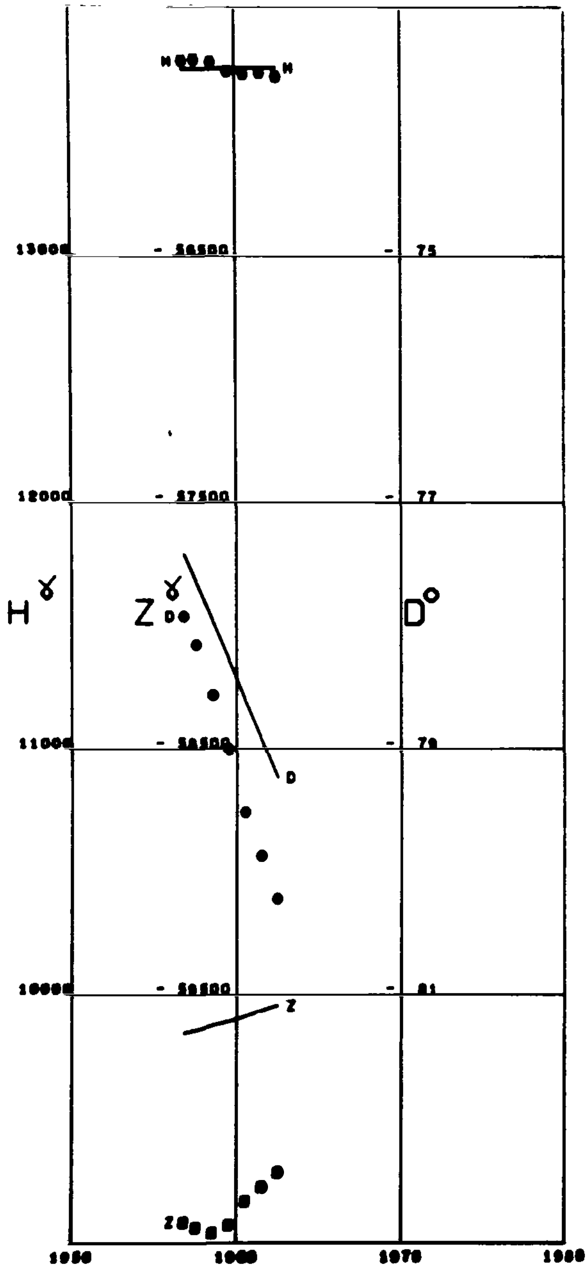

Figure A116

MISALLAT
Lat 29.51 Long 30.89 Alt 0.12

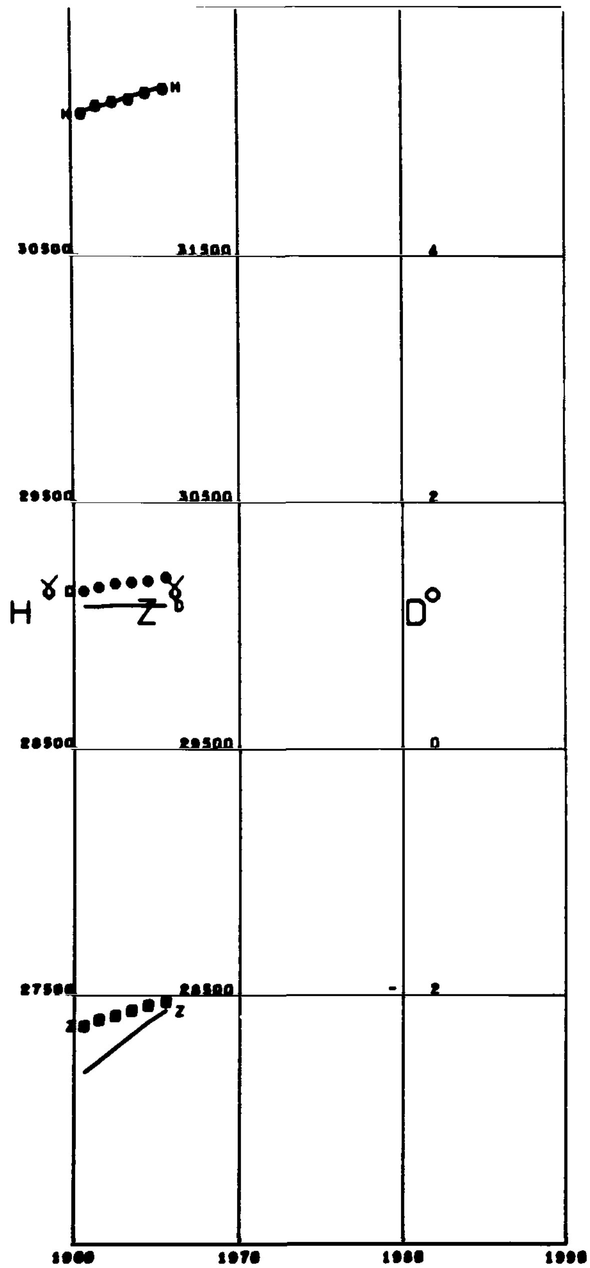

Figure A117

MOCA
Lat 3.34 Long 8.66 Alt 1.35

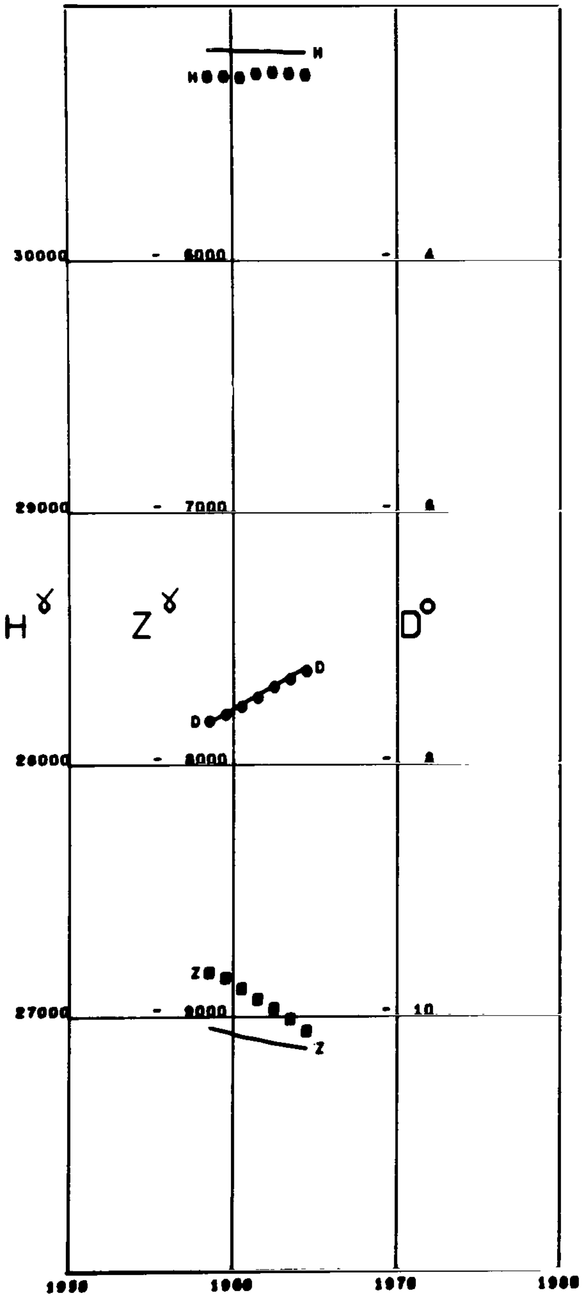

Figure A118

MONTE CAPPELLINO
Lat 44.55 Long 8.95

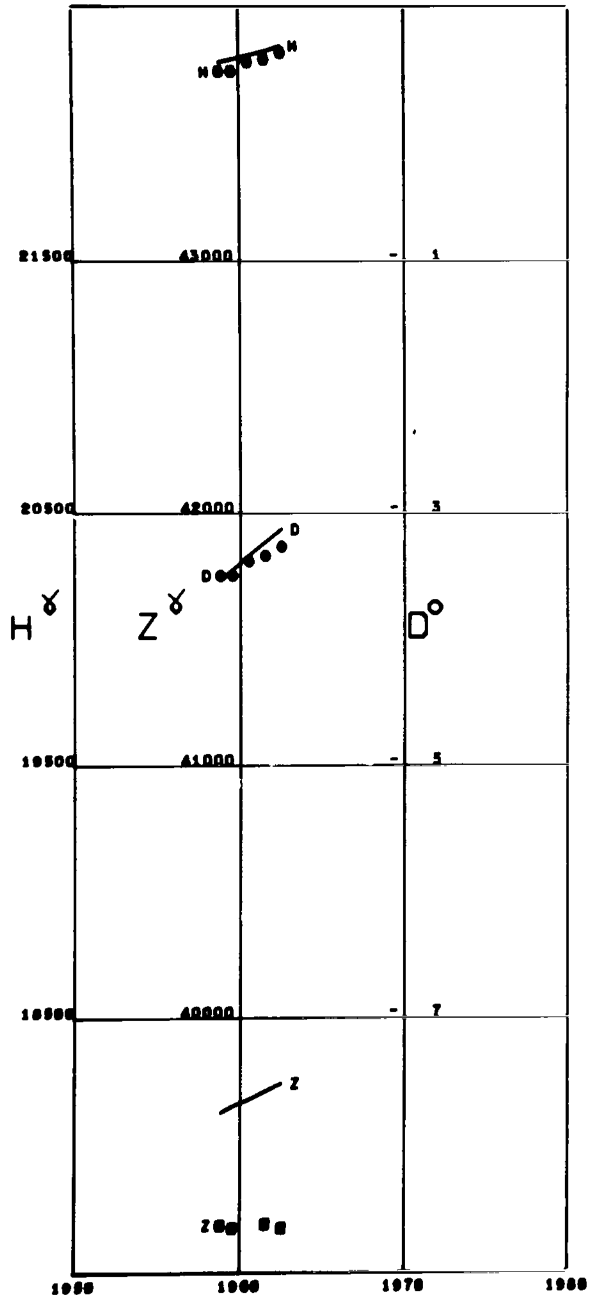

Figure A119

MUNICH
Lat 48.14 Long 11.60

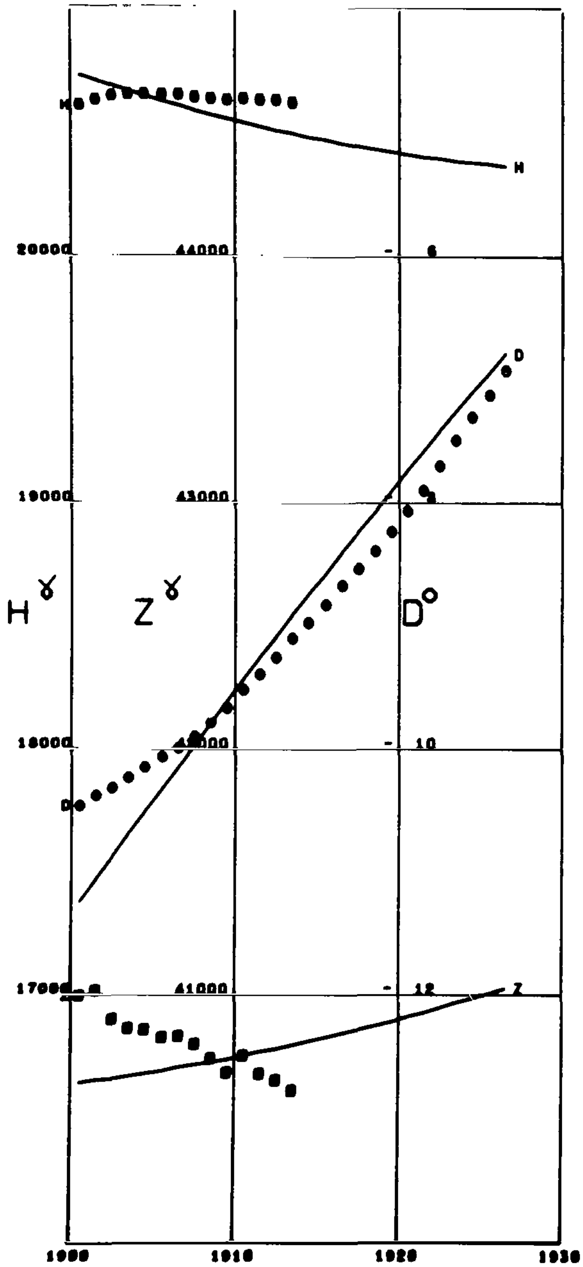

Figure A120

MUNTINLUPA
Lat 14.37 Long 121.01 Alt 0.06

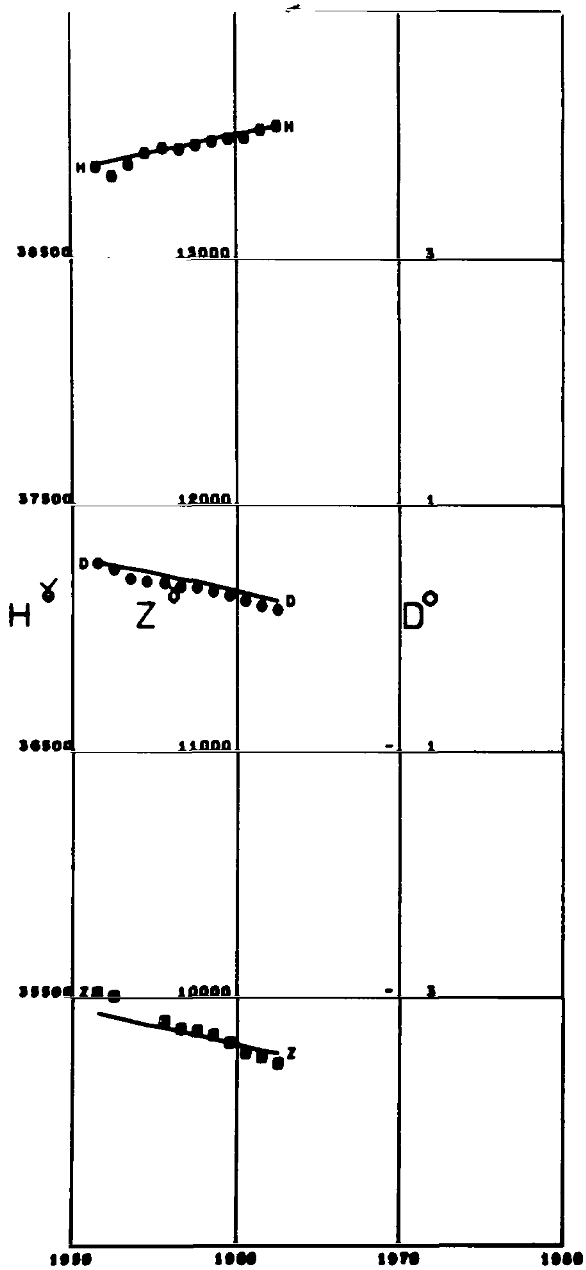

Figure A121

NANTES
Lat 47.24 Long -1.56

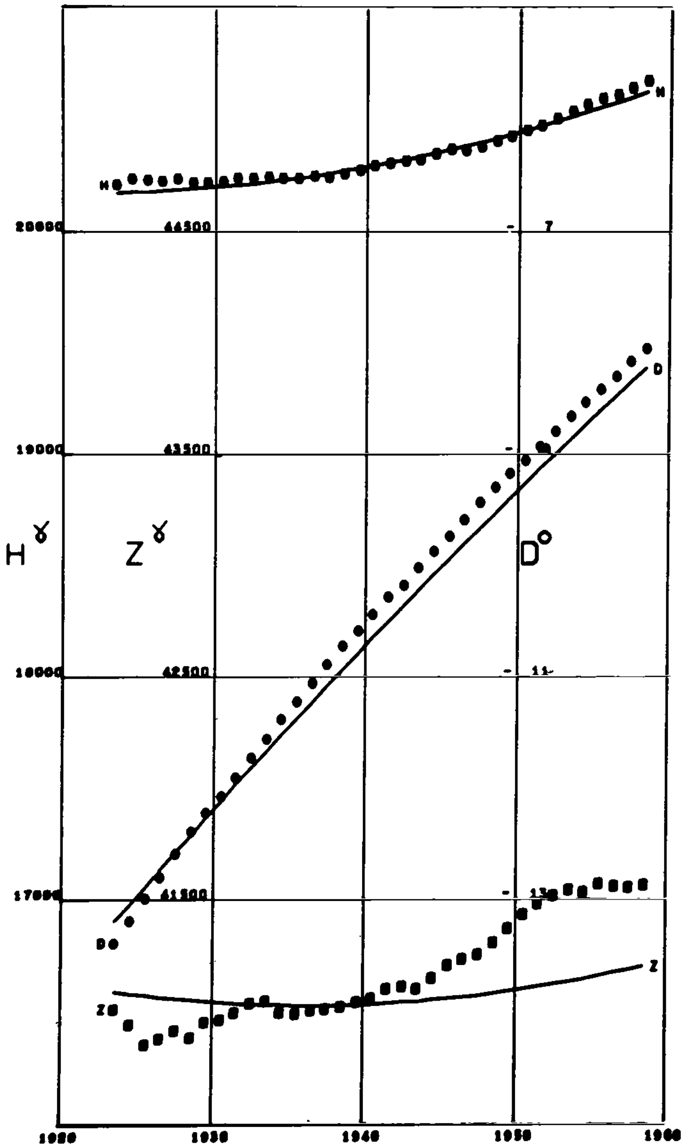

Figure A122

NEW YEARS ISLAND
Lat -54.65 Long -64.15

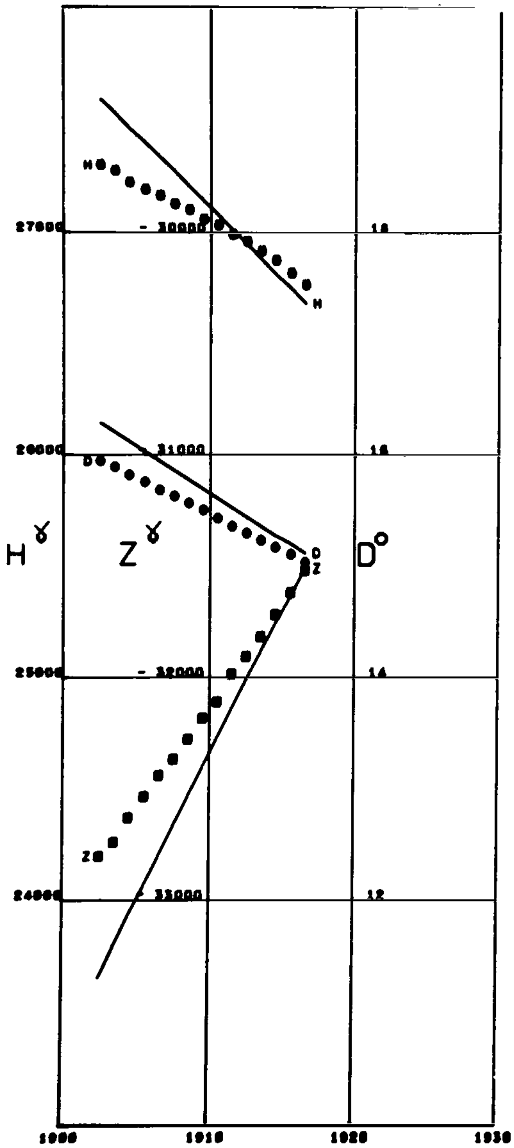

Figure A123

NIEMEGK
Lat 52.07 Long 12.67

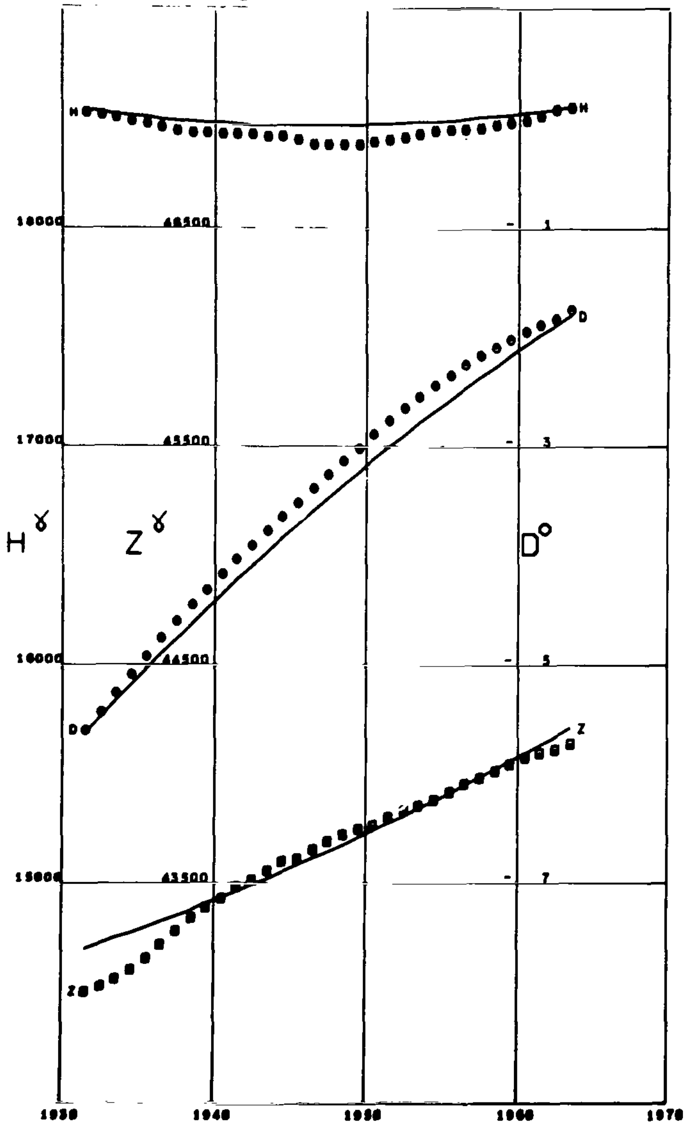

Figure A124

NIZHNEDEVISTSK
Lat 51.51 Long 38.36

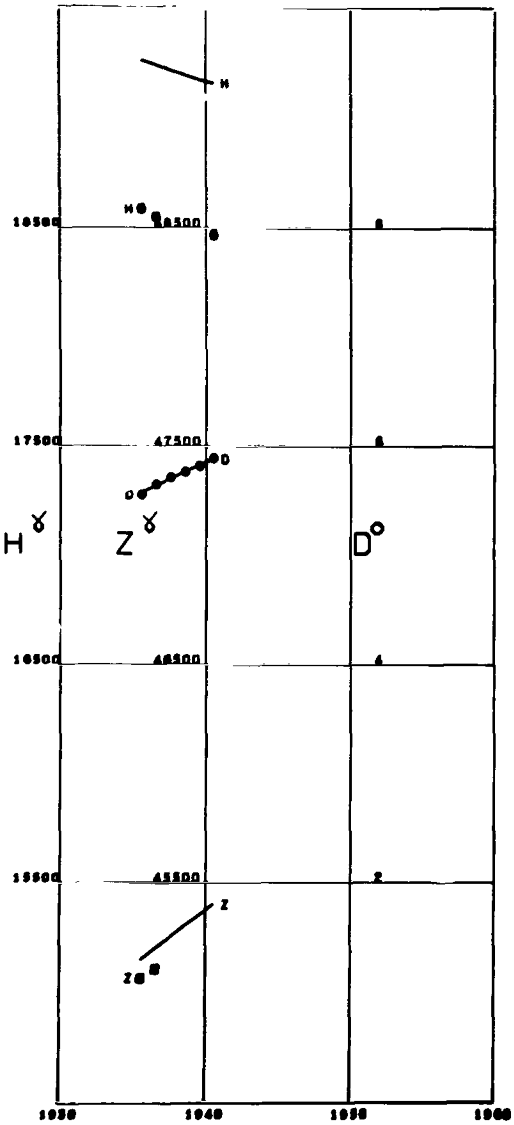

Figure A125

NURMIJARVI
Lat 60.50 Long 24.65 Alt 0.11

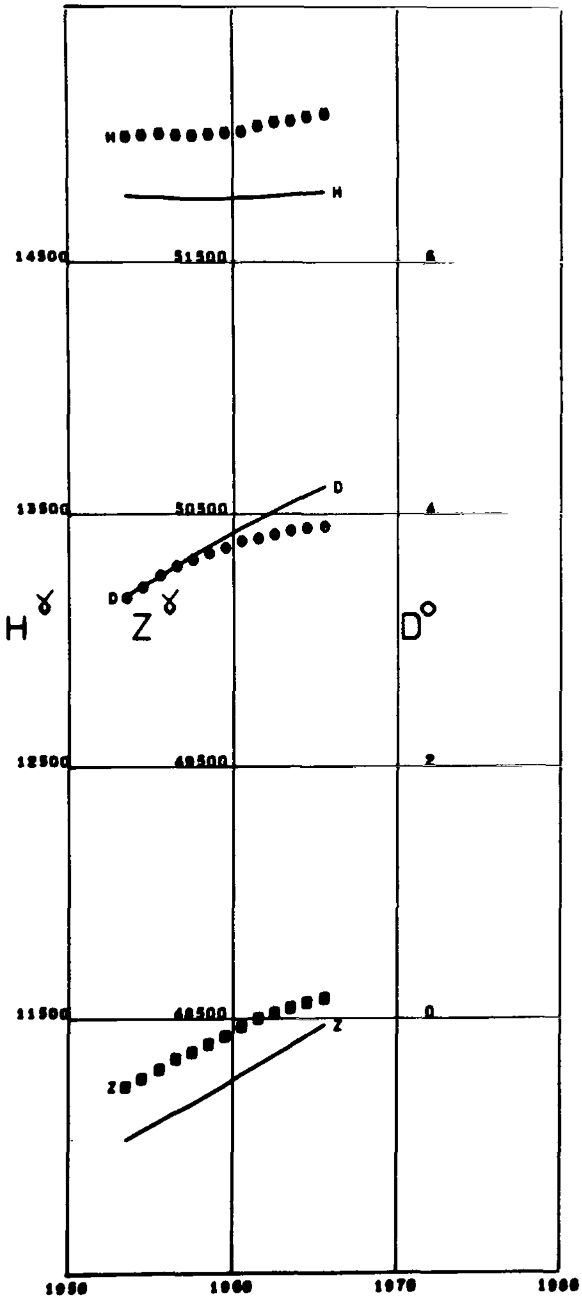

Figure A126

O GYALLA PESTH
Lat 47.87 Long 18.19

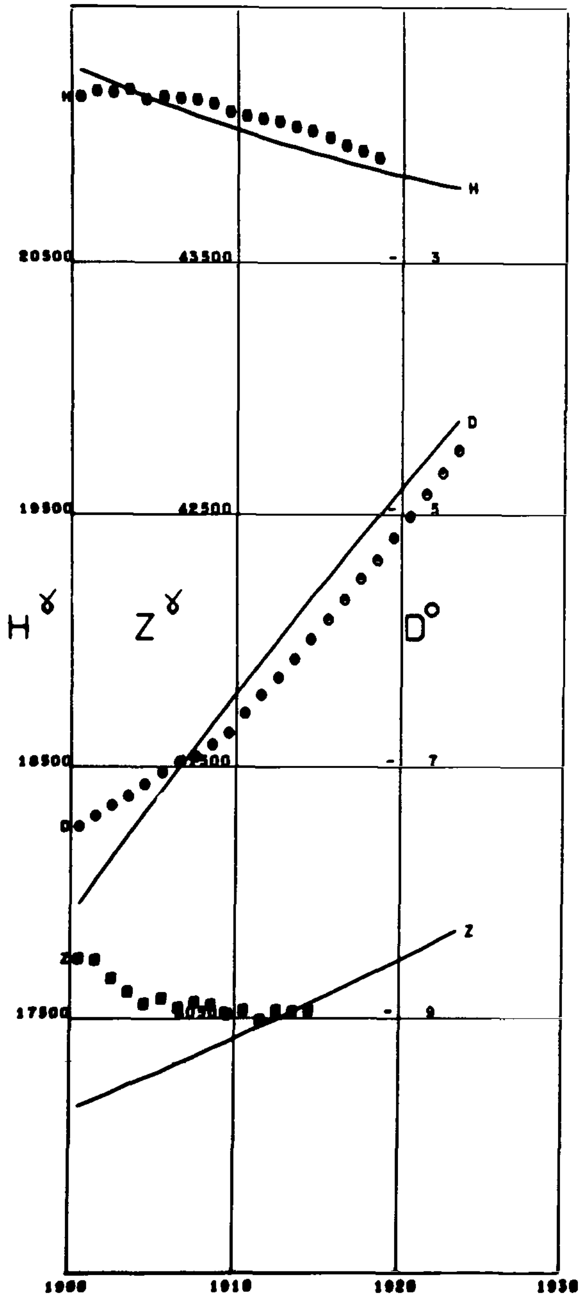

Figure A127

ODESSA
Lat 46.66 Long 30.77

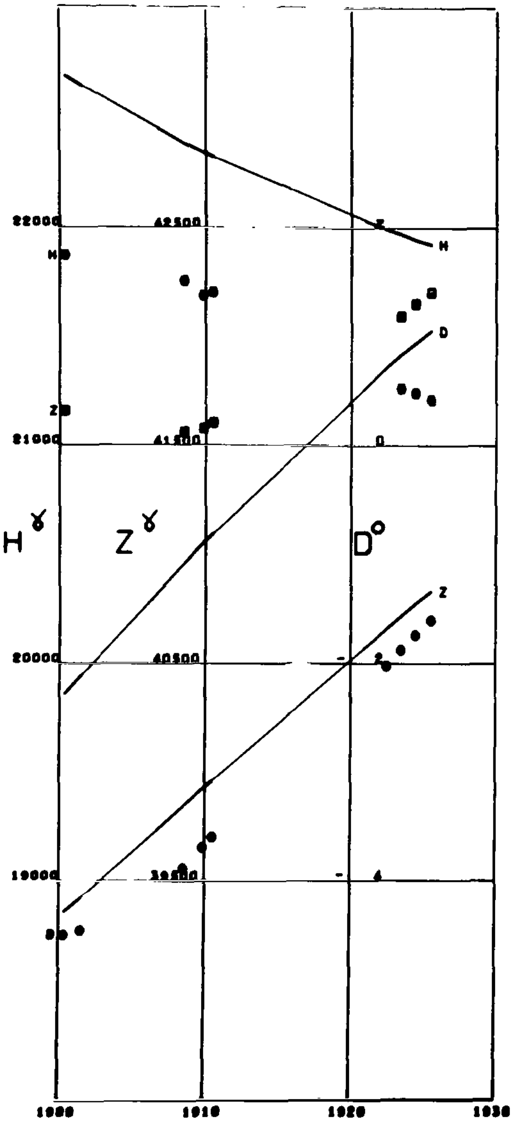

Figure A128

OSLO
Lat 59.91 Long 10.72

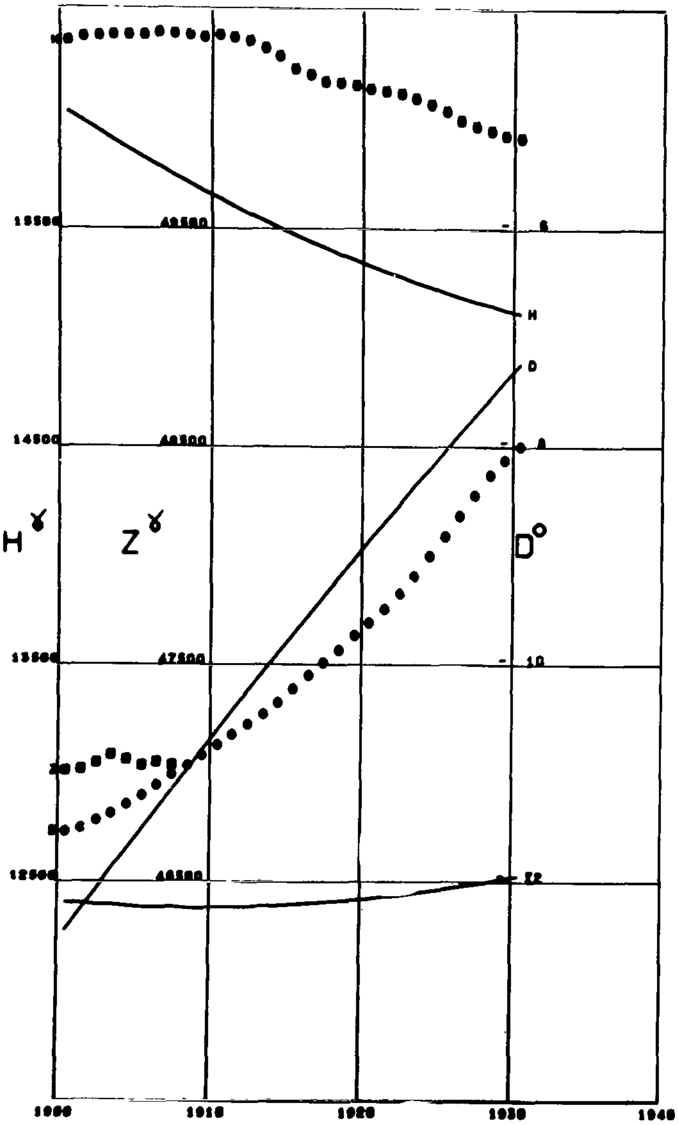

Figure A129

OTOMARI
Lat 46.65 Long 142.76

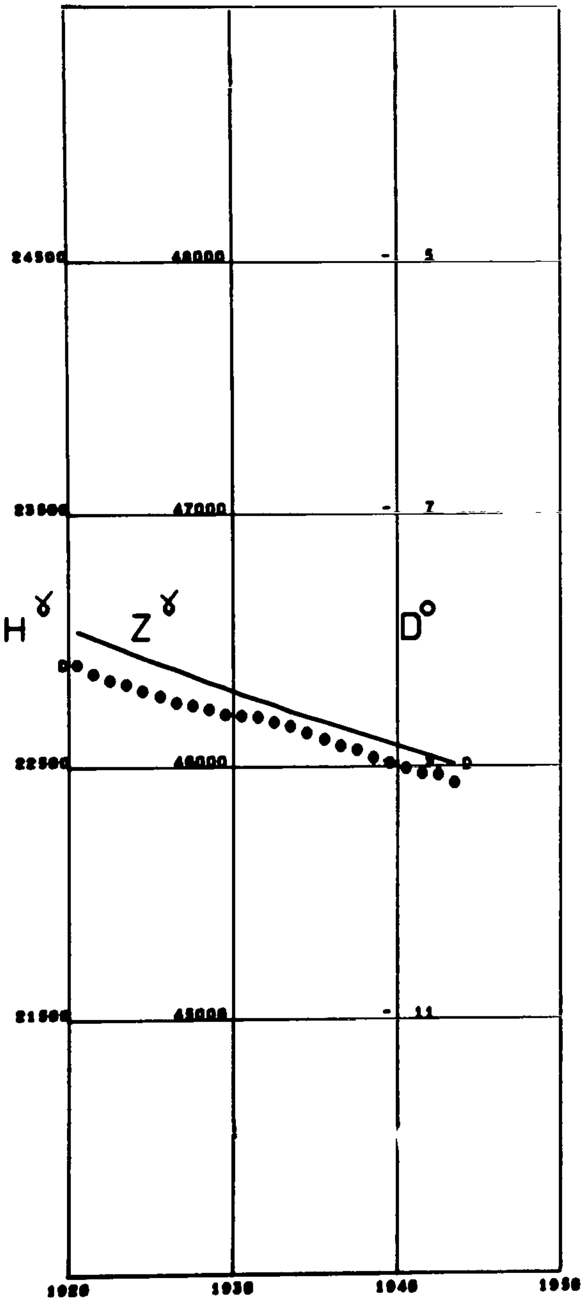

Figure A130

PALAU
Lat 7.33 Long 134.48

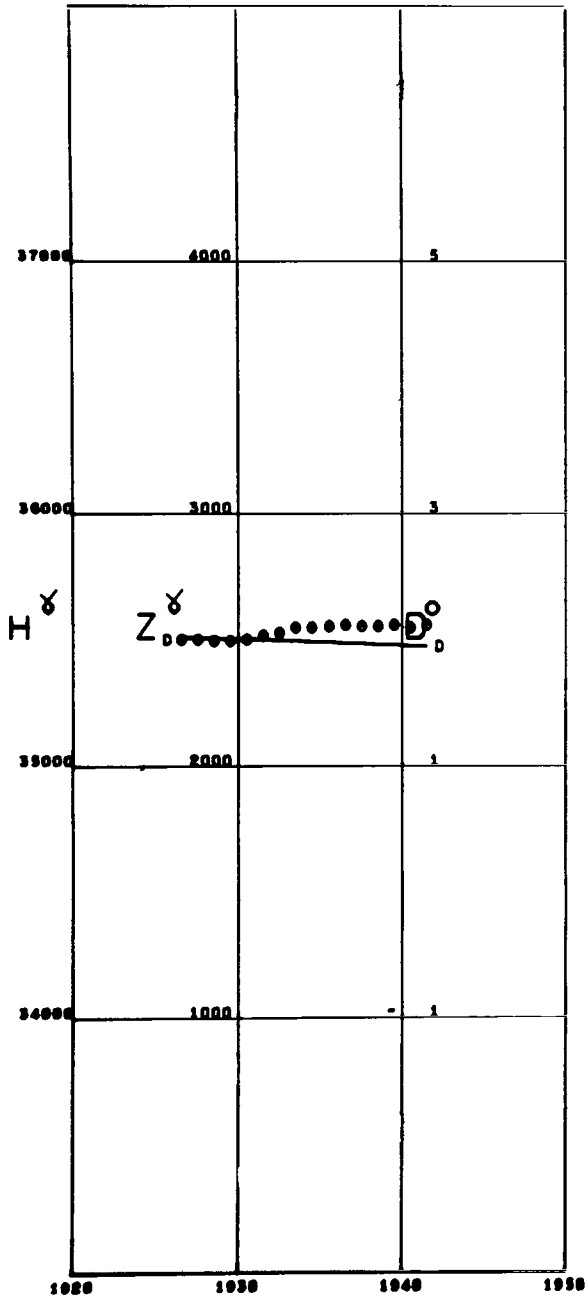

Figure A131

PANAGYURISHTE
Lat 42.51 Long 24.18

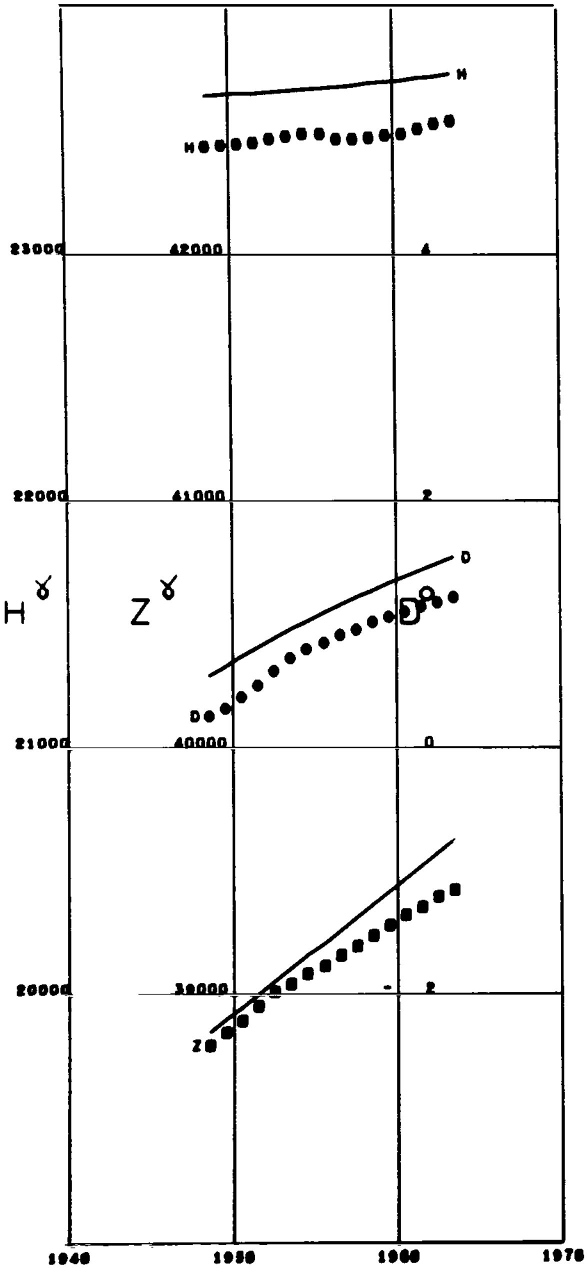

Figure A132

PARAMARIBO
Lat 5.81 Long -55.22 Alt 0.10

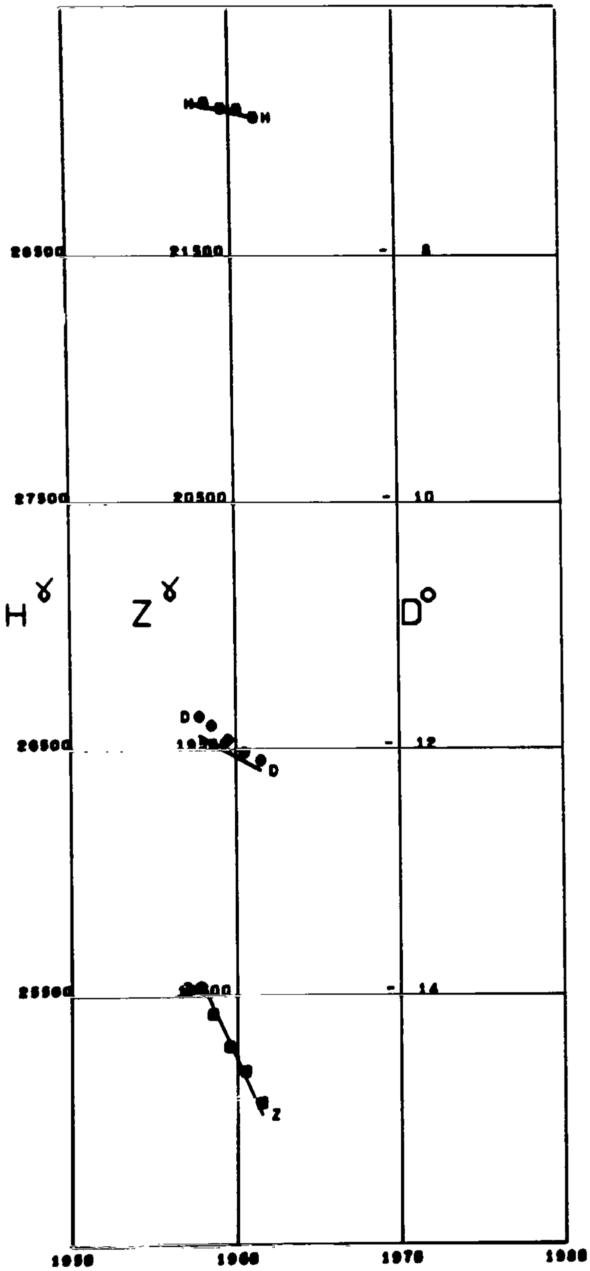

Figure A133

PATRONY
Lat 52.16 Long 104.45 Alt 0.76

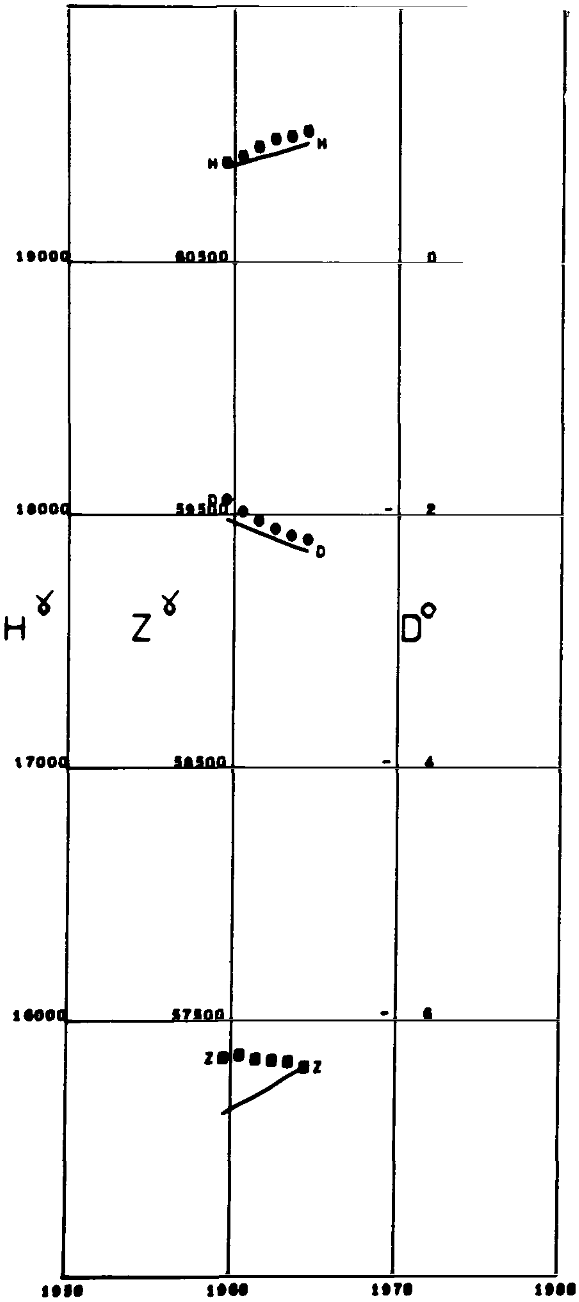

Figure A134

PERPIGNAN
Lat 42.70 Long 2.88

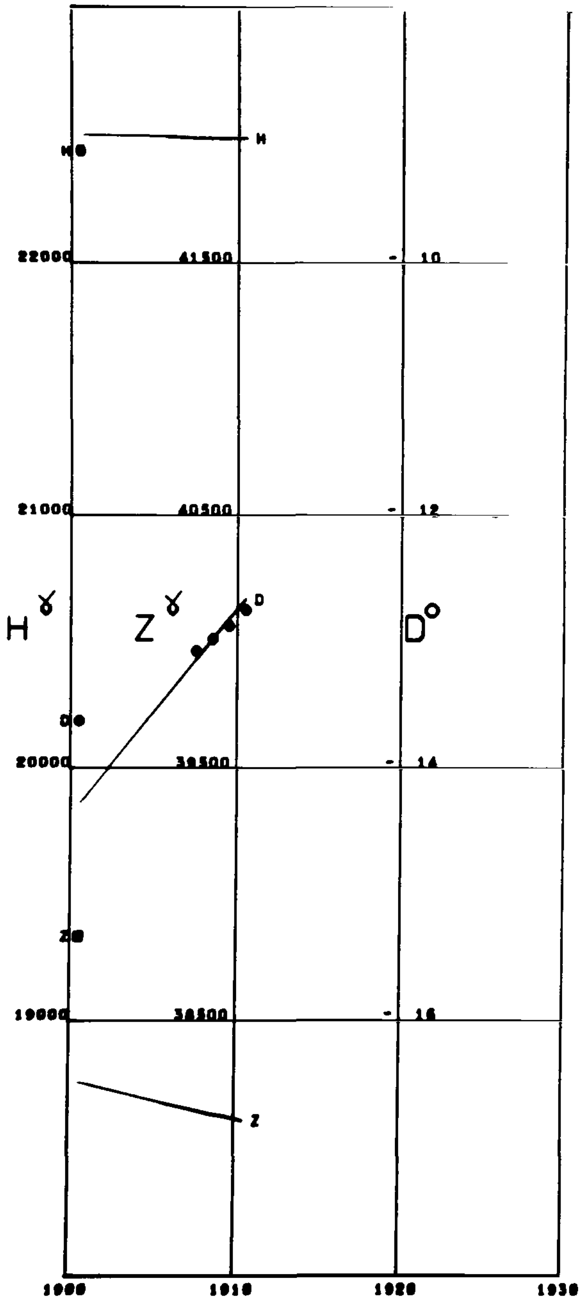

Figure A135

PILAR
Lat -31.66 Long -63.88 Alt 0.34

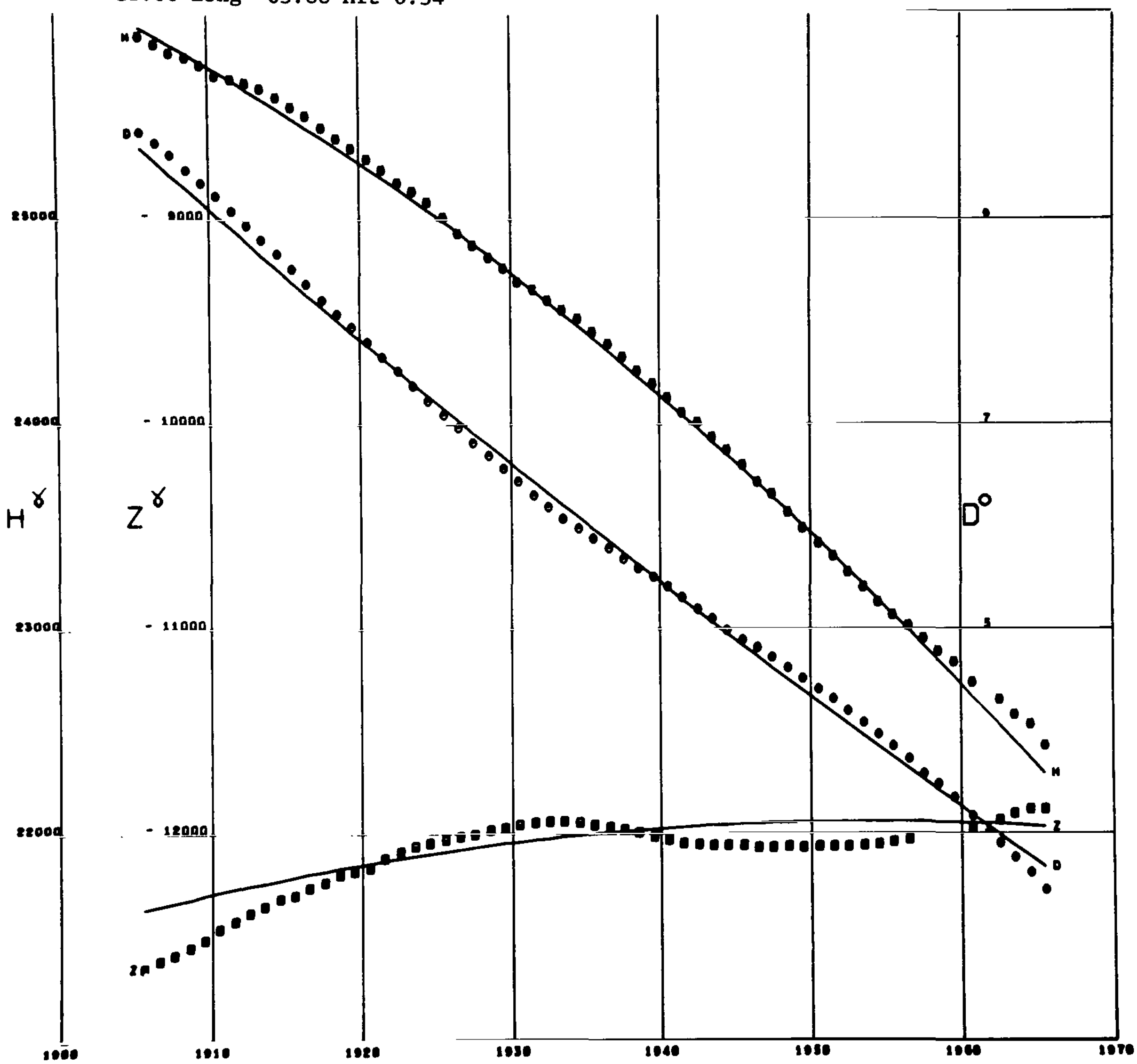

Figure A136

POLA
Lat 44.86 Long 13.84

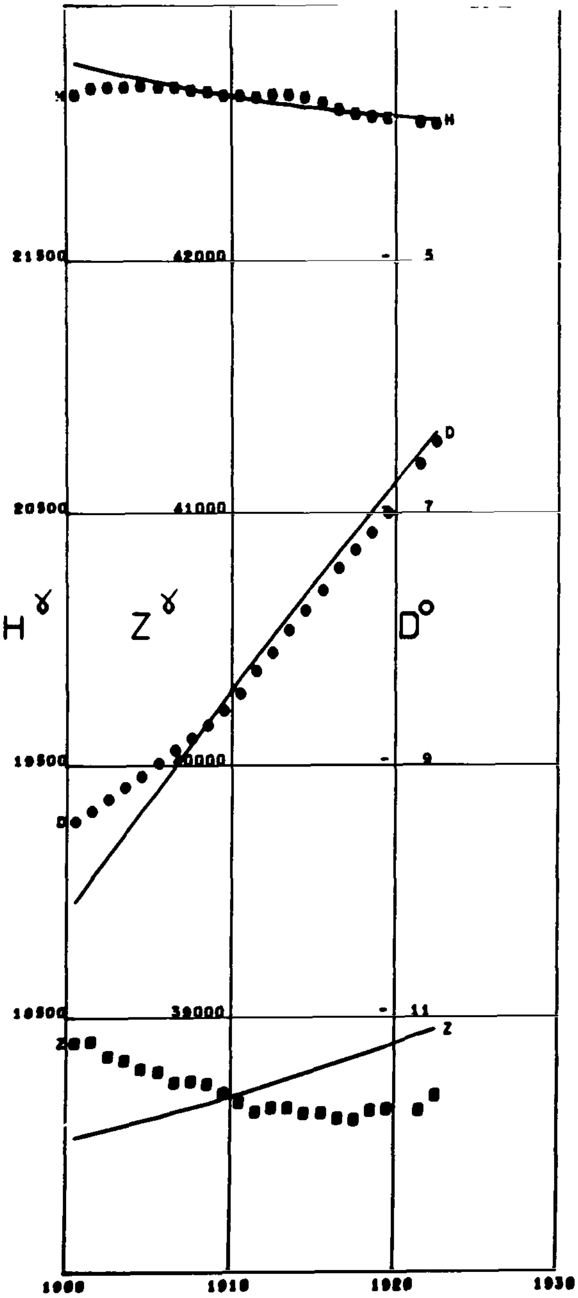

Figure A137

PORT MORESBY
Lat -9.40 Long 147.15 Alt 0.08

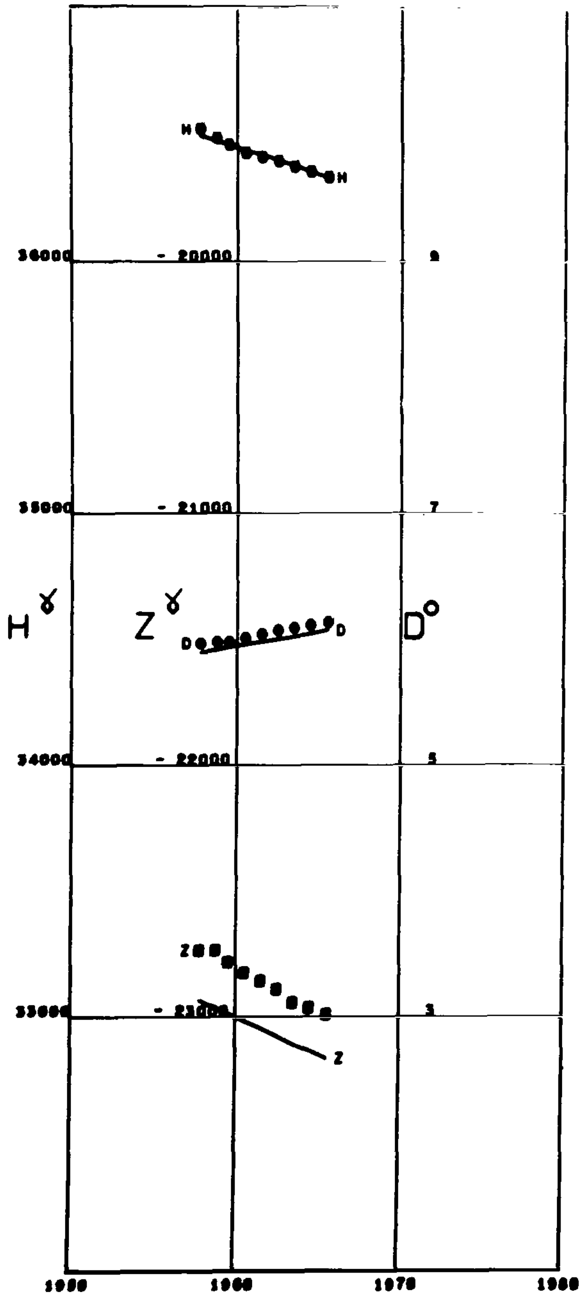

Figure A138

POTSDAM
Lat 52.38 Long 13.06

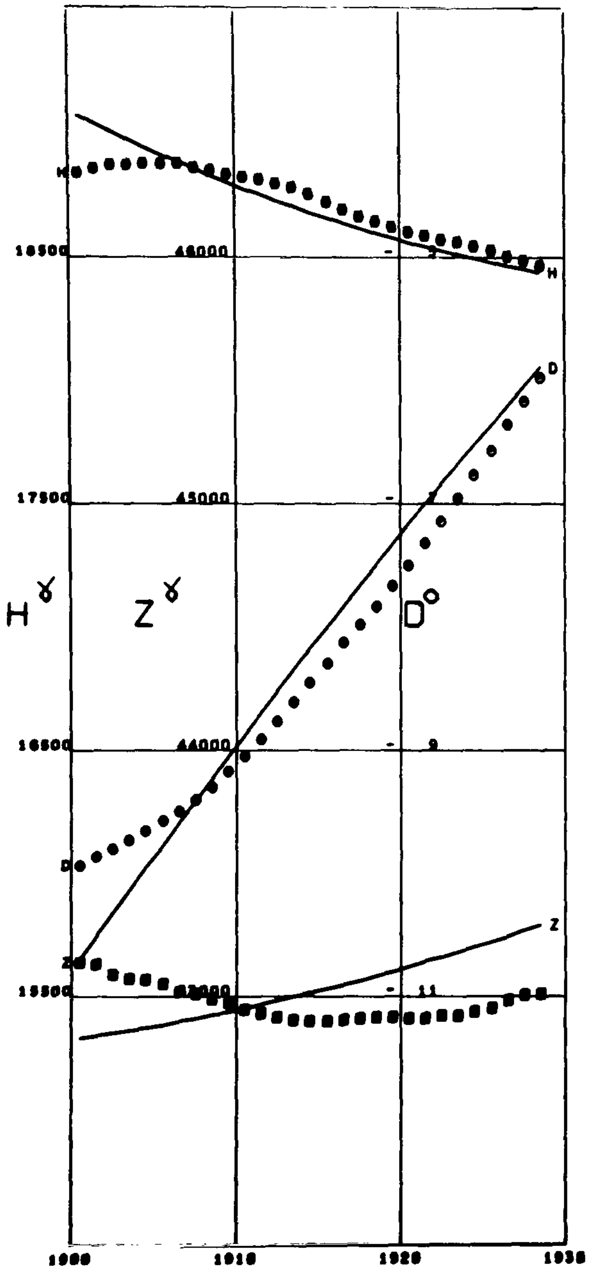

Figure A139

PRAGUE
Lat 50.08 Long 14.41

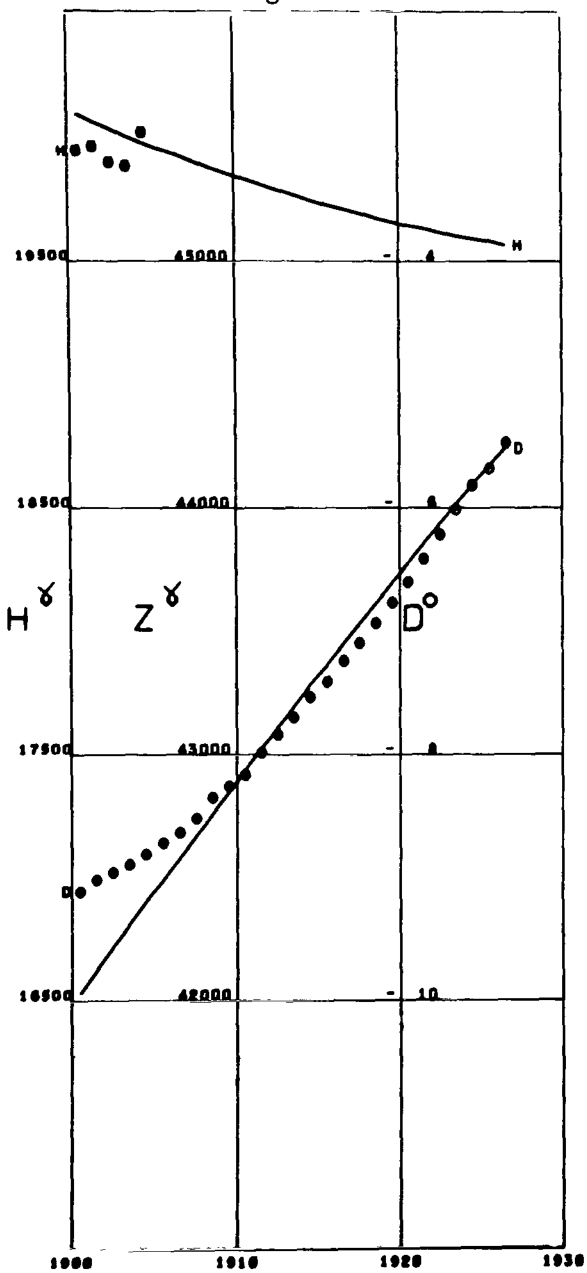

Figure A140

PRUHONICE
Lat 49.99 Long 14.54

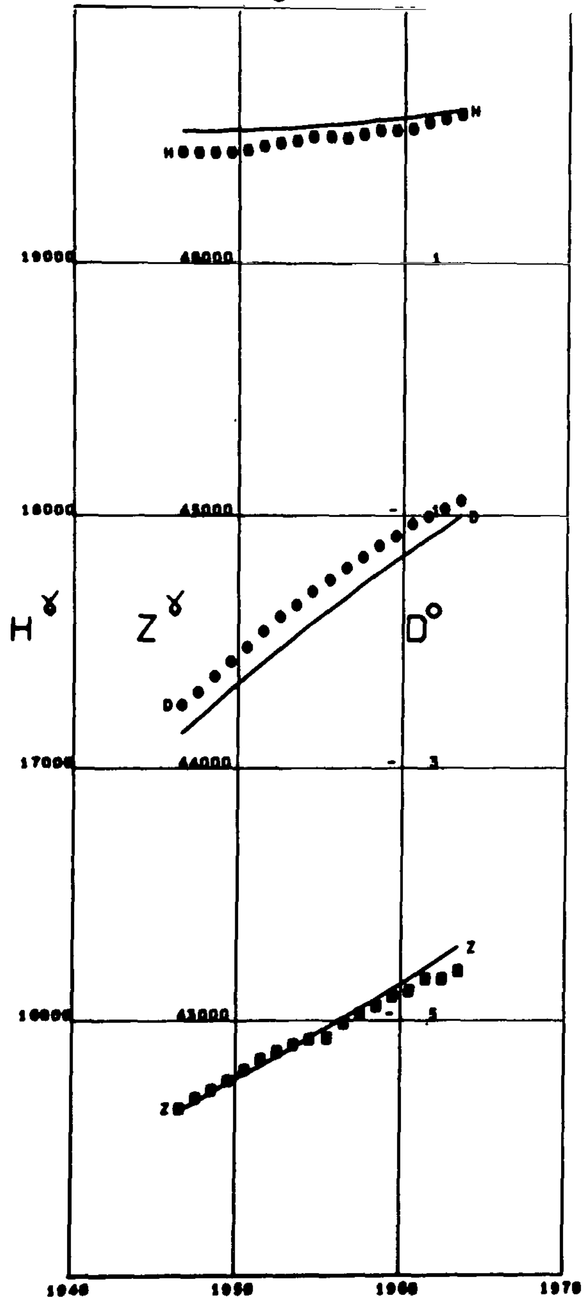

Figure A141

QUETTA
Lat 30.18 Long 66.95

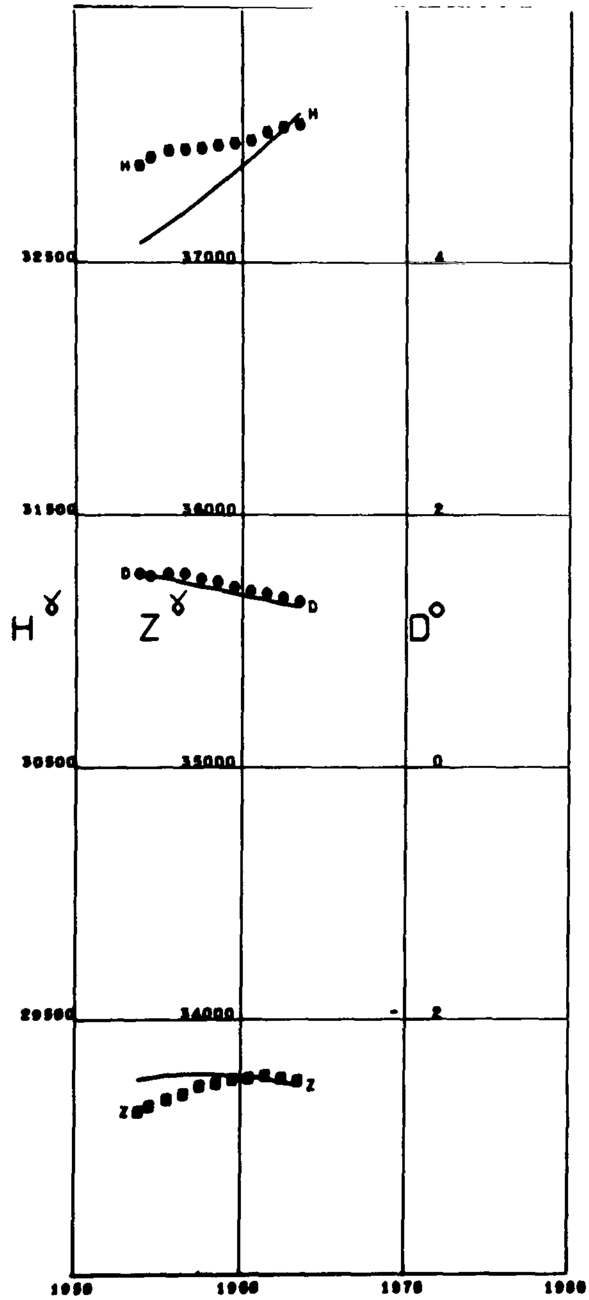

Figure A142

QUIACA
Lat -22.10 Long -65.60

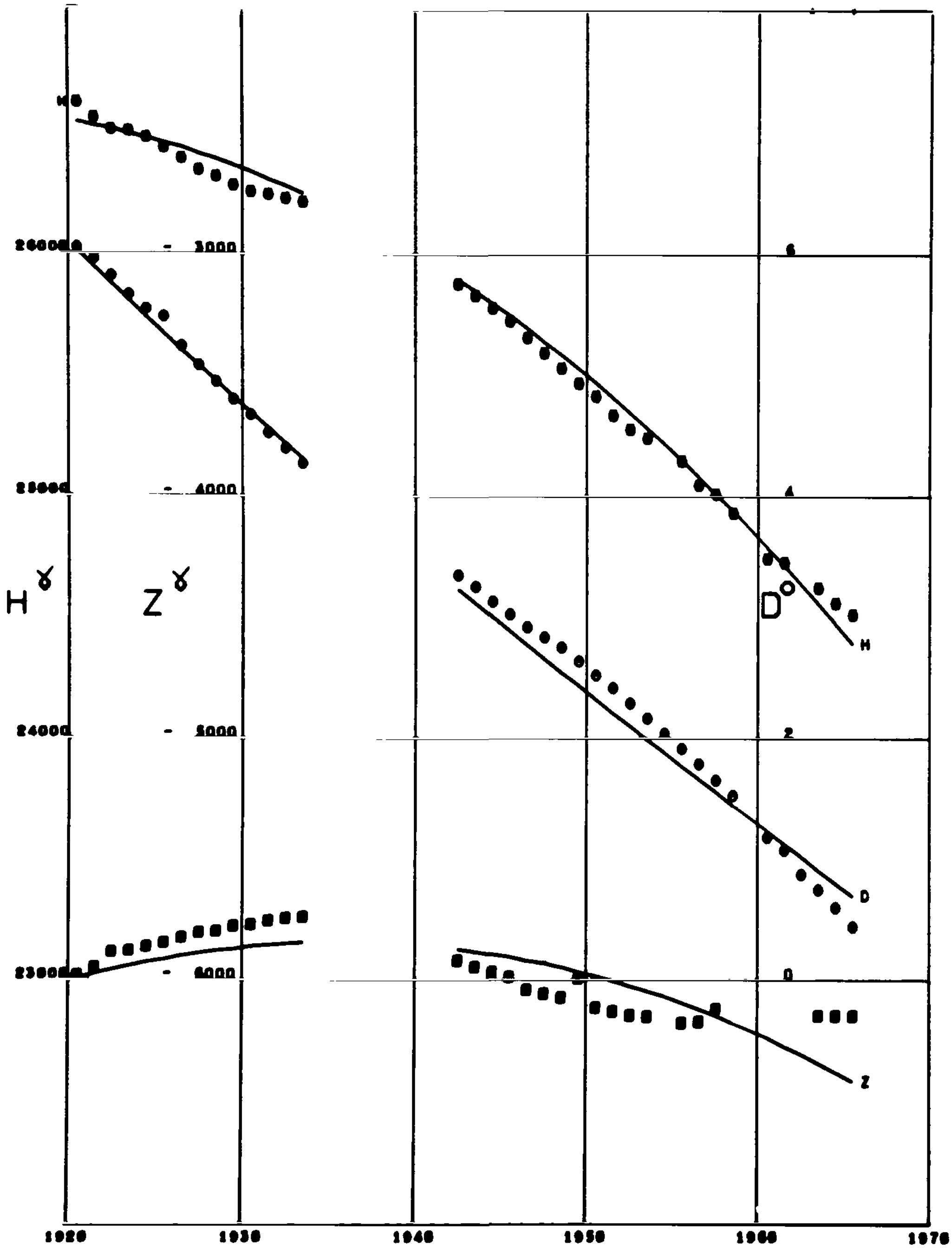

Figure A143

REGENSBERG
Lat 47.48 Long 8.44

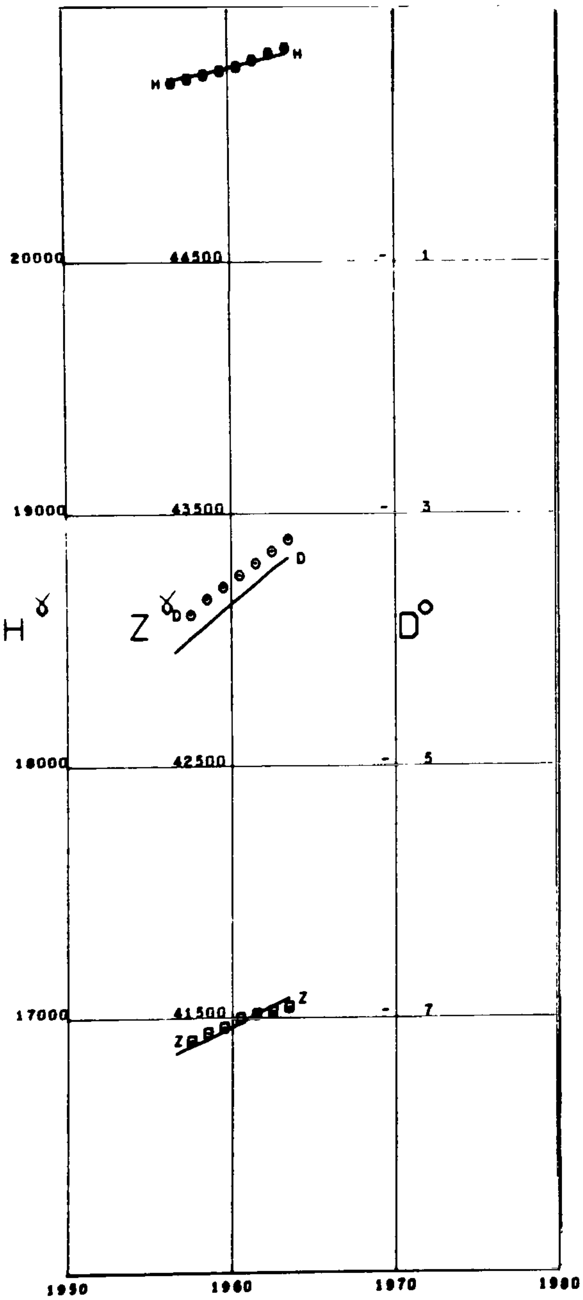

Figure A144

RIO DE JANEIRO
Lat -22.90 Long -43.17

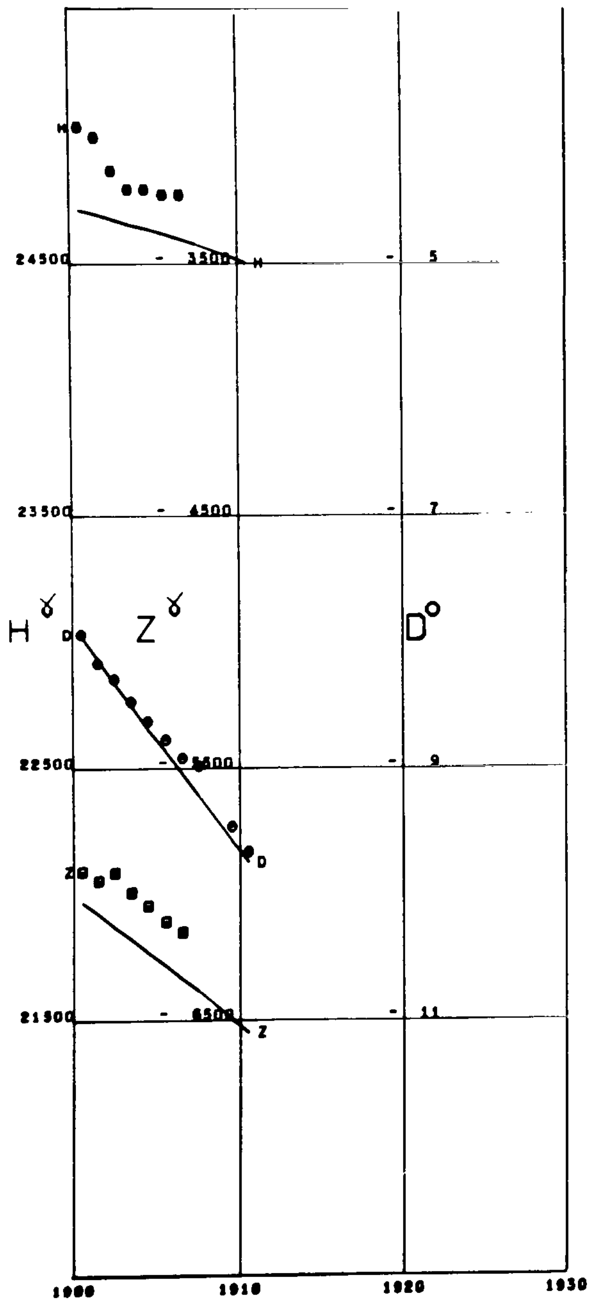

Figure A145

RUDE SKOV
Lat 55.84 Long 12.45 Alt 0.05

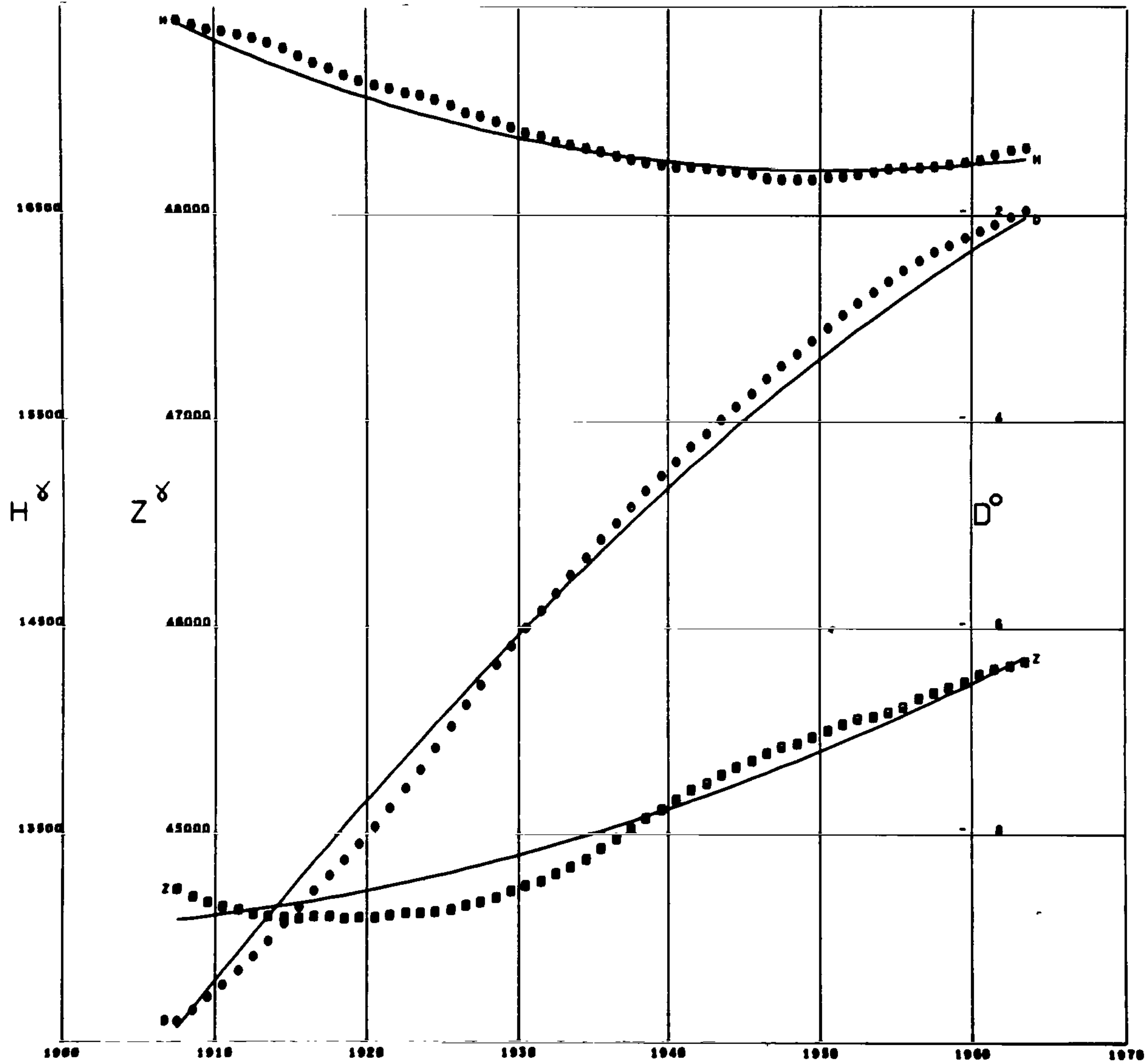

Figure A146

SAN FERNANDO
Lat 36.46 Long -6.20

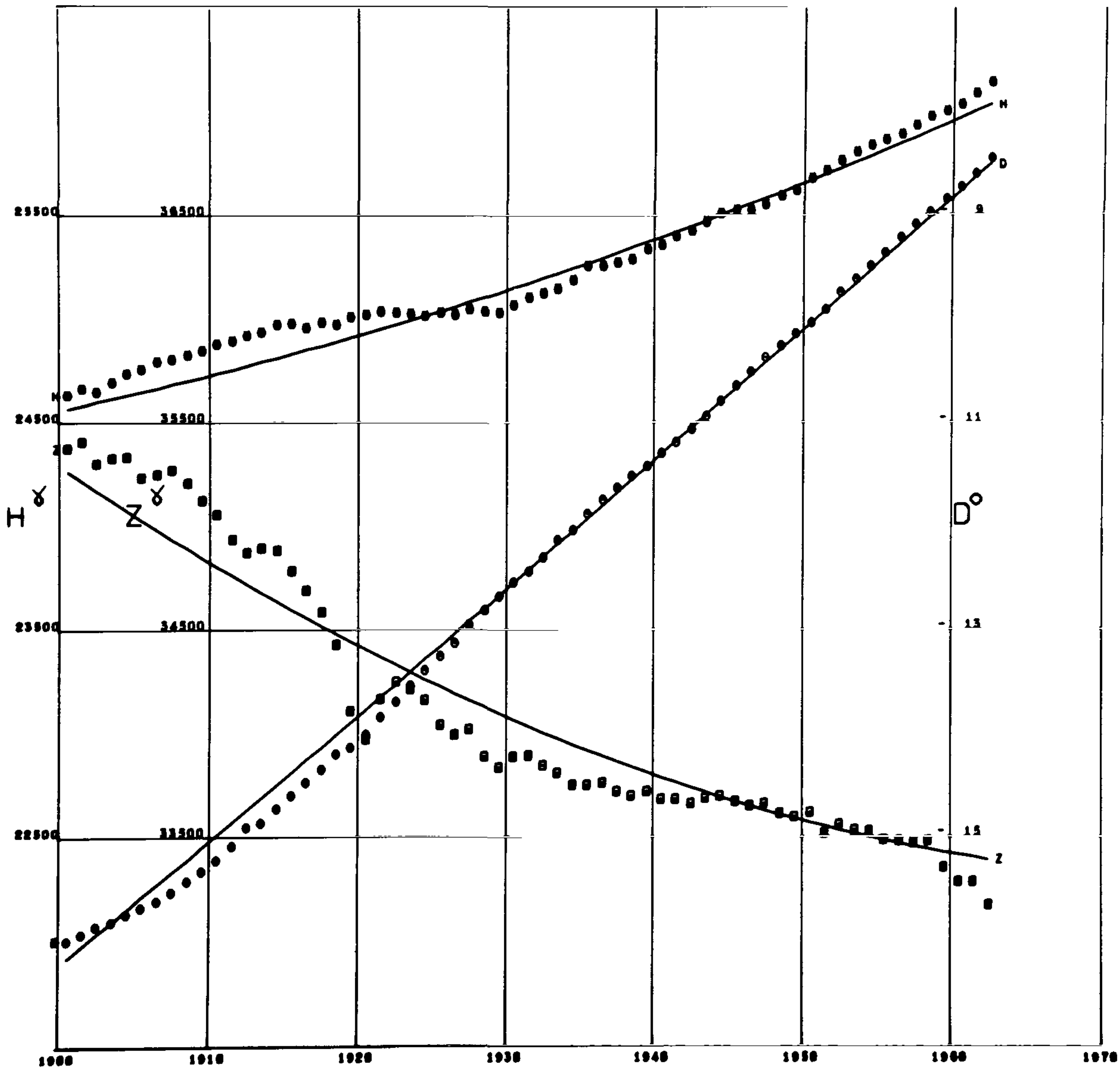

Figure A147

SAN JUAN
Lat 18.11 Long -66.15 Alt 0.40

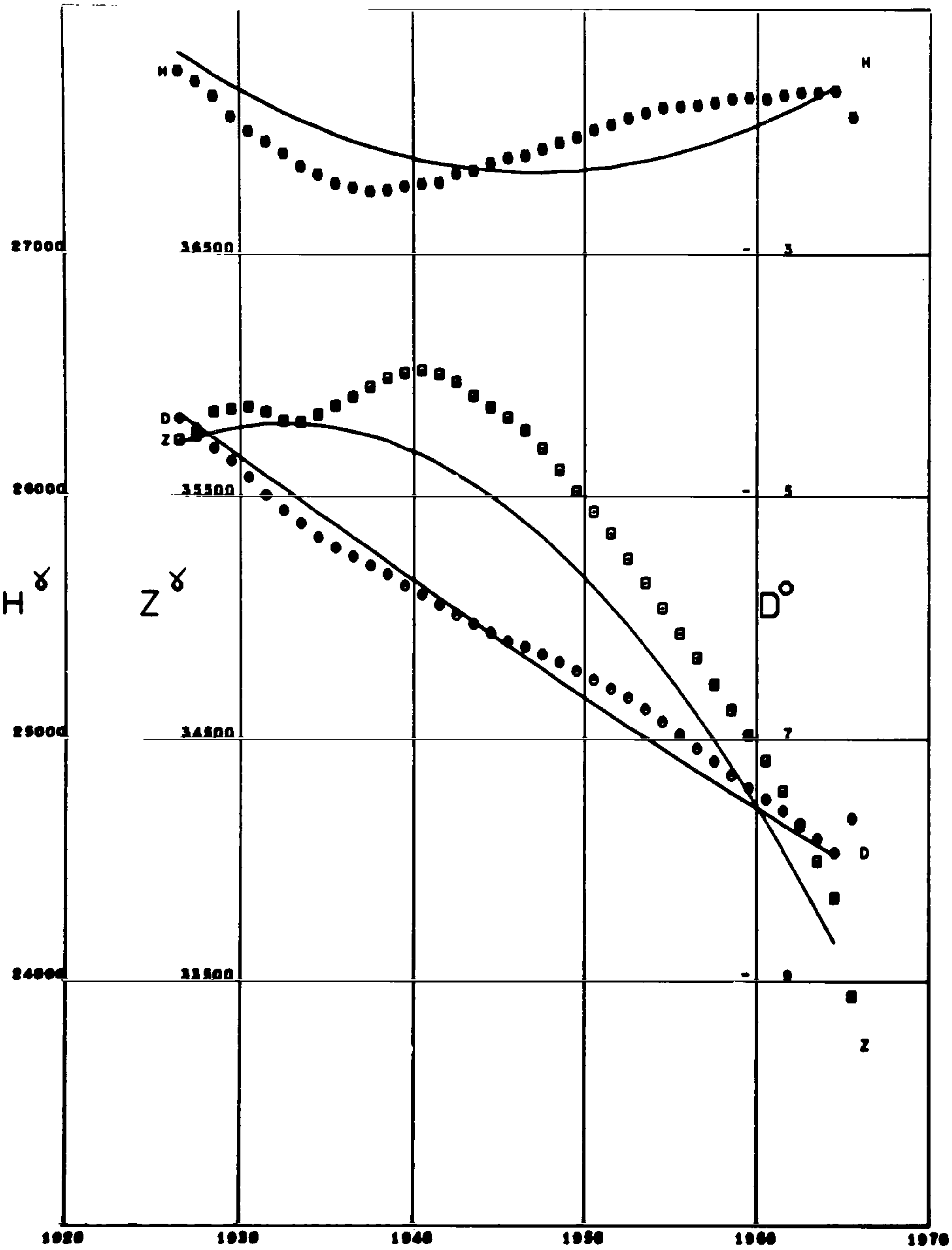

Figure A148

SAN MIGUEL
Lat 37.76 Long -25.65

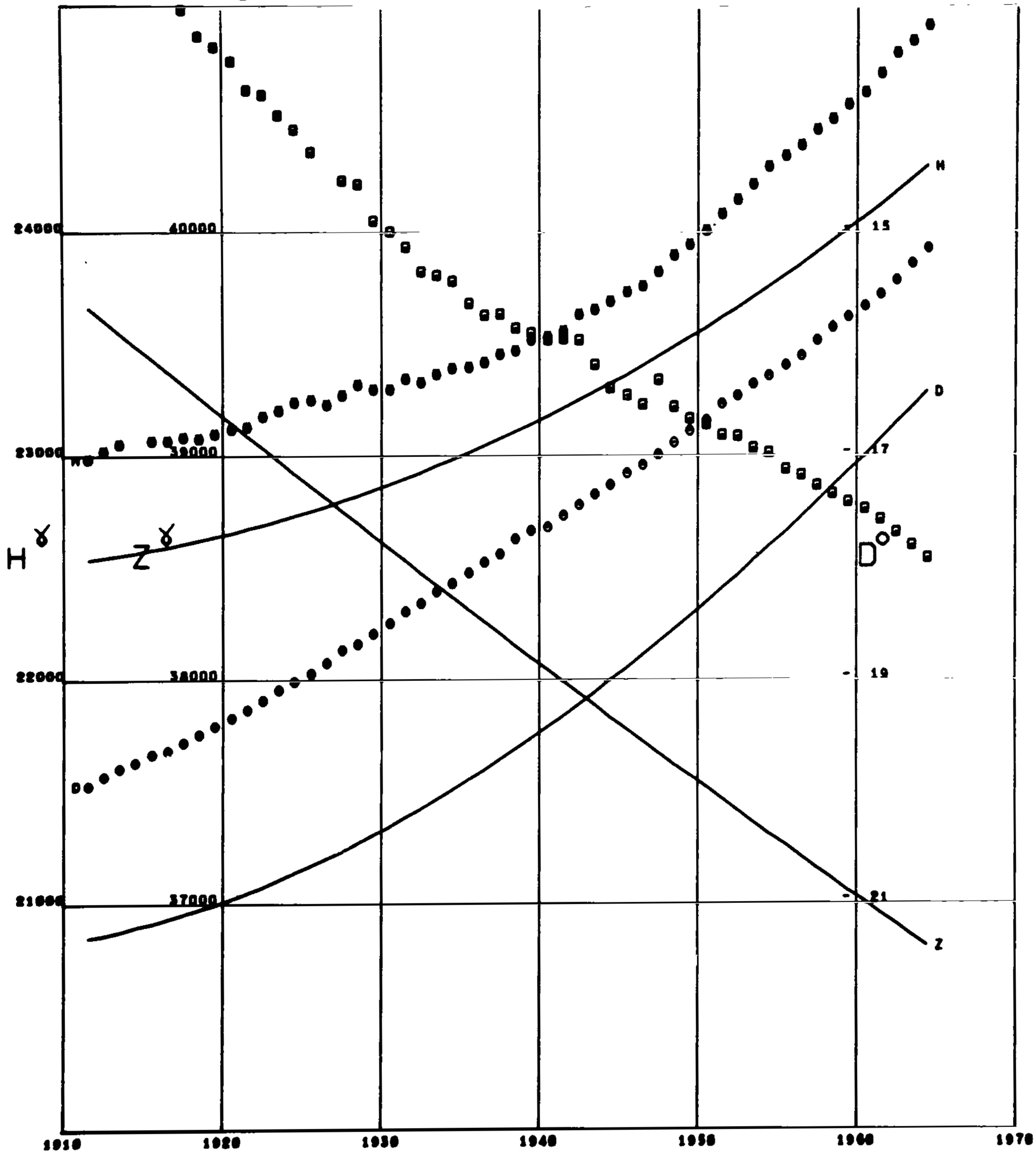

Figure A149

SANTIAGO
Lat -33.45 Long -70.70

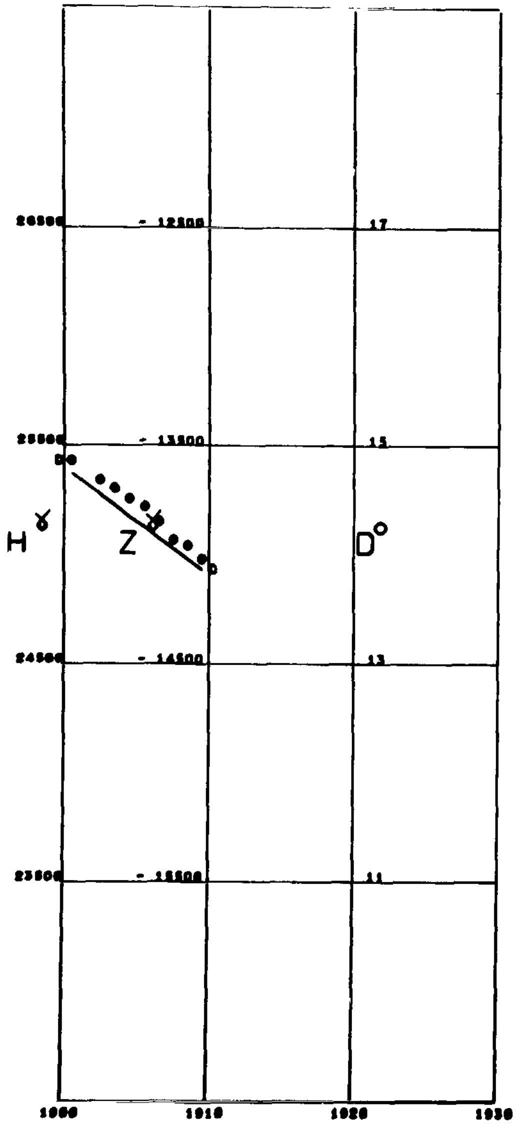

Figure A150

SEDDIN
Lat 52.27 Long 13.01

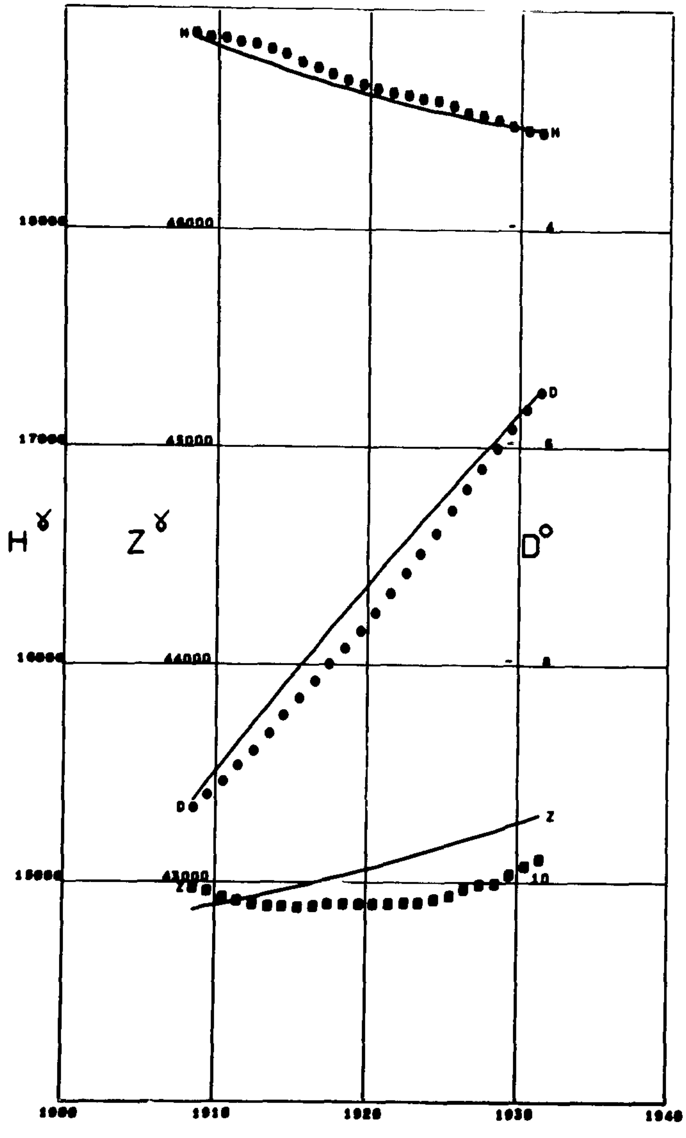

Figure A151

SIMOSATO
Lat 33.57 Long 135.94

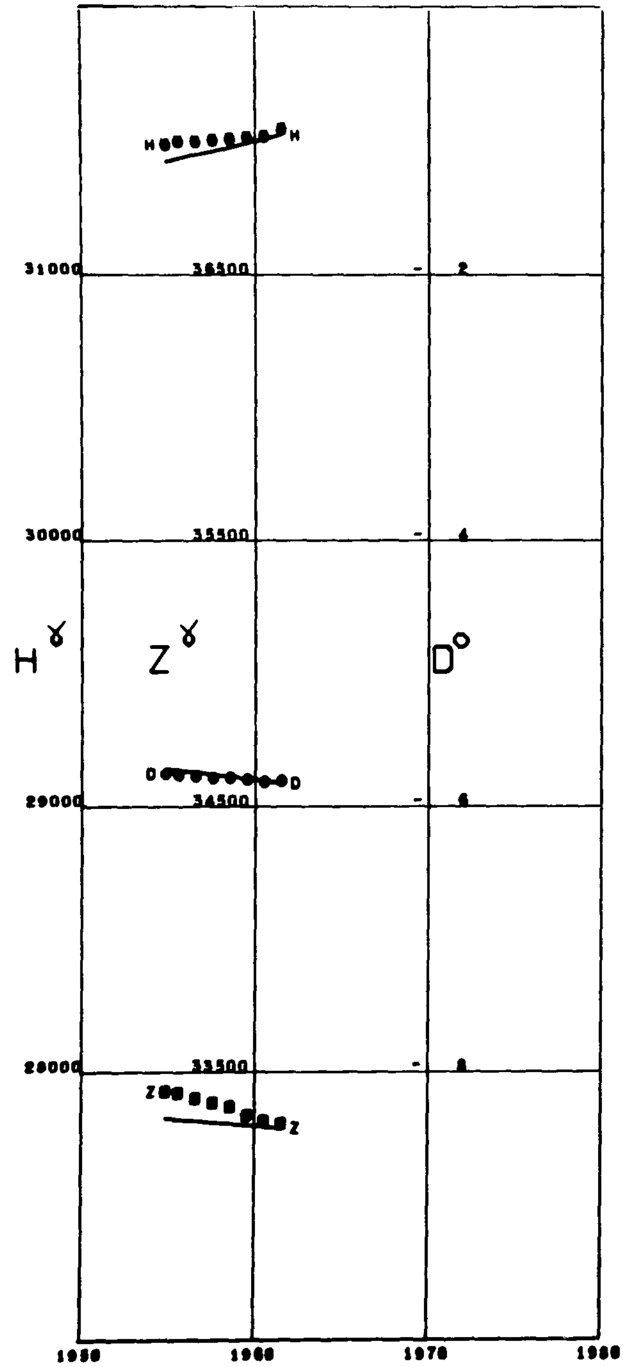

Figure A152

SITKA
Lat 57.05 Long -135.32 Alt 0.02

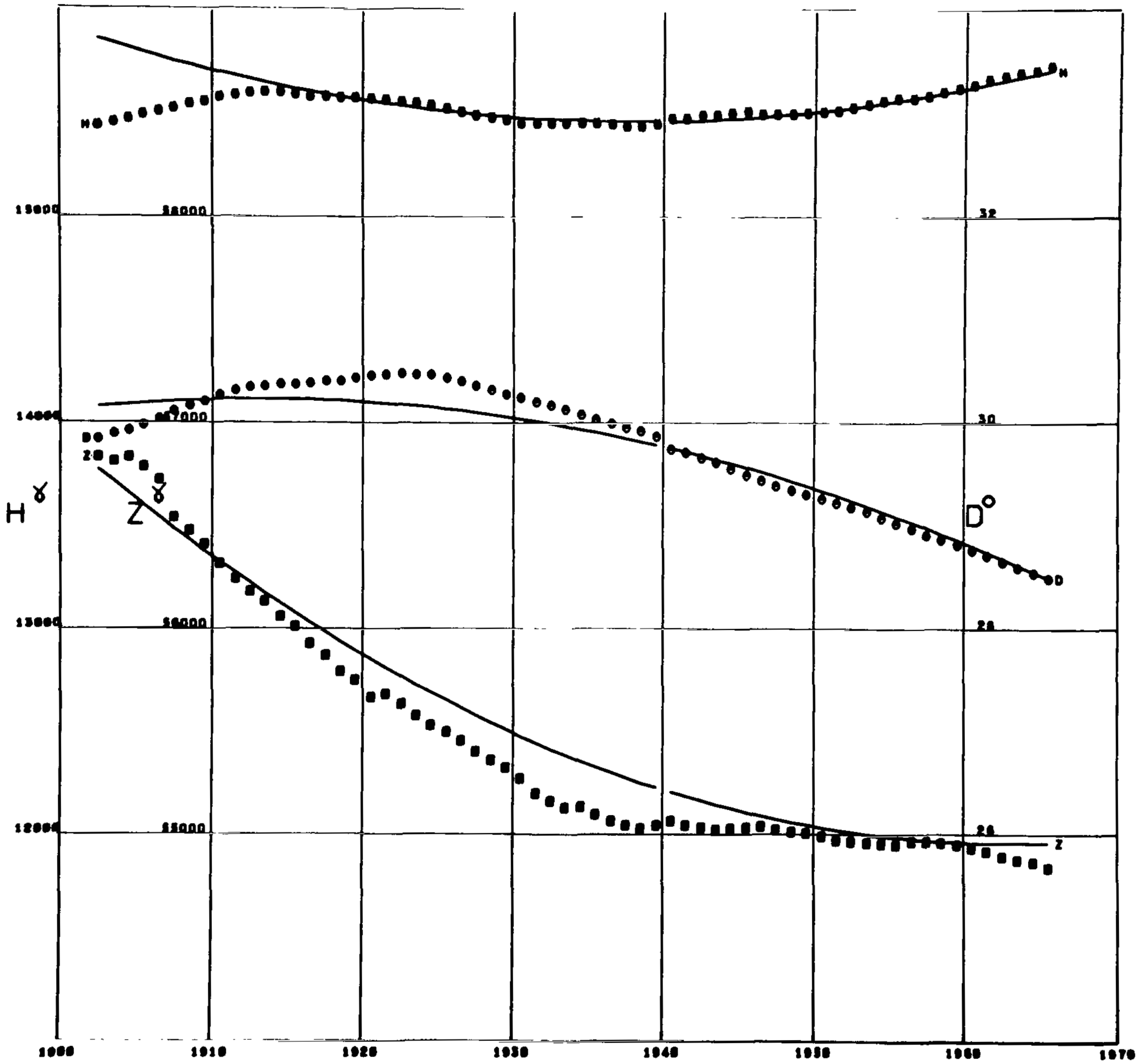

Figure A153

SLUTZK
Lat 59.68 Long 30.48

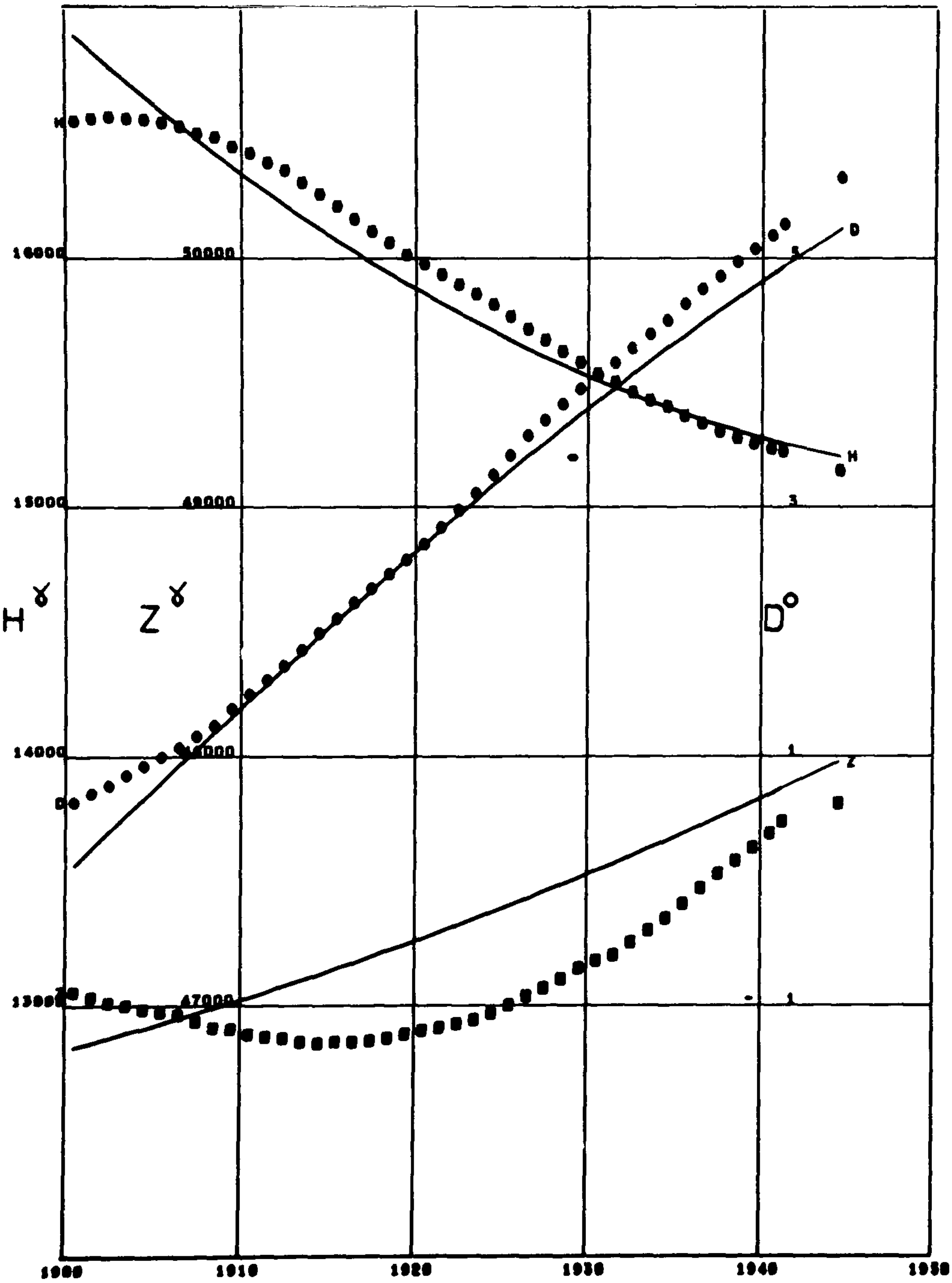

Figure A154

SODANKYLA
Lat 67.36 Long 26.63

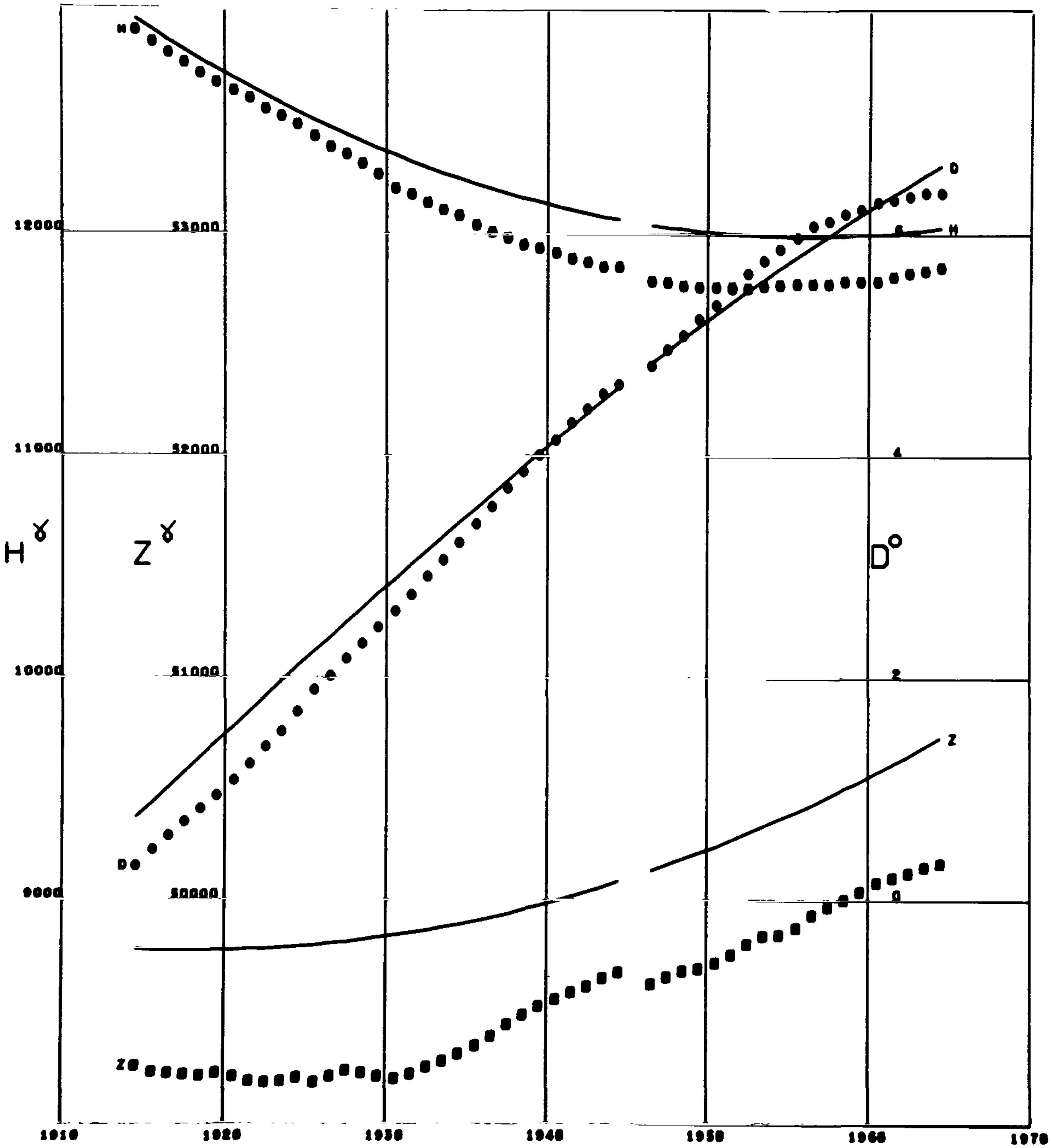

Figure A155

SOUTH POLE
Lat -89.99 Long -13.32 Alt 2.80

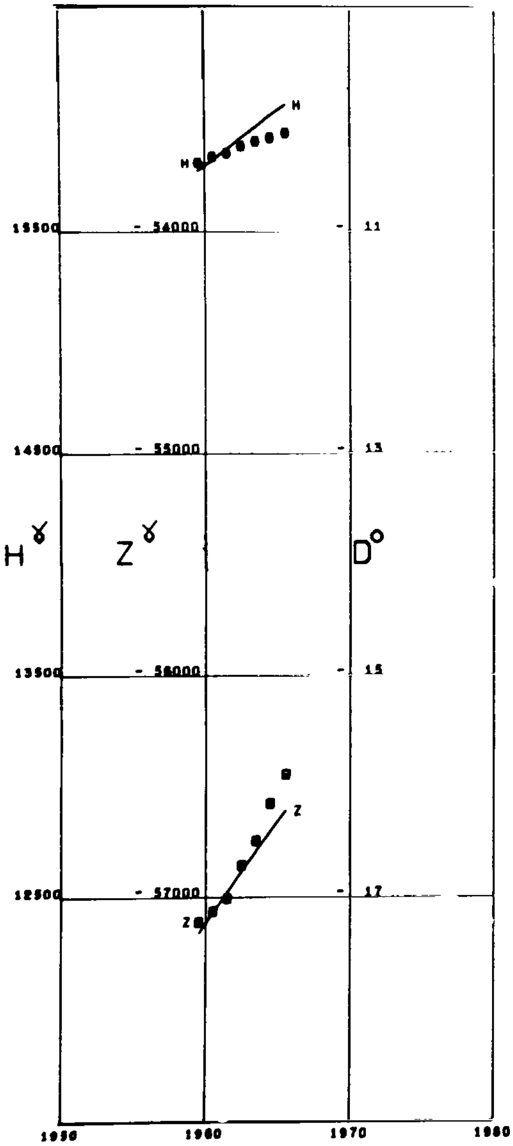

Figure A156

SREDNIKAN
Lat 62.44 Long 152.31

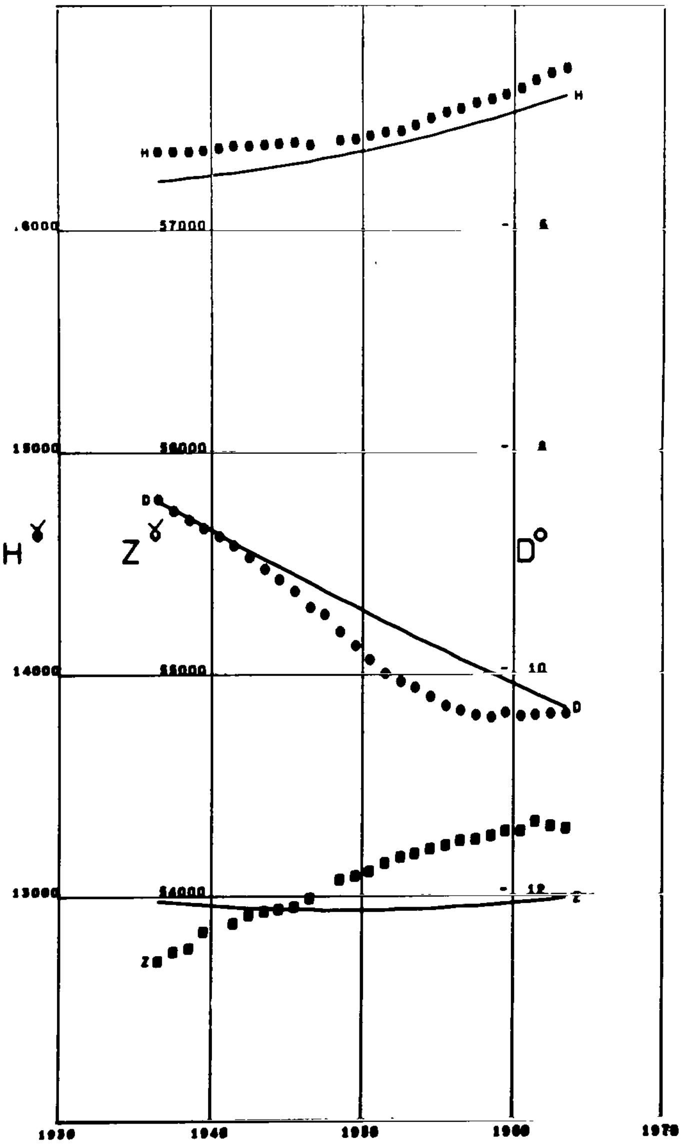

Figure A157

ST. HELIER
Lat 49.19 Long-2.09

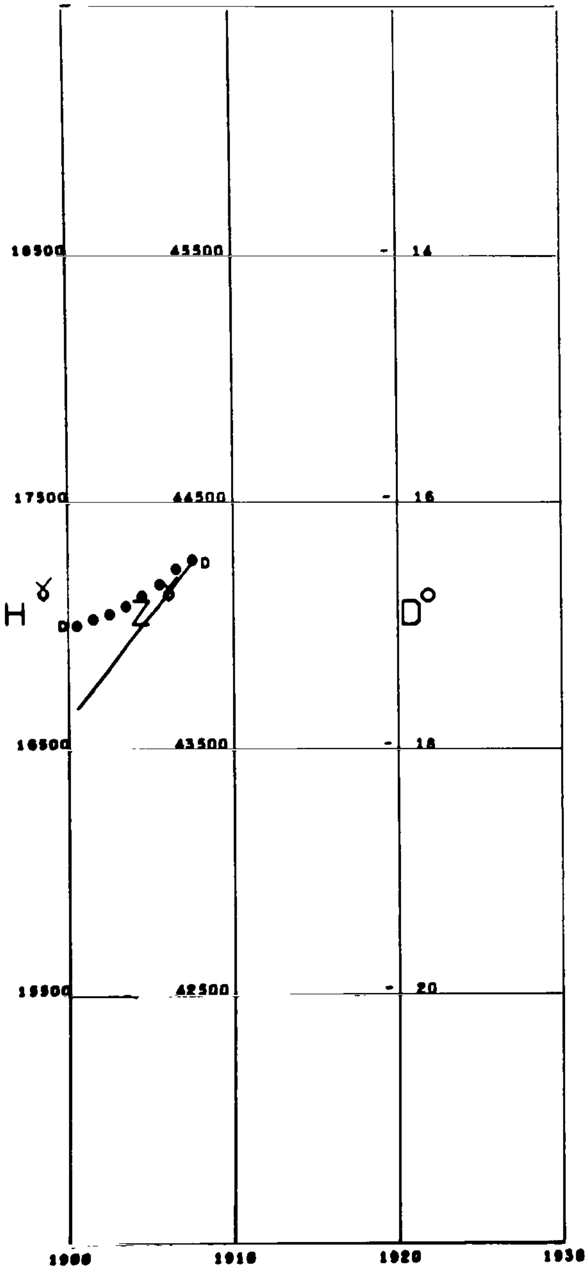

Figure A158

STARA DALA
Lat 47.87 Long 18.19

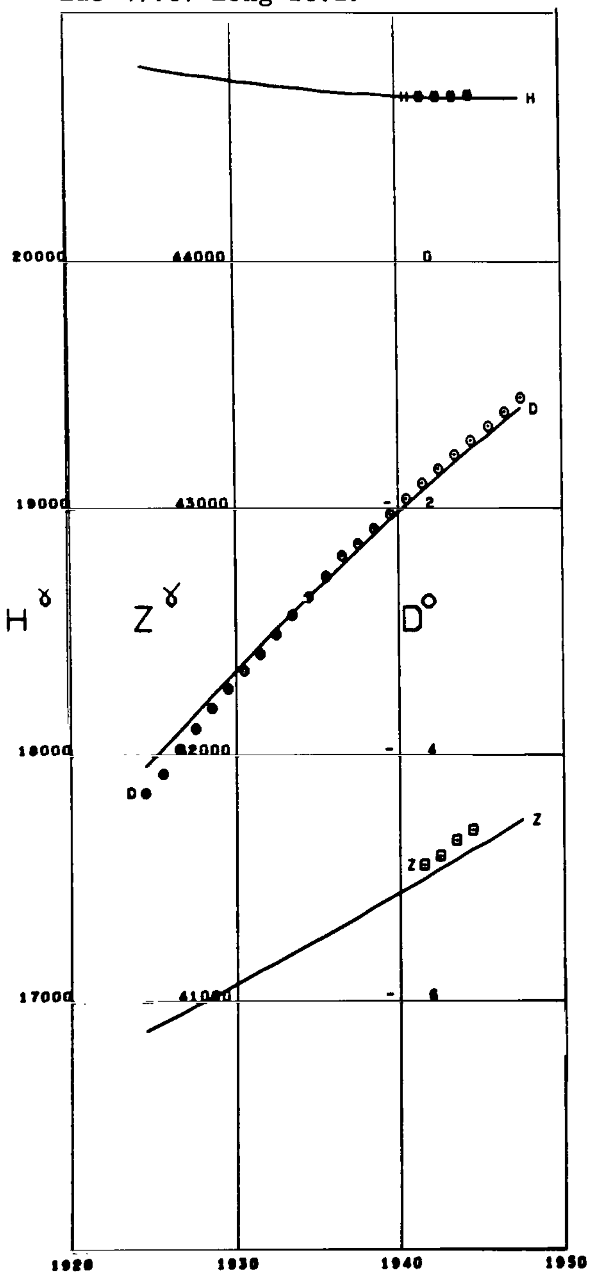

Figure A159

STEPANOVKA
Lat 46.78 Long 30.88 Alt 0.14

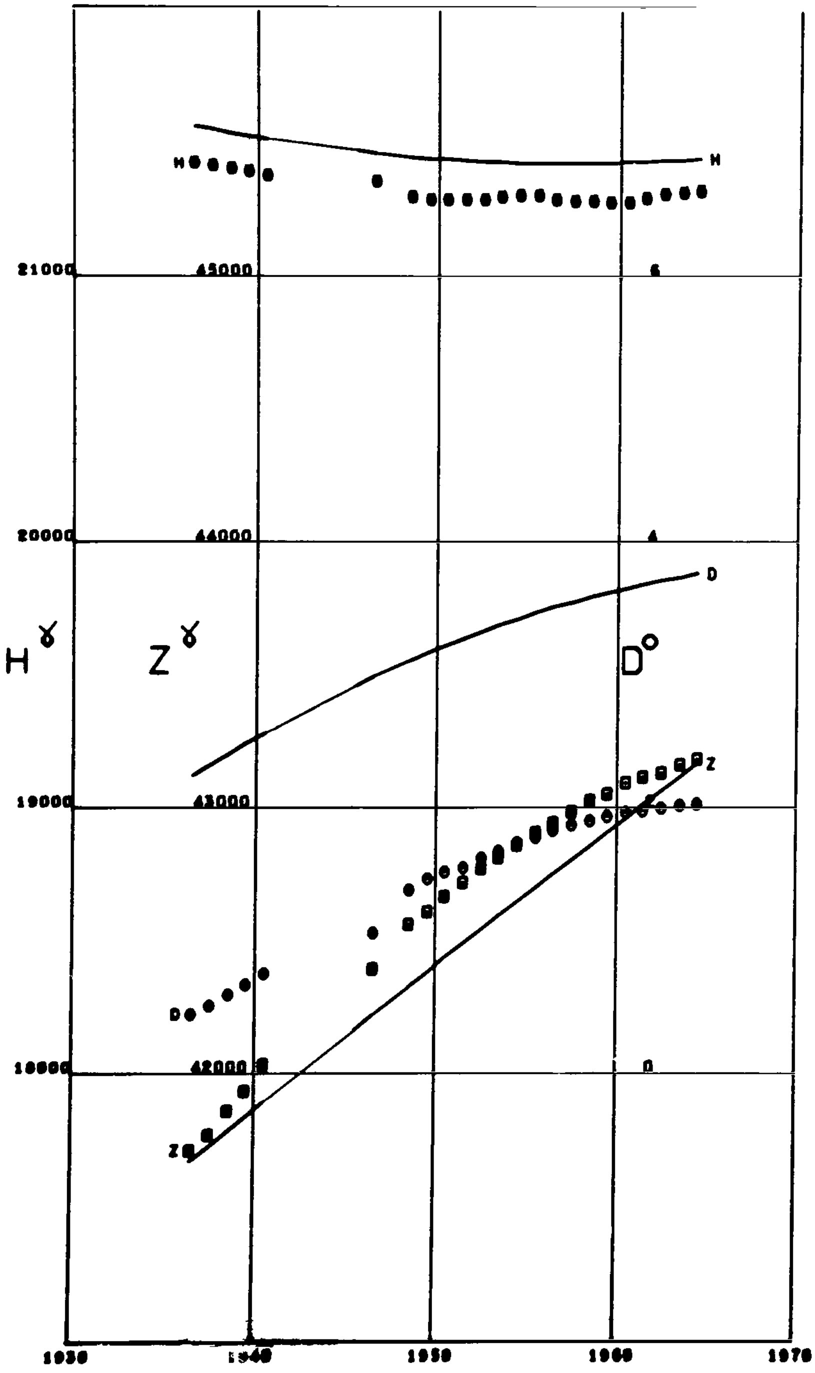

Figure A160

STONYHURST
Lat 53.84 Long -2.47

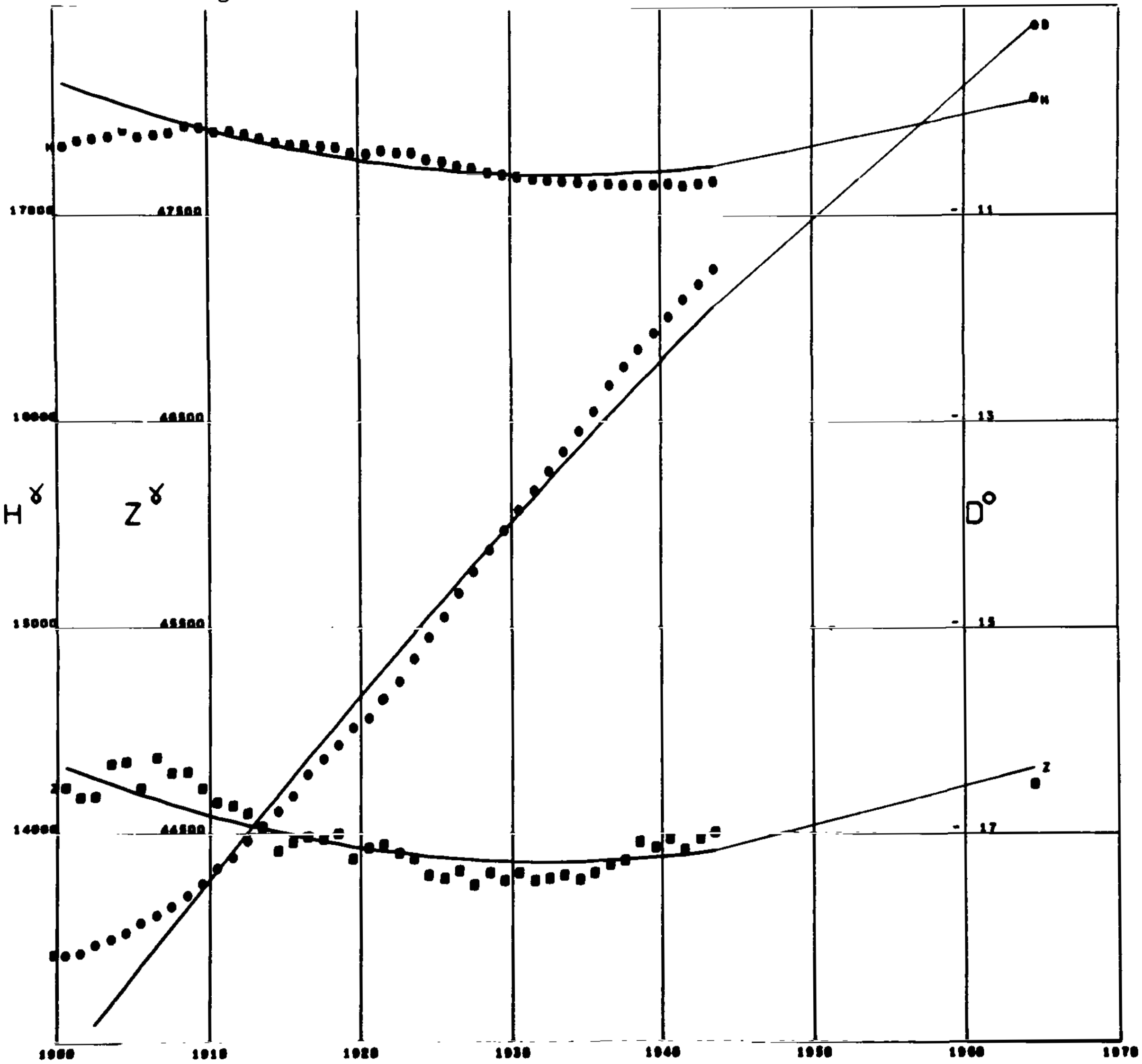

Figure A161

SURLARI
Lat 44.68 Long 26.25 Alt 0.08

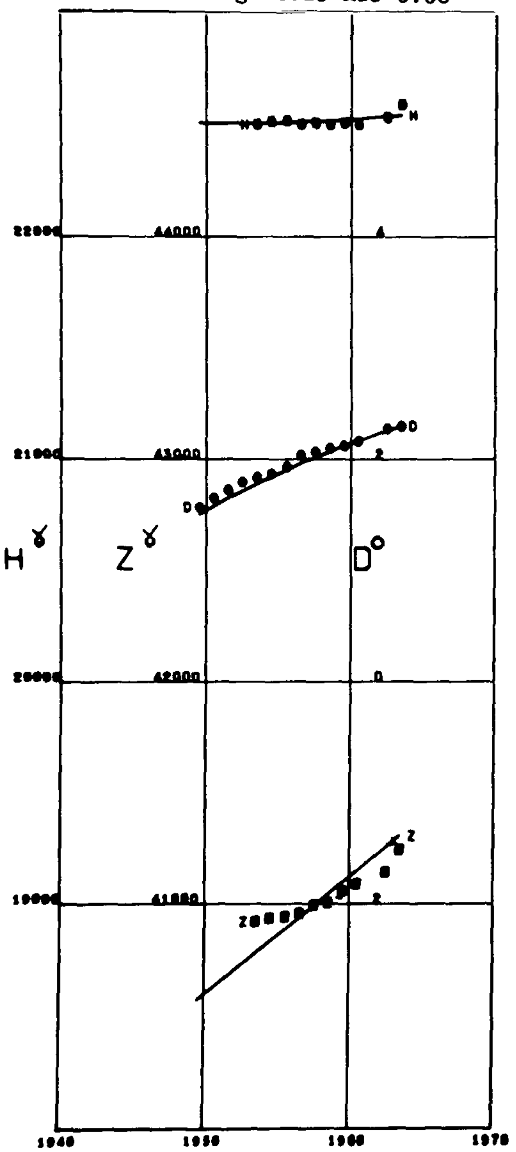

Figure A162

SVERDLOVSK
Lat 56.82 Long 60.63

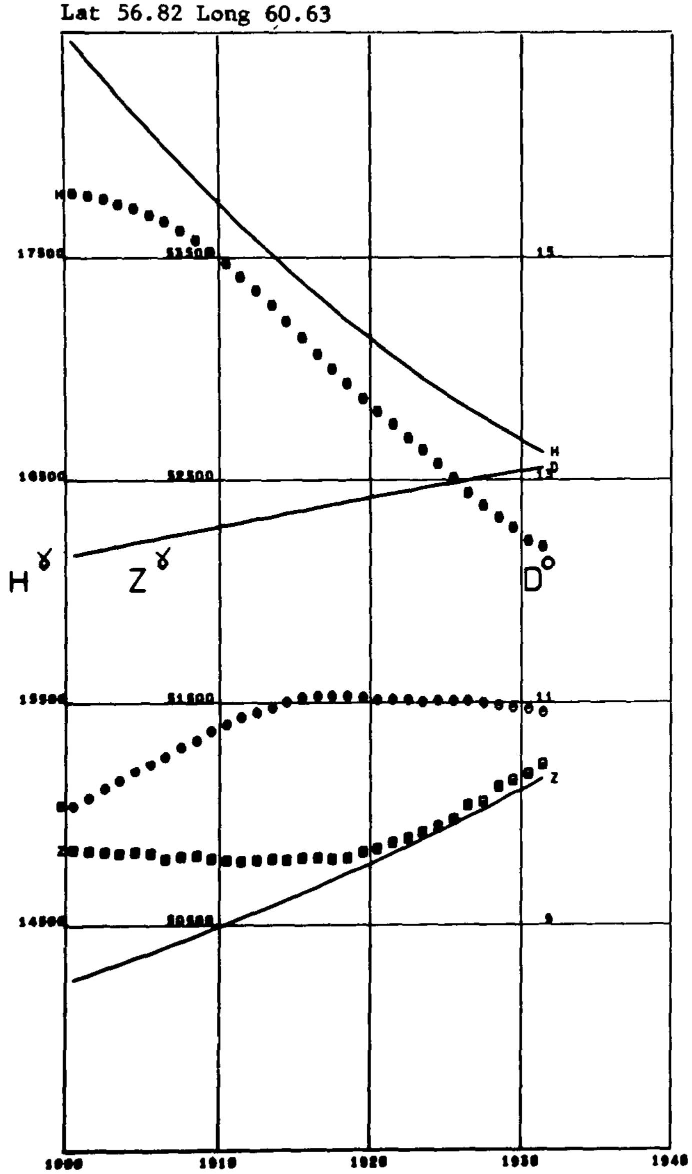

Figure A163

SWIDER
Lat 52.11 Long 21.25

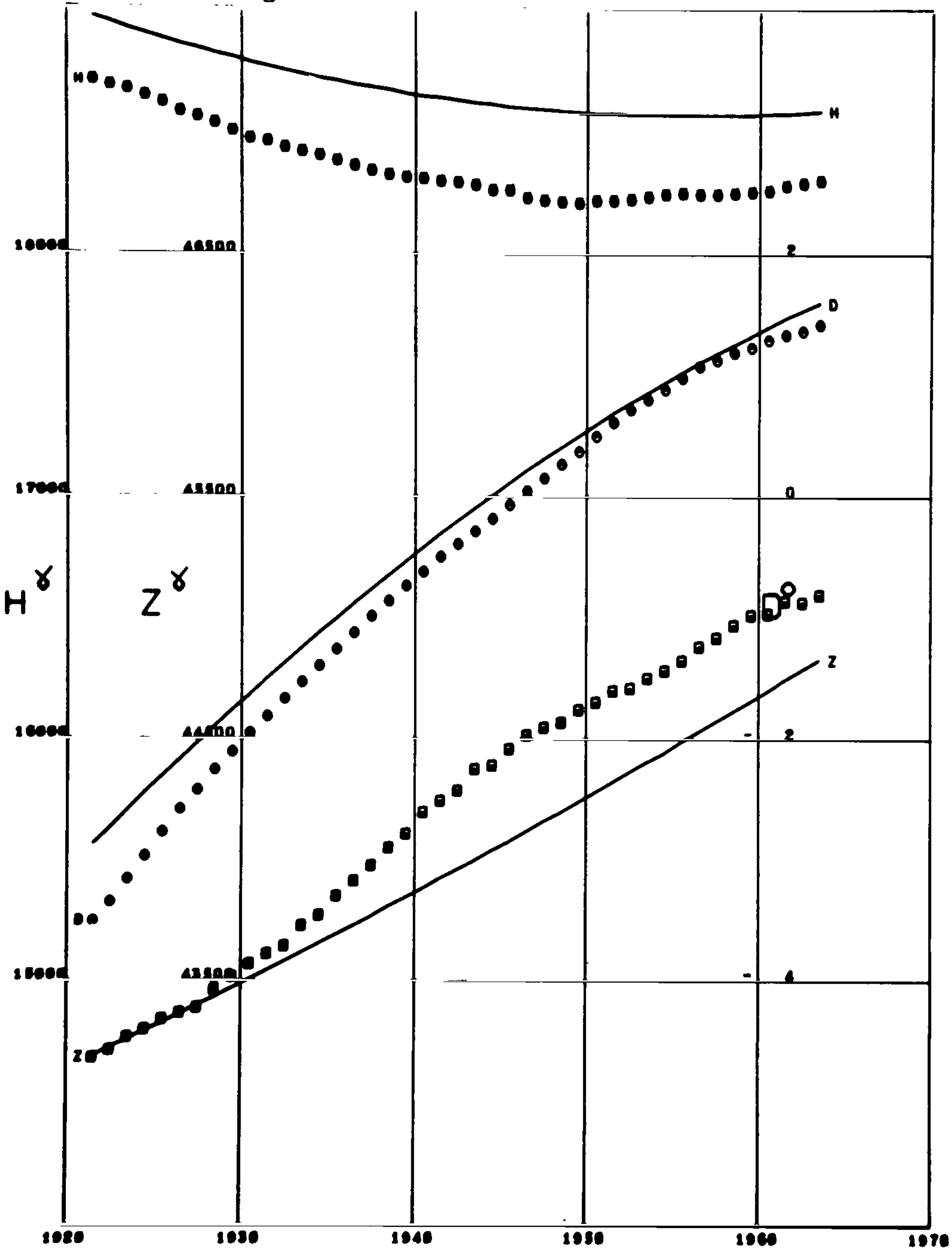

Figure A164

TAIPEI
Lat 25.03 Long 121.51

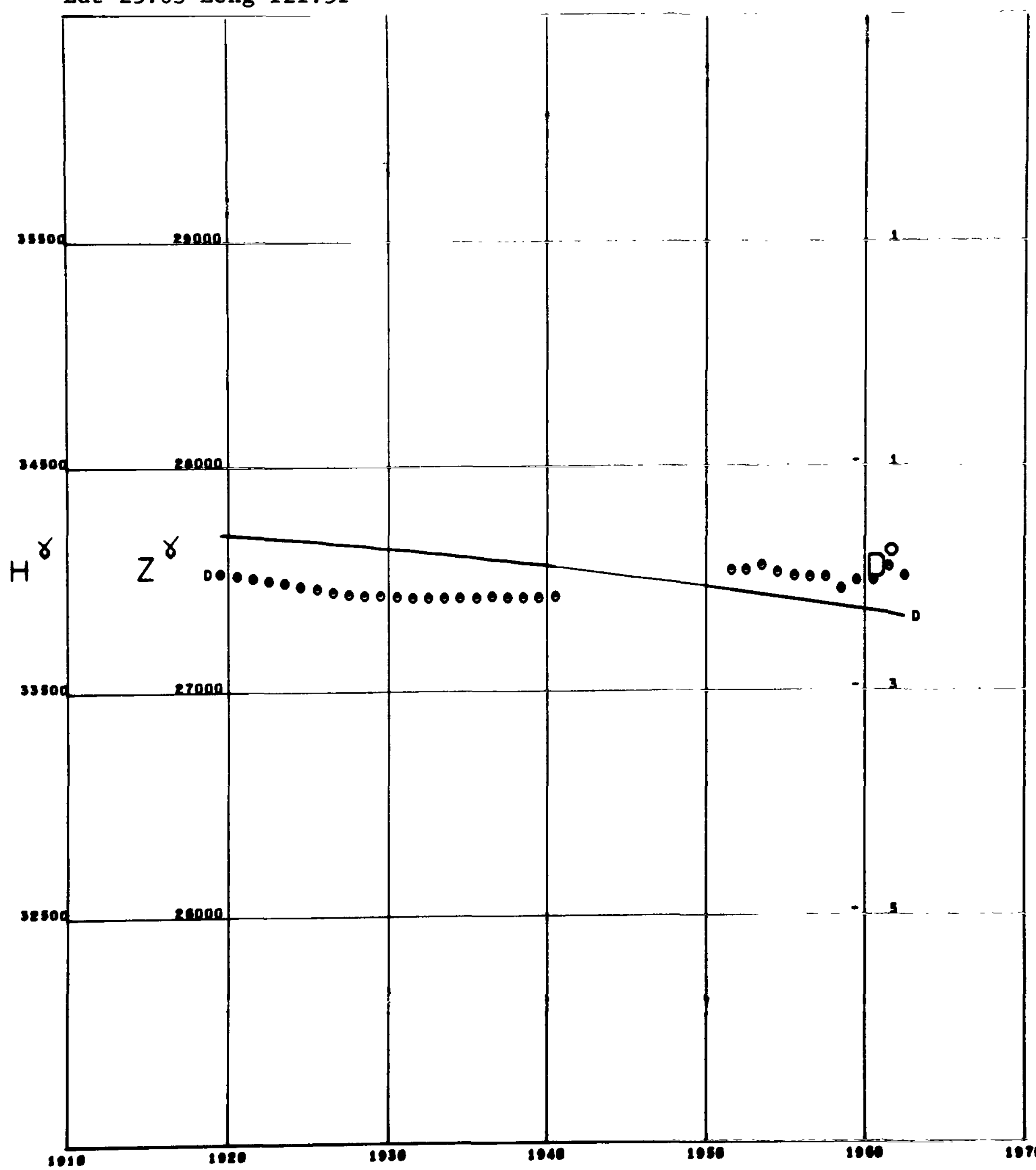

Figure A165

TAMANRASSET
Lat 22.79 Long 5.52

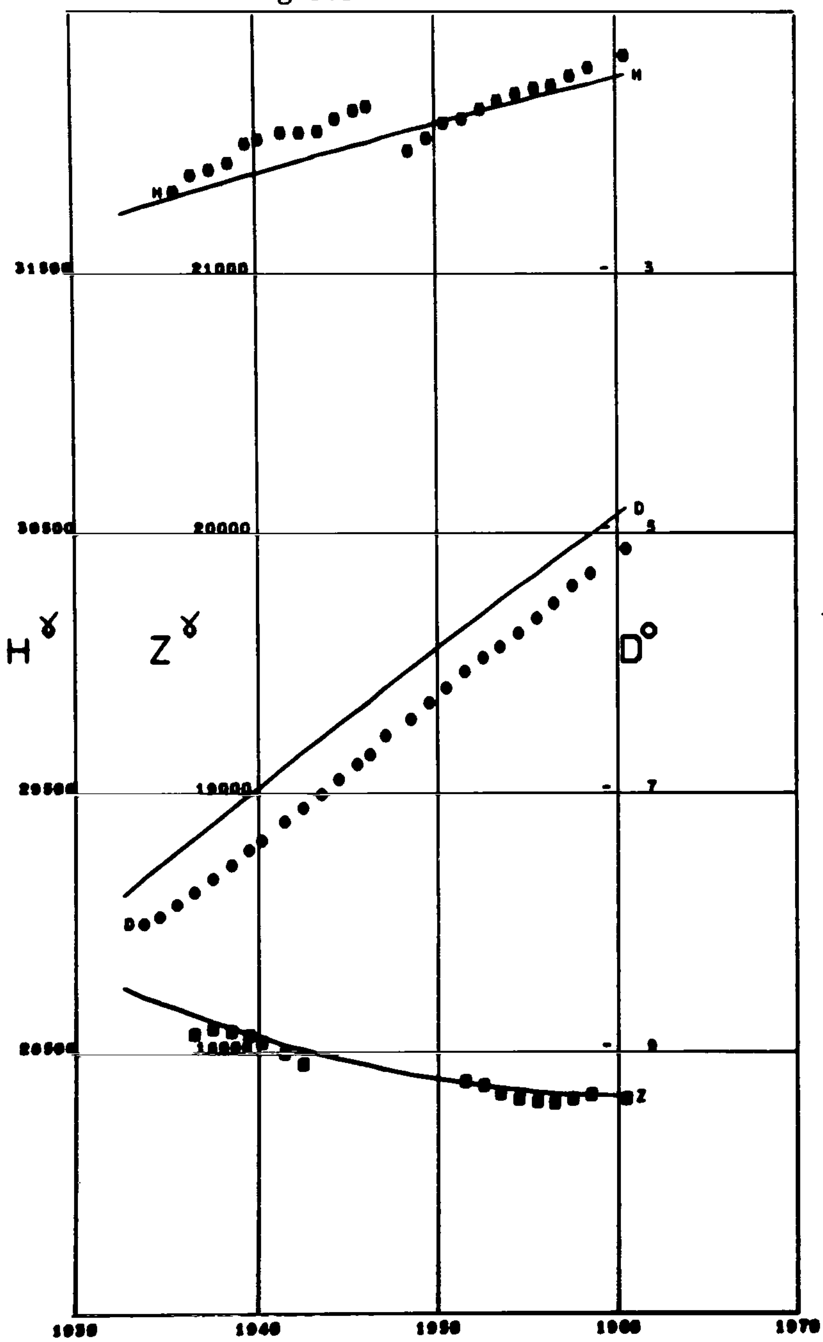

Figure A166

TANANARIVE
Lat -18.91 Long 47.55

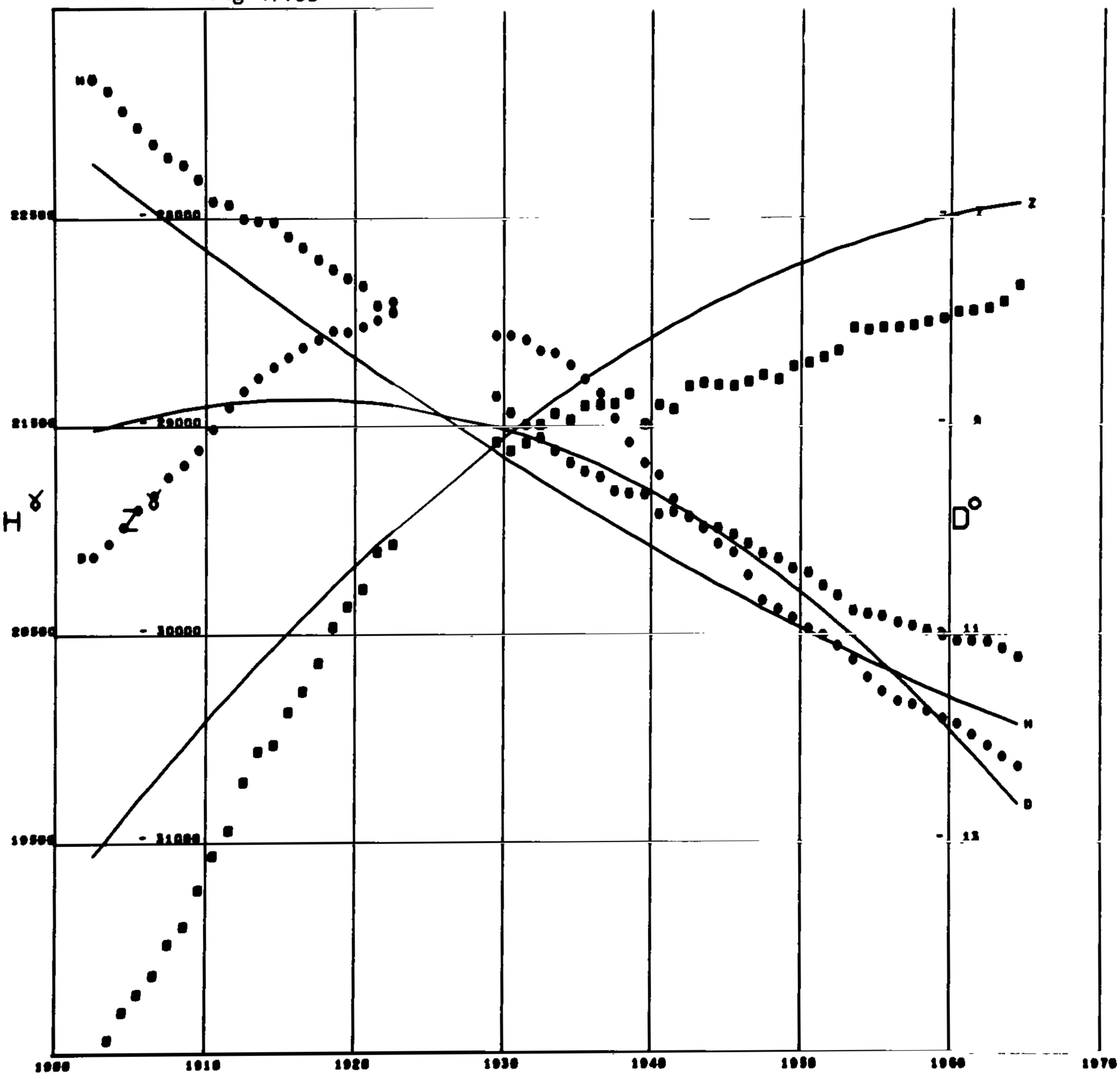

Figure A167

TASHKENT
Lat 41.33 Long 69.30

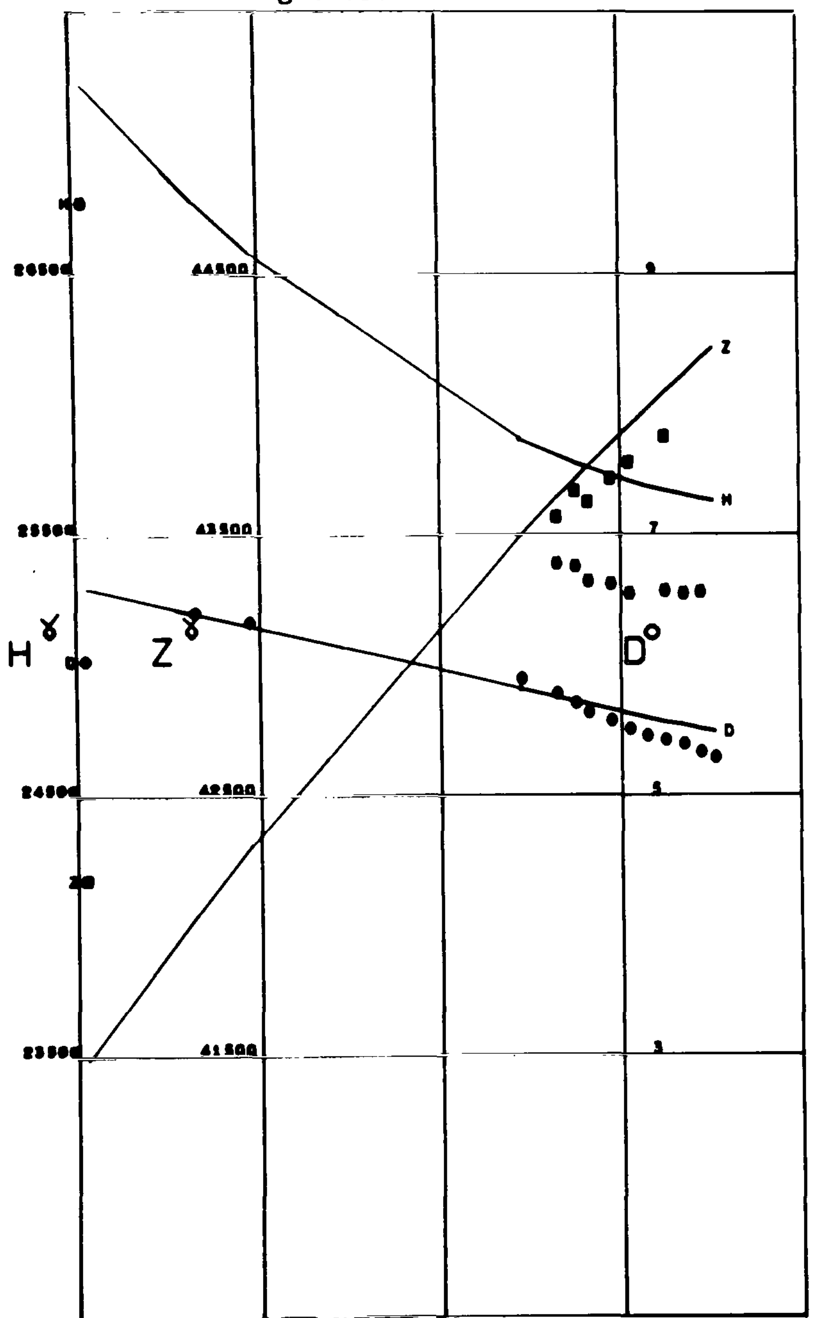

Figure A168

TATUOCA
Lat -1.20 Long -48.51

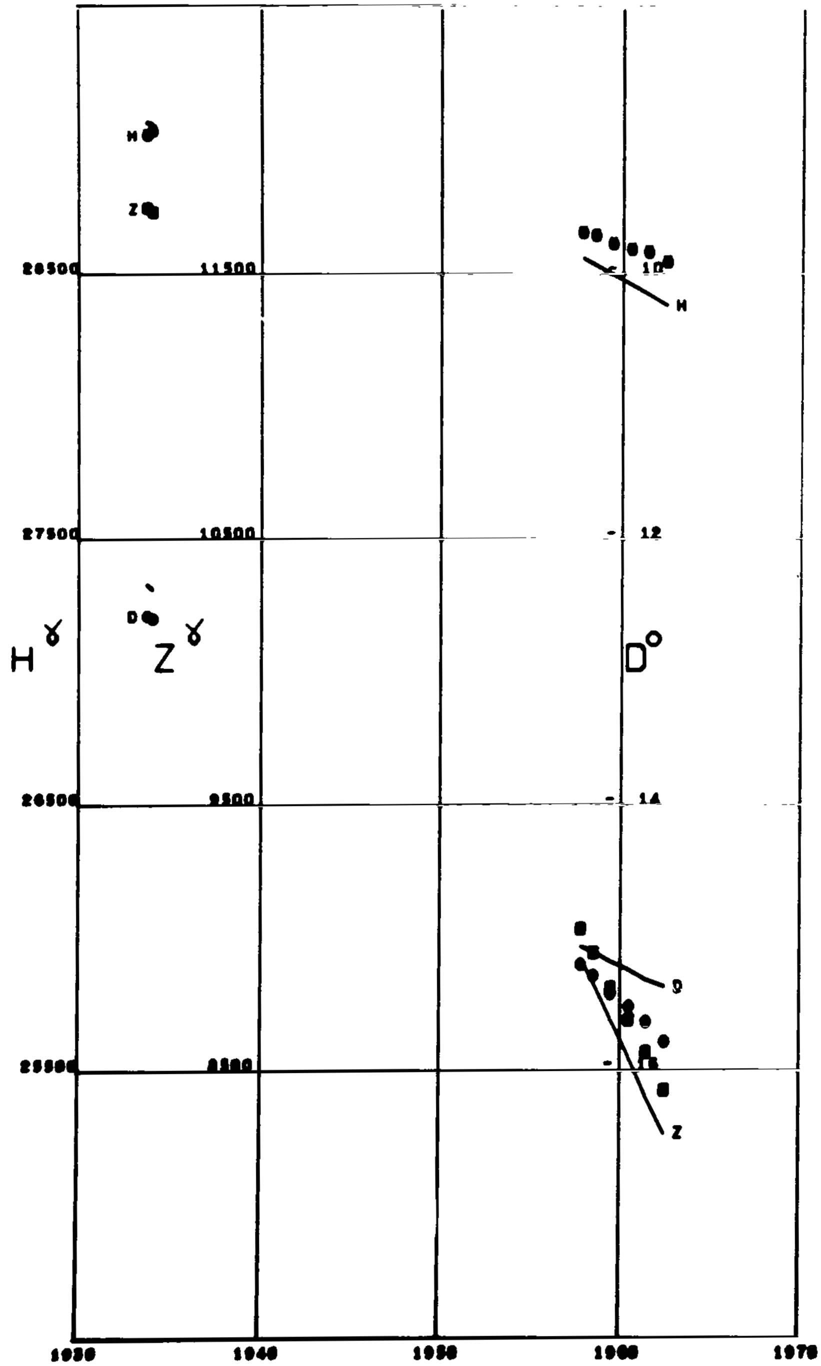

Figure A169

TBILISI
Lat 41.71 Long 44.79

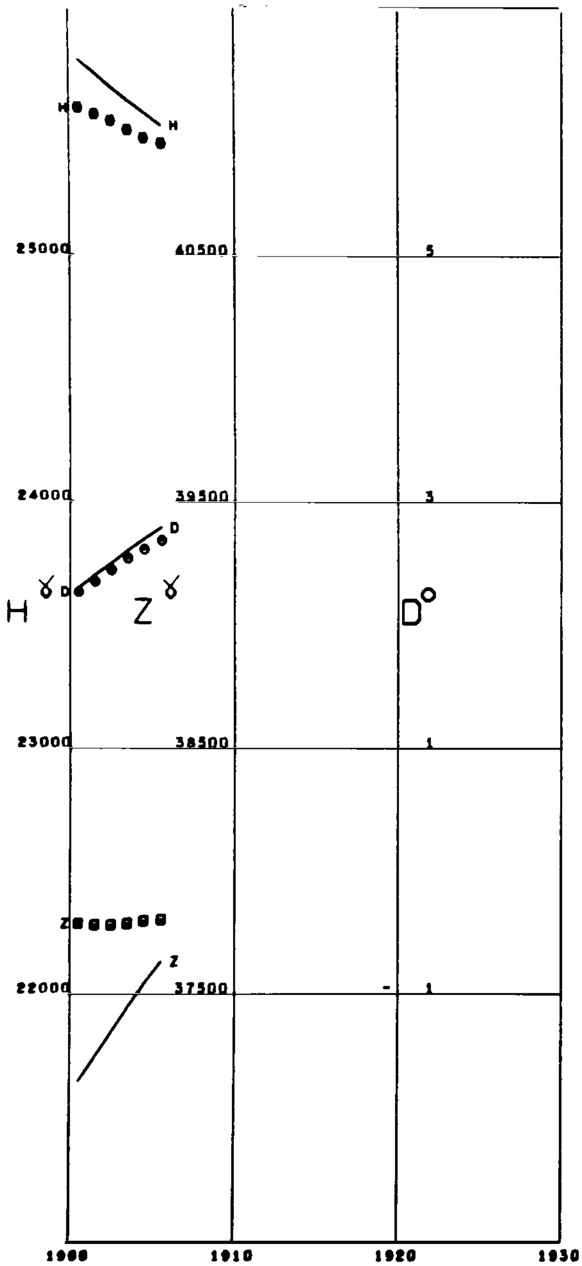

Figure A170

TEHRAN
Lat 35.73 Long 51.38

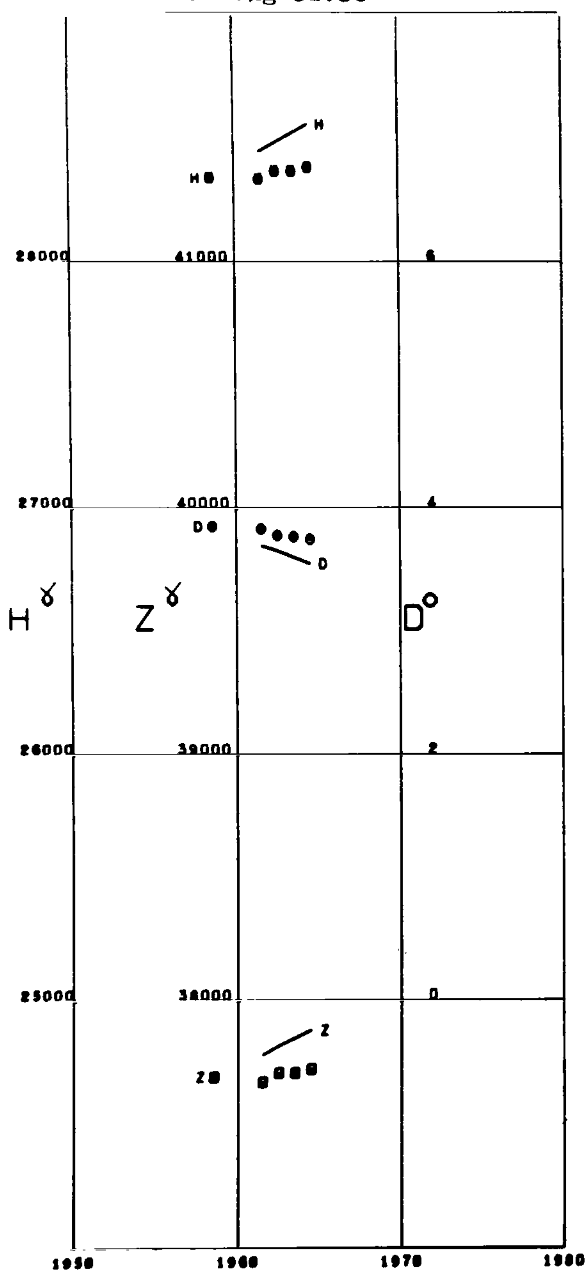

Figure A171

TENERIFE
Lat 28.47 Long -16.27 Alt 0.40

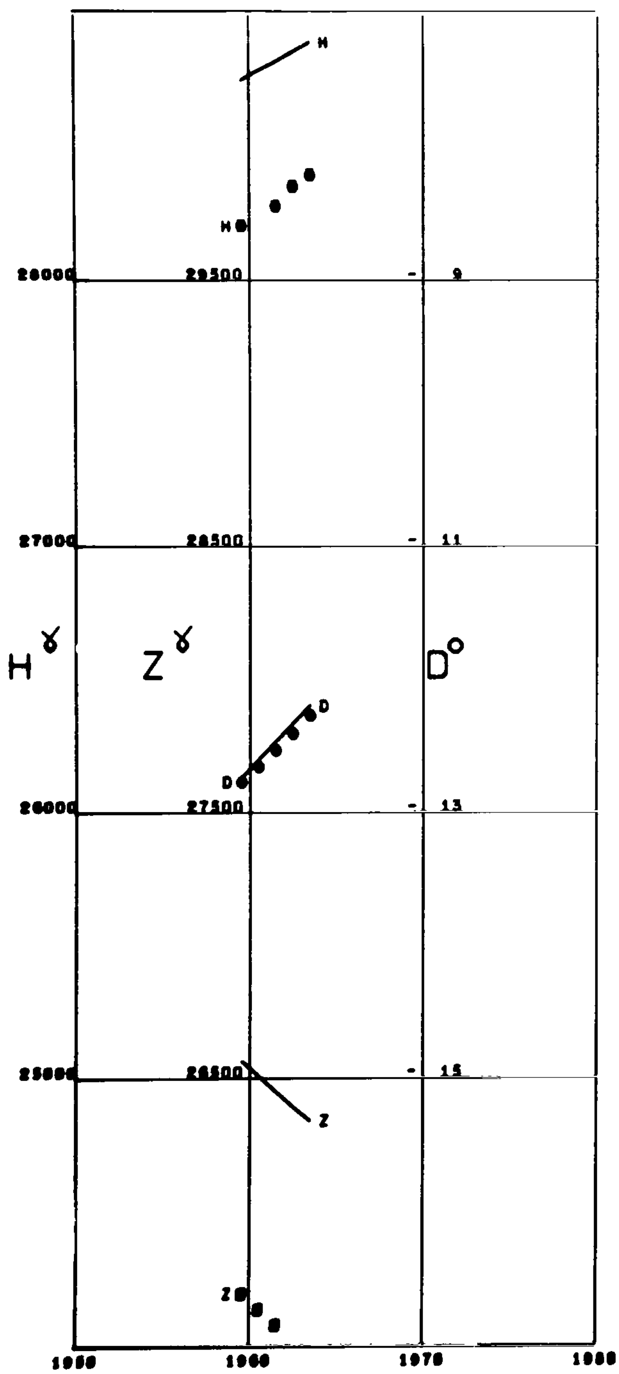

Figure A172

TEOLOYUCAN
Lat 19.74 Long -99.18

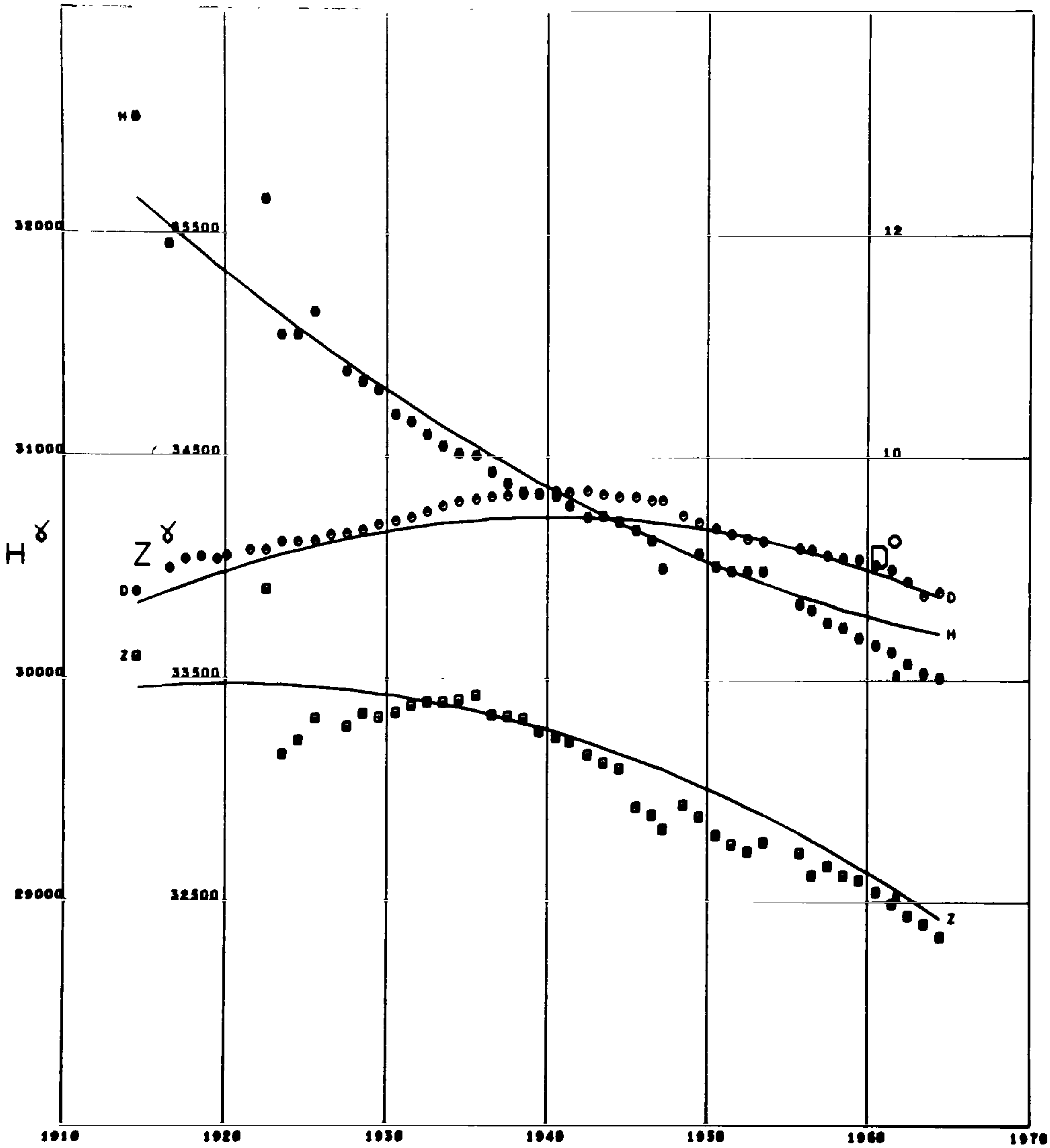

Figure A173

THULE II
Lat 77.48 Long -69.16

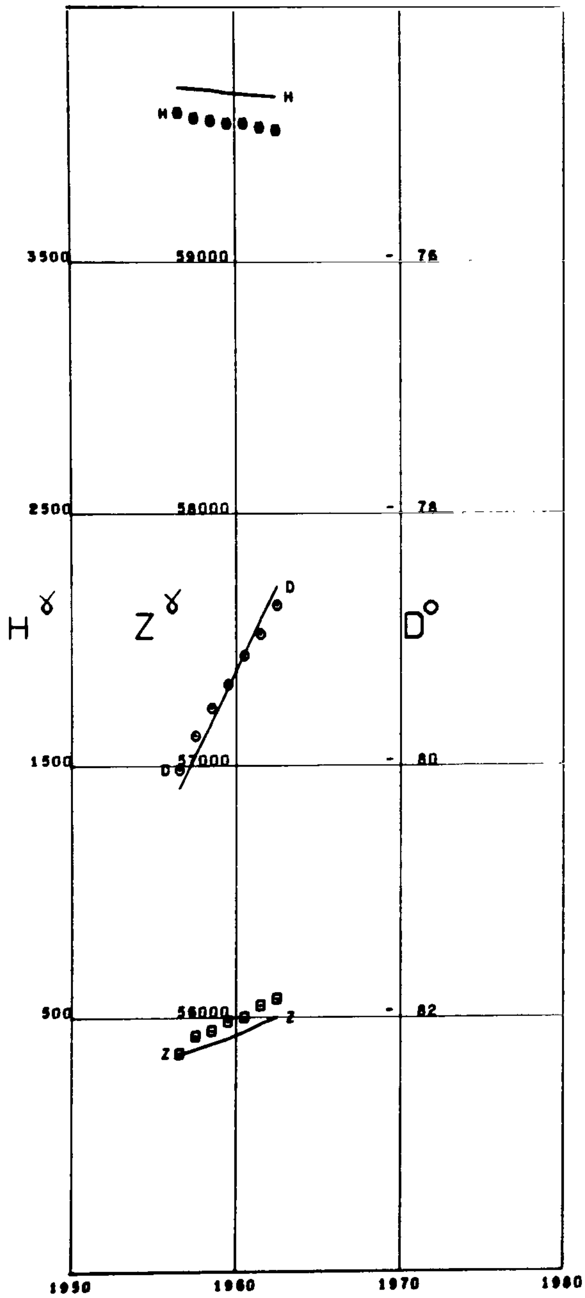

Figure A174

TIHANY
Lat 46.90 Long 17.89

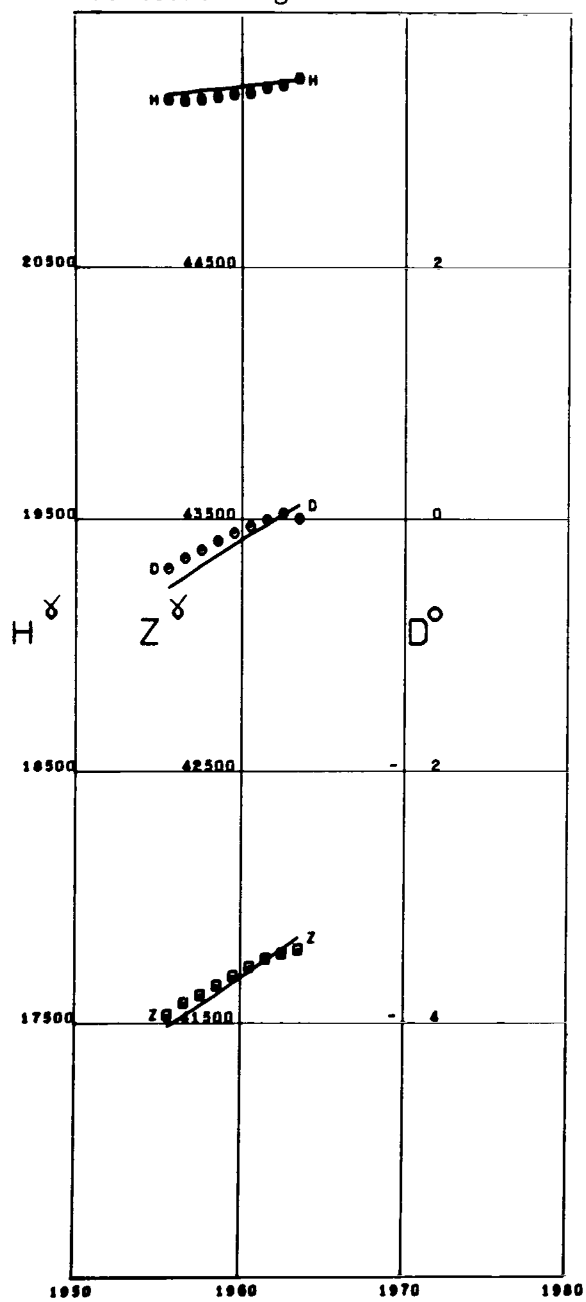

Figure A175

TIKHAYA BAY
Lat 80.33 Long 52.80

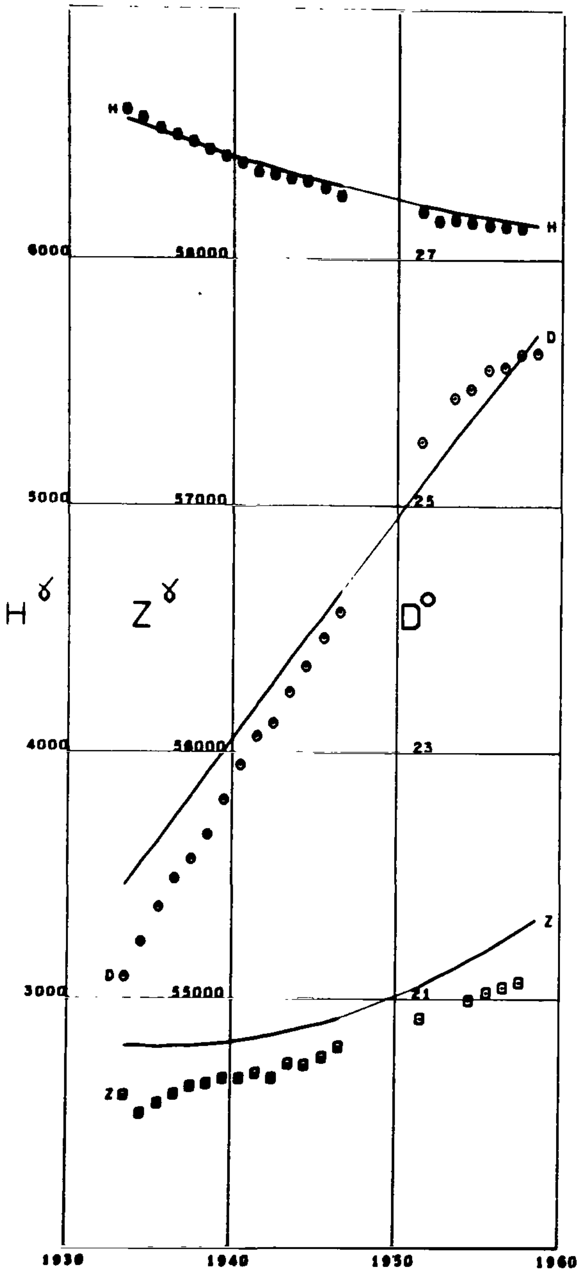

Figure A176

TIKSI
Lat 71.58 Long 129.00

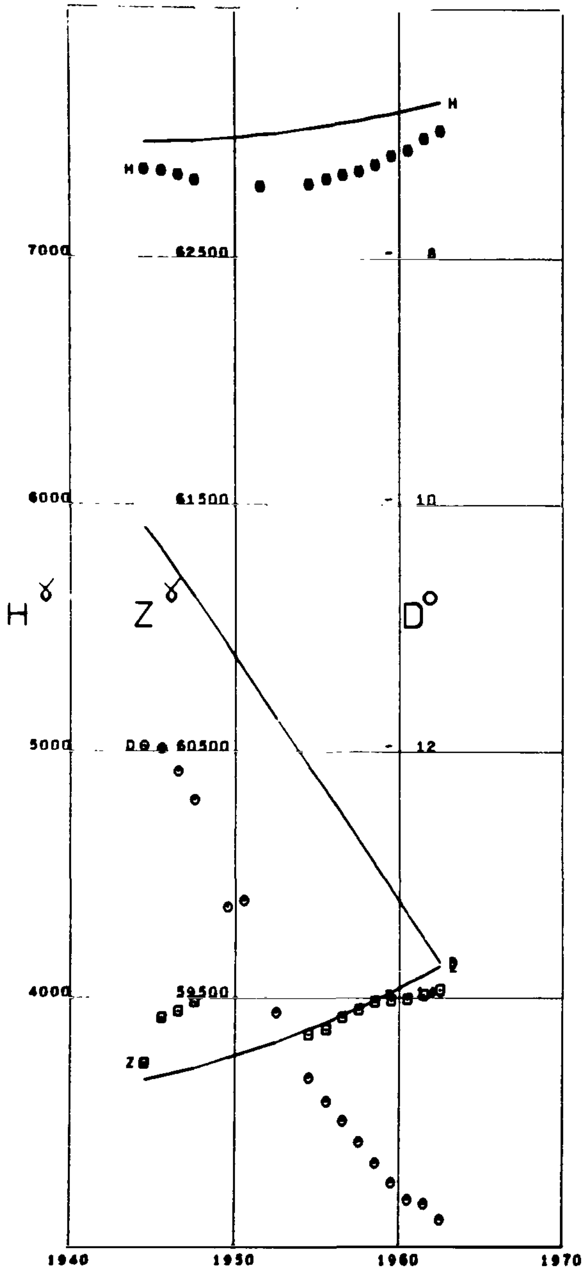

Figure A177

TOKYO
Lat 35.68 Long 139.75

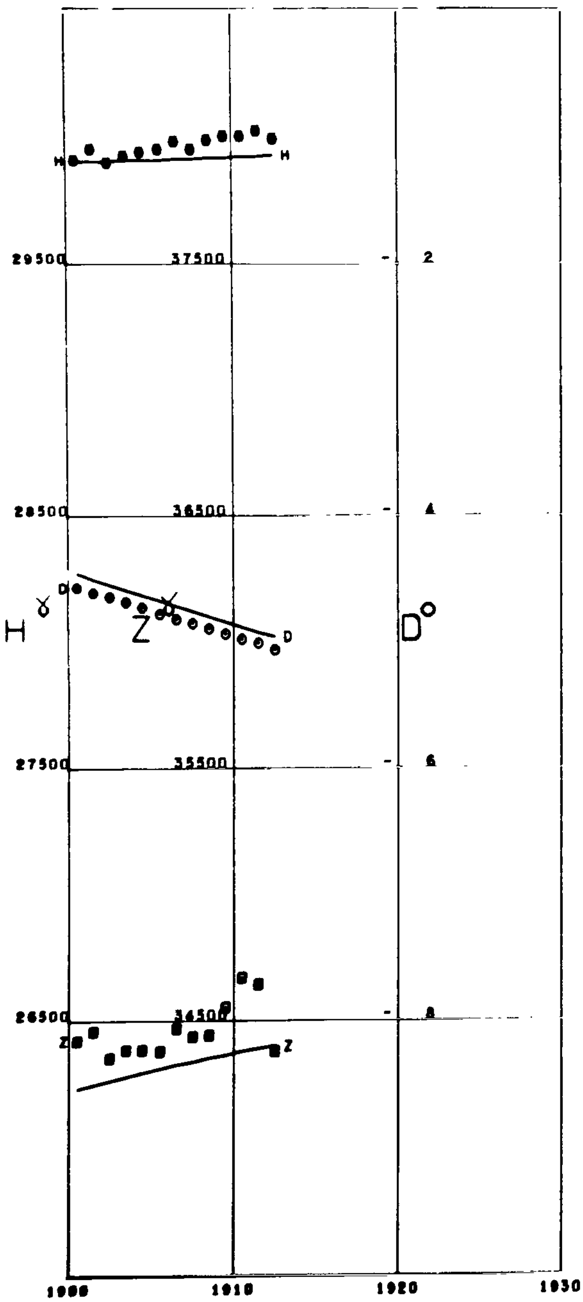

Figure A178

TOLEDO
Lat 39.88 Long -4.04 Alt 0.50

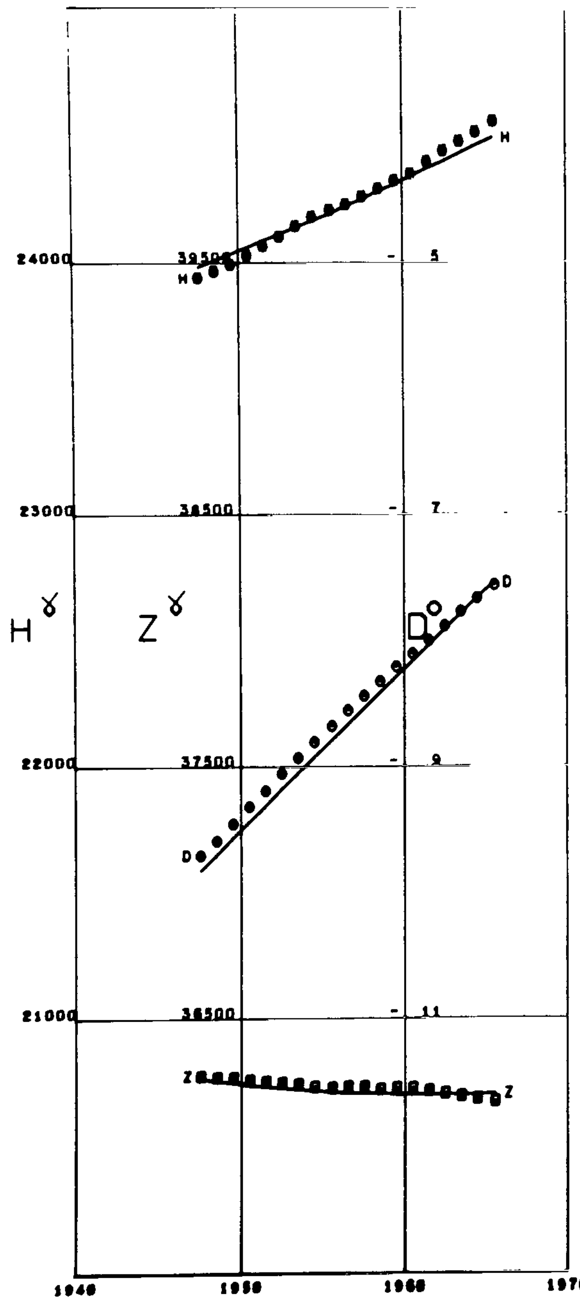

Figure A179

TOOLANGI
Lat -37.53 Long 145.46 Alt 0.48

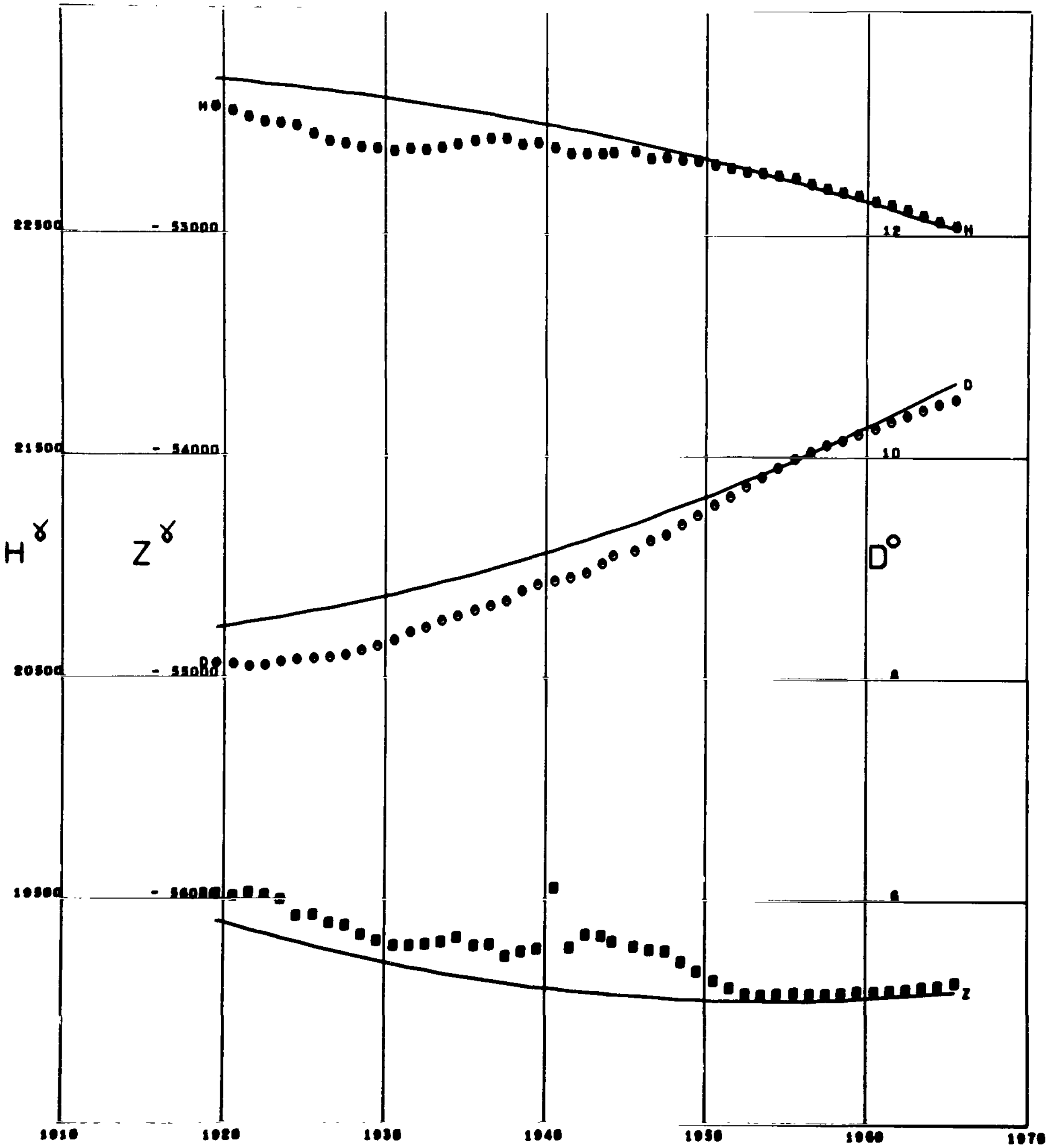

Figure A180

TOULOUSE
Lat 43.61 Long 1.45

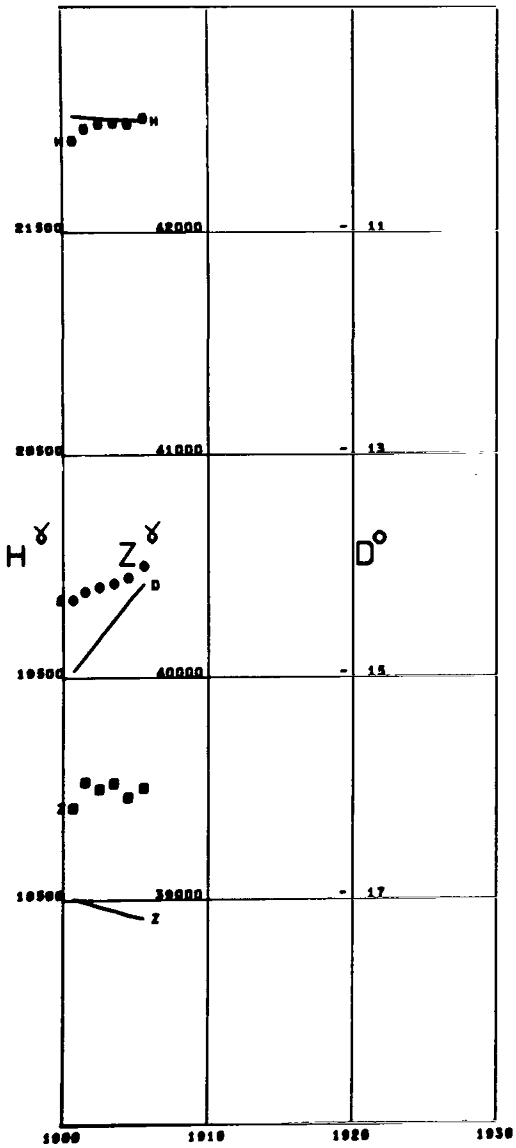

Figure A181

TOUNGOO
Lat 18.93 Long 96.45

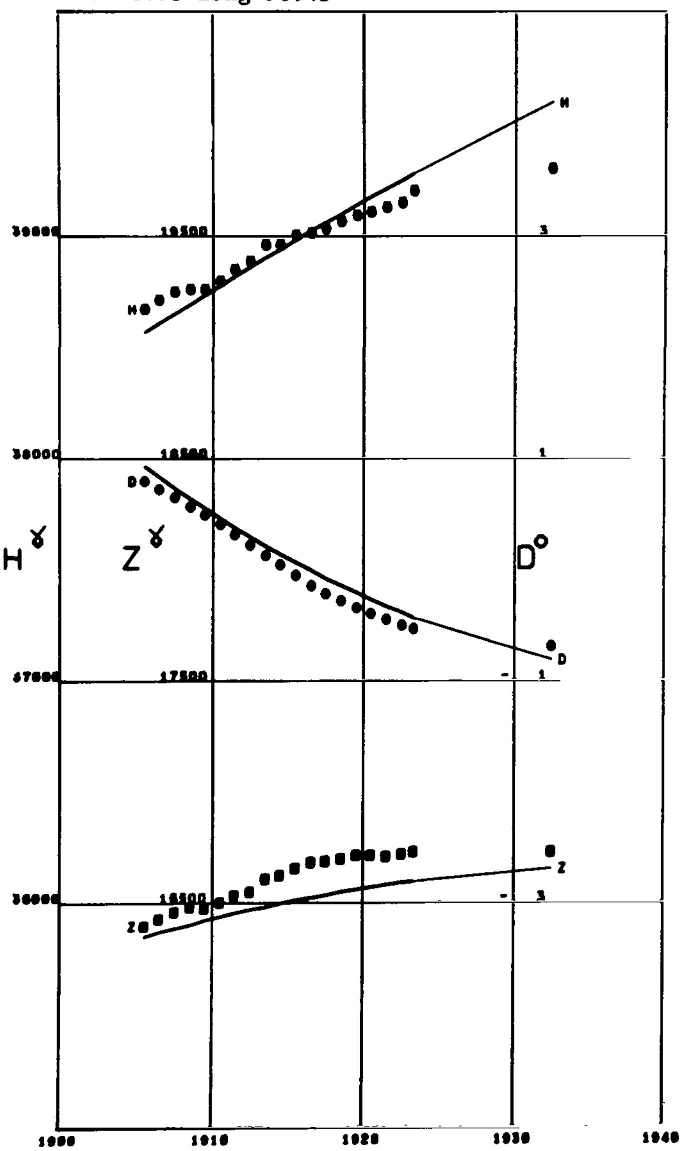

Figure A182

TOYOHARA
Lat 46.94 Long 142.74

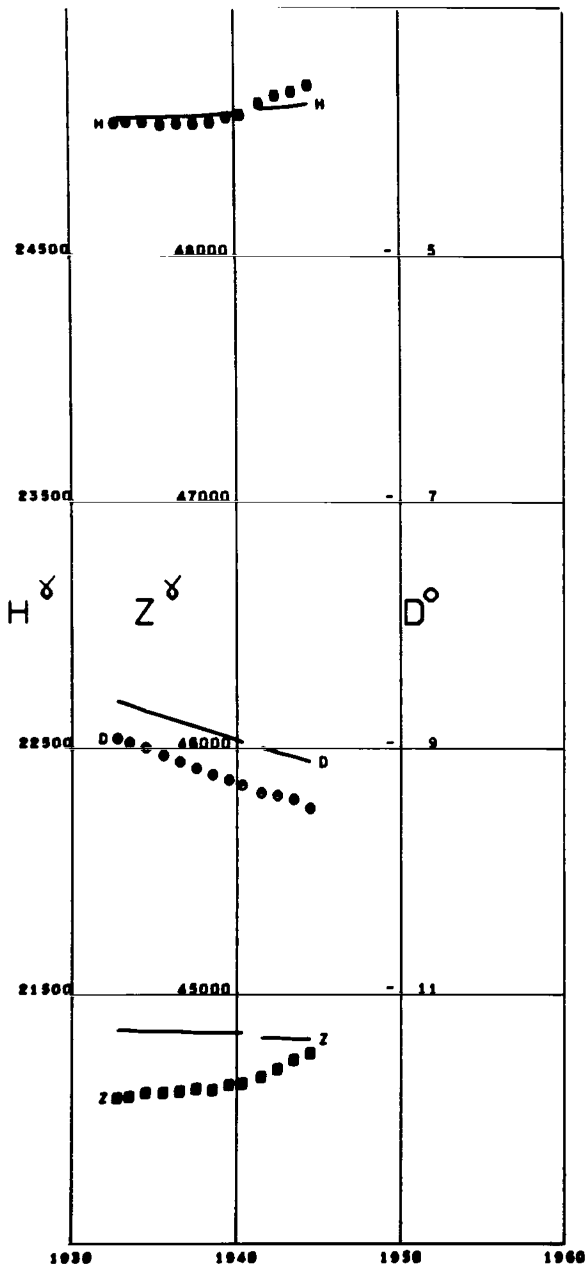

Figure A183

TRELEW
Lat -43.24 Long -65.31 Alt 0.03

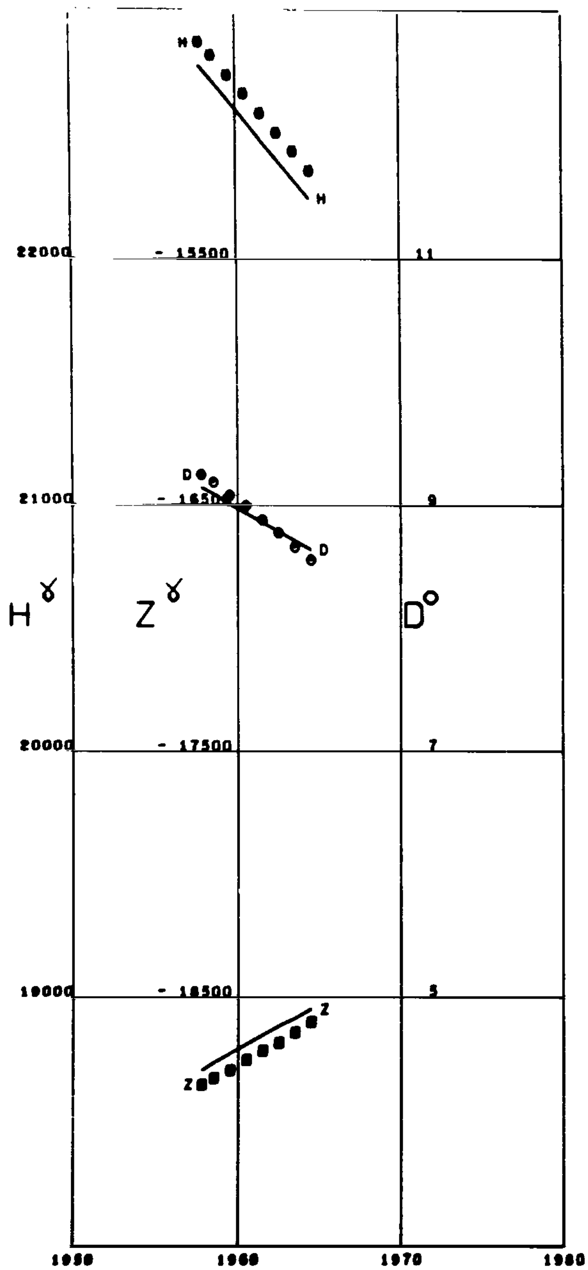

Figure A184

TRIVANDRUM
Lat 8.48 Long 76.95

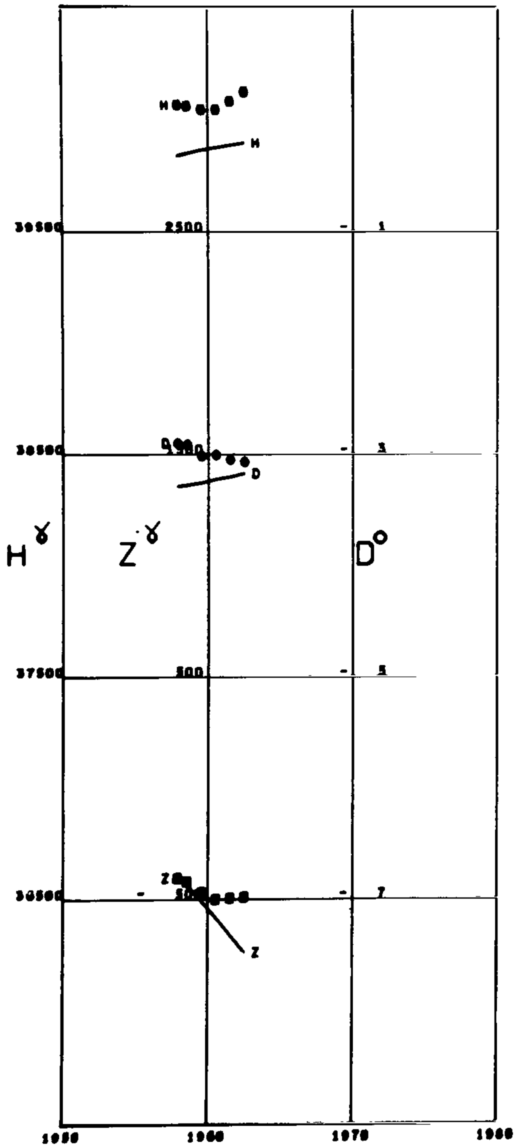

Figure A185

TROMSO
Lat 69.66 Long 18.94

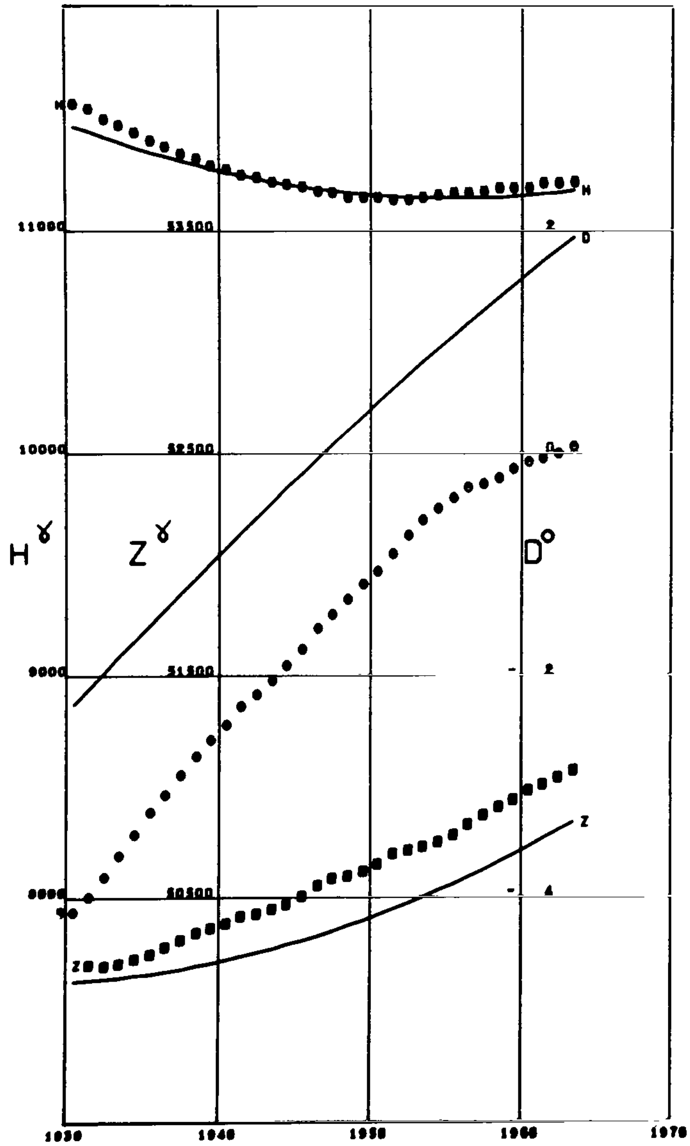

Figure A186

TSINGTAO
Lat 36.07 Long 120.32

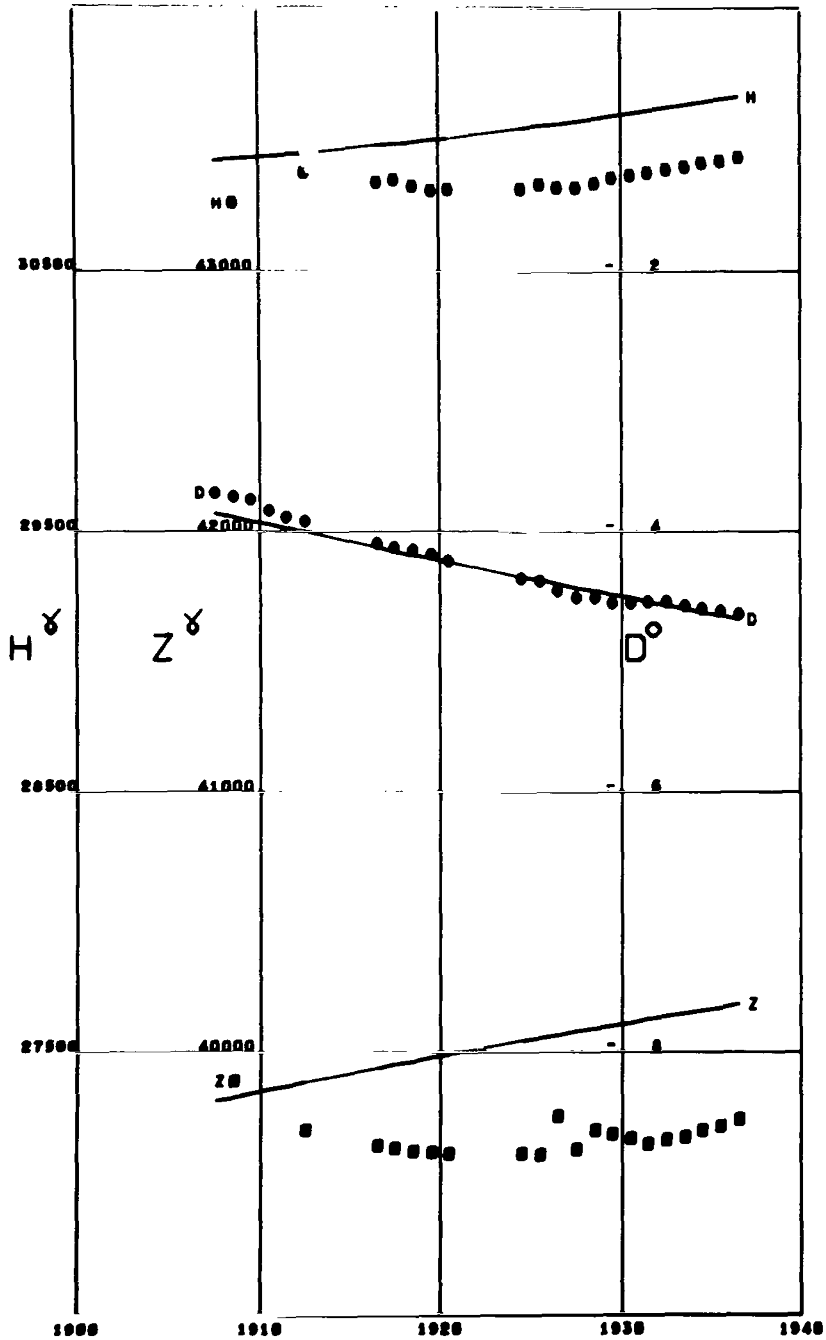

Figure A187

TUCSON
Lat 32.24 Long -110.83 Alt 0.77

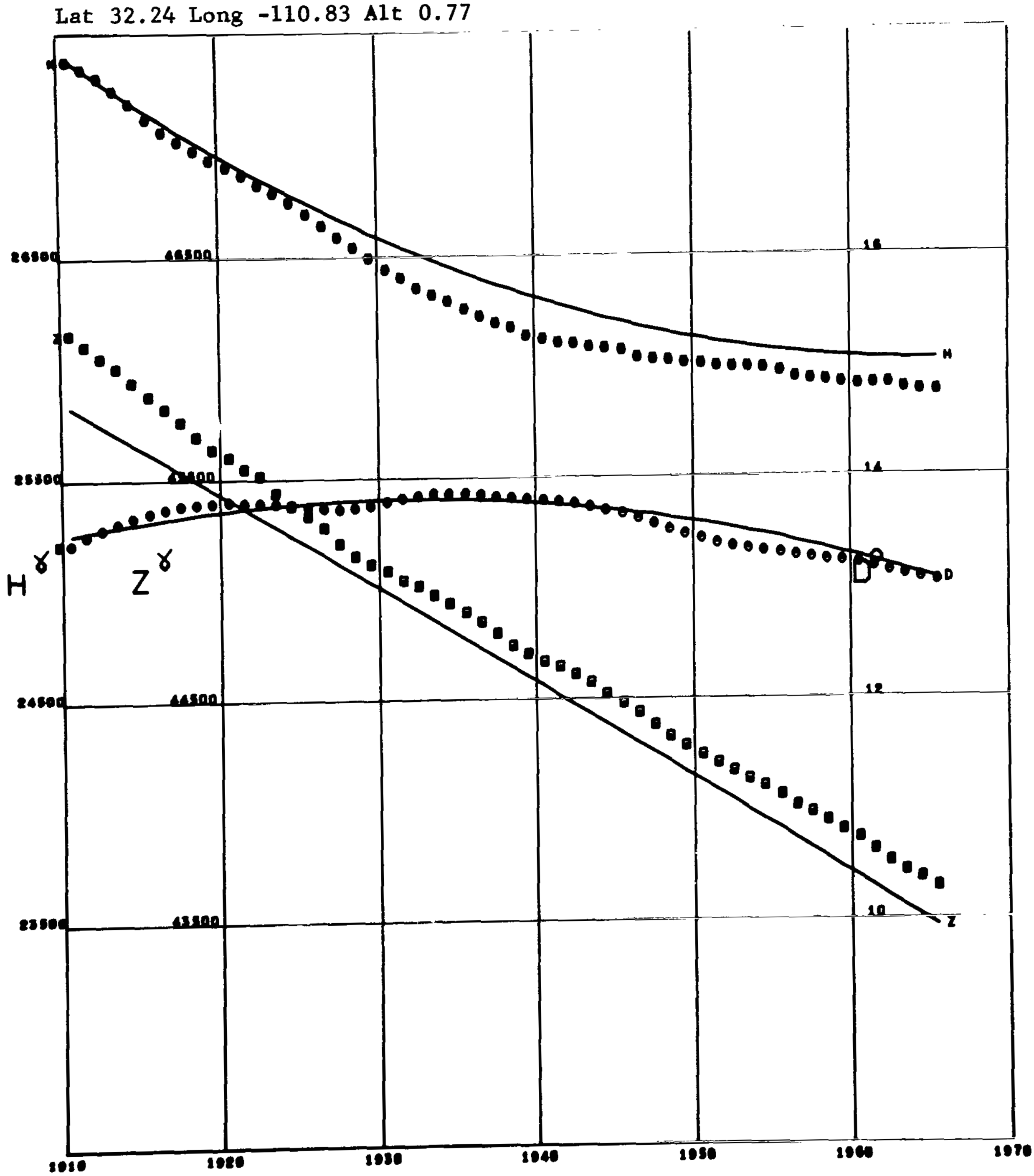

Figure A188

UCCLE
Lat 50.79 Long 4.36

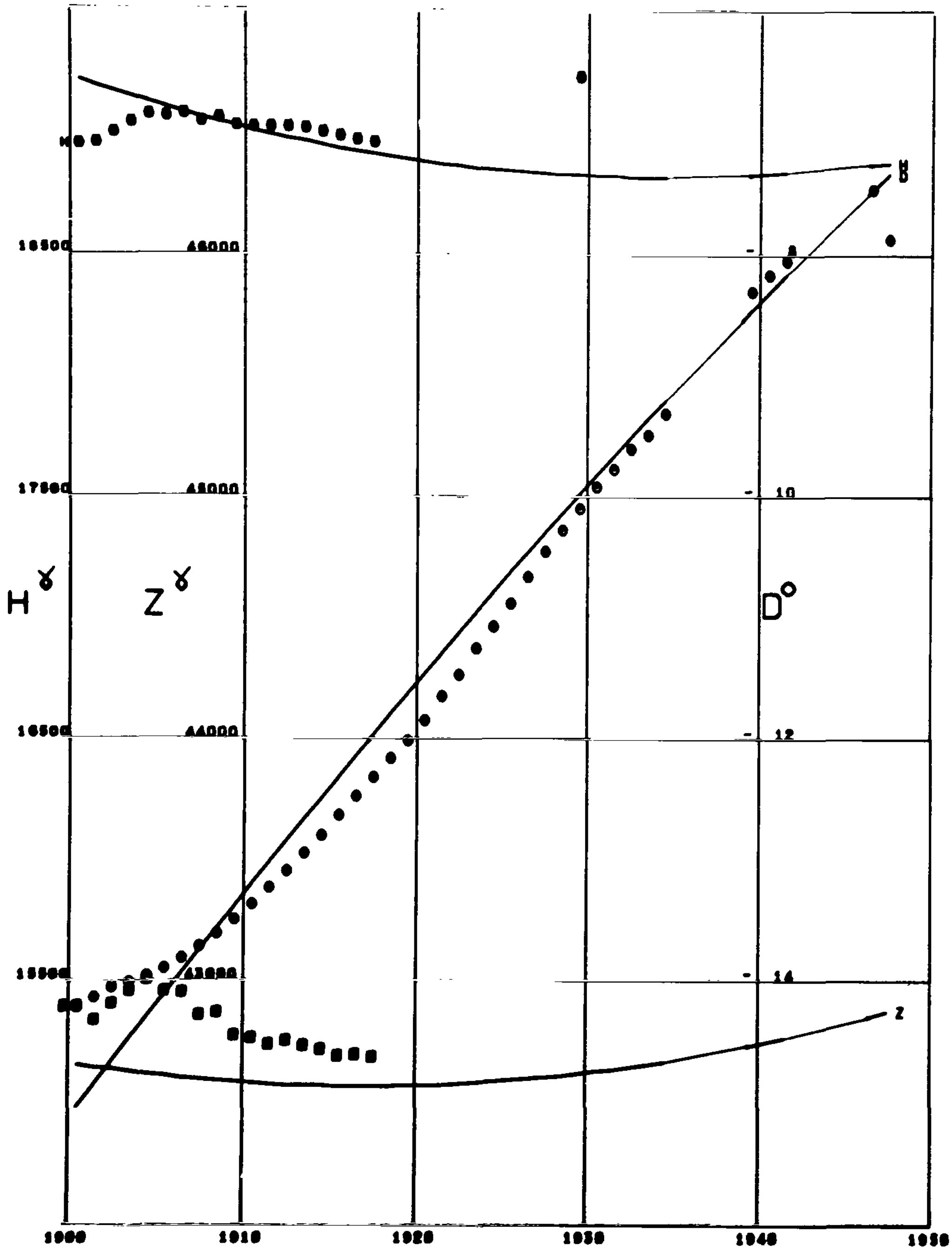

Figure A189

UELEN
Lat 66.16 Long -169.83

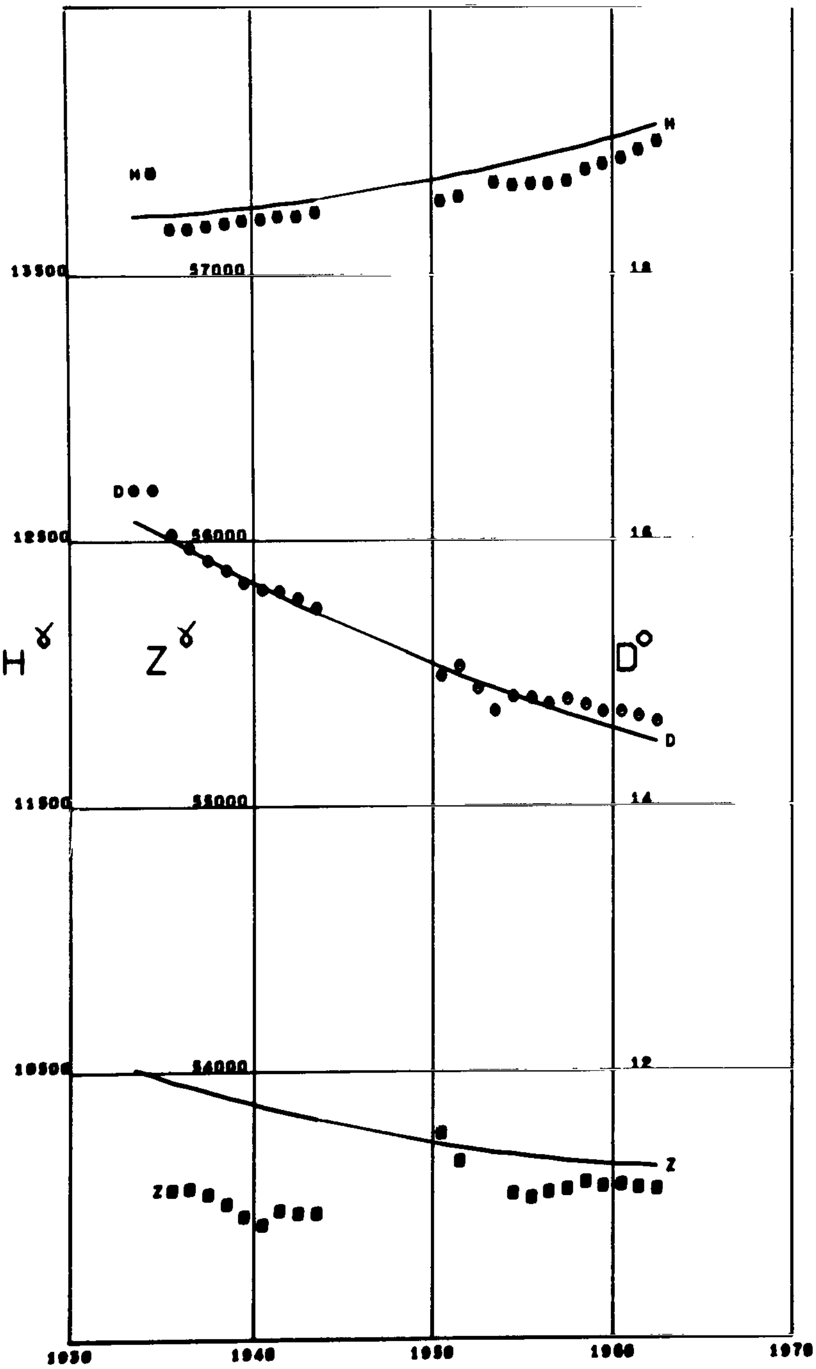

Figure A190

VAL JOYEUX
Lat 48.82 Long 2.01

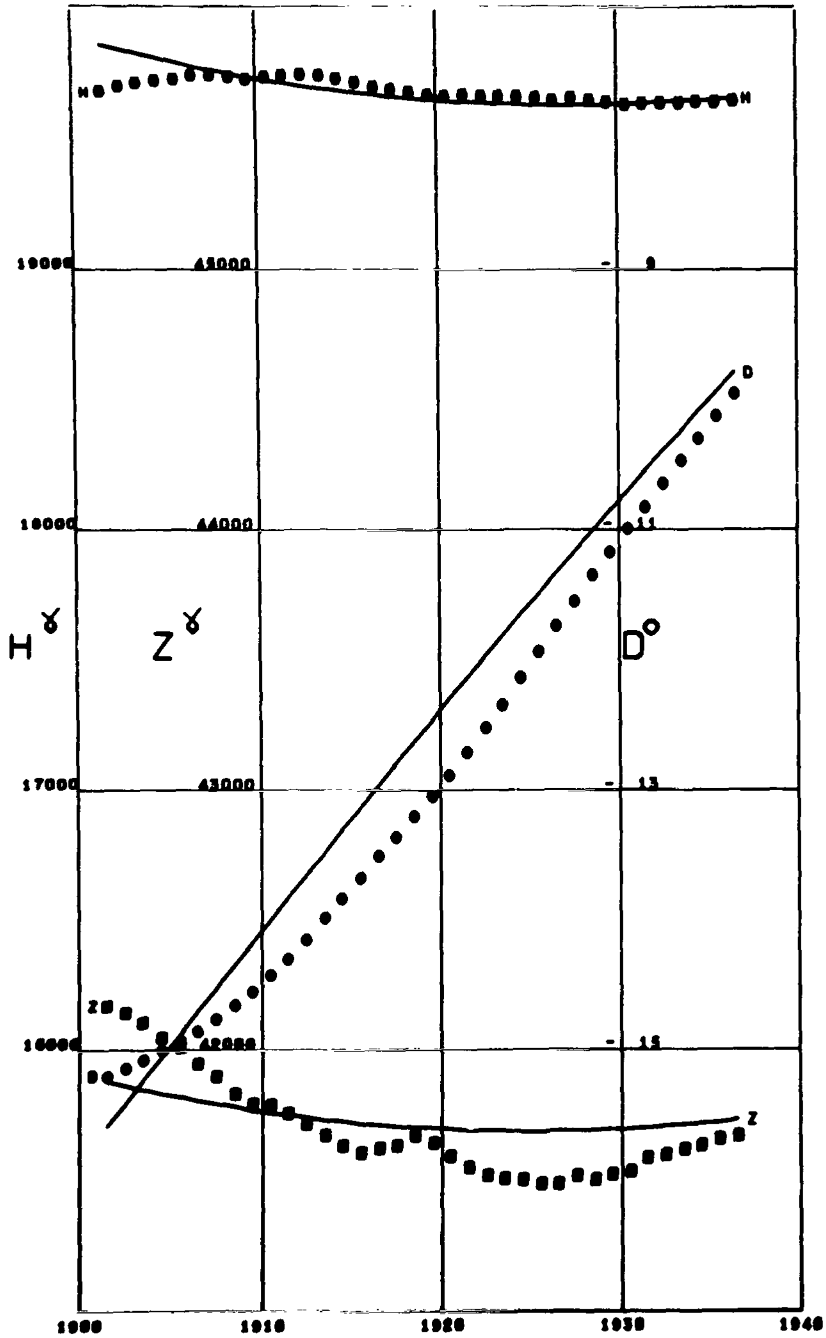

Figure A191

VALENTIA
Lat 51.93 Long -10.25

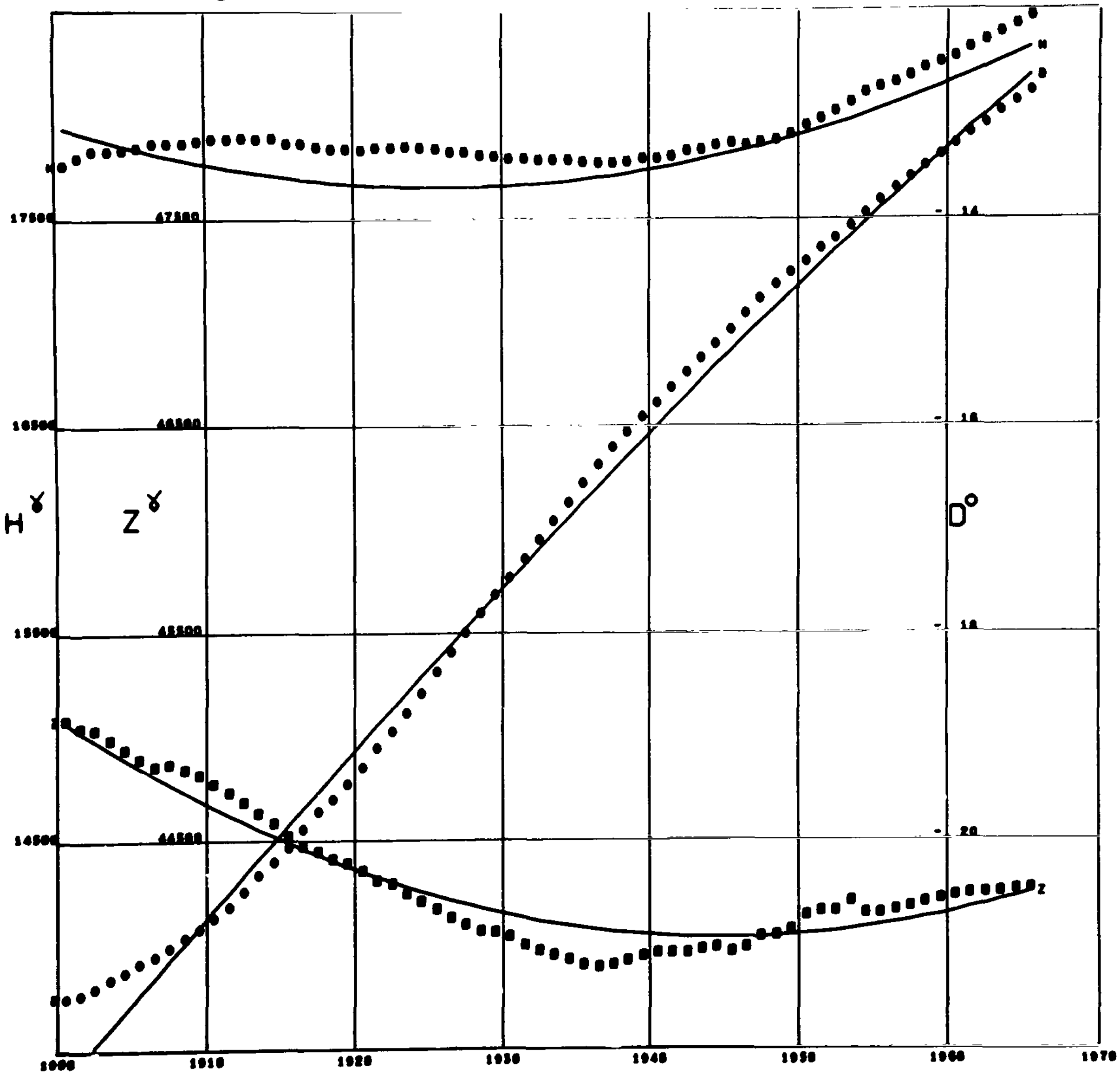

Figure A192

VASSOURAS
Lat -22.40 Long -43.65 Alt 0.46

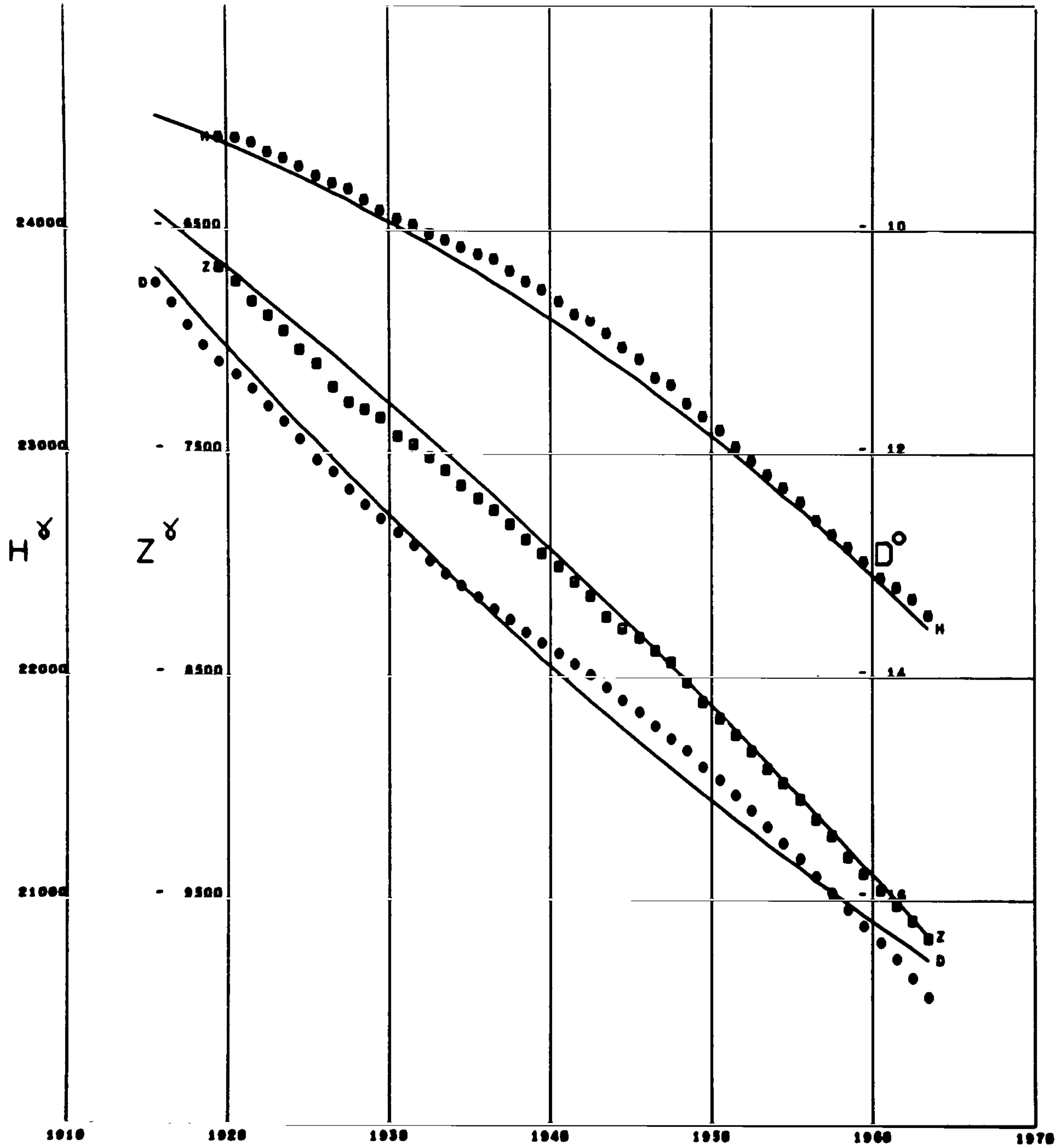

Figure A193

VYKHODNOY
Lat 73.23 Long 56.73

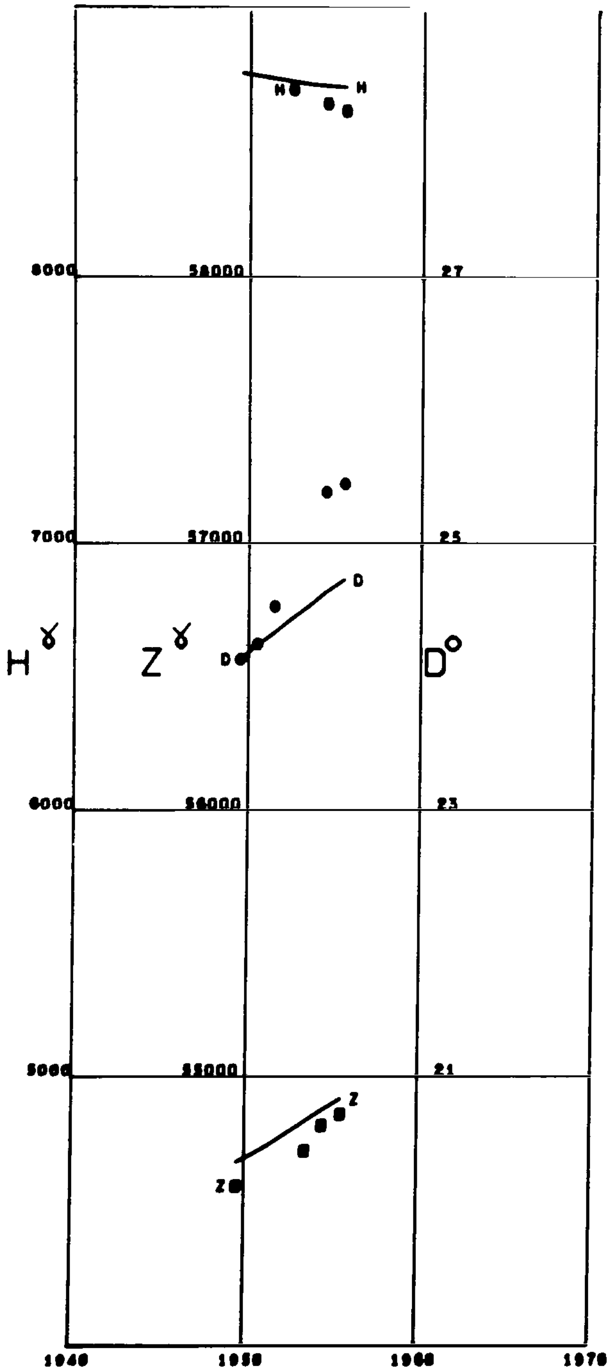

Figure A198

VYSOKAYA DUBRAVA
Lat 56.73 Long 61.06 Alt 0.29

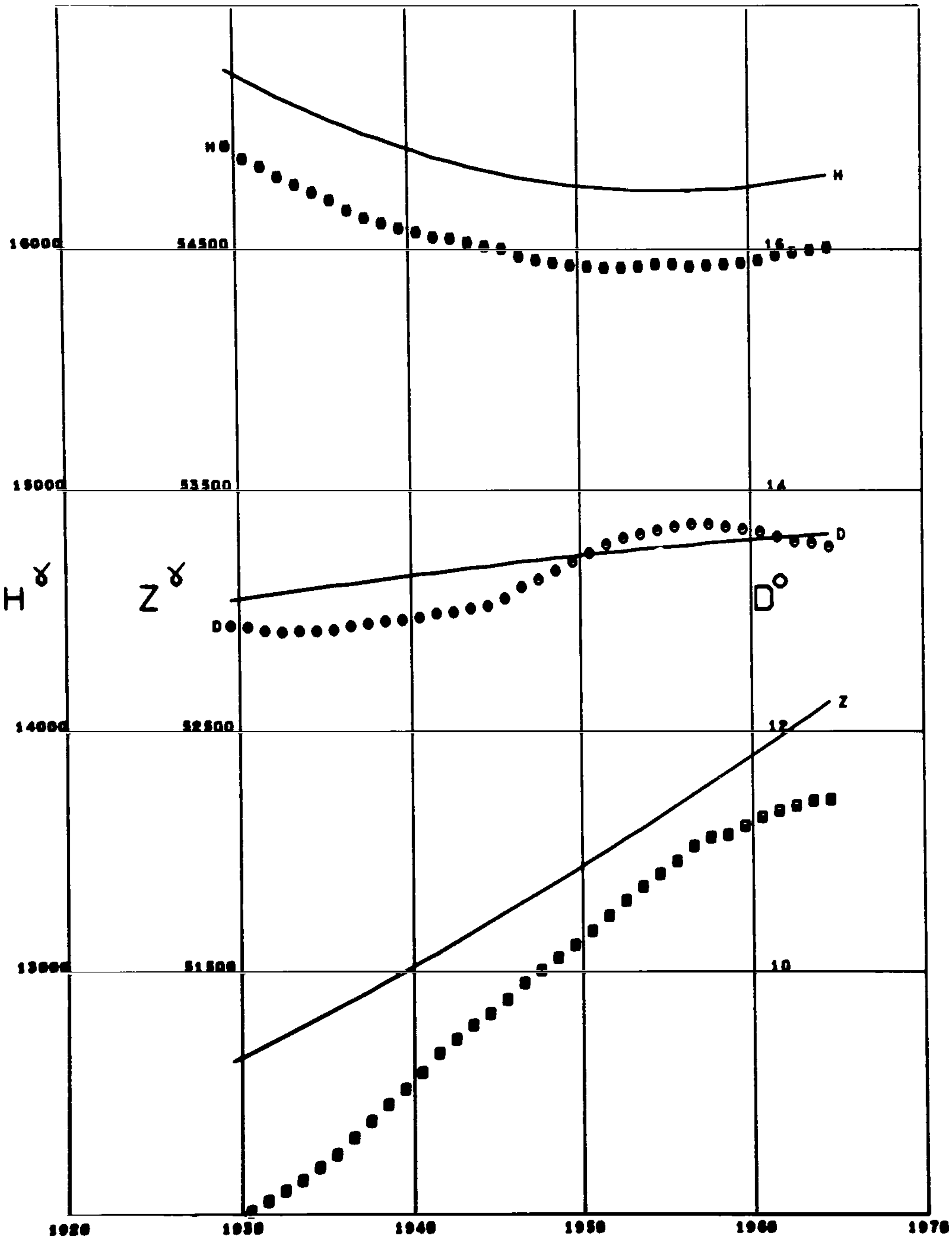

Figure A199

WATHEROO
Lat -30.31 Long 115.87

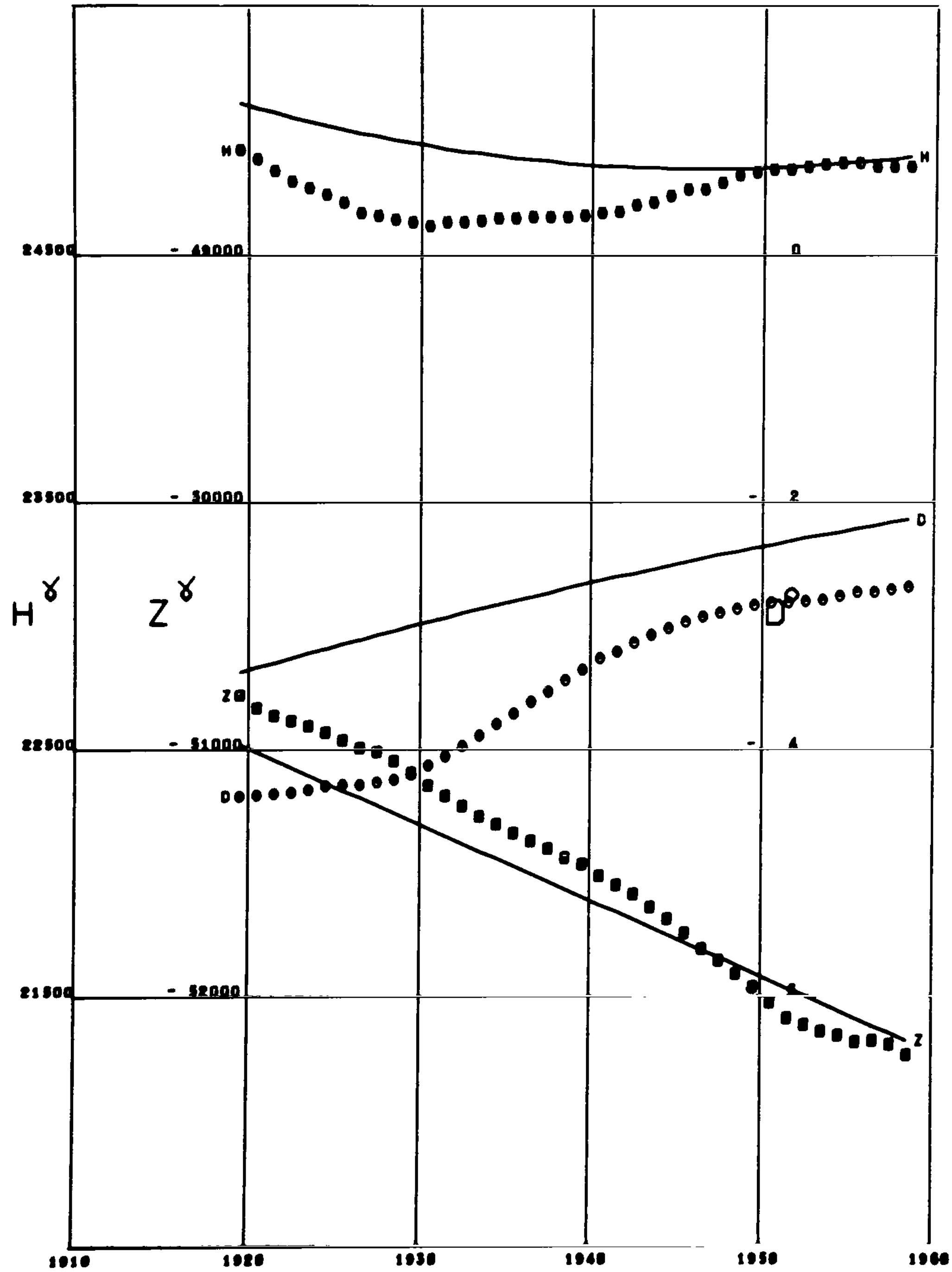

Figure A200

WIEN AUHOF
Lat 48.20 Long 16.23

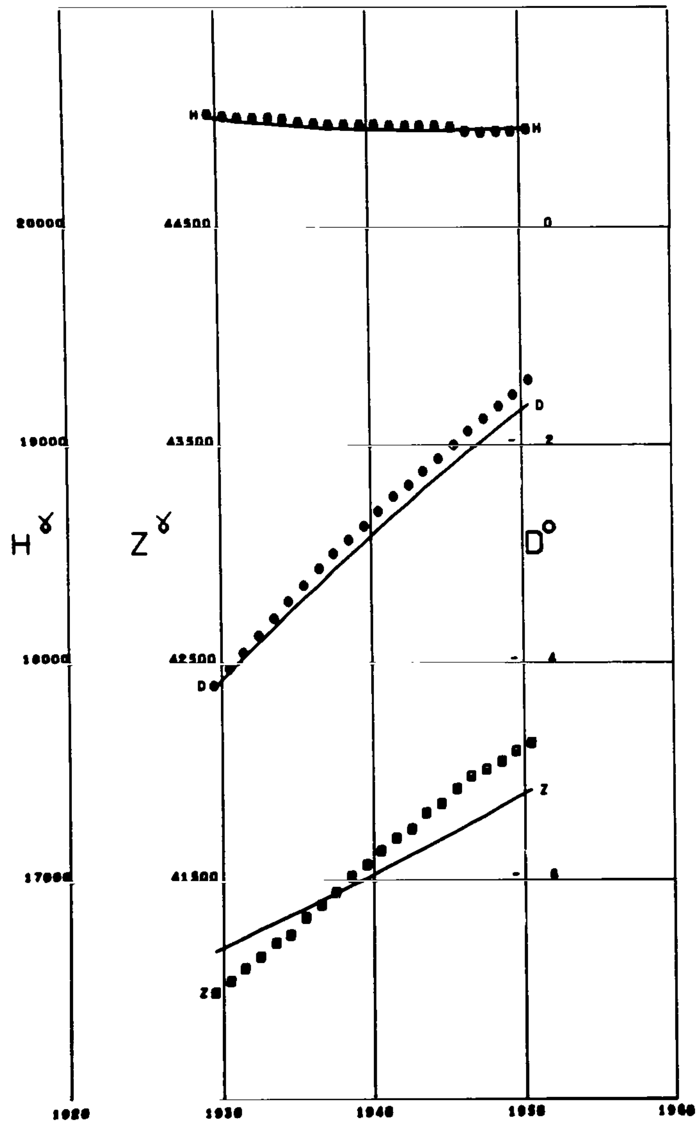

Figure A201

WIEN KOBENZL
Lat 48.26 Long 16.31

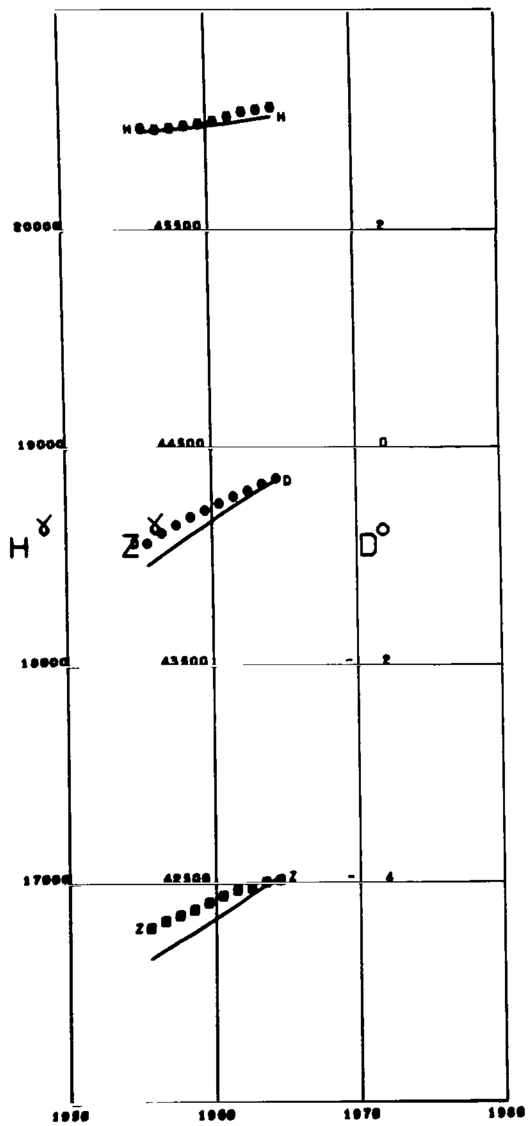

Figure A202

WILHELMSHAVEN
Lat 53.53 Long 8.14

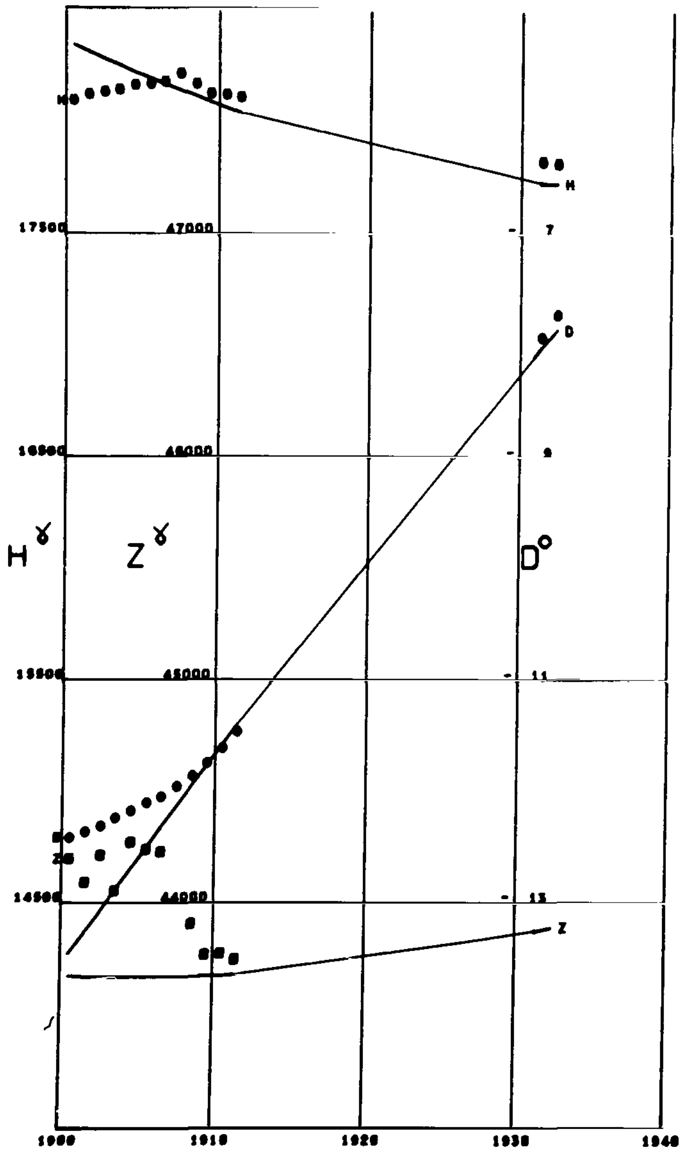

Figure A203

WILKES
Lat -66.25 Long 110.58 Alt 0.01

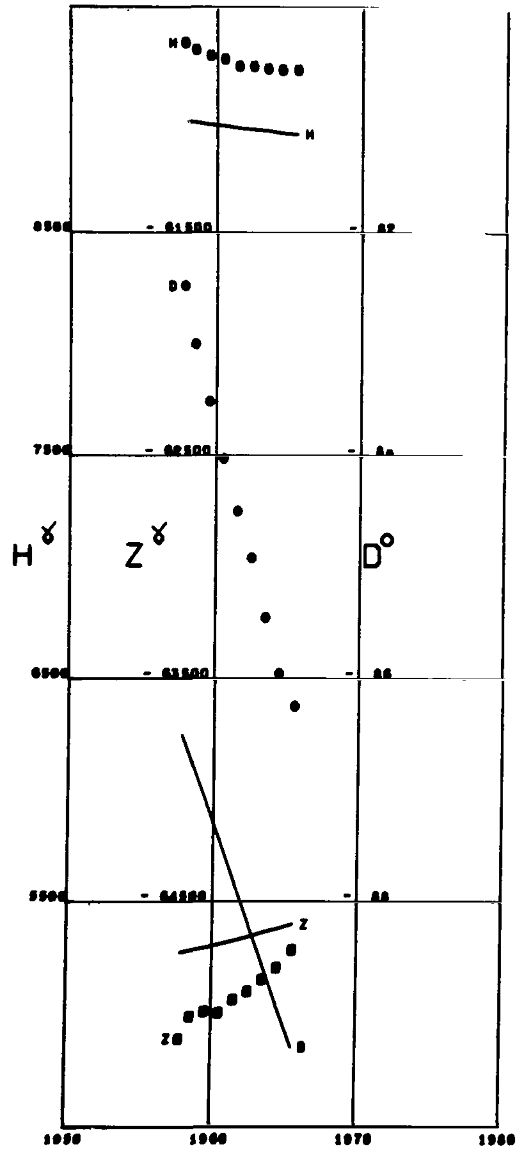

Figure A204

WINGST
Lat 53.74 Long 9.07

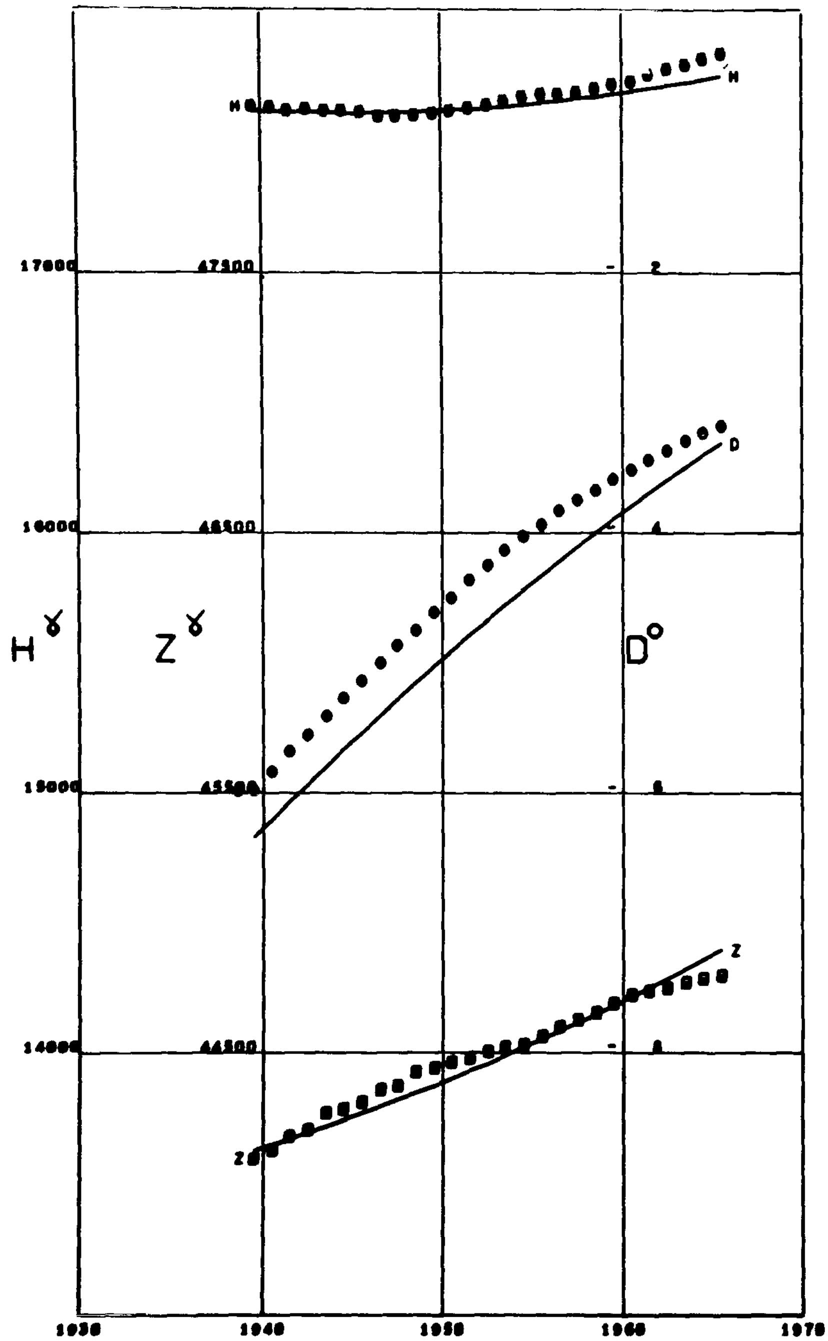

Figure A205

WITTEVEEN
Lat 52.81 Long 6.66

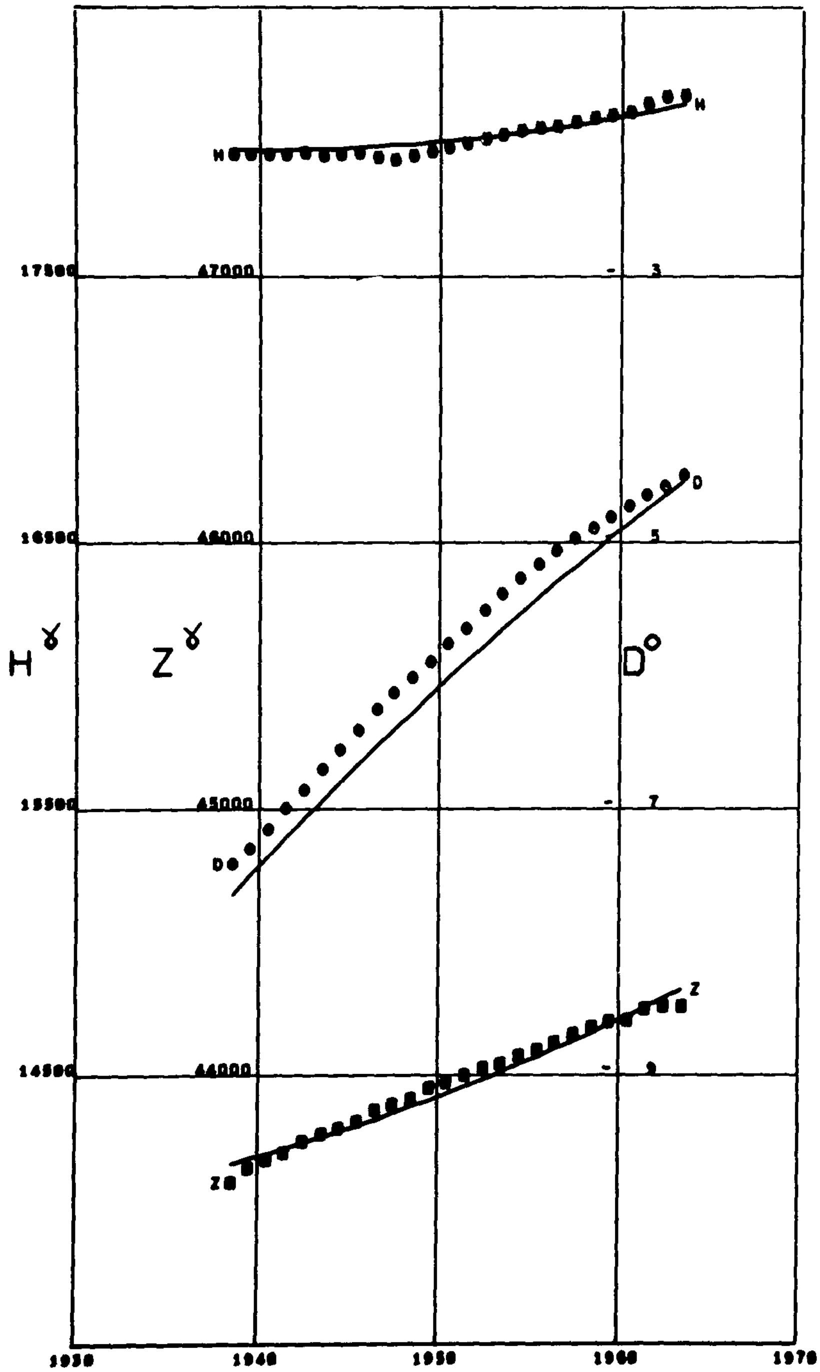

Figure A206

YAKUTSK
Lat 62.01 Long 129.71 Alt 0.10

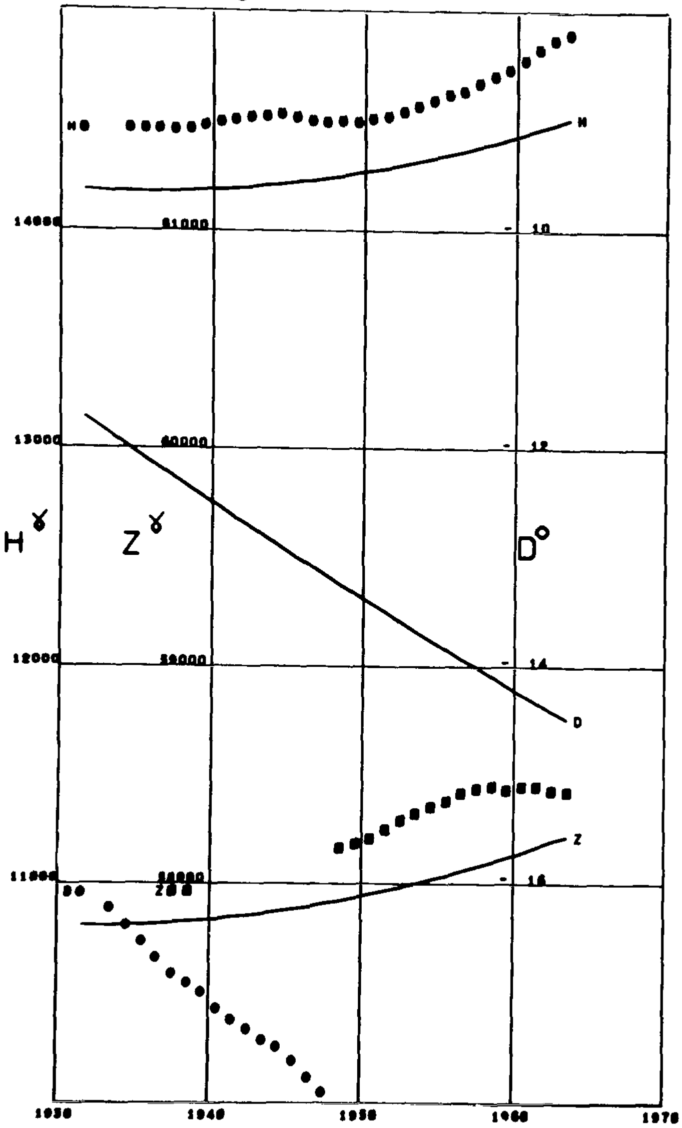

Figure A207

YUZHNO SAKHALINSK
Lat 46.95 Long 142.71

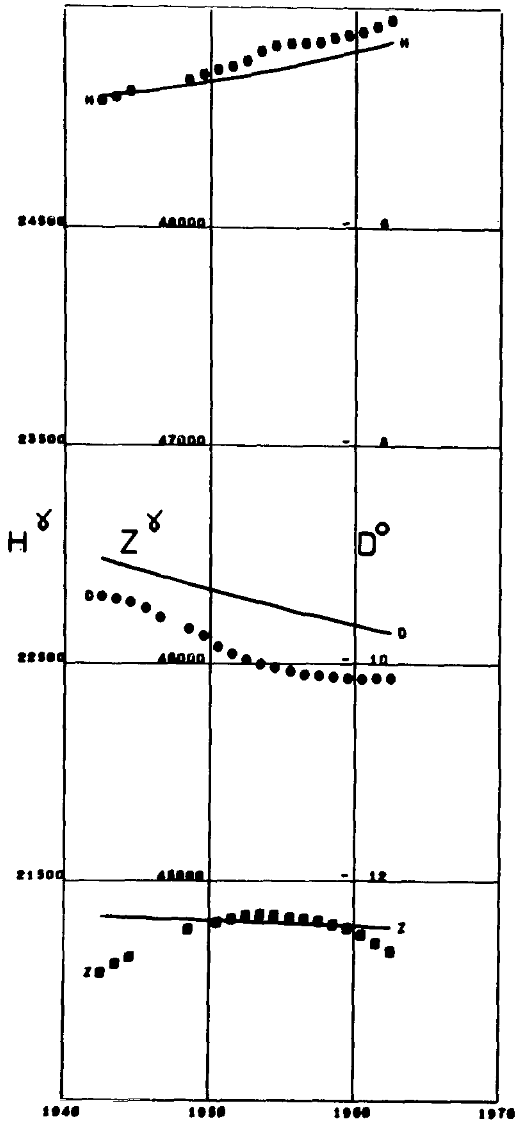

Figure A208

ZAYMISHCHE
Lat 55.83 Long 48.85

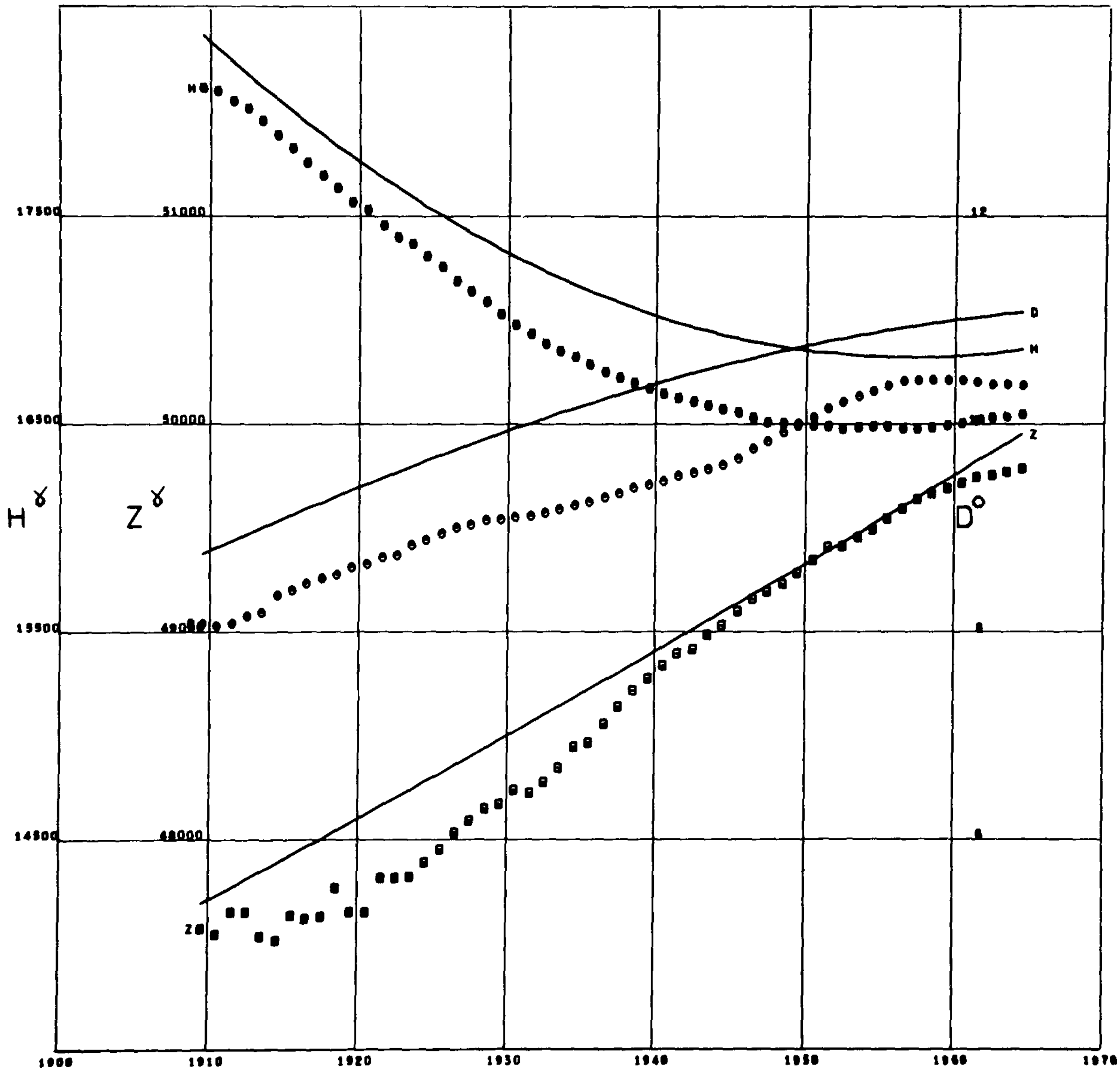

Figure A209

ZIKAWEI
Lat 31.20 Long 121.43

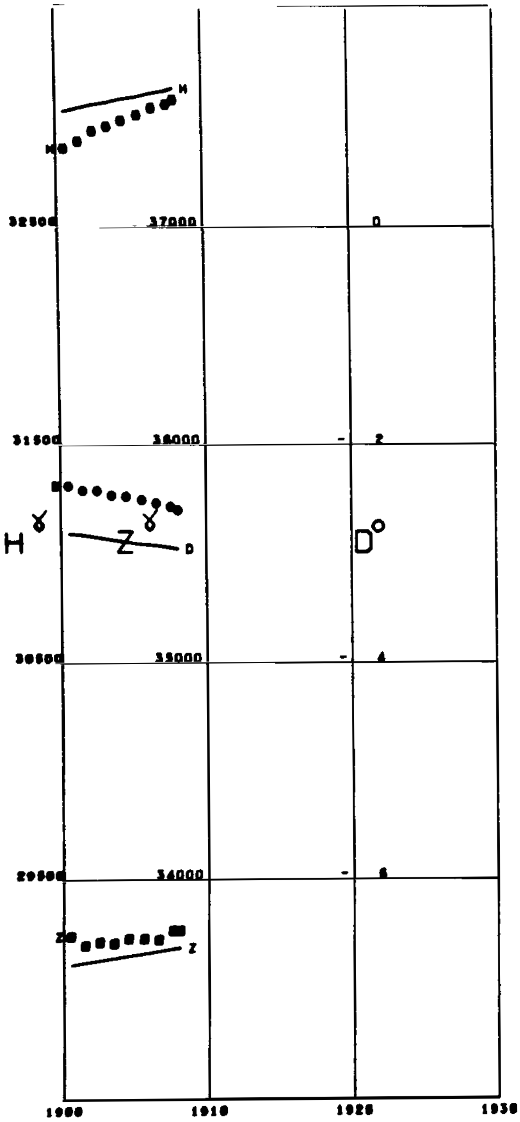

Figure A210

ZINSEN
Lat 37.47 Long 126.62

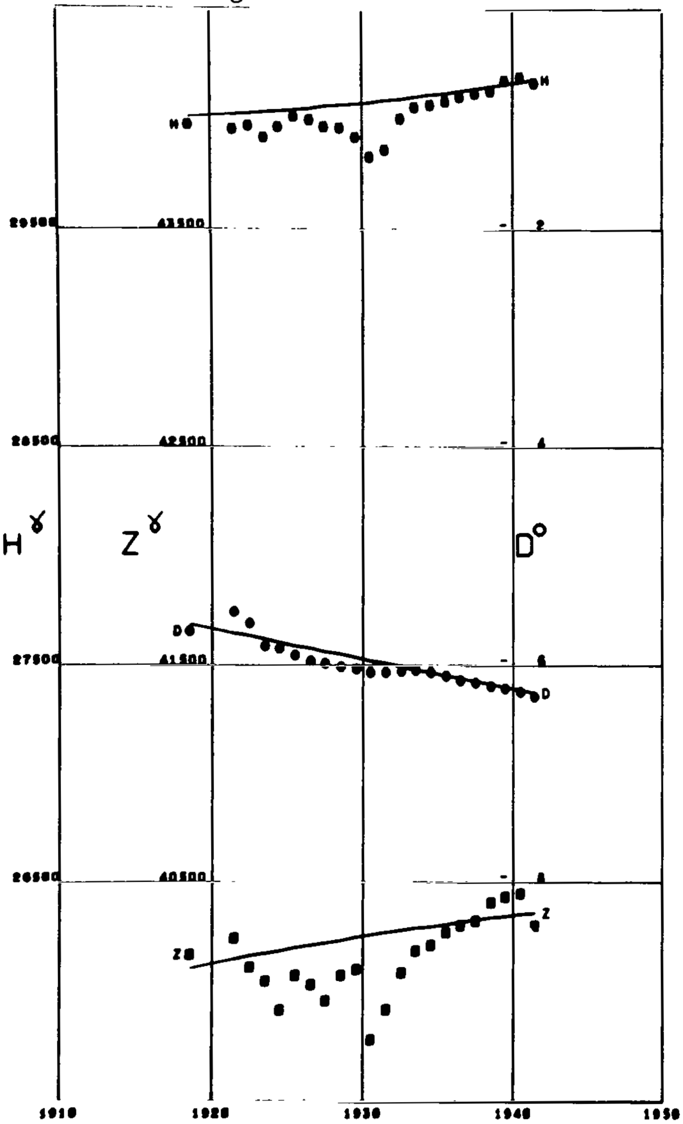

Figure A211

ZO SE
Lat 31.09 Long 121.18

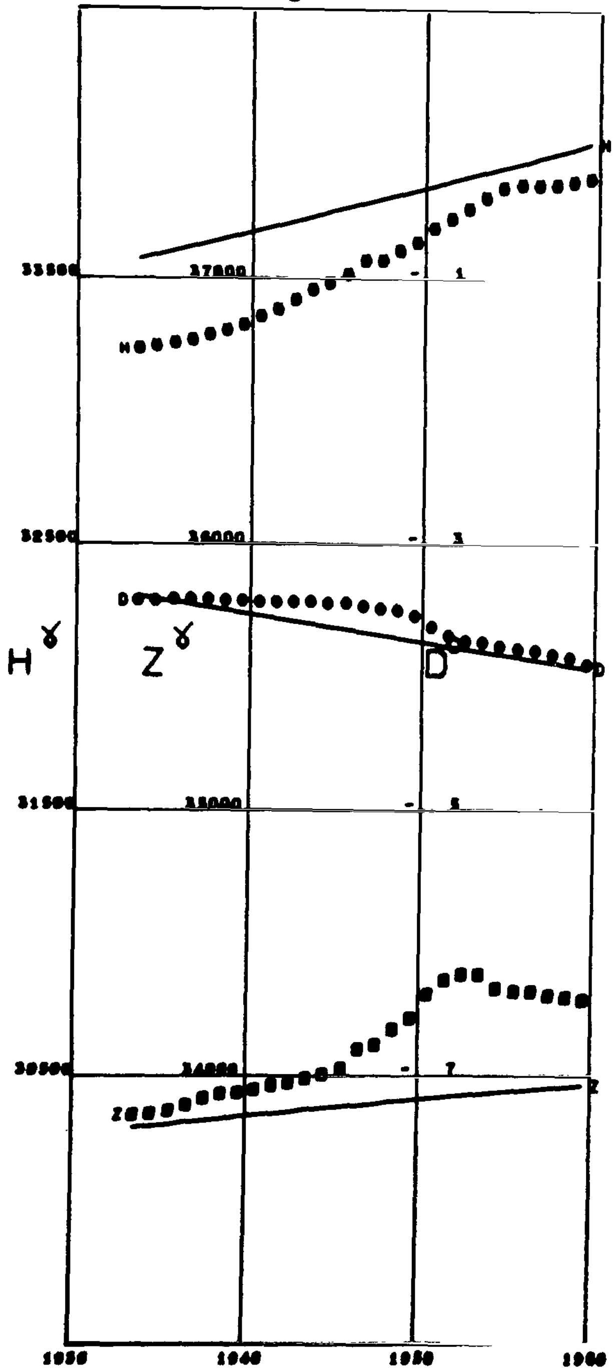

Figure A212

ZUY
Lat 52.46 Long 104.03

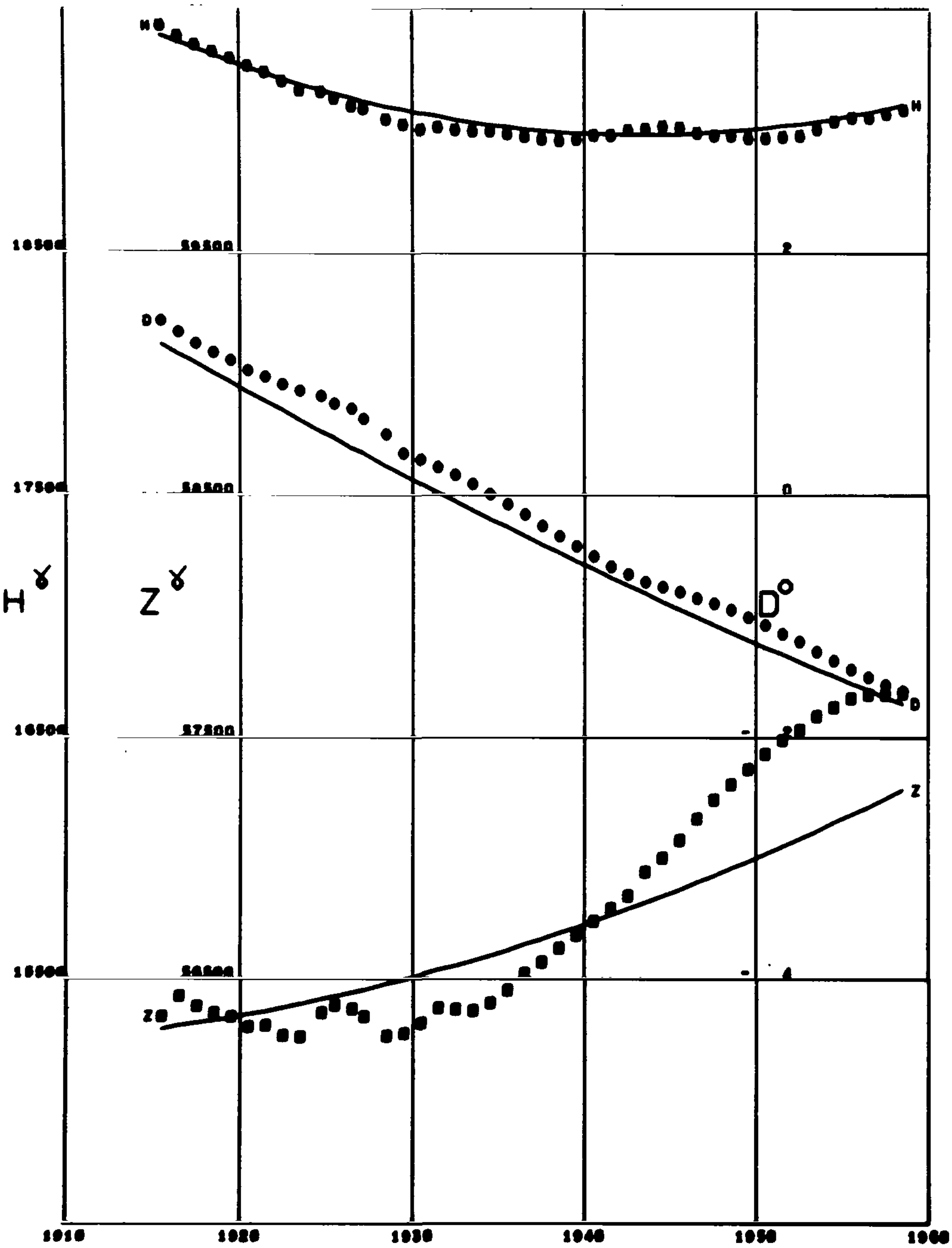

Figure A213

Appendix B

Comparison of Isoporic Charts (1912-1942) From GSFC (12/66) With Those From Vestine et al. (1947)

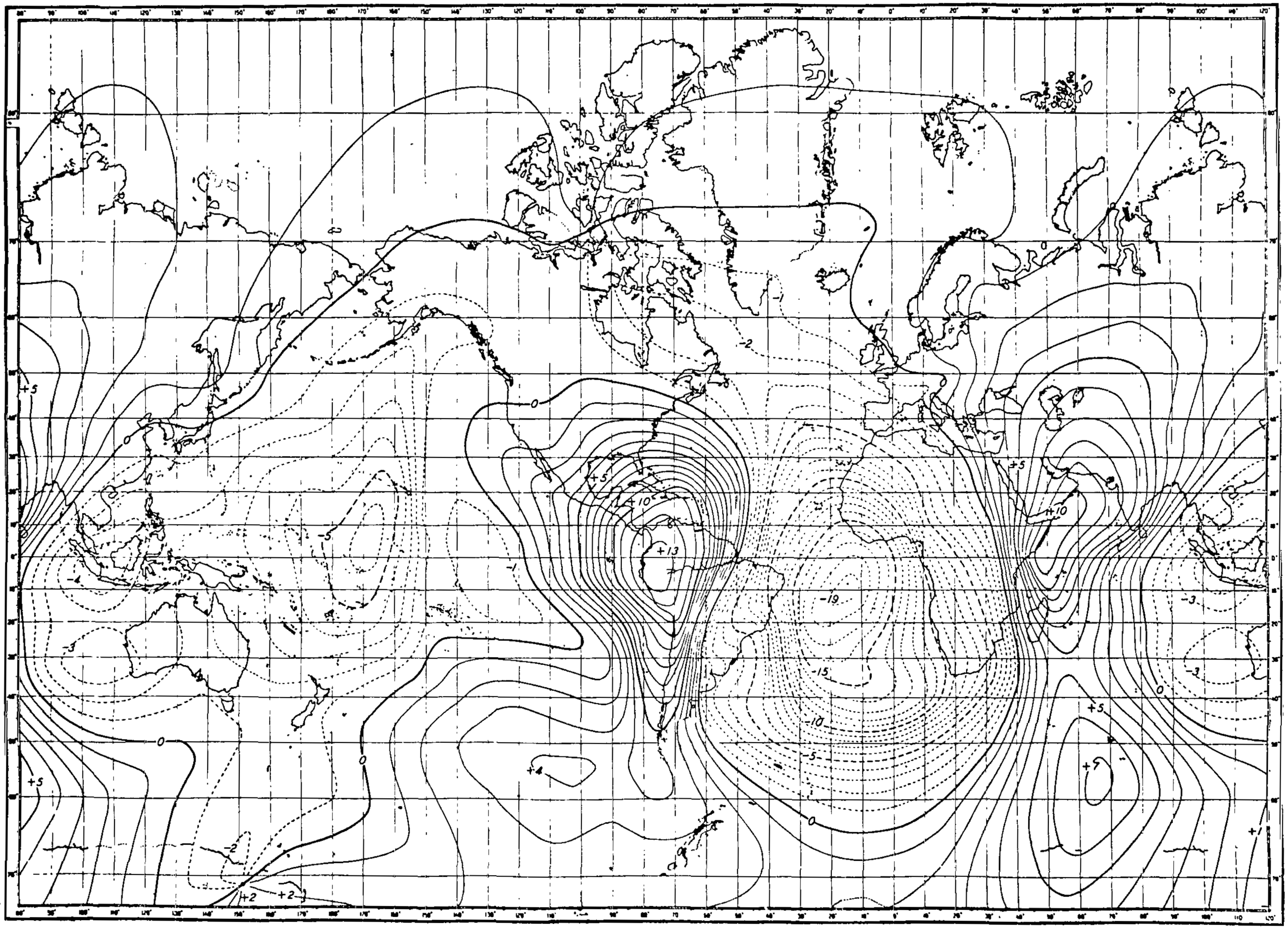

Figure B1-Geomagnetic secular change in minutes per year, inclination, epoch 1912.5. Vestine et al. (1947).

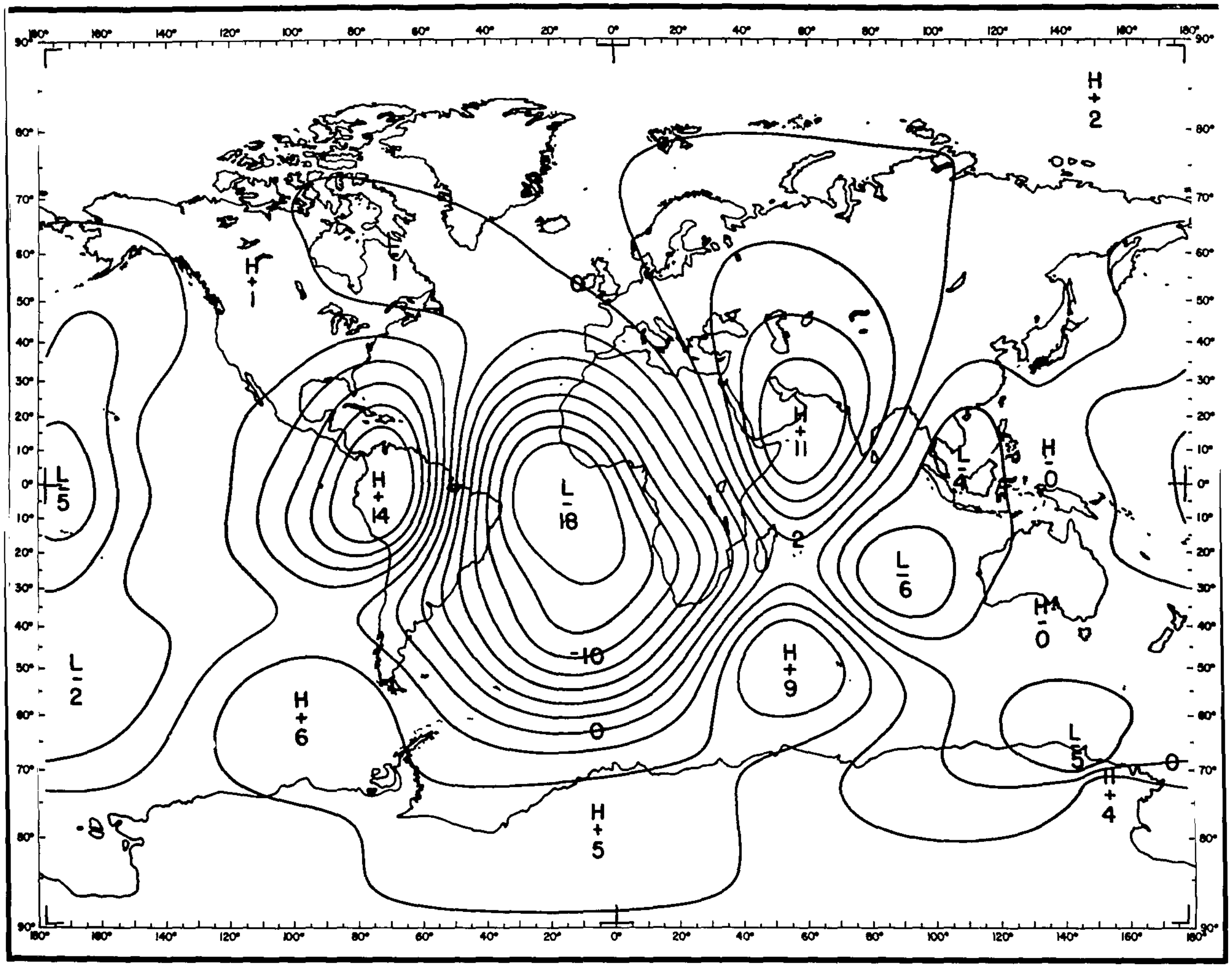

Figure B2—Geomagnetic secular change in minutes per year, inclination, epoch 1912.5. GSFC (12/66).

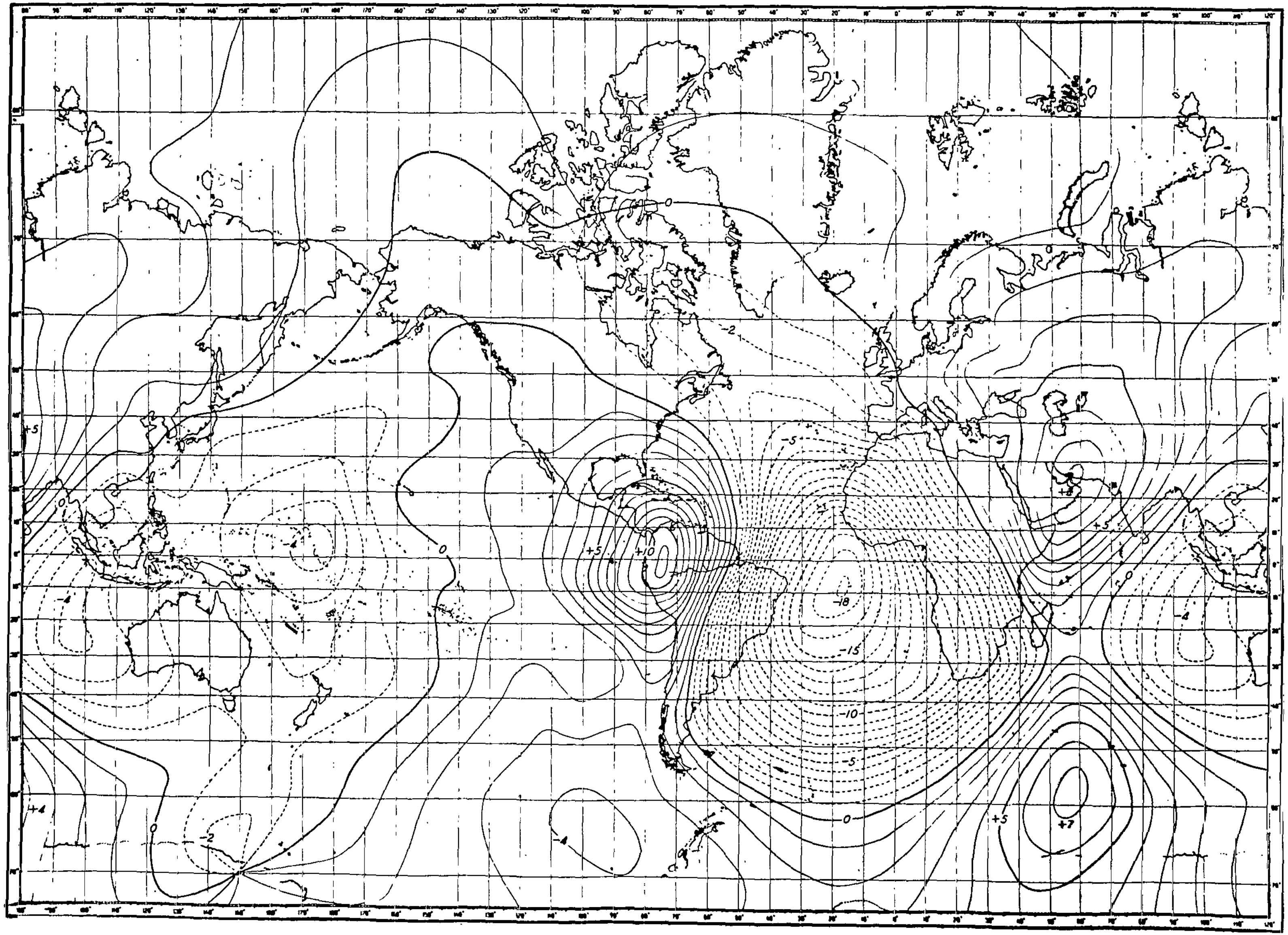

Figure B3-Geomagnetic secular change in minutes per year, inclination, epoch 1922.5. Vestine et al. (1947).

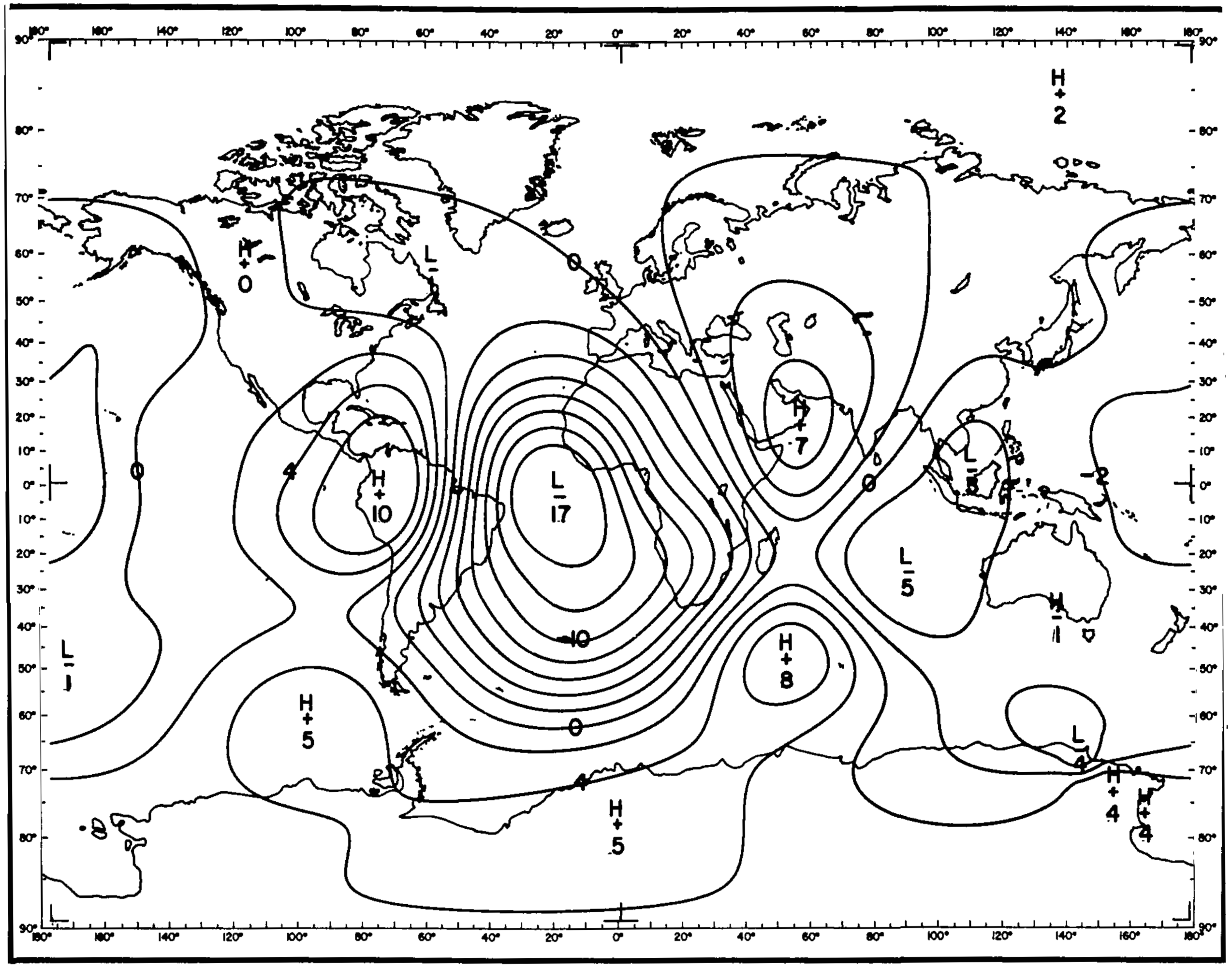

Figure B4—Geomagnetic secular change in minutes per year, inclination, epoch 1922.5. GSFC (12/66).

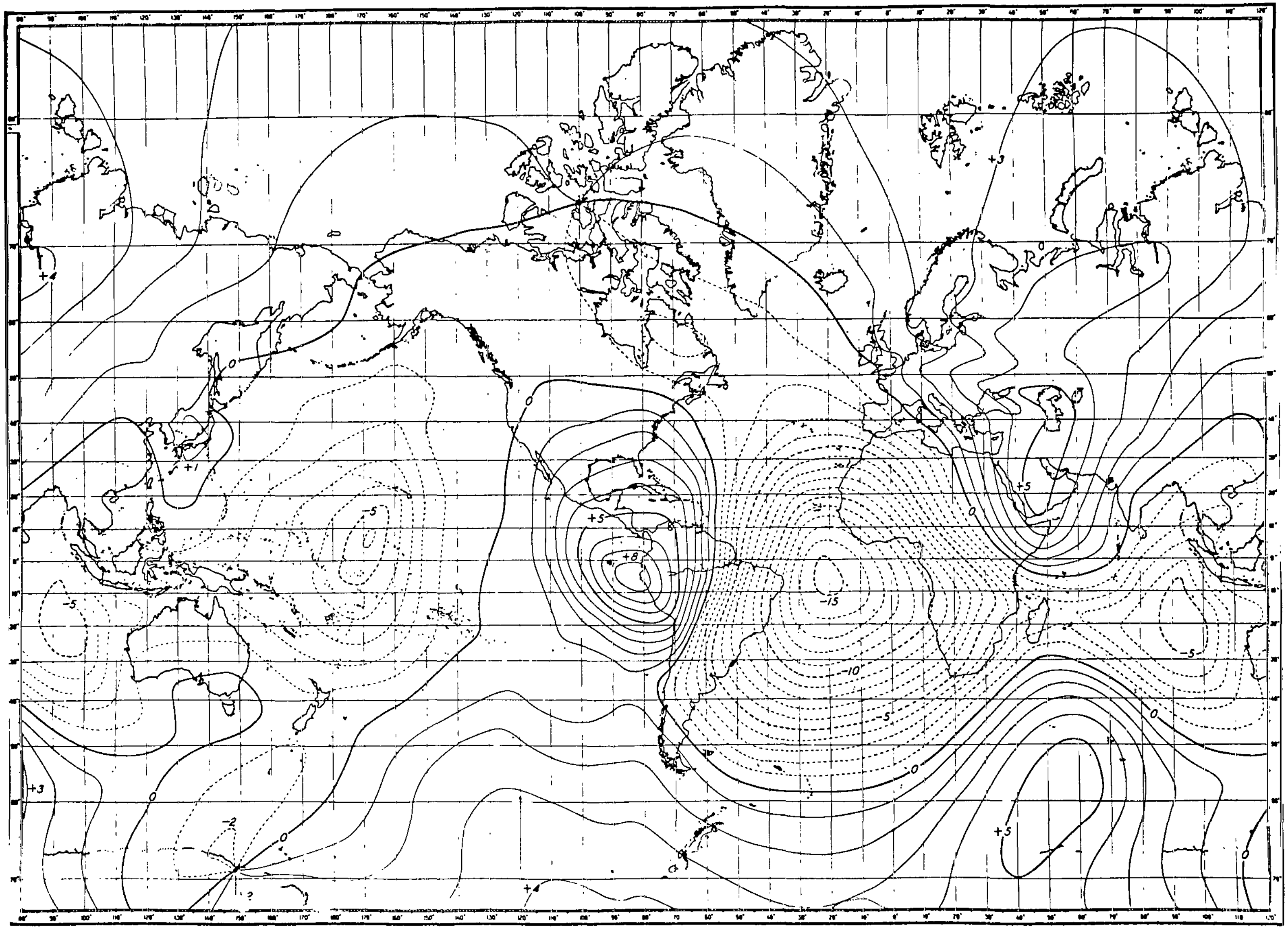

Figure B5–Geomagnetic secular change in minutes per year, inclination, epoch 1932.5. Vestine et al. (1947).

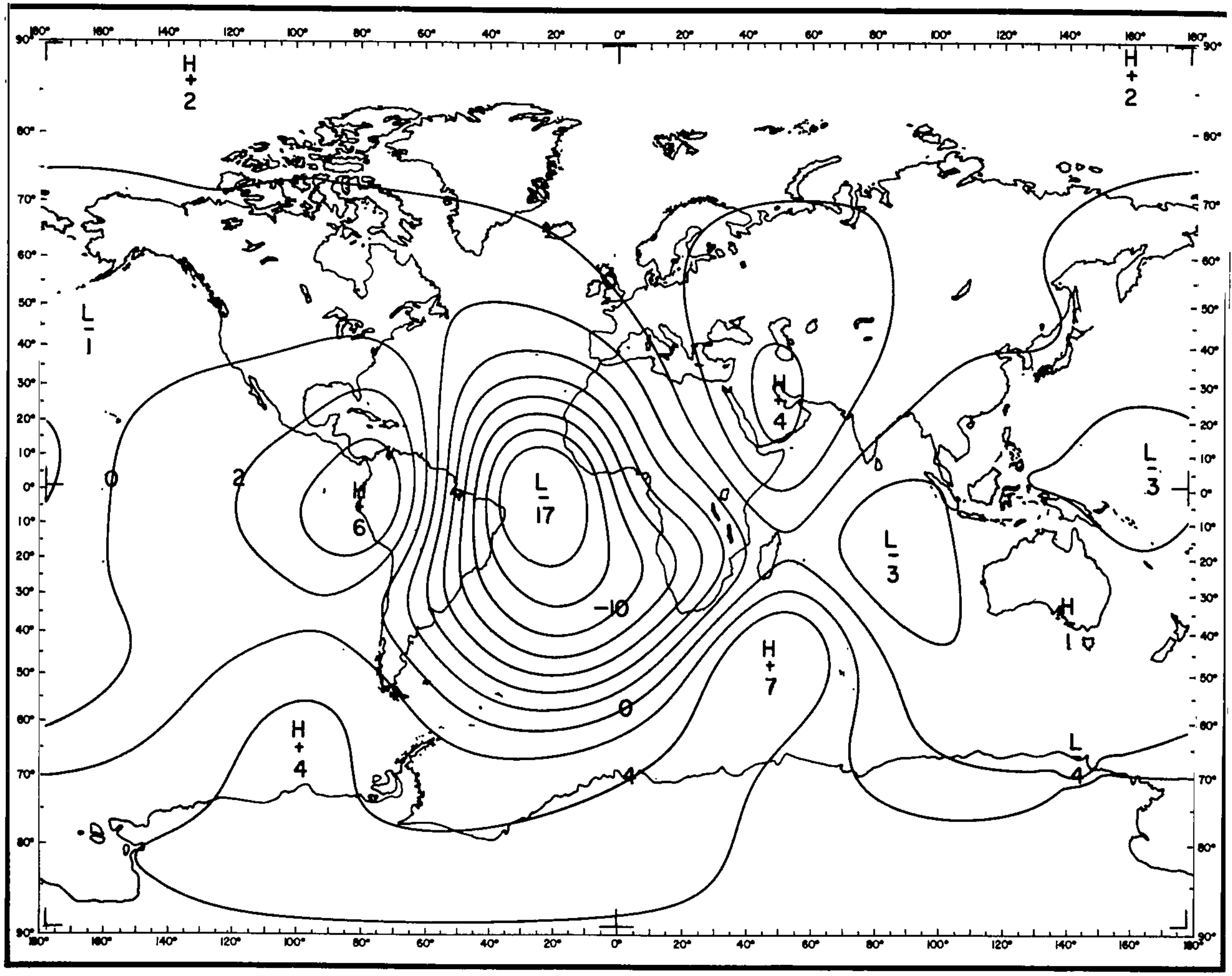

Figure B6—Geomagnetic secular change in minutes per year, inclination, epoch 1932.5. GSFC (12/66).

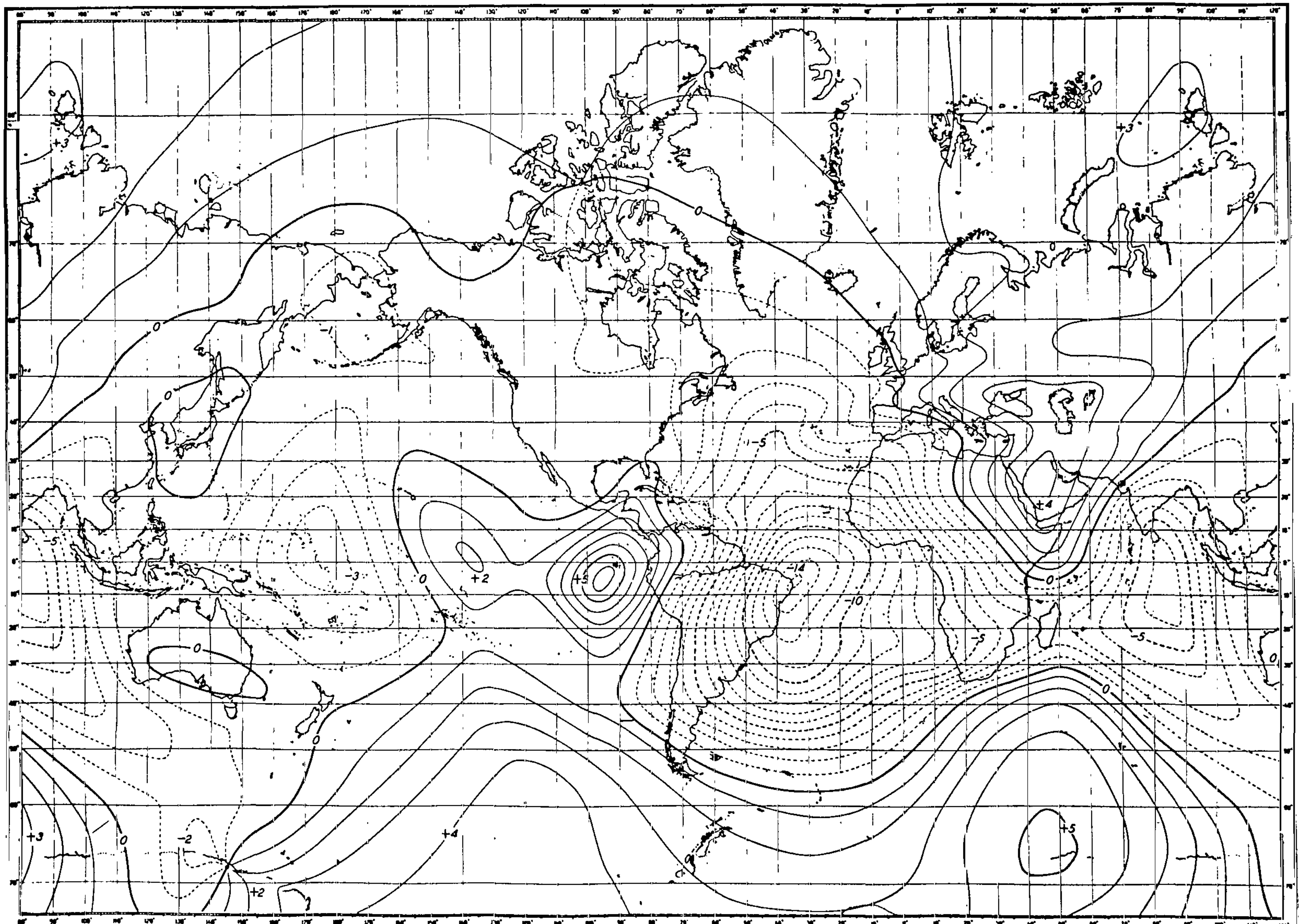

Figure B7-Geomagnetic secular change in minutes per year, inclination, epoch 1942.5. Vestine et al. (1947).

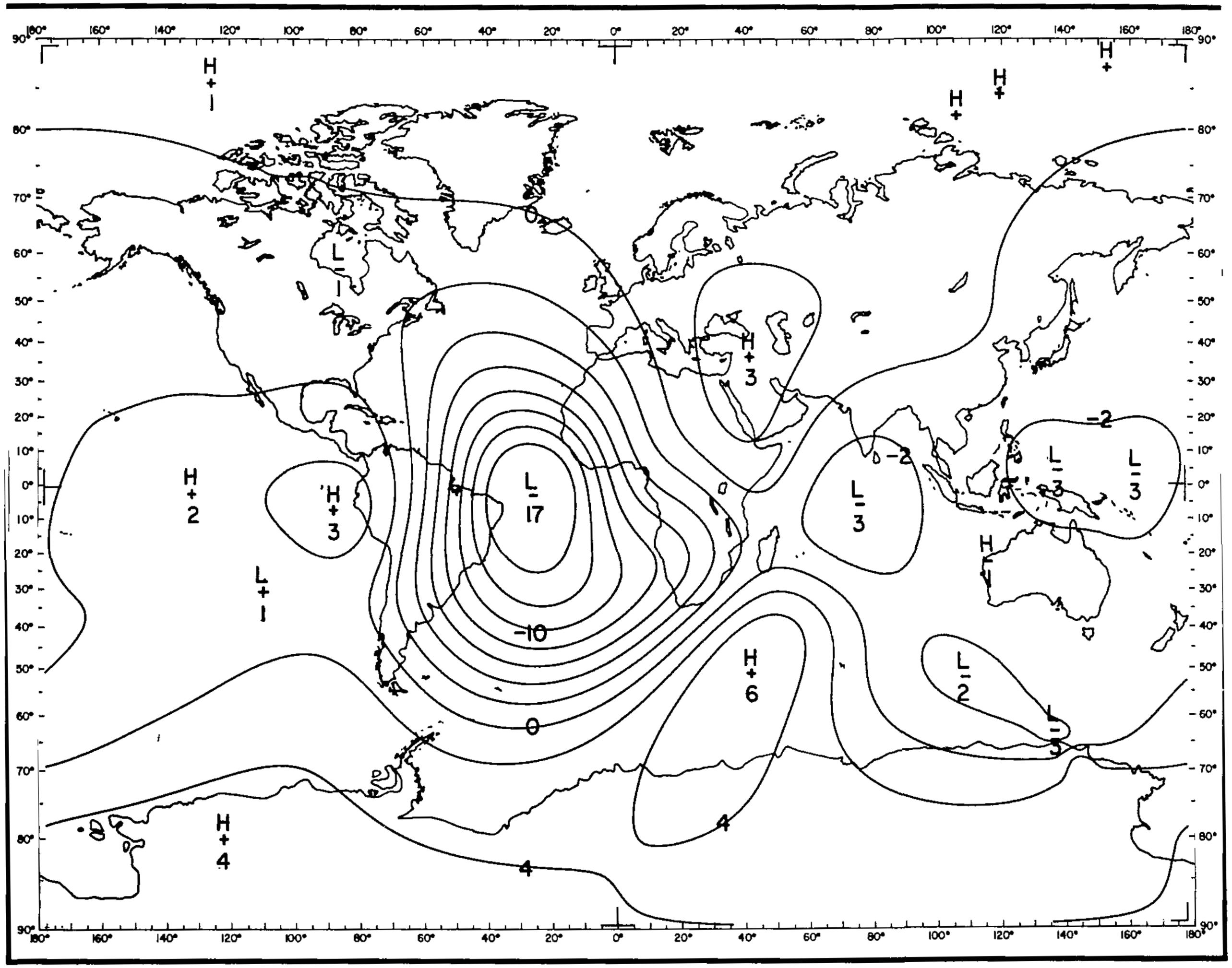

Figure B8—Geomagnetic secular change in minutes per year, inclination, epoch 1942.5. GSFC (12/66).

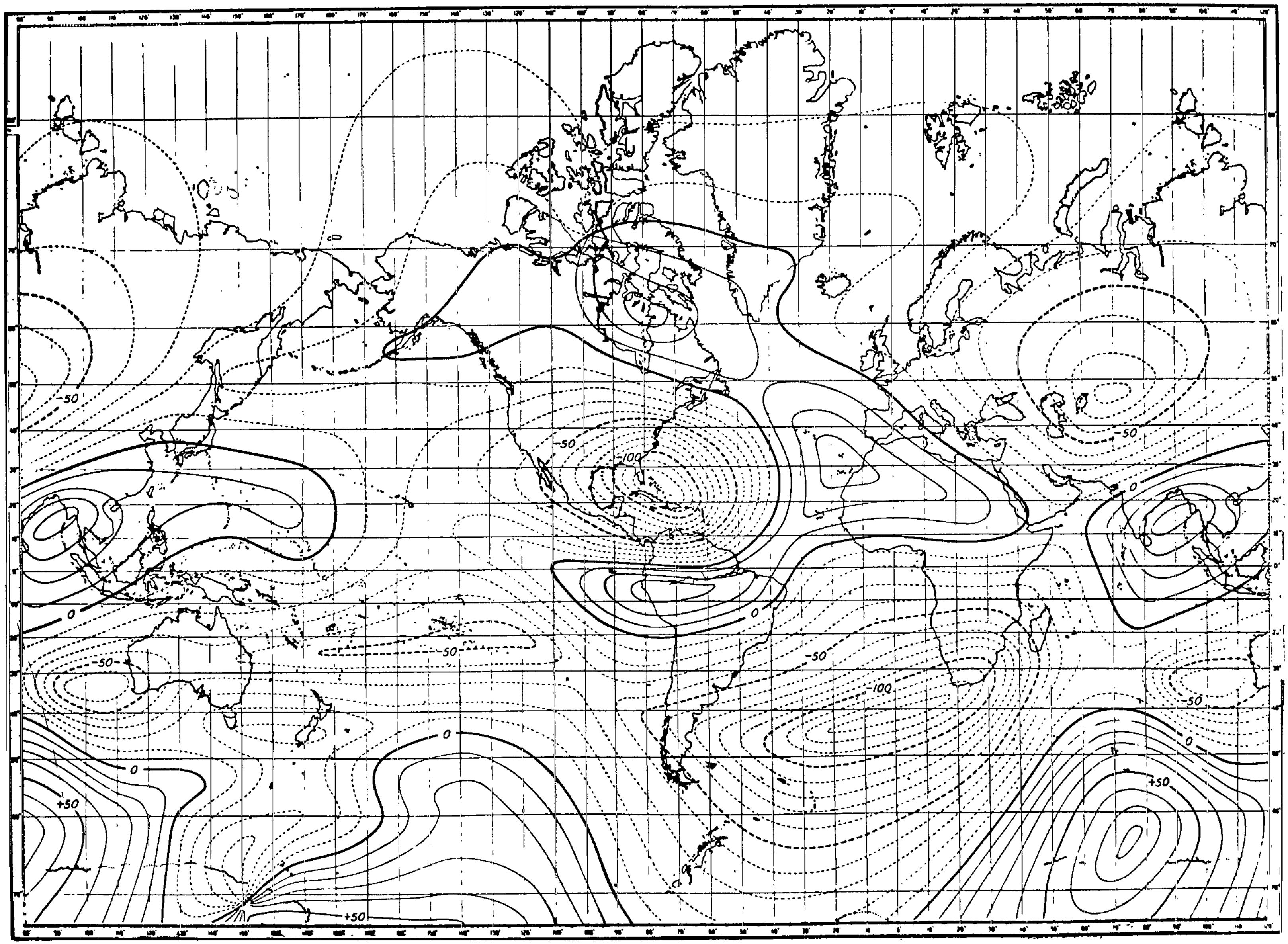

Figure B9–Geomagnetic secular change in gammas per year, horizontal component, epoch 1912.5. Vestine et al. (1947).

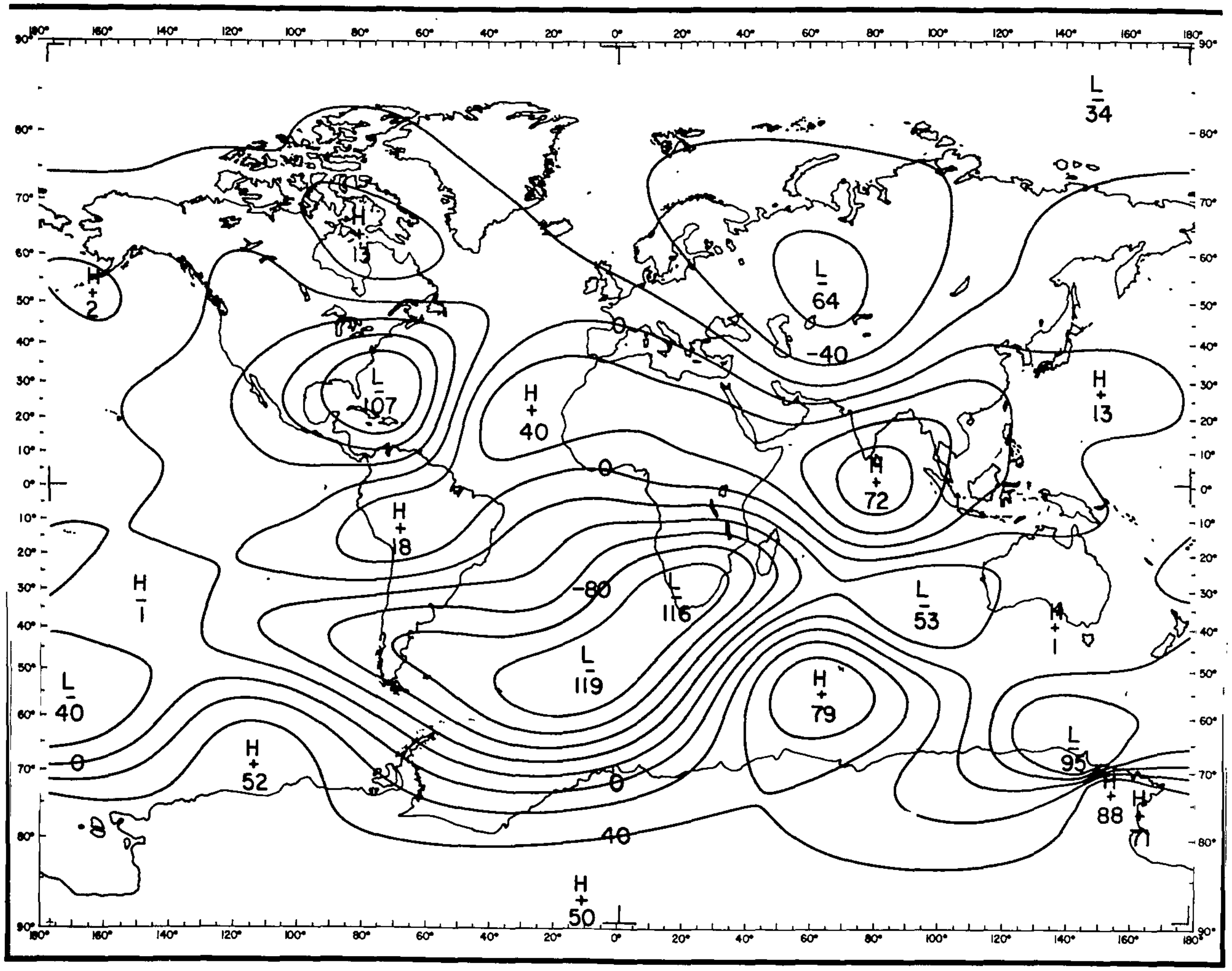

Figure B10—Geomagnetic secular change in gammas per year, horizontal component, epoch 1912.5. GSFC (12/66).

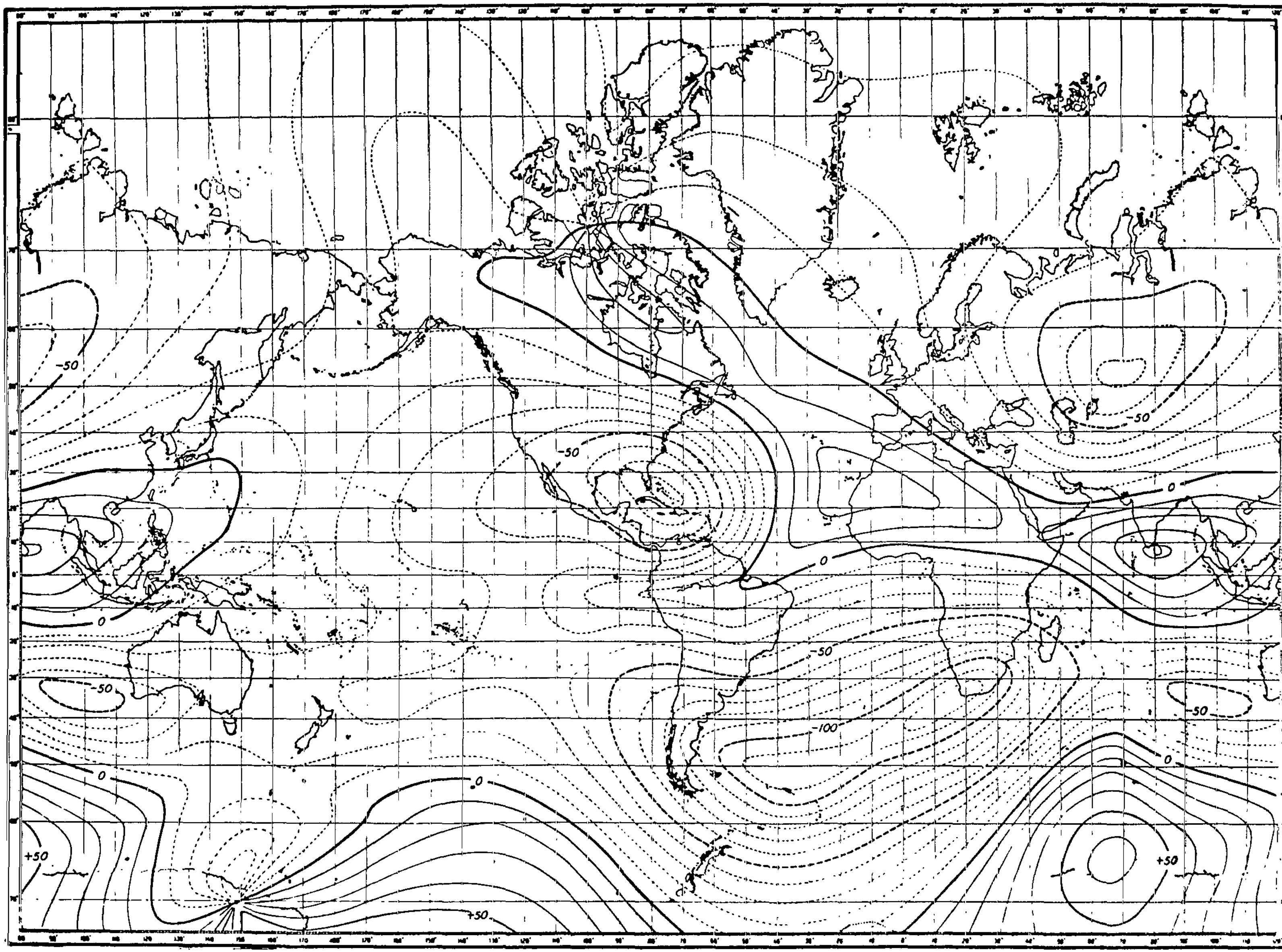

Figure B11–Geomagnetic secular change in gammas per year, horizontal component, epoch 1922.5. Vestine et al. (1947).

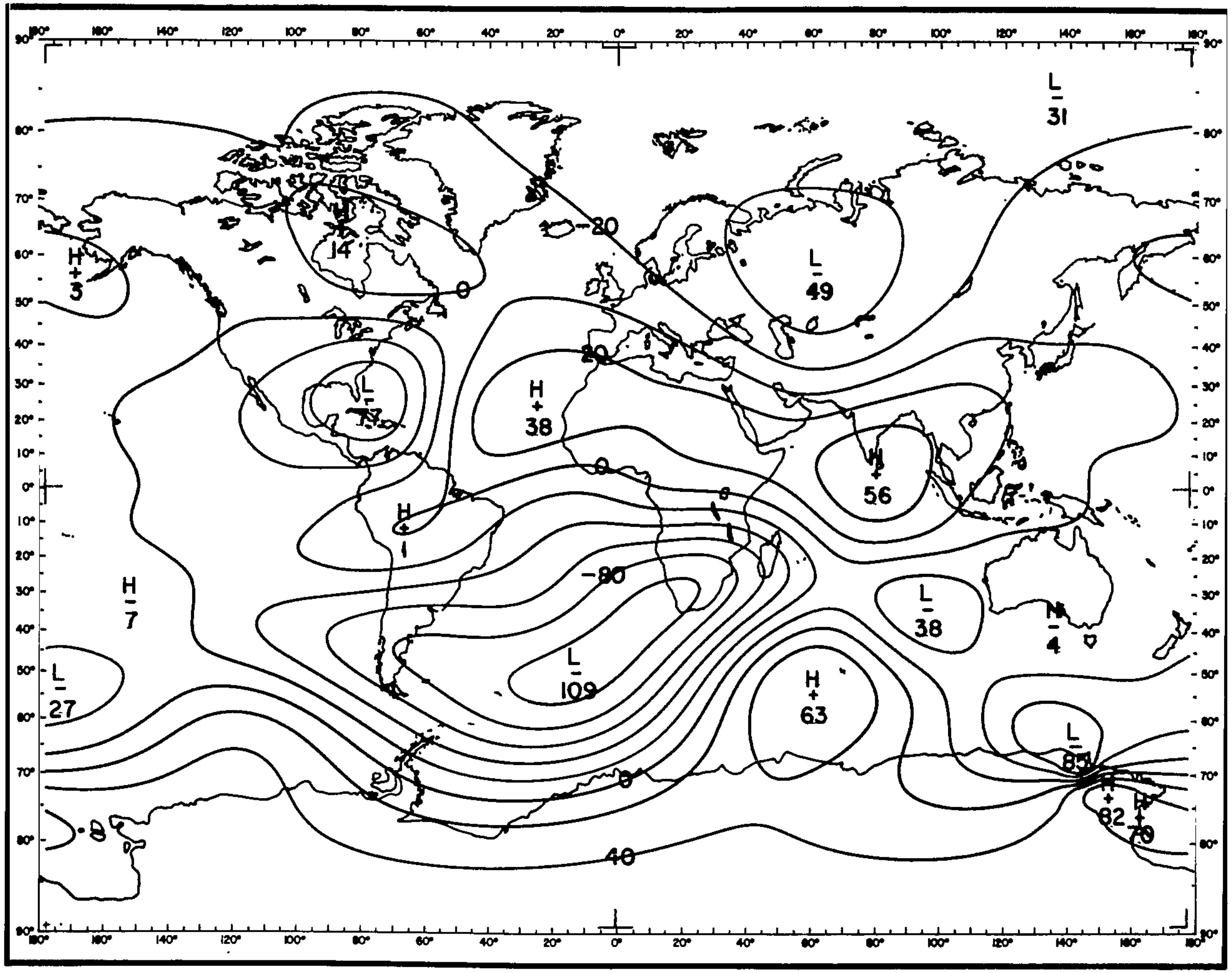

Figure B12—Geomagnetic secular change in gammas per year, horizontal component, epoch 1922.5. GSFC (12/66).

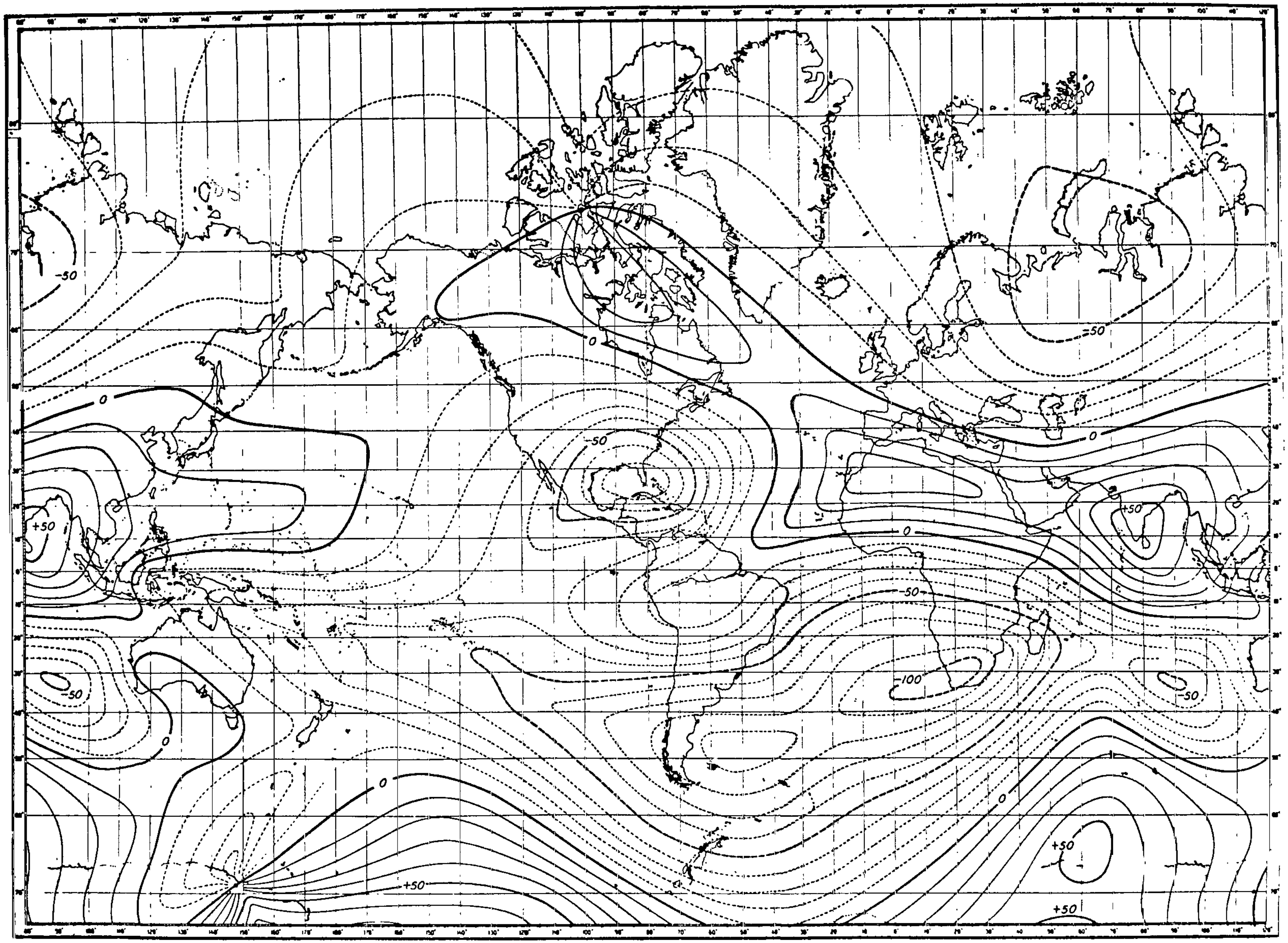

Figure B13–Geomagnetic secular change in gammas per year, horizontal component, epoch 1932.5. Vestine et al. (1947).

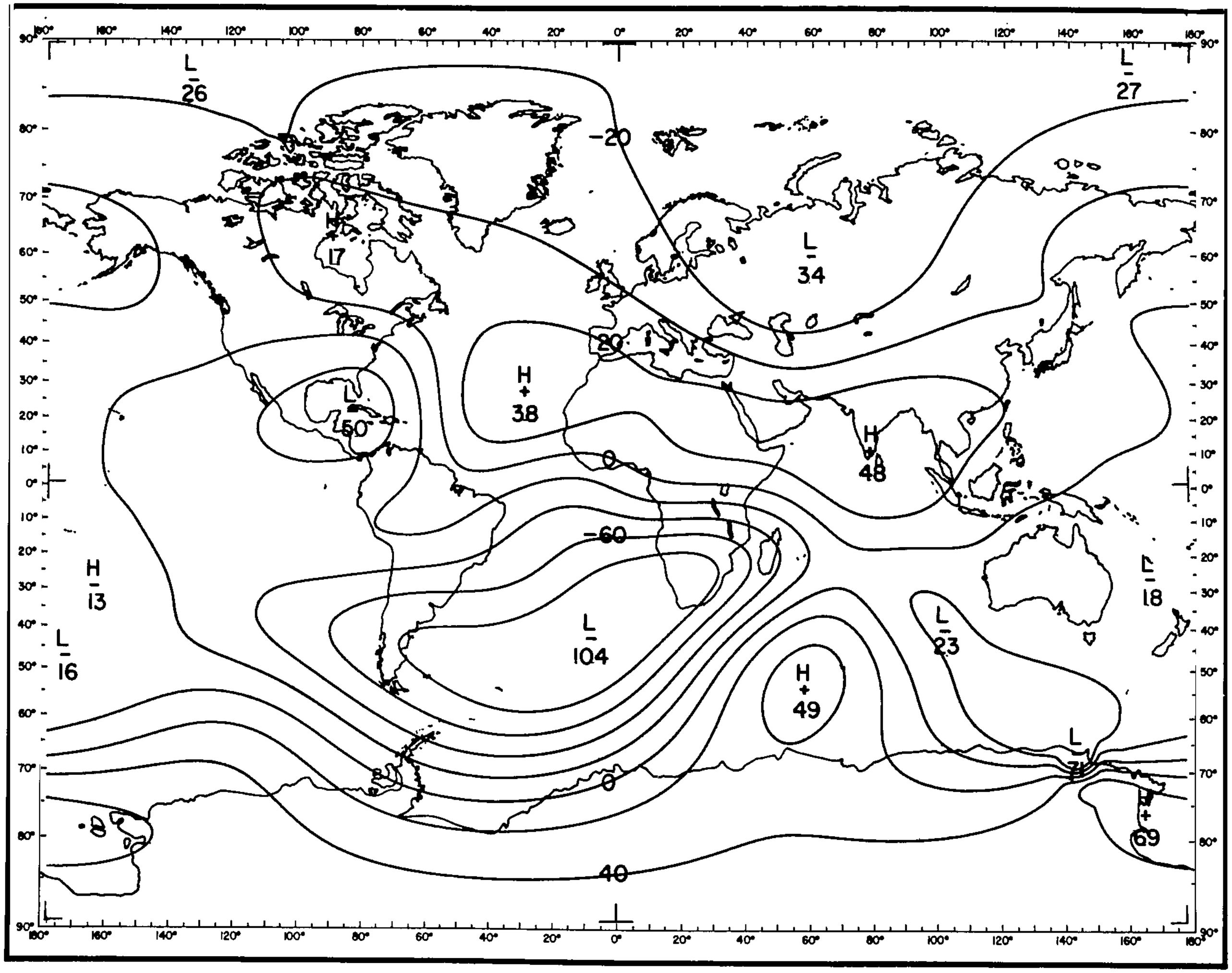

Figure B14—Geomagnetic secular change in gammas per year, horizontal component, epoch 1932.5. GSFC (12/66).

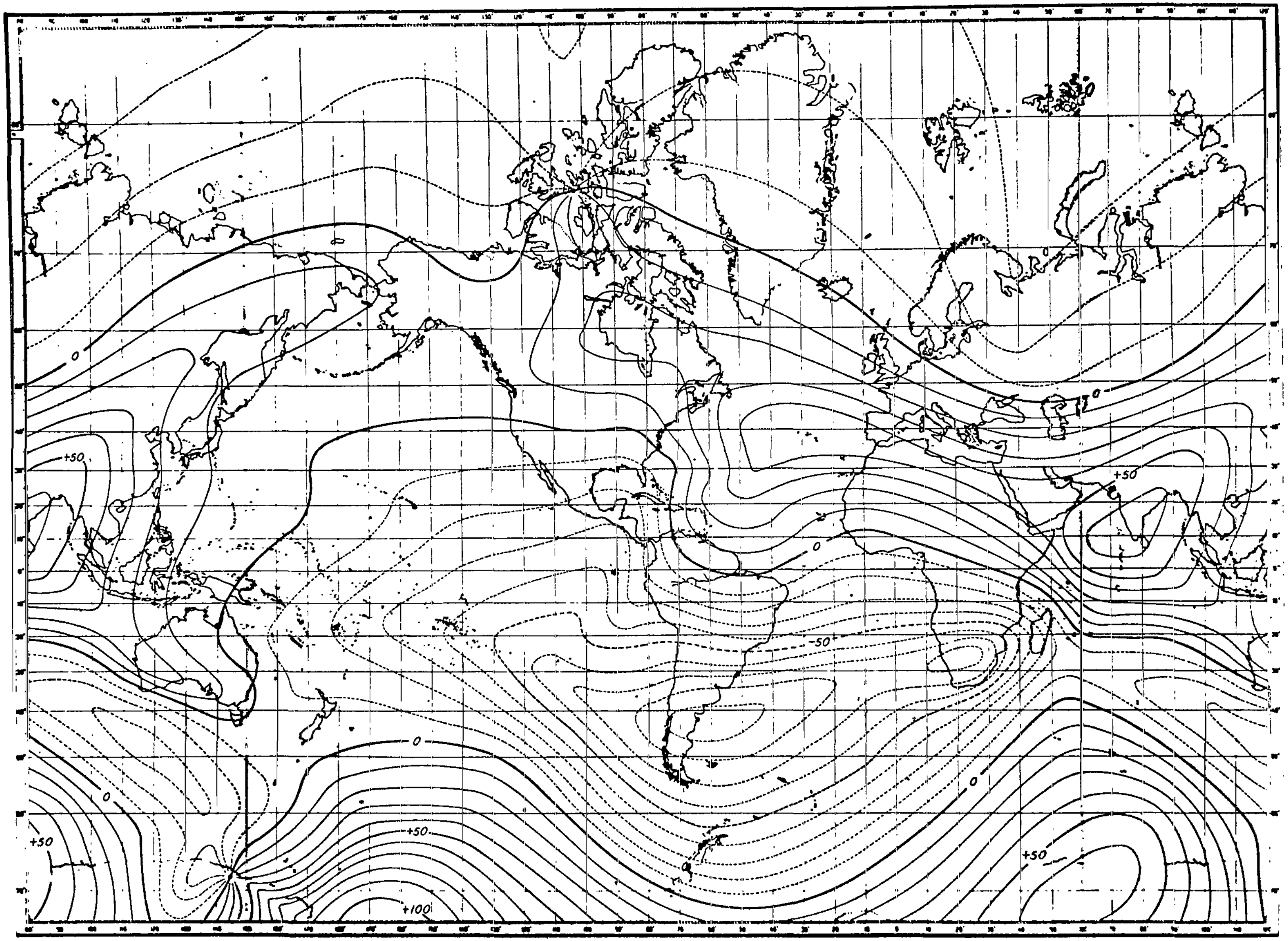

Figure B15–Geomagnetic secular change in gammas per year, horizontal component, epoch 1942.5. Vestine et al. (1947).

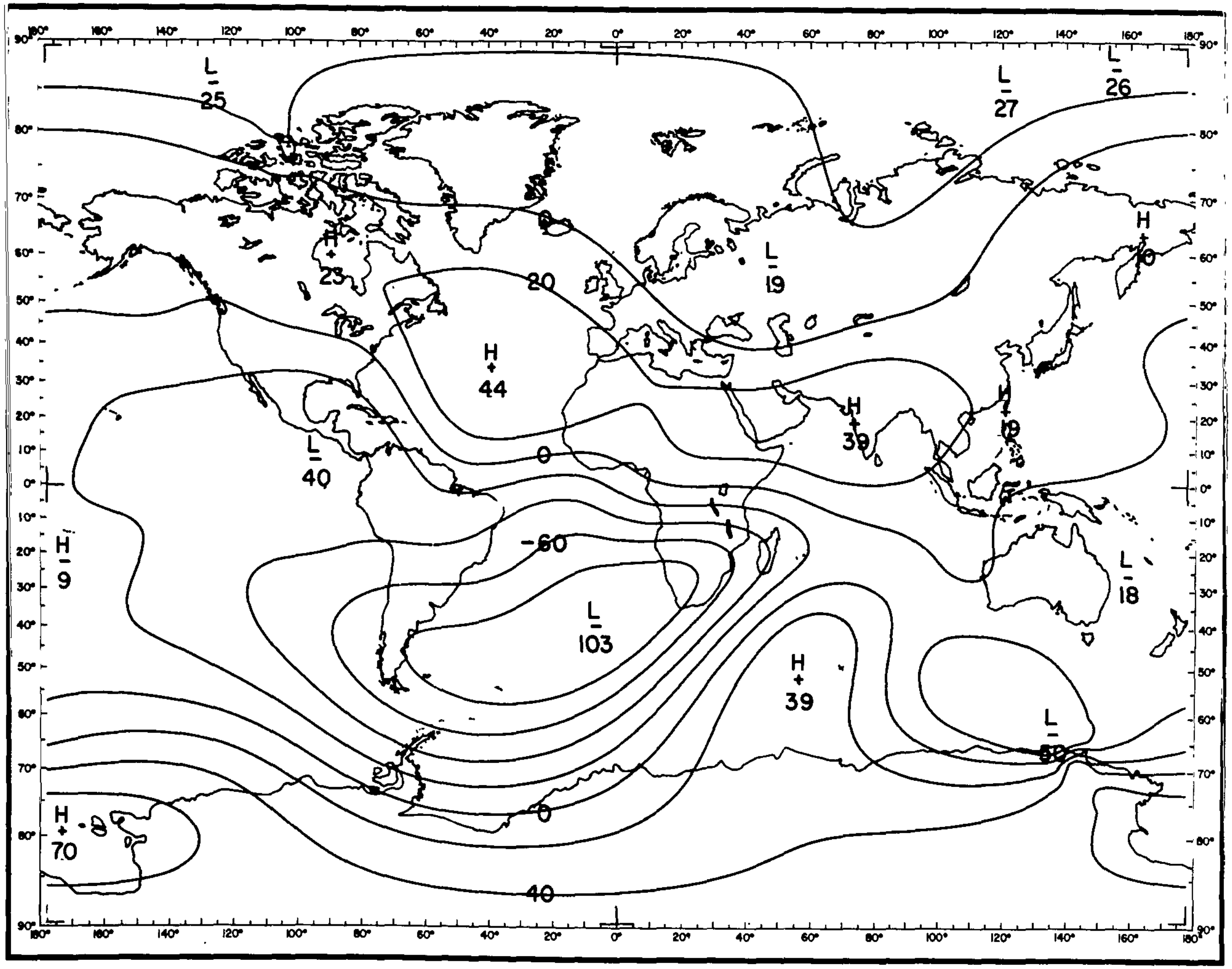

Figure B16–Geomagnetic secular change in gammas per year, horizontal component, epoch 1942.5. GSFC (12/66).

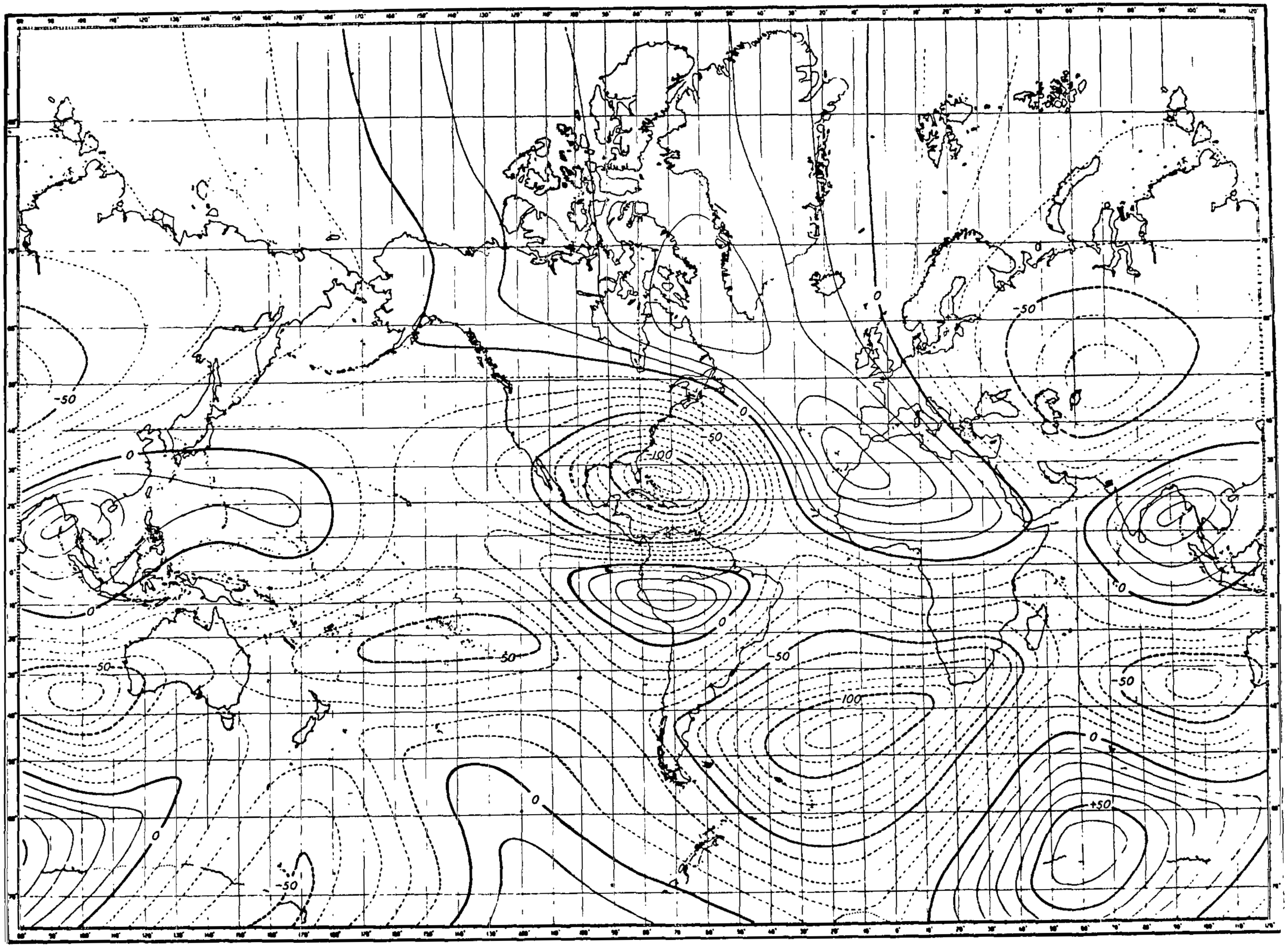

Figure B17–**Geomagnetic** secular change in gammas per year, north component, epoch 1912.5. Vestine et al. (1947).

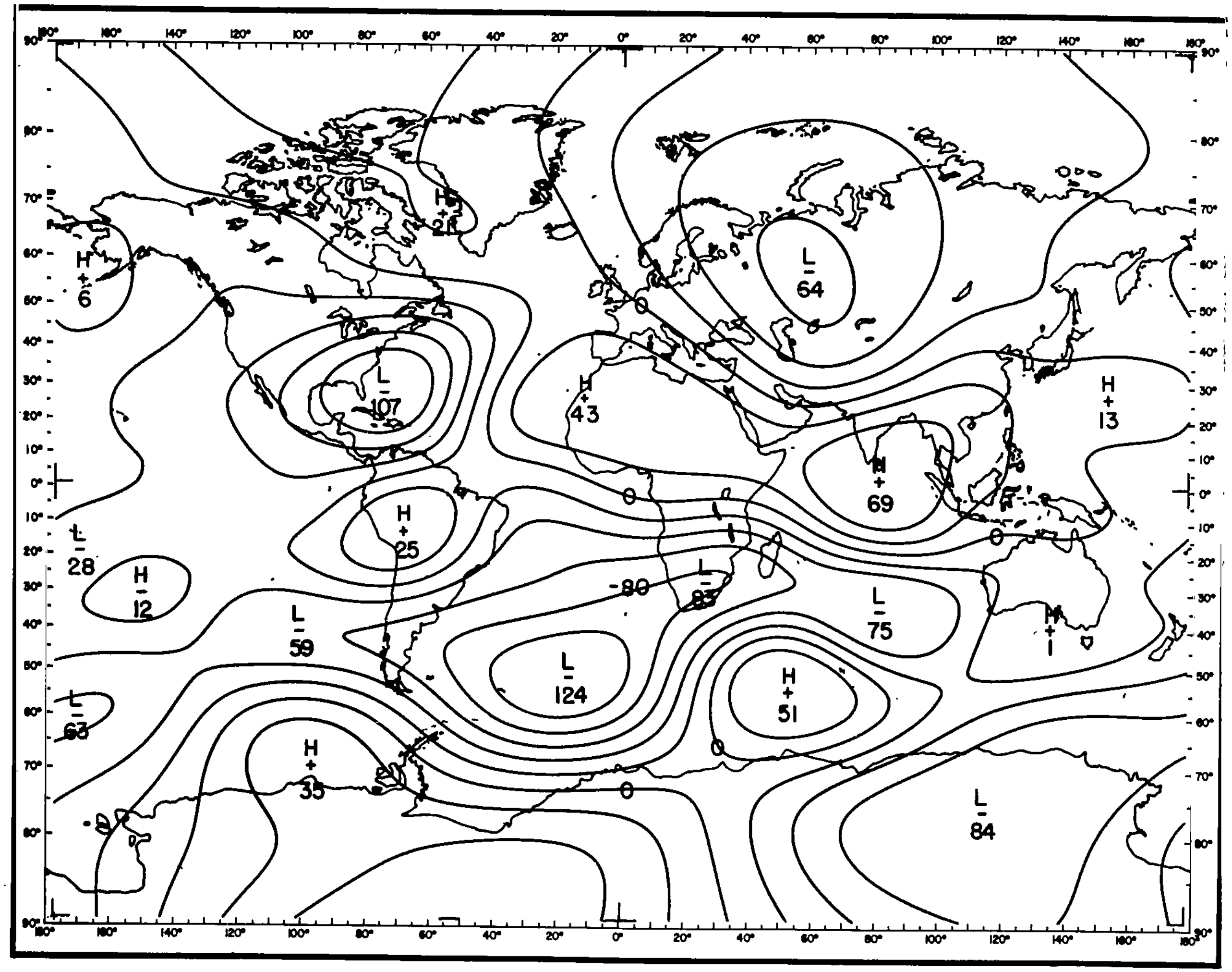

Figure B18—Geomagnetic secular change in gammas per year, north component, epoch 1912.5. GSFC (12/66).

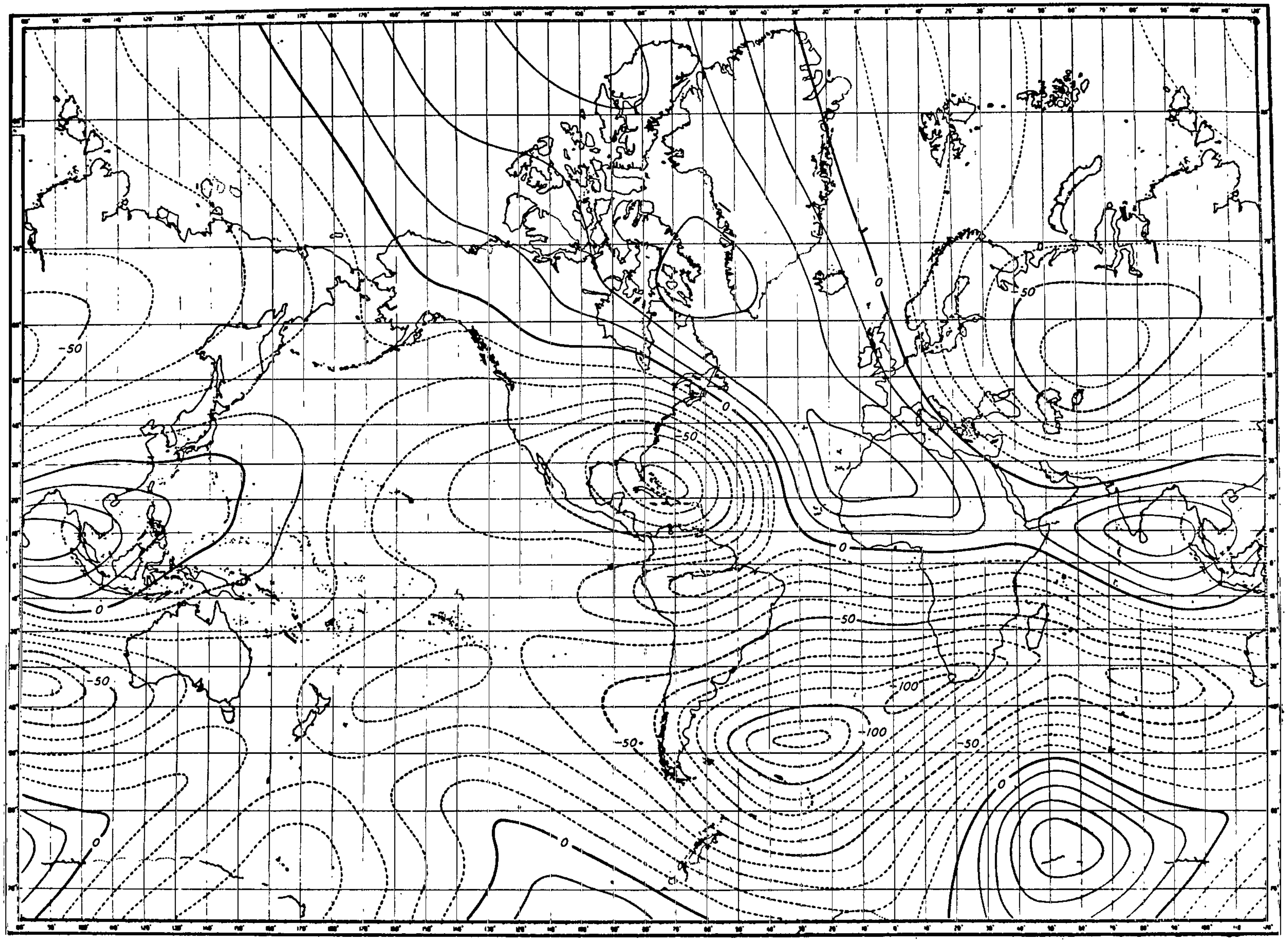

Figure B19–Geomagnetic secular change in gammas per year, north component, epoch 1922.5. Vestine et al. (1947).

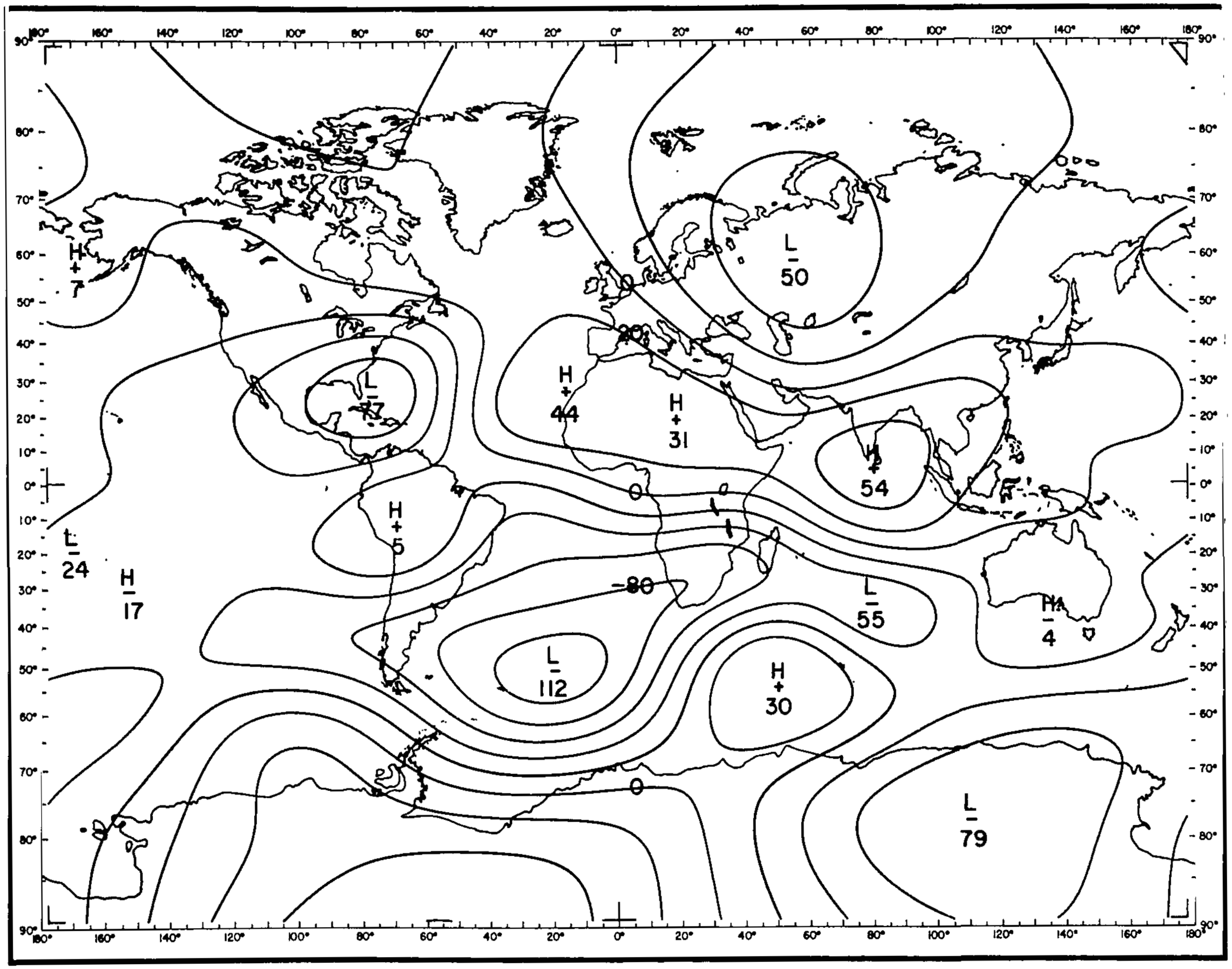

Figure B20—Geomagnetic secular change in gammas per year, north component, epoch 1922.5. GSFC (12/66).

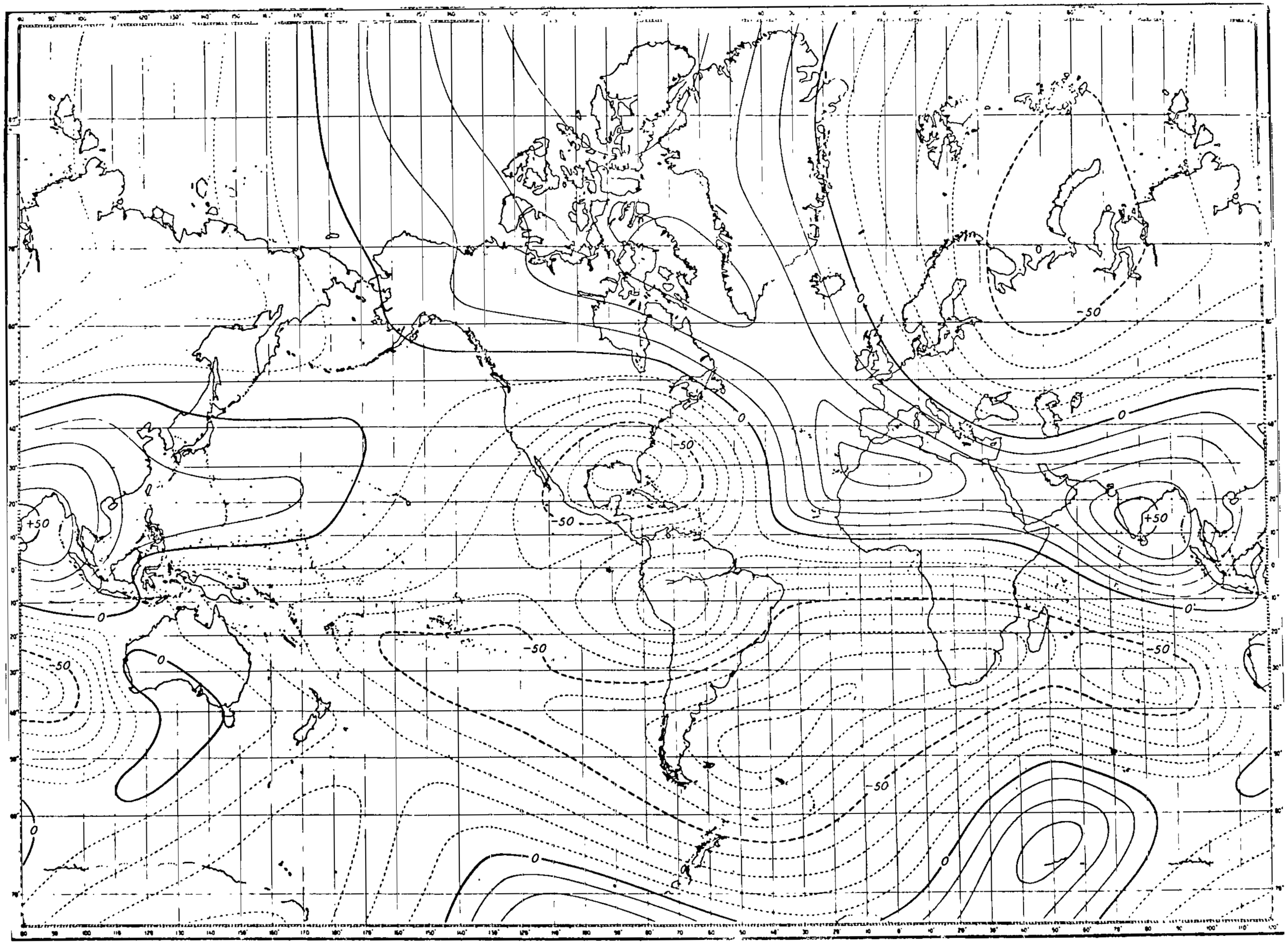

Figure B21-Geomagnetic secular change in gammas per year, north component, epoch 1932.5. Vestine et al. (1947).

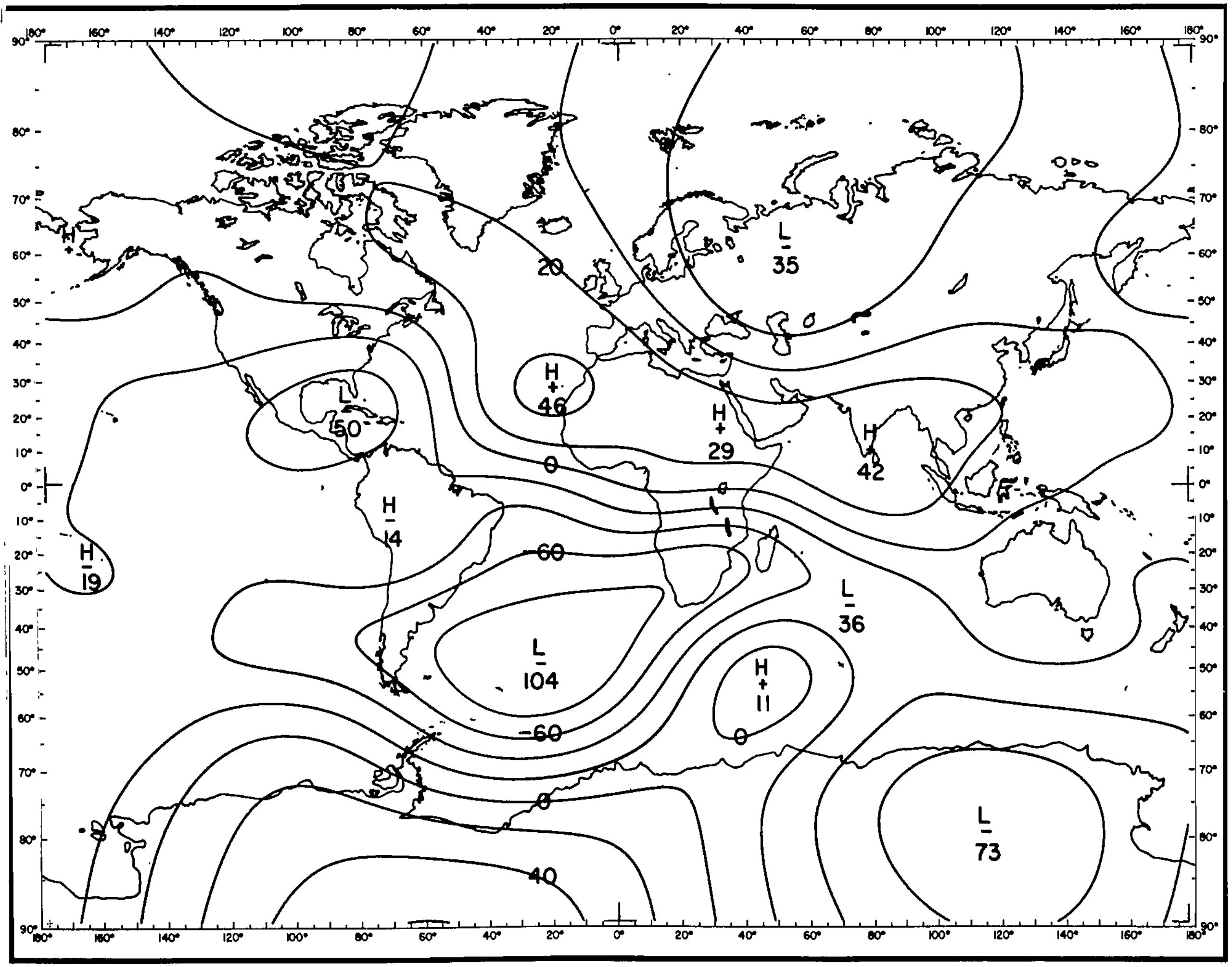

Figure B22—Geomagnetic secular change in gammas per year, north component, epoch 1932.5. GSFC (12/66).

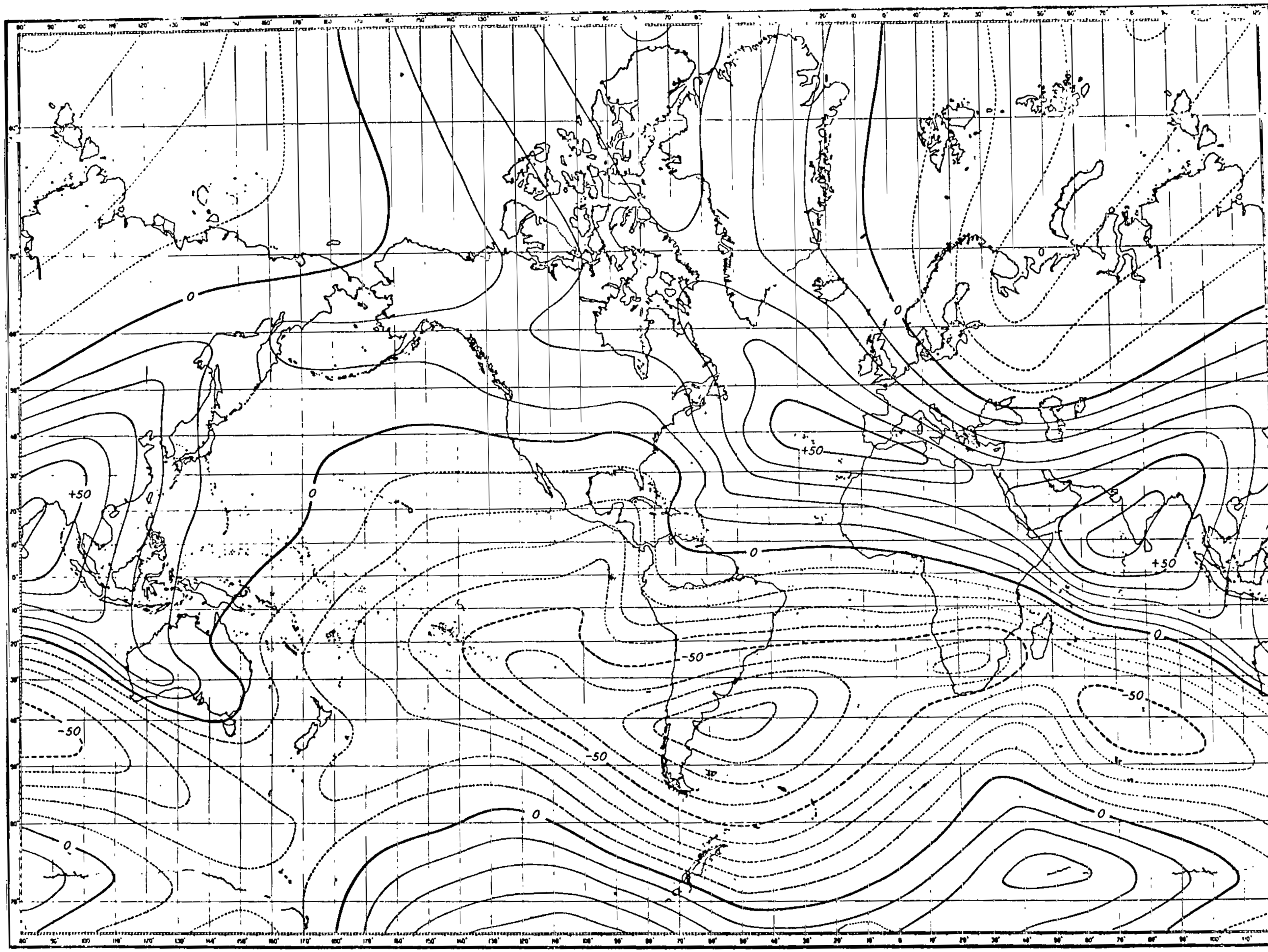

Figure B23–Geomagnetic secular change in gammas per year, north component, epoch 1942.5. Vestine et al. (1947).

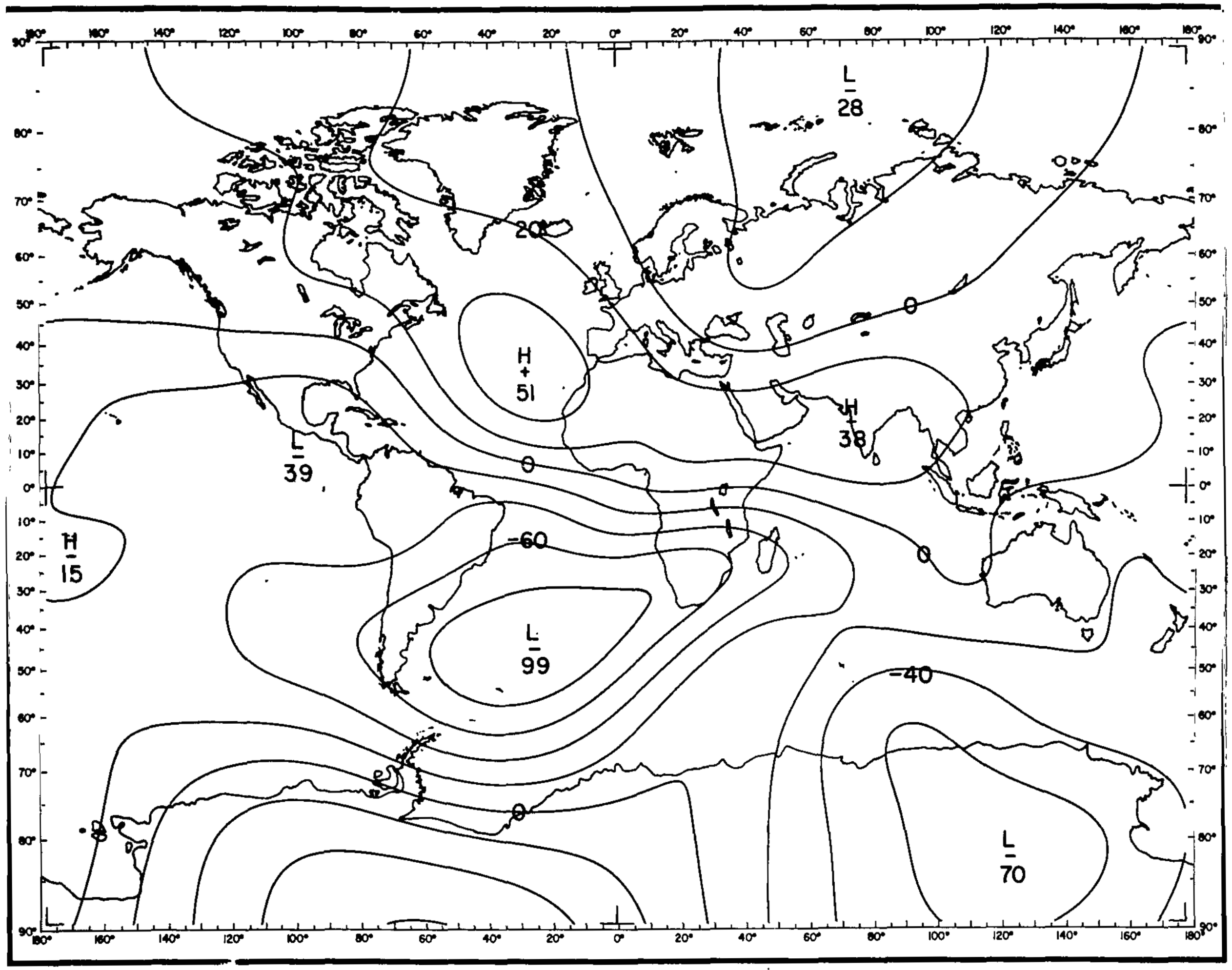

Figure B24—Geomagnetic secular change in gammas per year, north component, epoch 1942.5. GSFC (12/66).

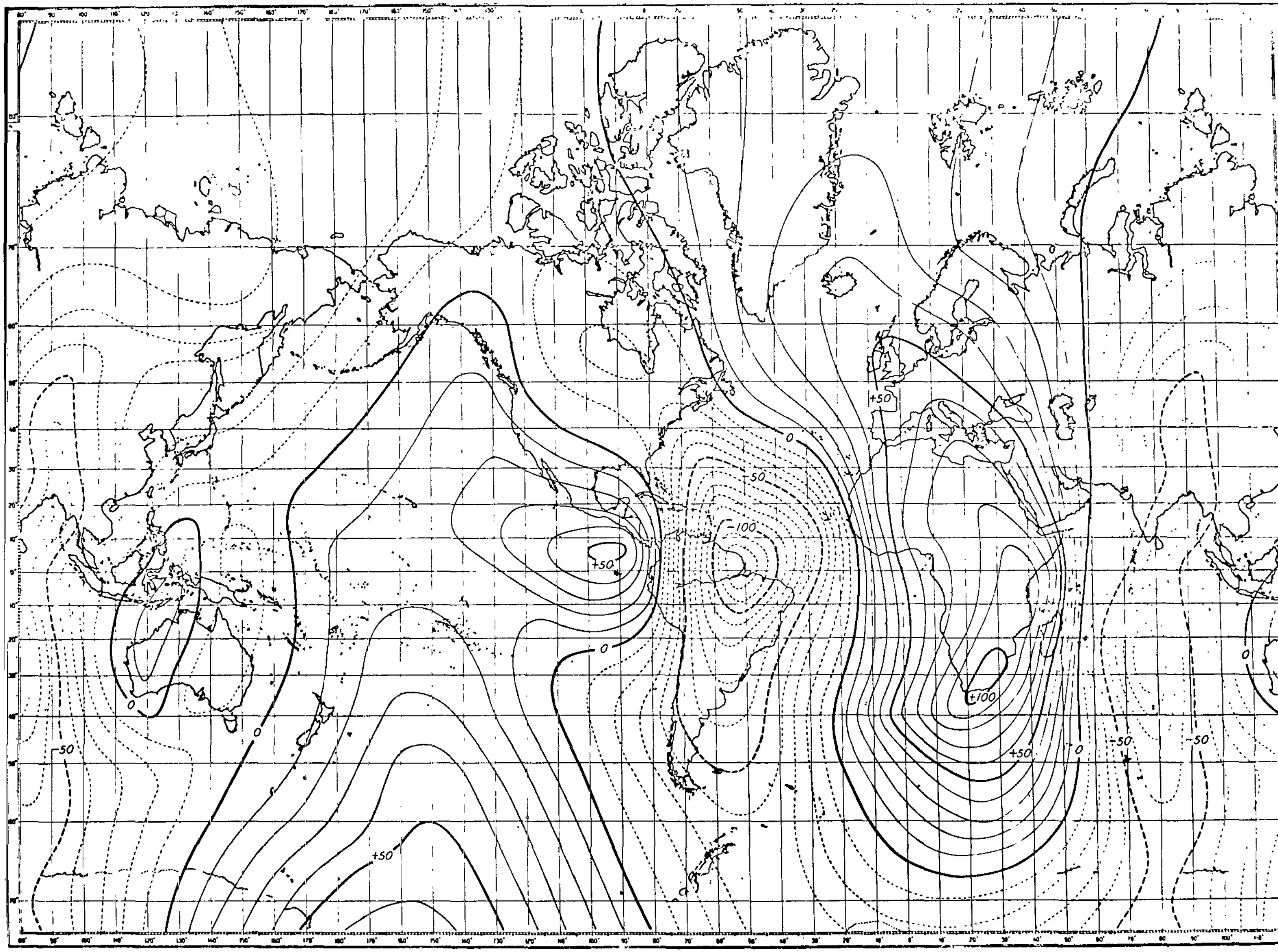

Figure B25–Geomagnetic secular change in gammas per year, east component, epoch 1912.5. Vestine et al. (1947).

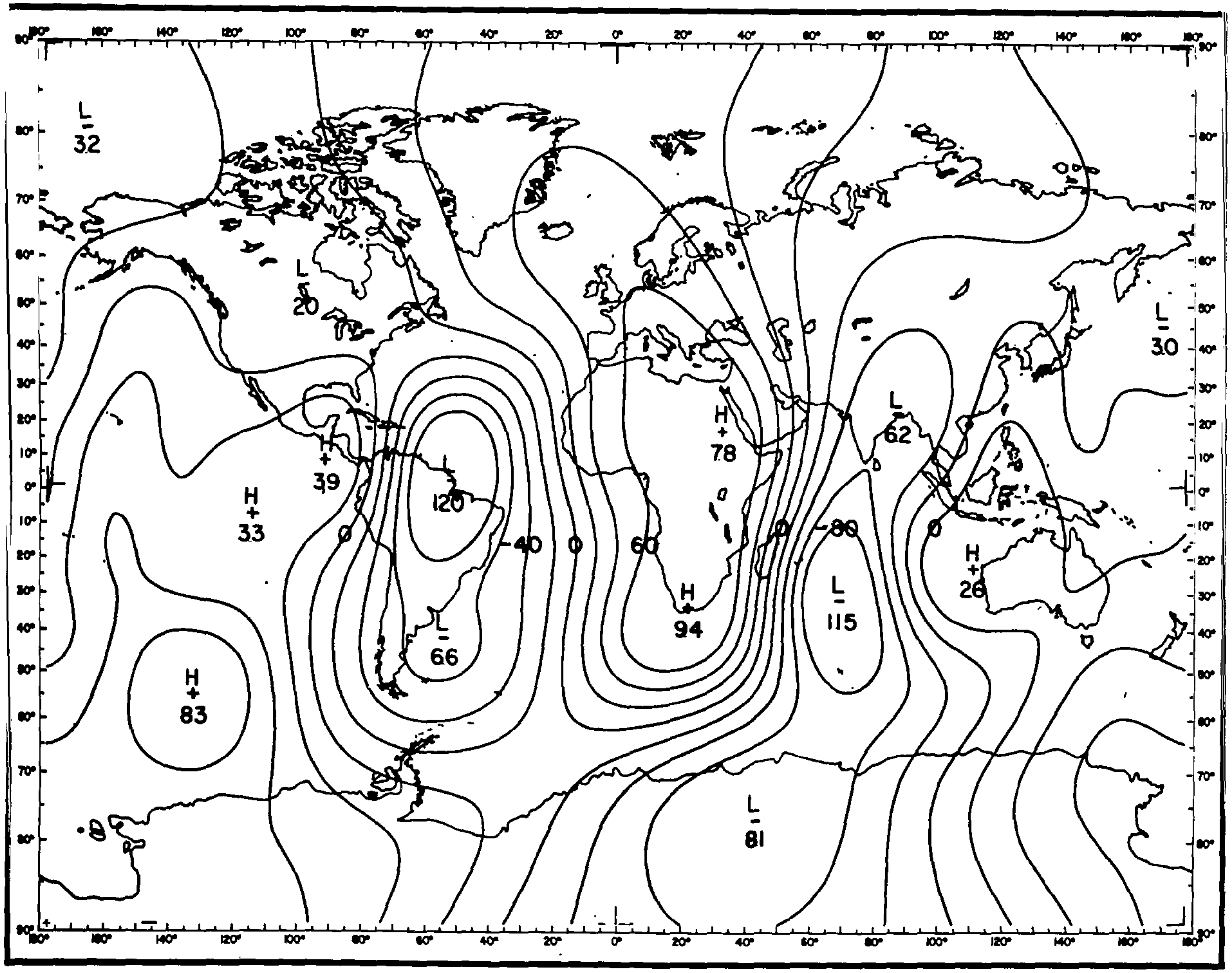

Figure B26—Geomagnetic secular change in gammas per year, east component, epoch 1912.5. GSFC (12/66).

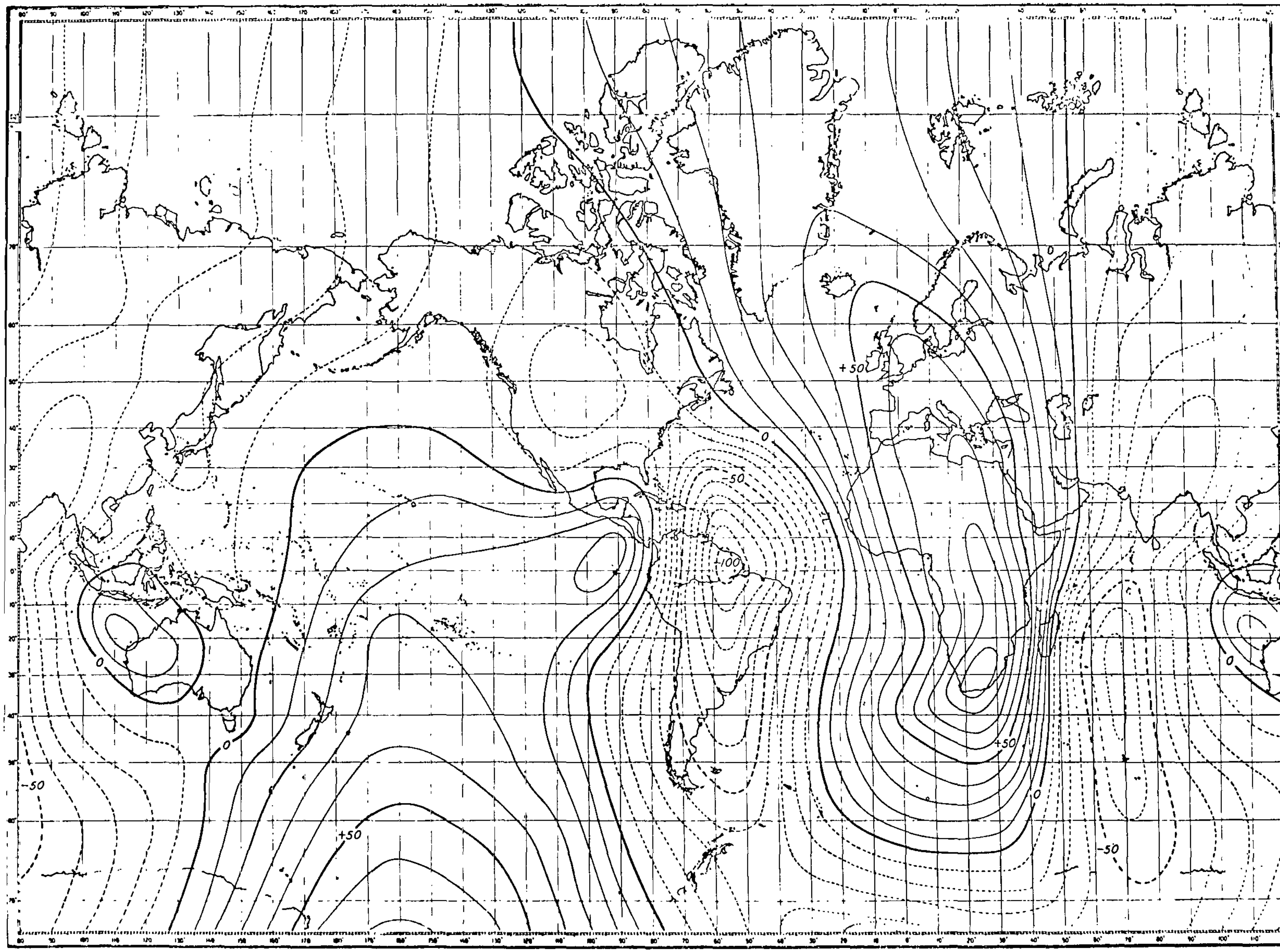

Figure B27-Geomagnetic secular change in gammas per year, east component, epoch 1922.5. Vestine et al. (1947).

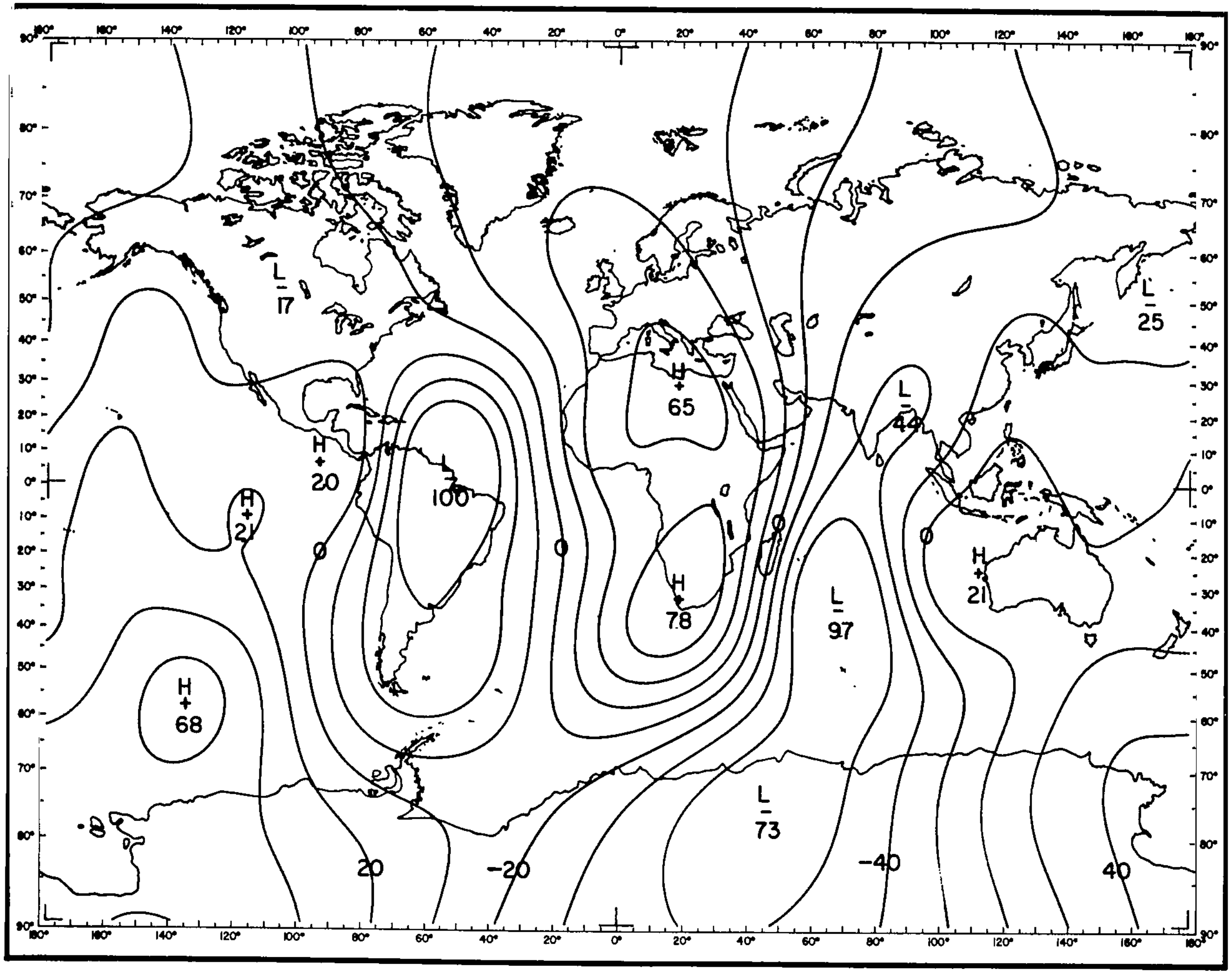

Figure B28—Geomagnetic secular change in gammas per year, east component, epoch 1922.5. GSFC (12/66).

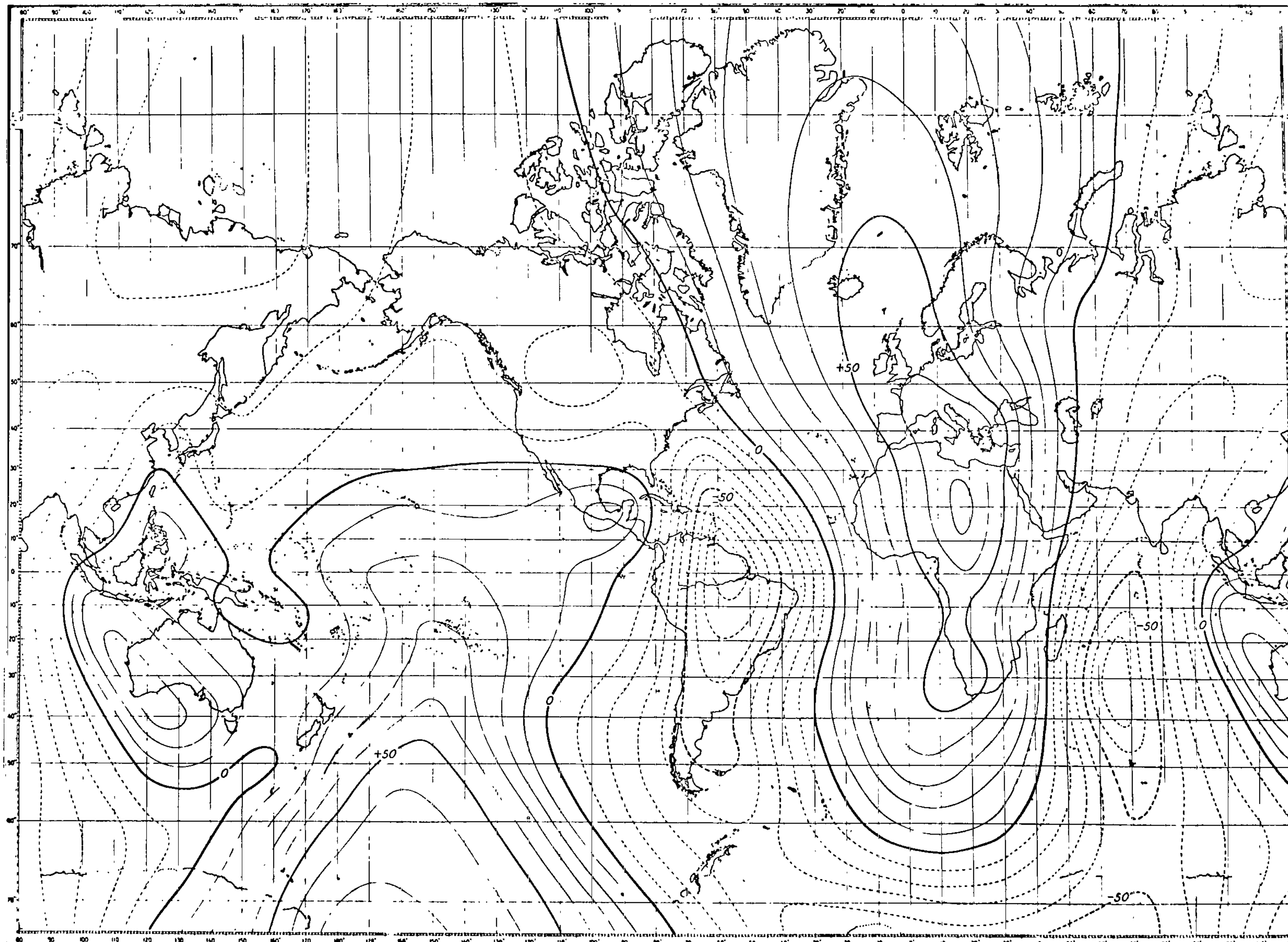

Figure B29-Geomagnetic secular change in gammas per year, east component, epoch 1932.5. Vestine et al. (1947).

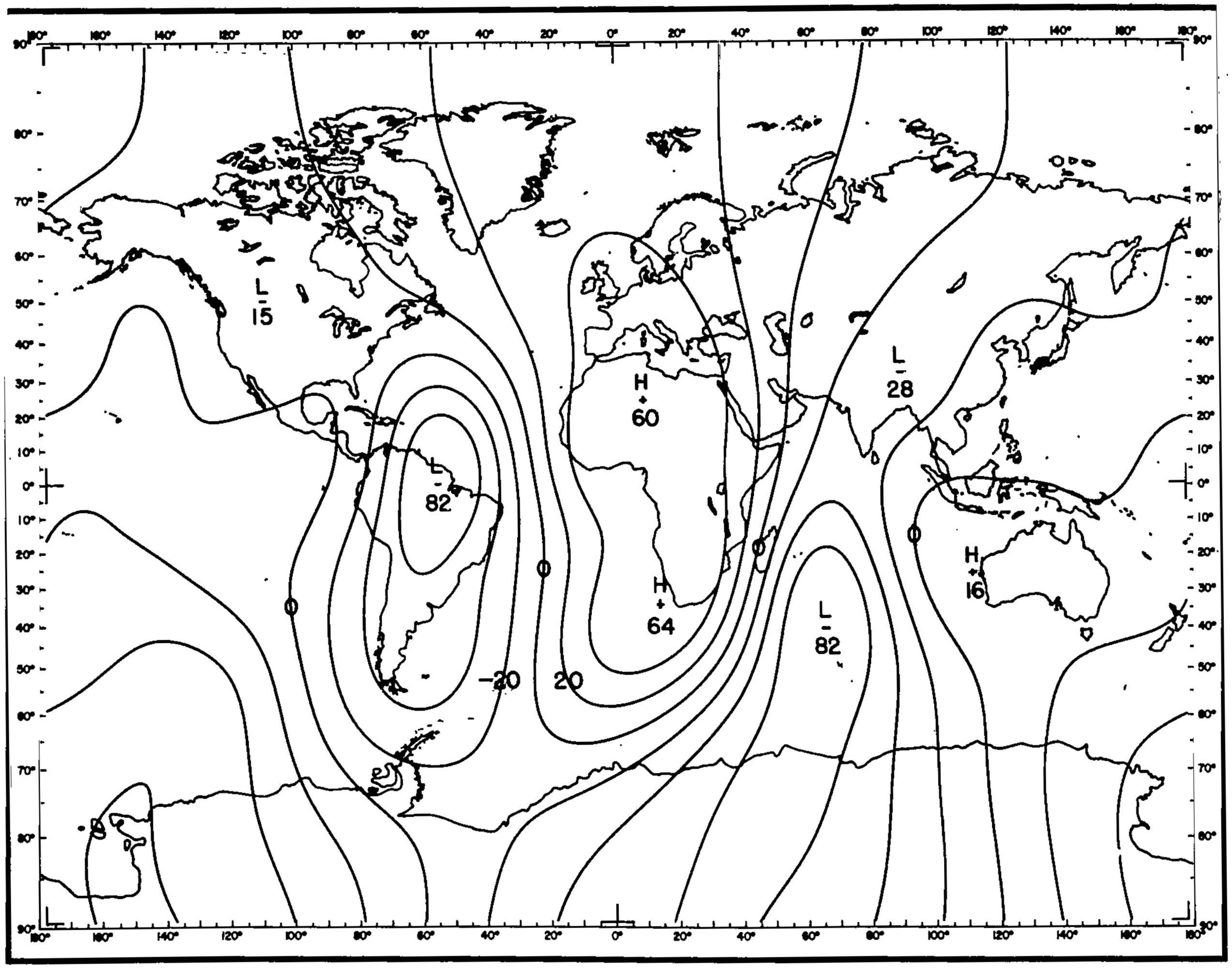

Figure B30—Geomagnetic secular change in gammas per year, east component, epoch 1932.5. GSFC (12/66).

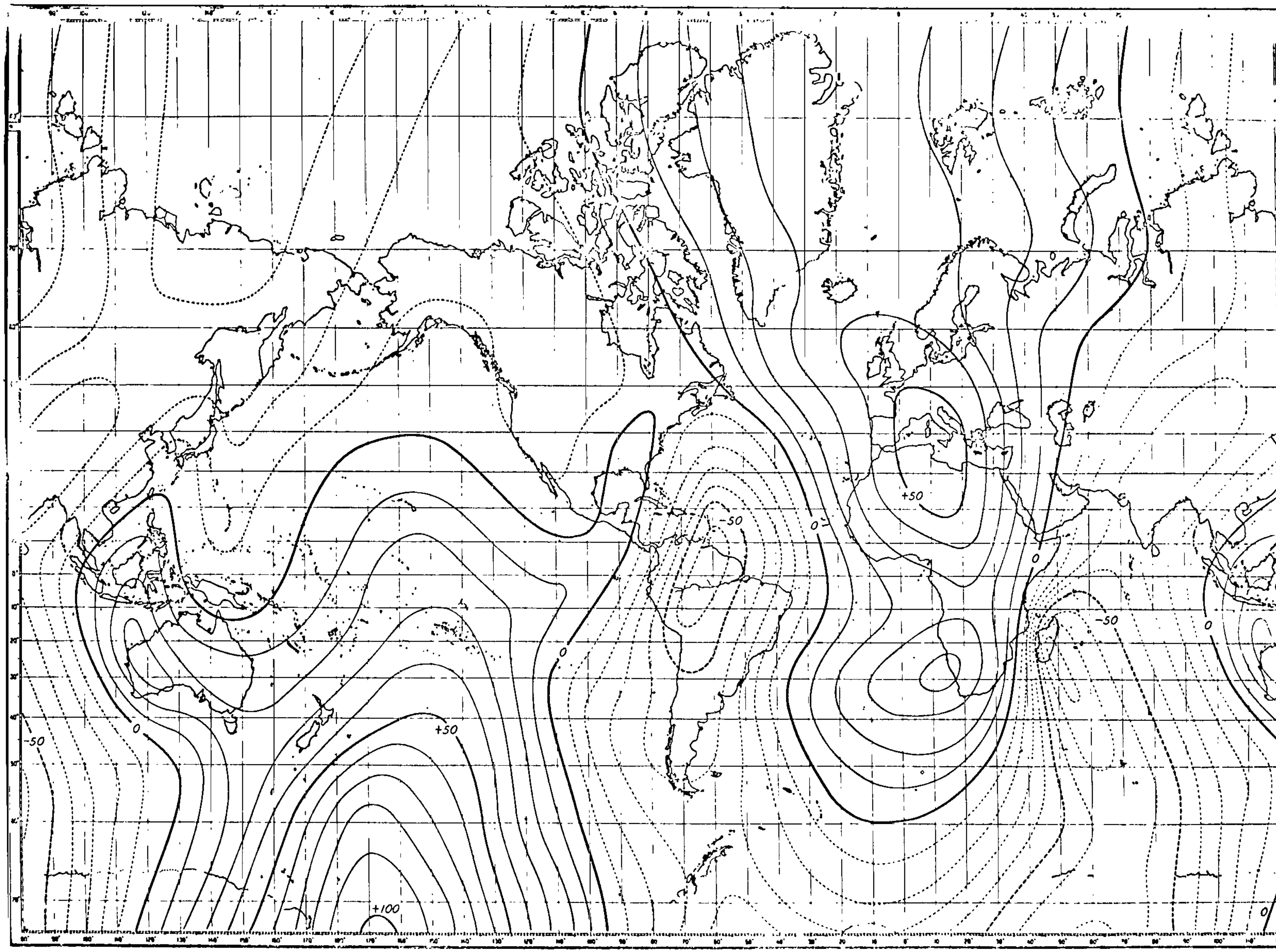

Figure B31–Geomagnetic secular change in gammas per year, east component, epoch 1942.5. Vestine et al. (1947).

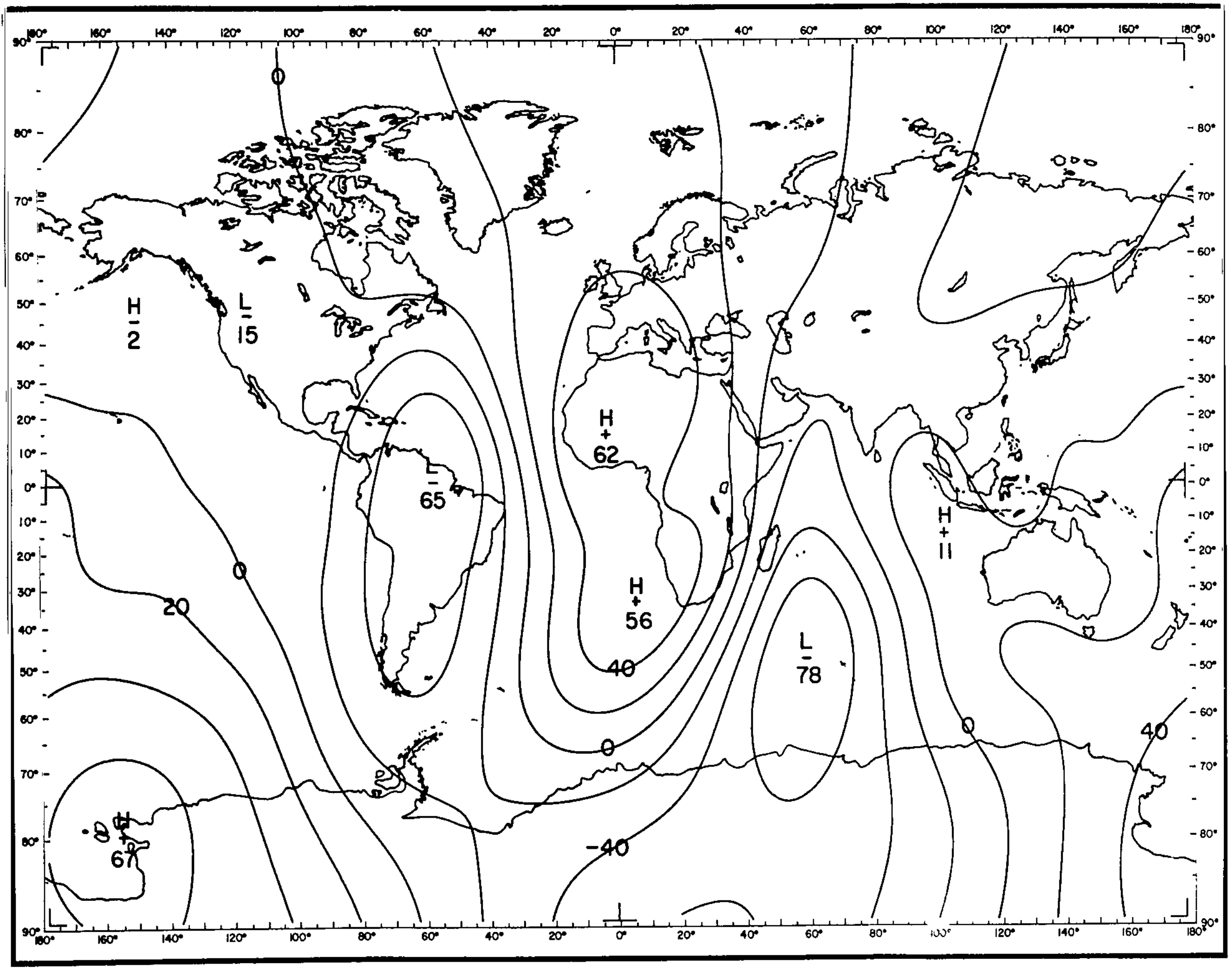

Figure B32—Geomagnetic secular change in gammas per year, east component, epoch 1942.5. GSFC (12/66).

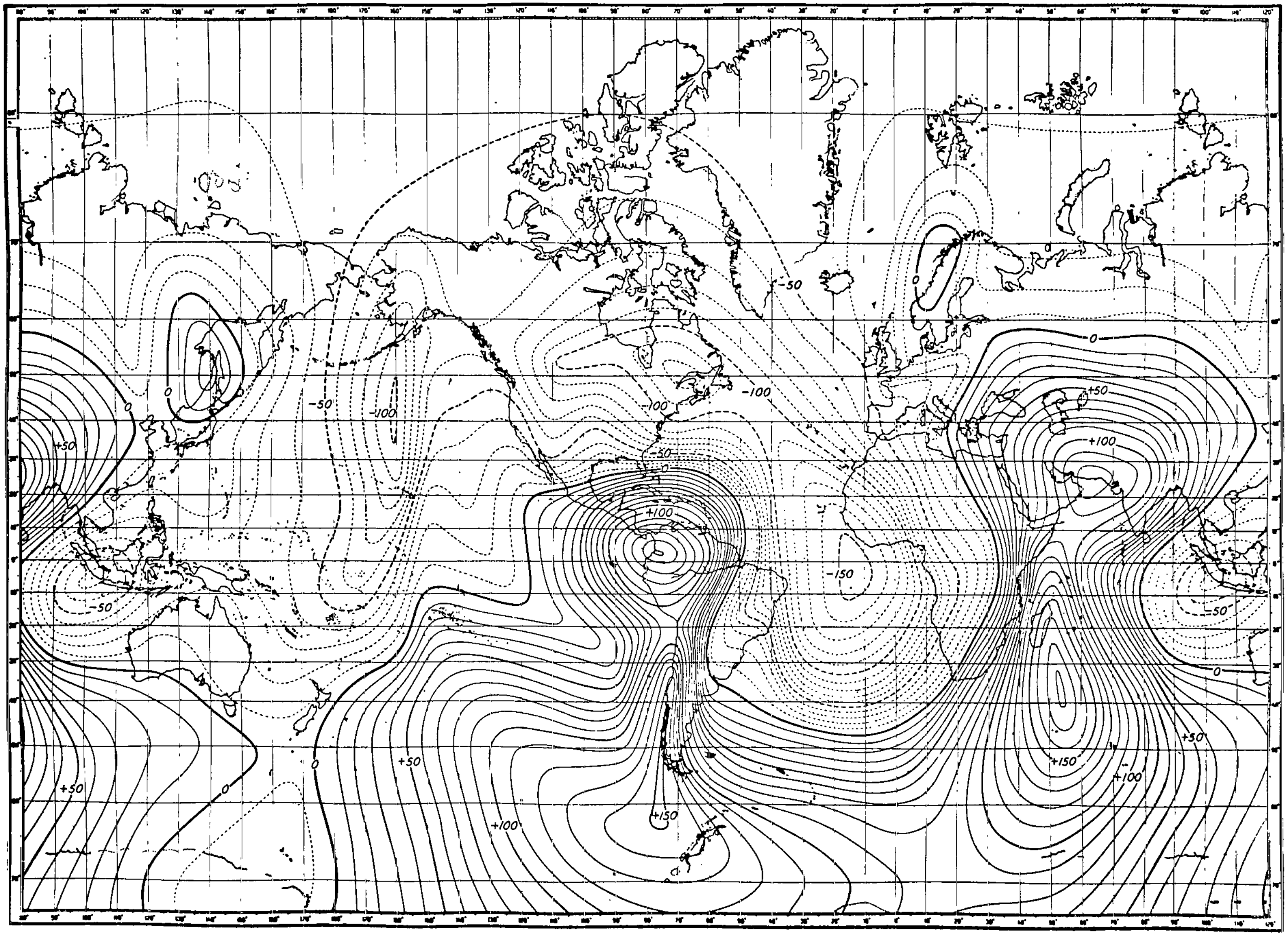

Figure B33–Geomagnetic secular change in gammas per year, vertical component, epoch 1912.5. Vestine et al. (1947).

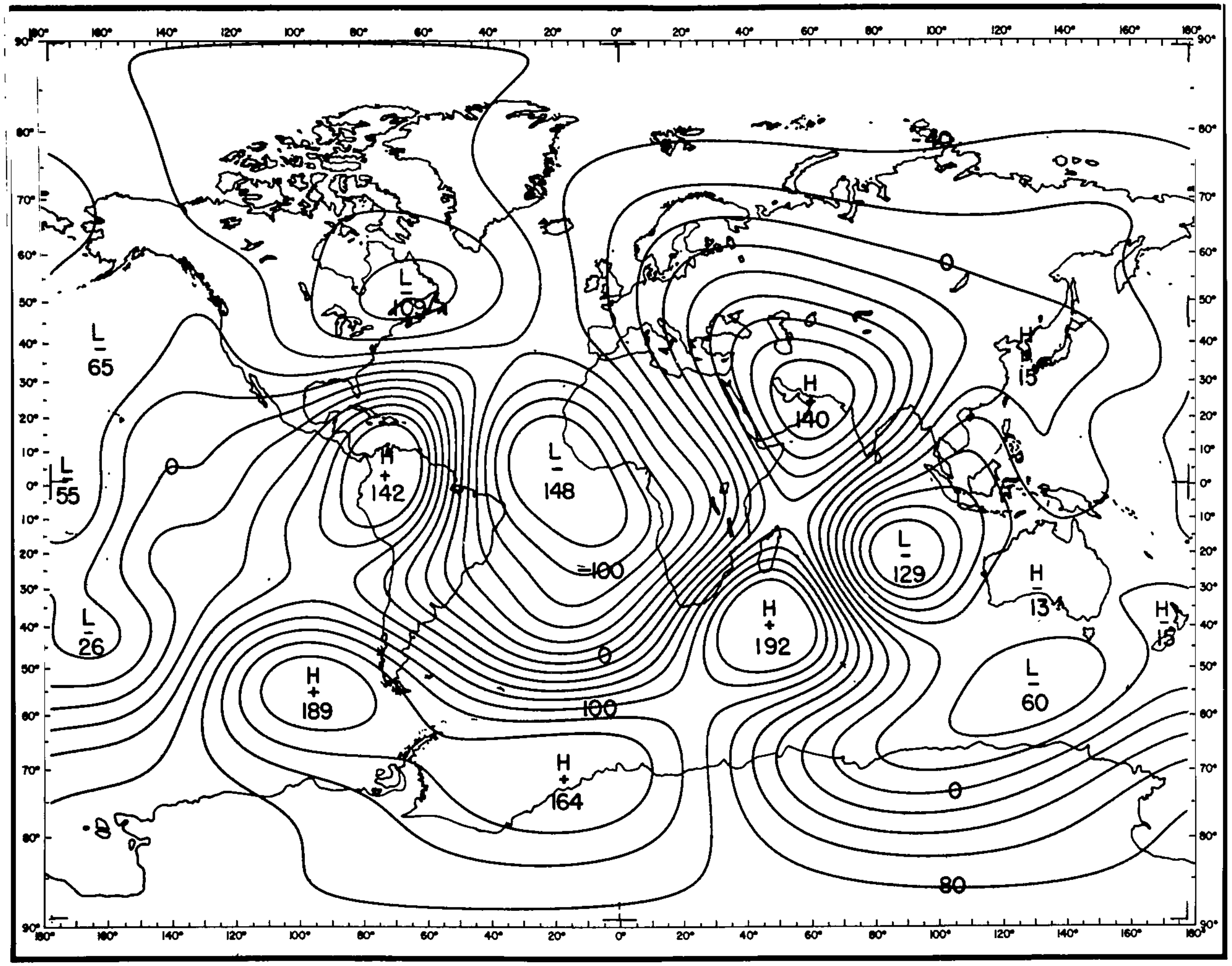

Figure B34—Geomagnetic secular change in gammas per year, vertical component, epoch 1912.5. GSFC (12/66).

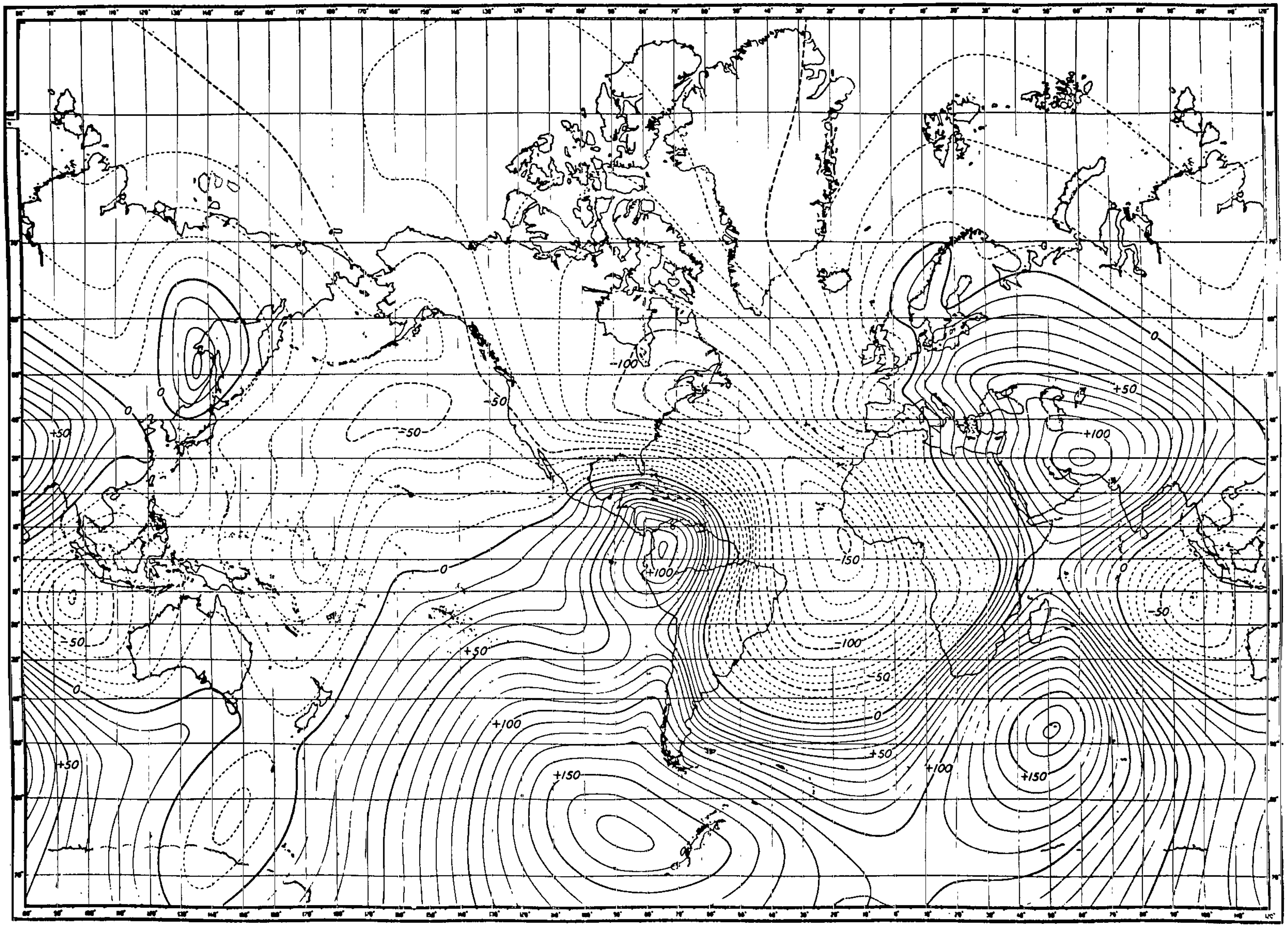

Figure B35–Geomagnetic secular change in gammas per year, vertical component, epoch 1922.5. Vestine et al. (1947).

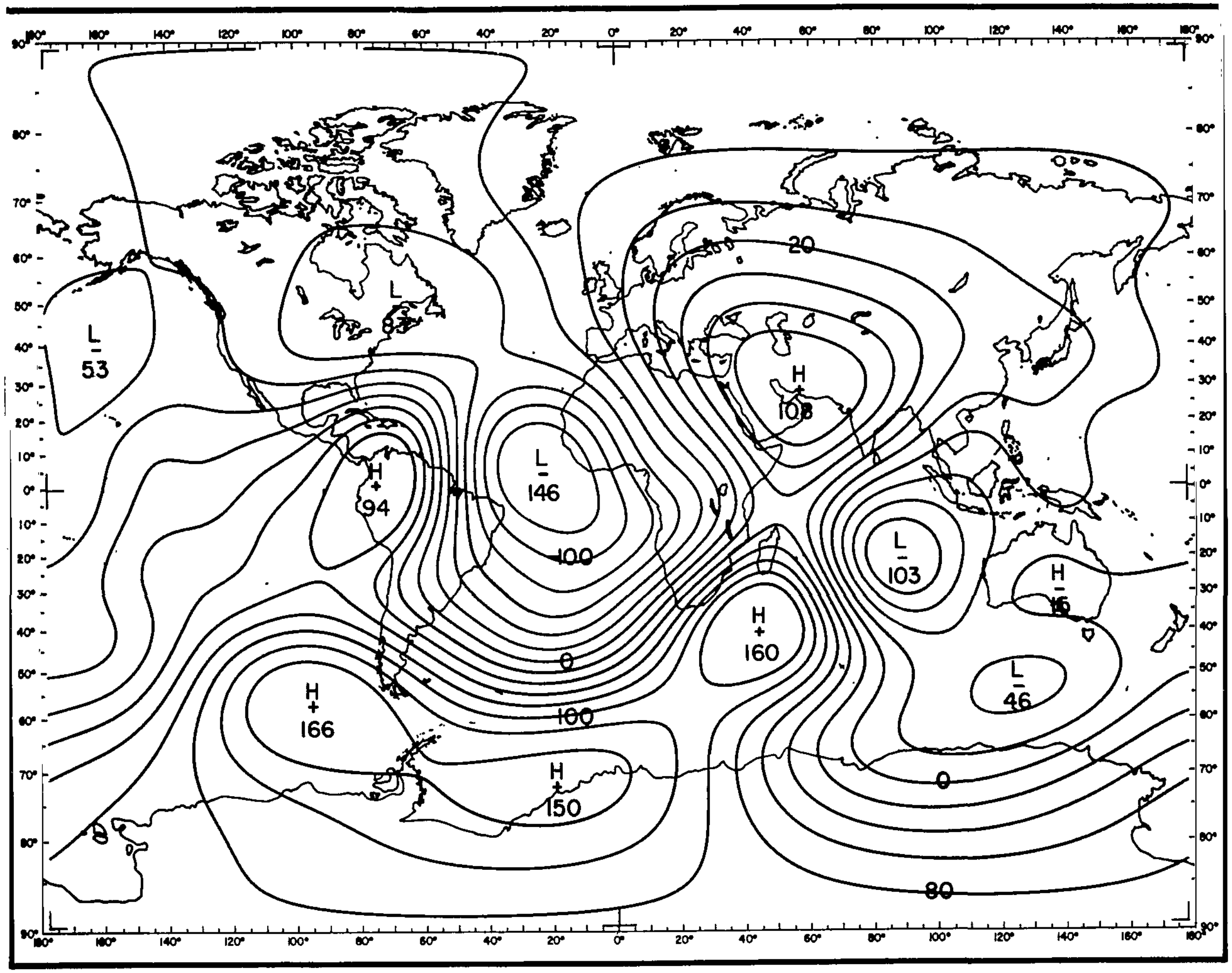

Figure B36—Geomagnetic secular change in gammas per year, vertical component, epoch 1922.5. GSFC (12/66).

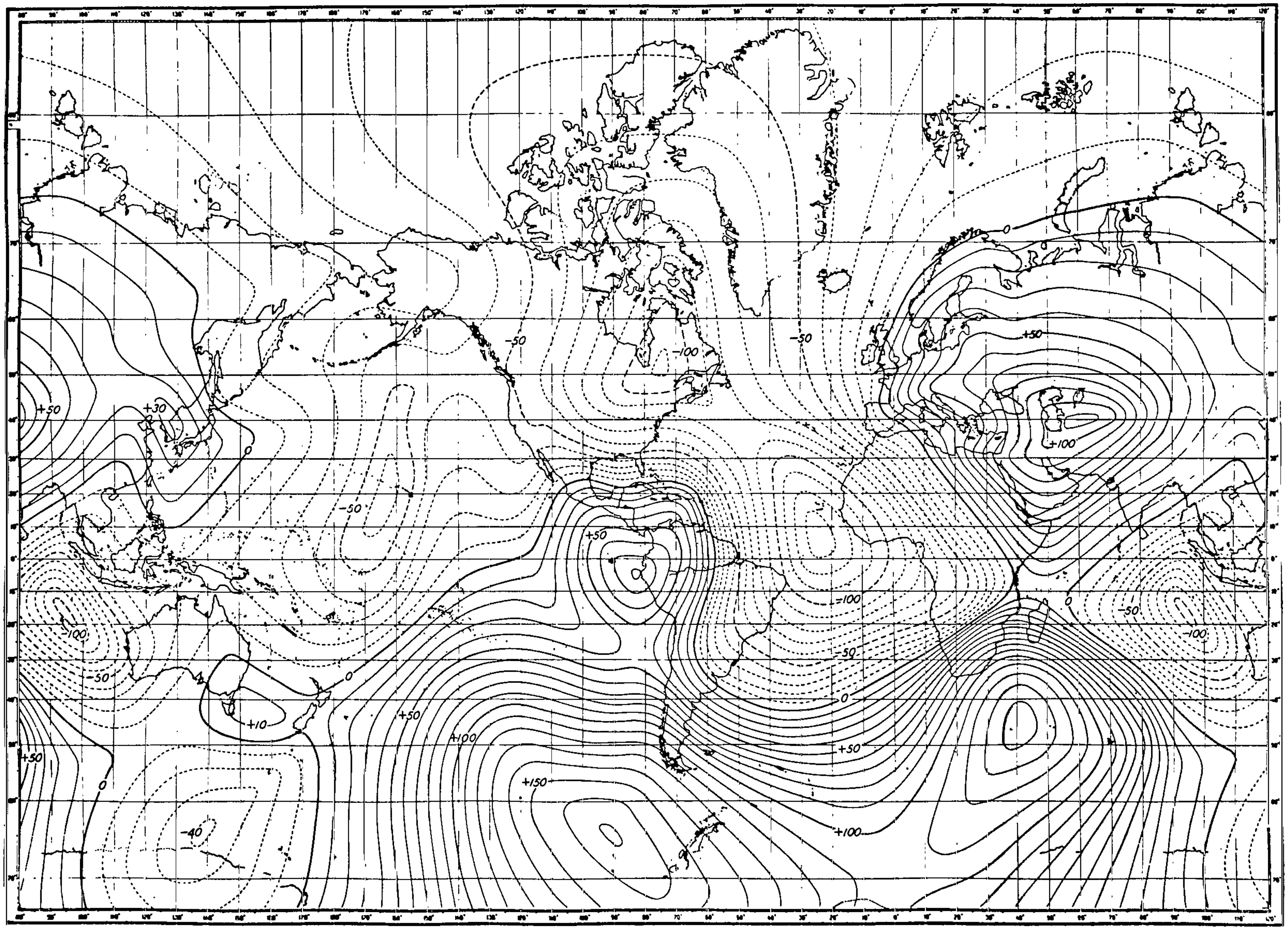

Figure B37–Geomagnetic secular change in gammas per year, vertical component, epoch 1932.5. Vestine et al. (1947).

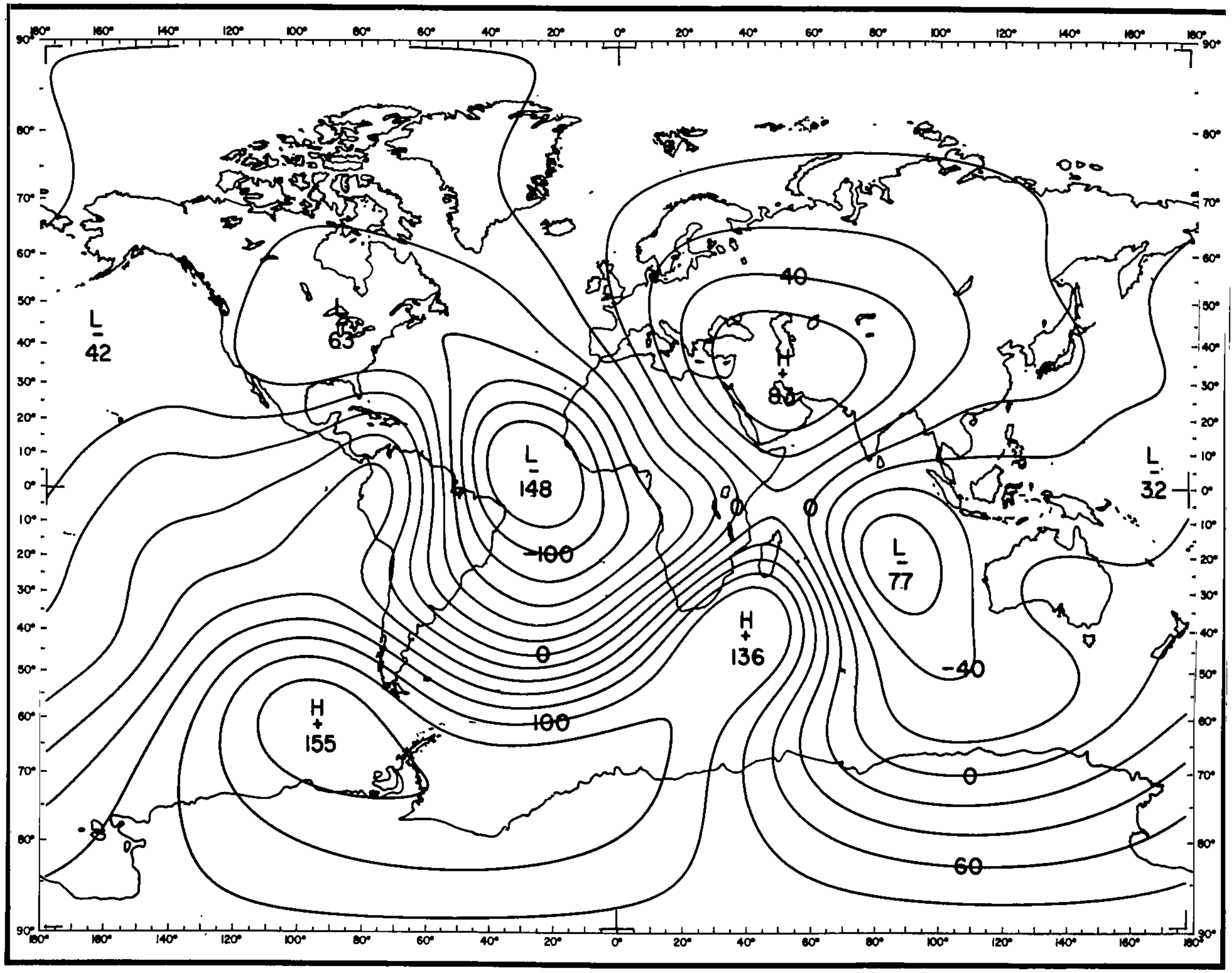

Figure B38—Geomagnetic secular change in gammas per year, vertical component, epoch 1932.5. GSFC (12/66).

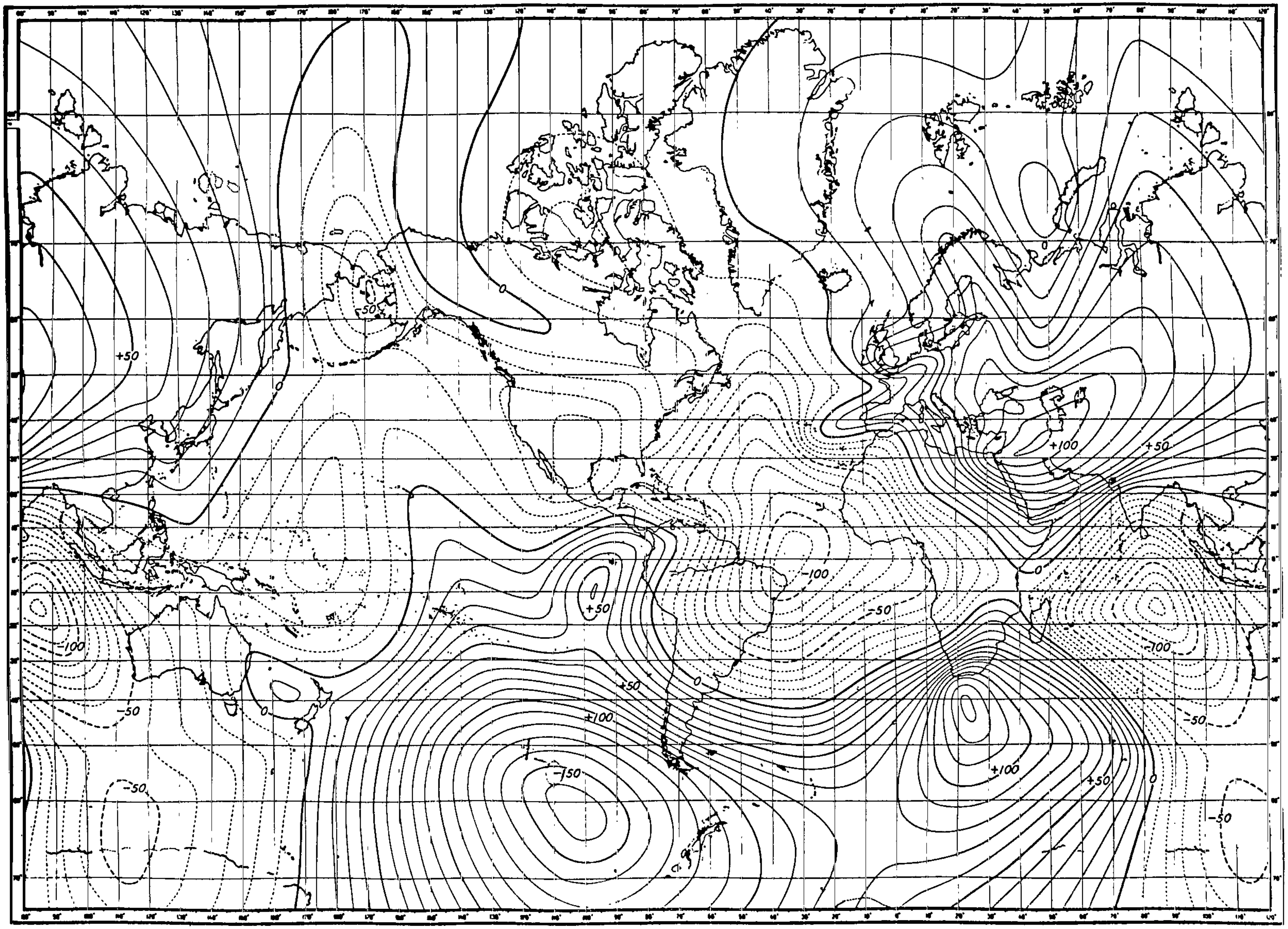

Figure B39–Geomagnetic secular change in gammas per year, vertical component, epoch 1942.5. Vestine et al. (1947).

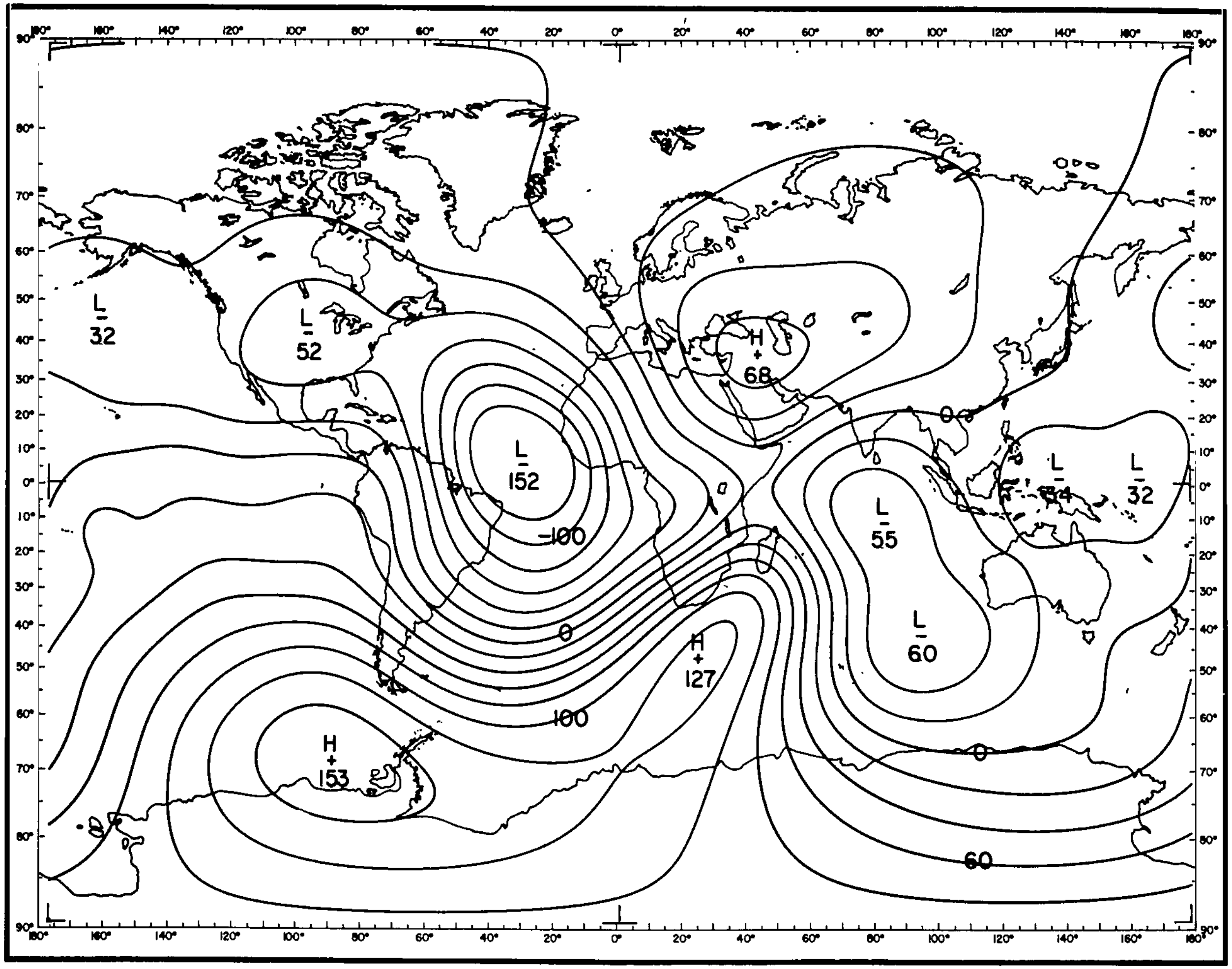

Figure B40—Geomagnetic secular change in gammas per year, vertical component, epoch 1942.5. GSFC (12/66).

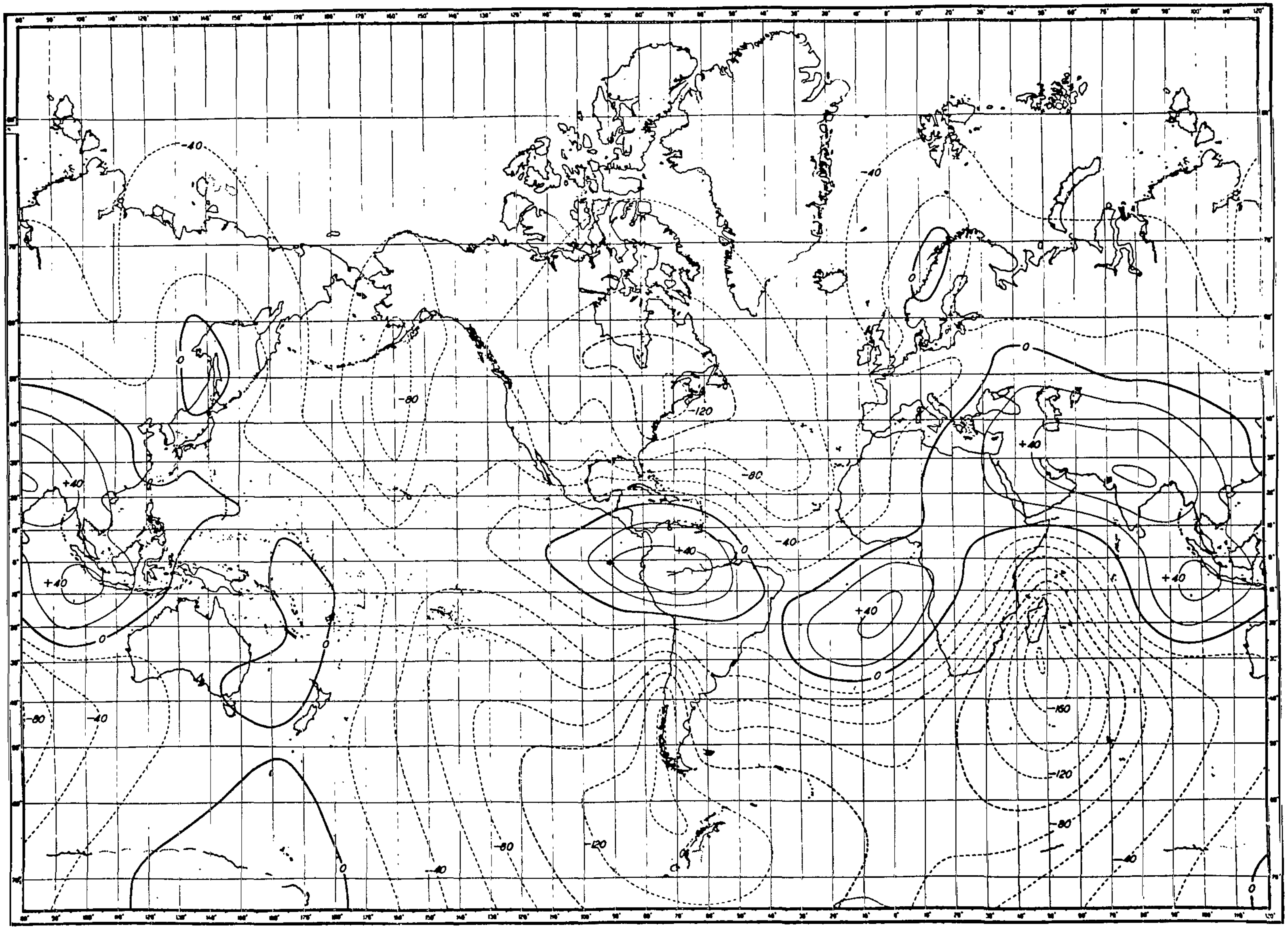

Figure B41-Geomagnetic secular change in gammas per year, total intensity, epoch 1912.5. Vestine et al. (1947).

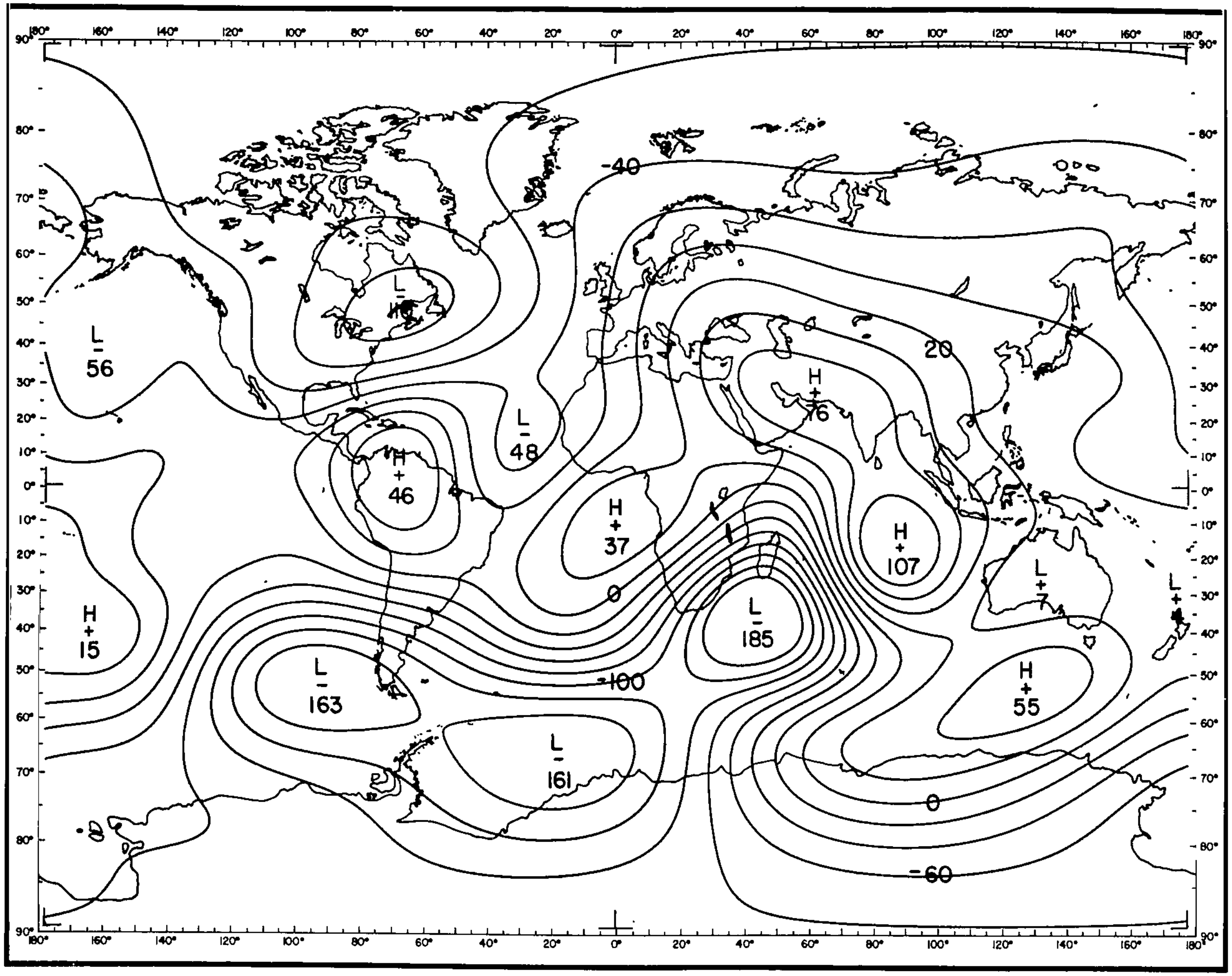

Figure B42—Geomagnetic secular change in gammas per year, total intensity, epoch 1912.5. GSFC (12/66).

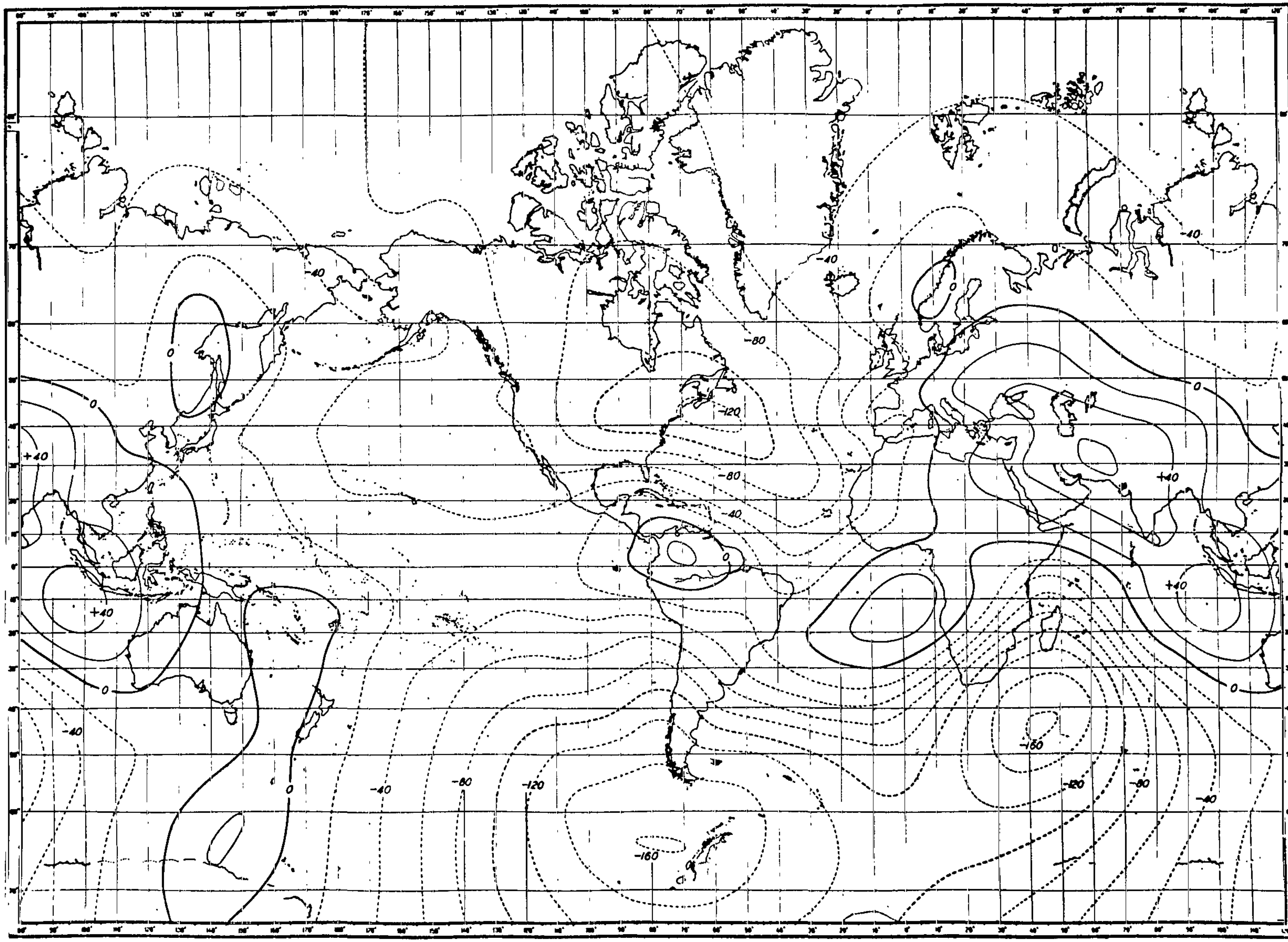

Figure B43–Geomagnetic secular change in gammas per year, total intensity, epoch 1922.5. Vestine et al. (1947).

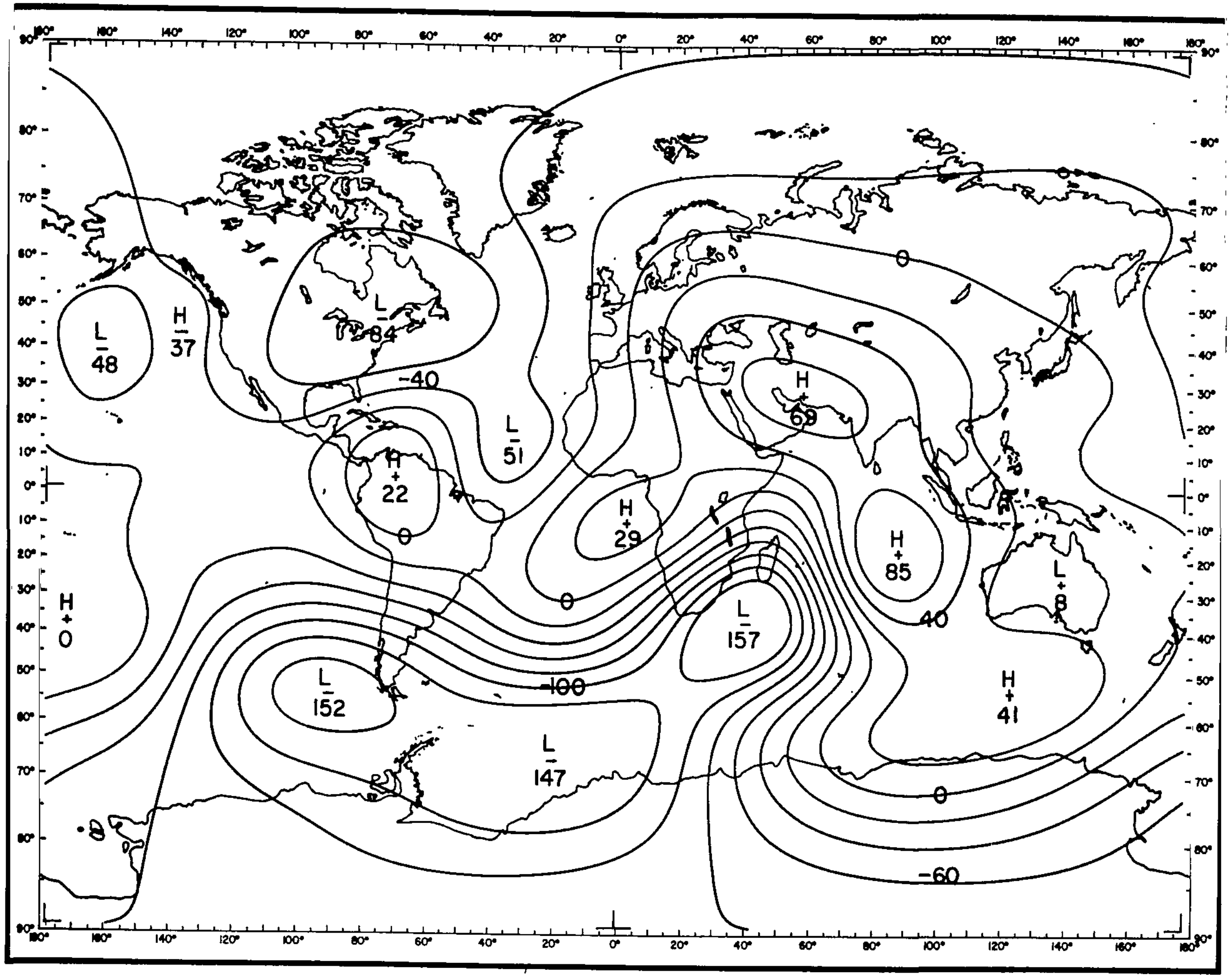

Figure B44—Geomagnetic secular change in gammas per year, total intensity, epoch 1922.5. GSFC (12/66).

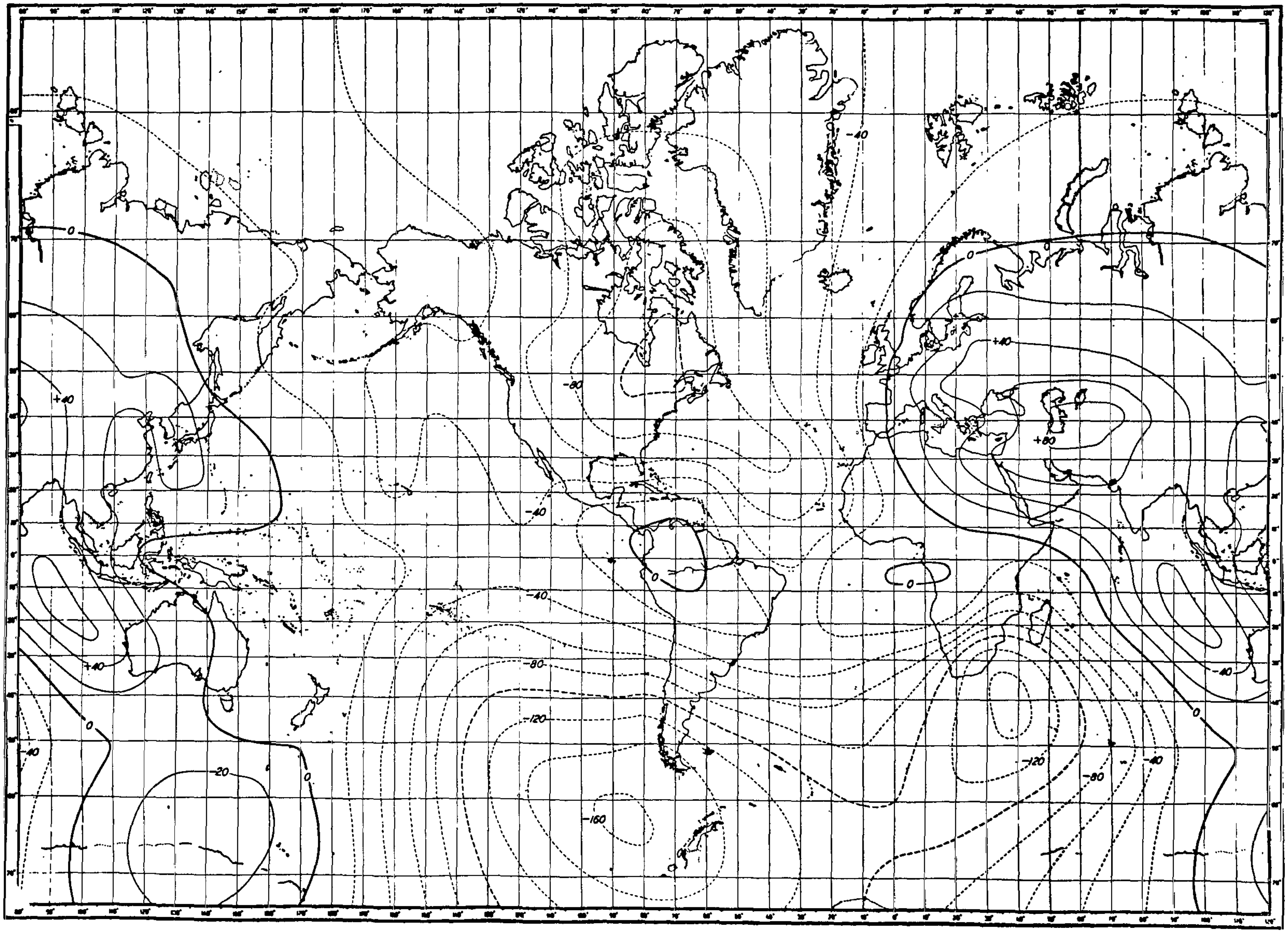

Figure B45–Geomagnetic secular change in gammas per year, total intensity, epoch 1932.5. Vestine et al. (1947).

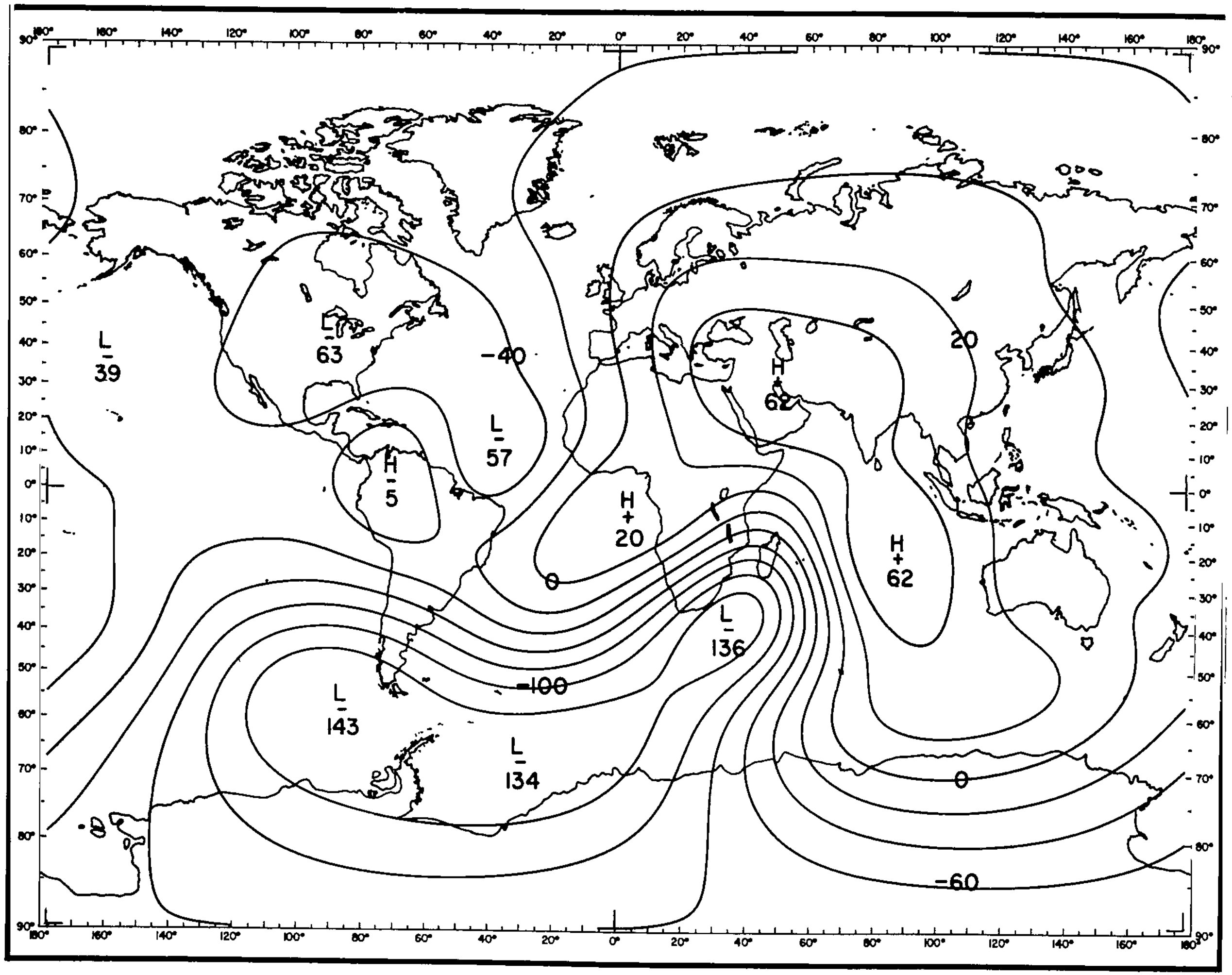

Figure B46—Geomagnetic secular change in gammas per year, total intensity, epoch 1932.5. GSFC (12/66).

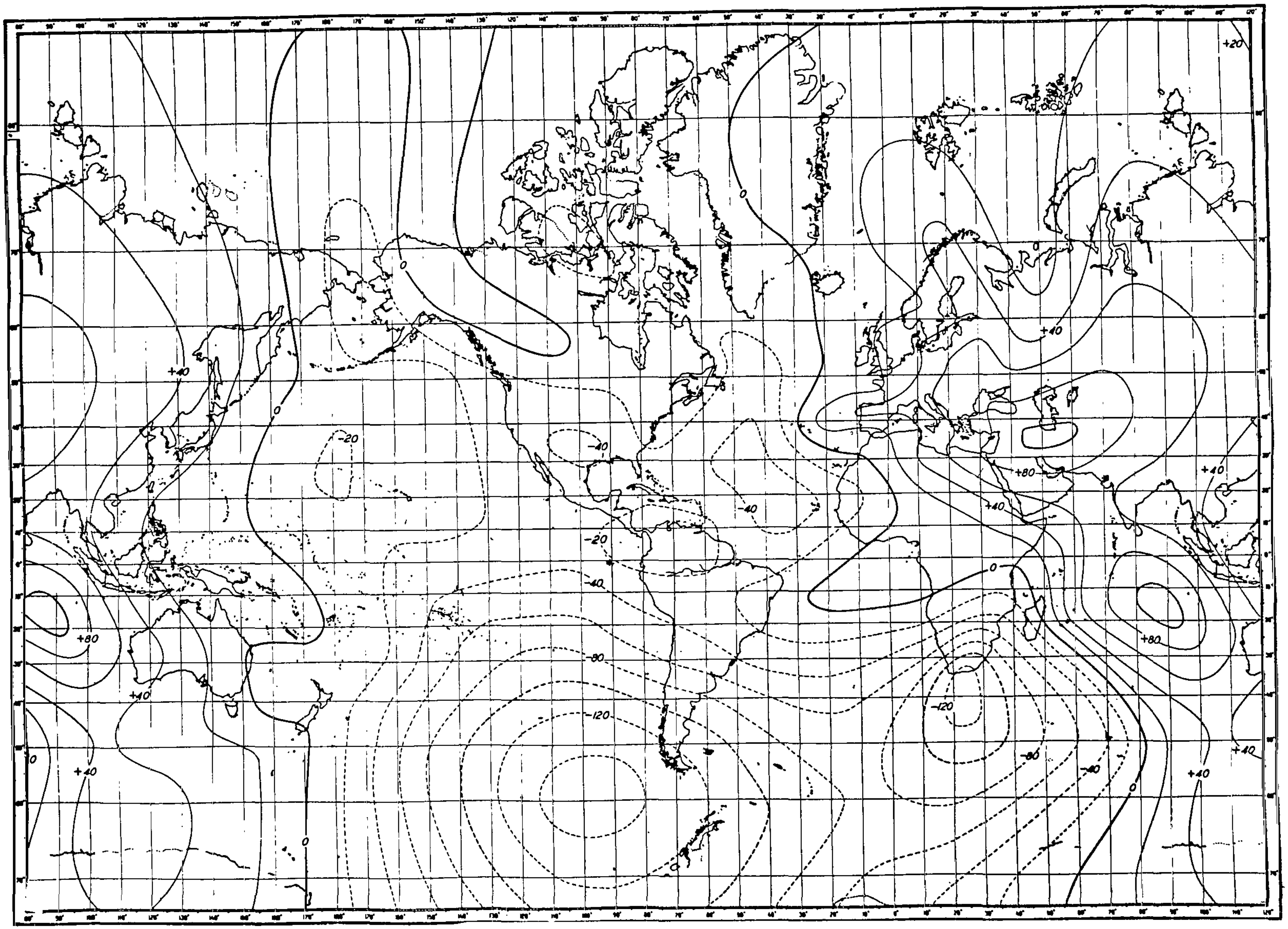

Figure B47–Geomagnetic secular change in gammas per year, total intensity, epoch 1942.5. Vestine et al. (1947).

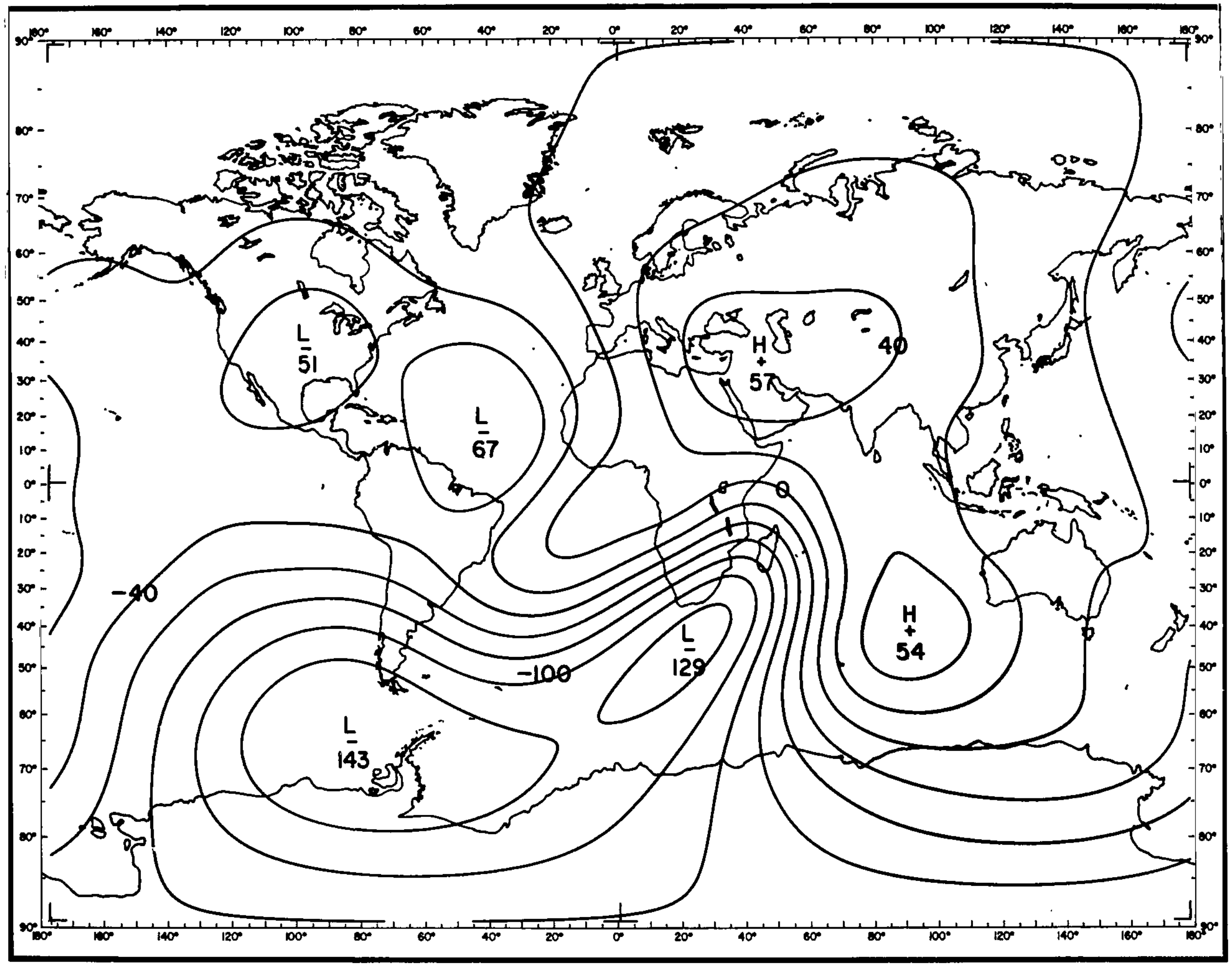

Figure B48—Geomagnetic secular change in gammas per year, total intensity, epoch 1942.5. GSFC (12/66).

Appendix C

Main Field Component and Isoporic Charts Computed From GSFC (12/66) for 1965.0 at the Earth's Surface

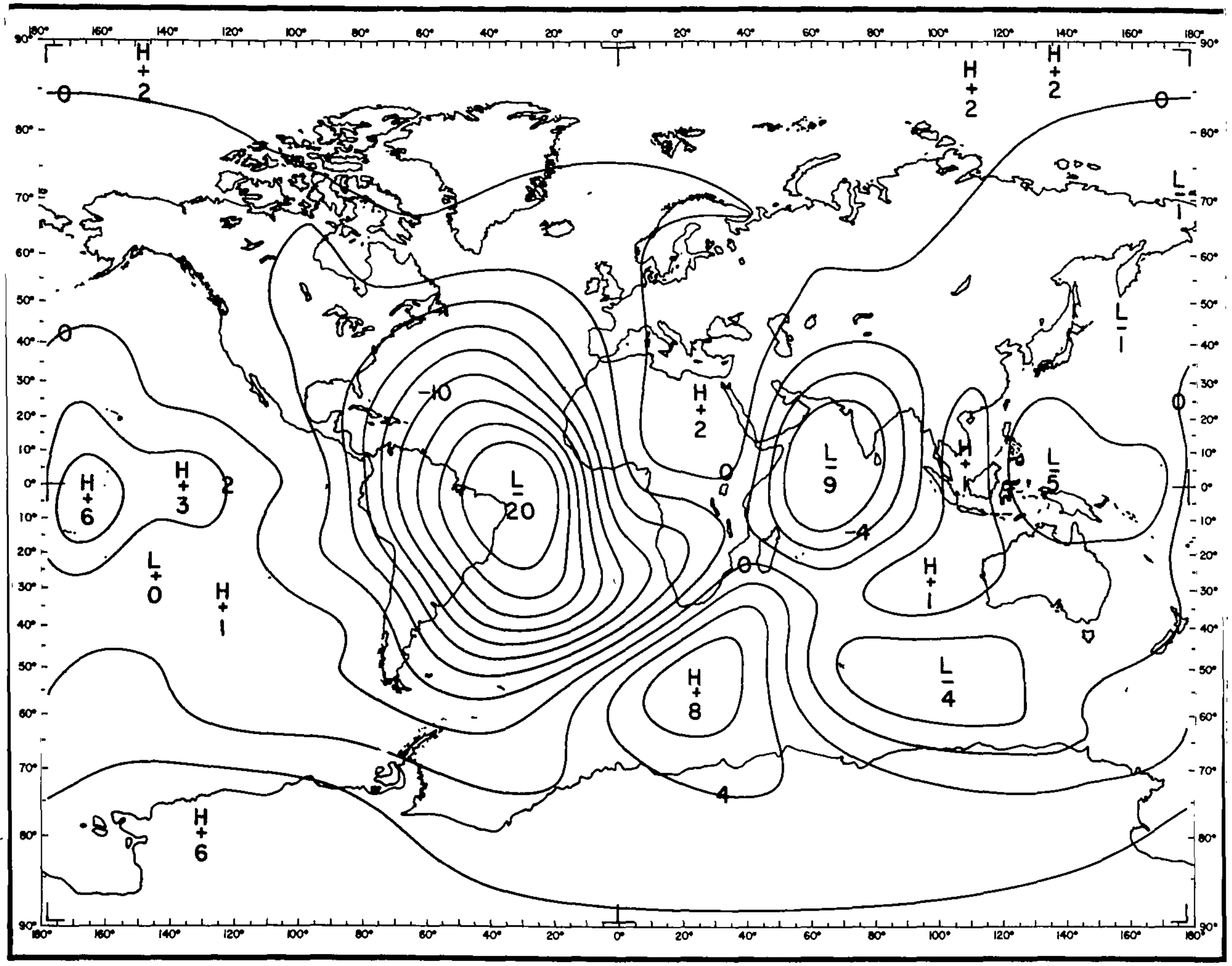

Figure C1—Geomagnetic secular change in minutes per year, inclination, epoch 1965.0. GSFC (12/66).

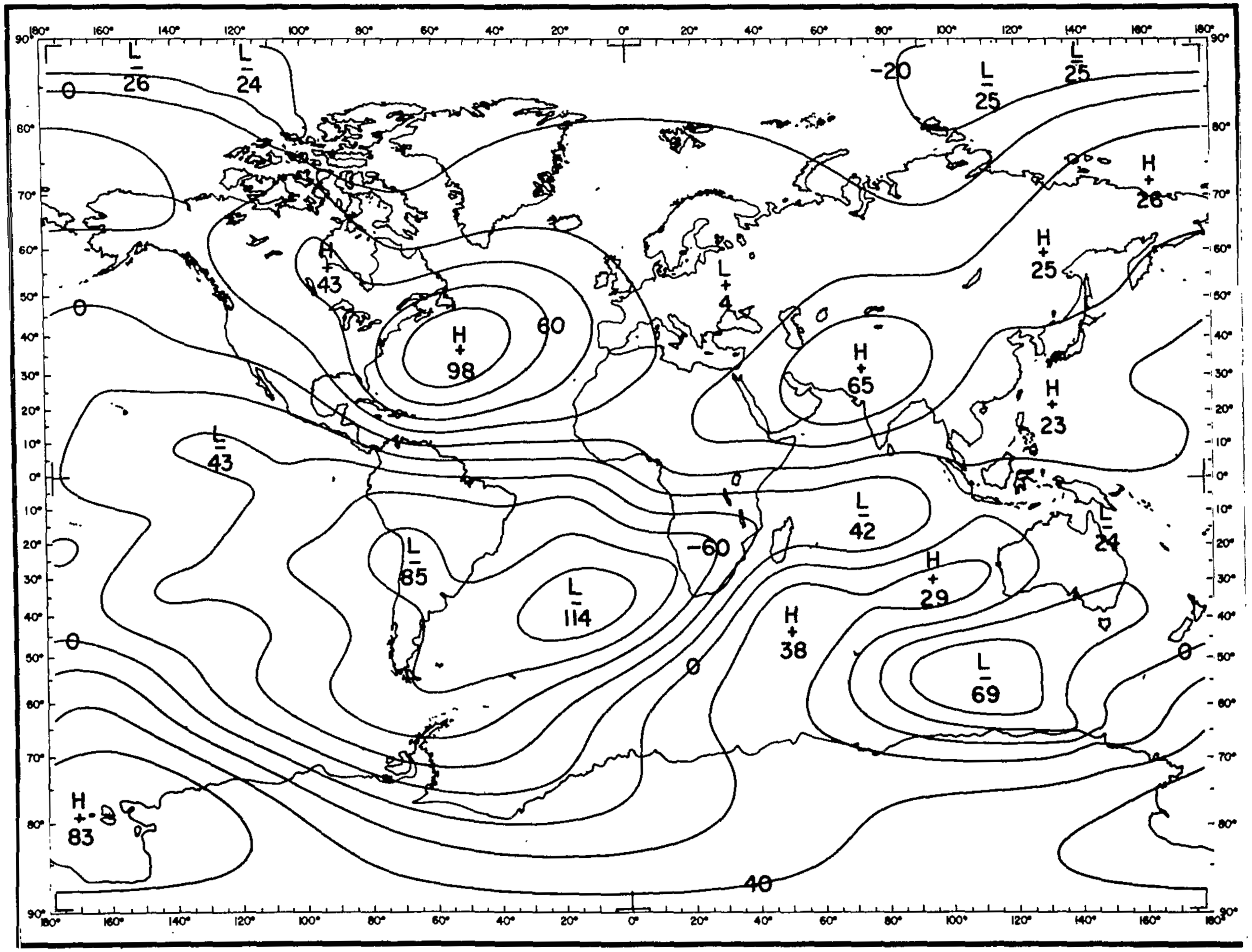

Figure C2—Geomagnetic secular change in gammas per year, horizontal component, epoch 1965.0. GSFC (12/66).

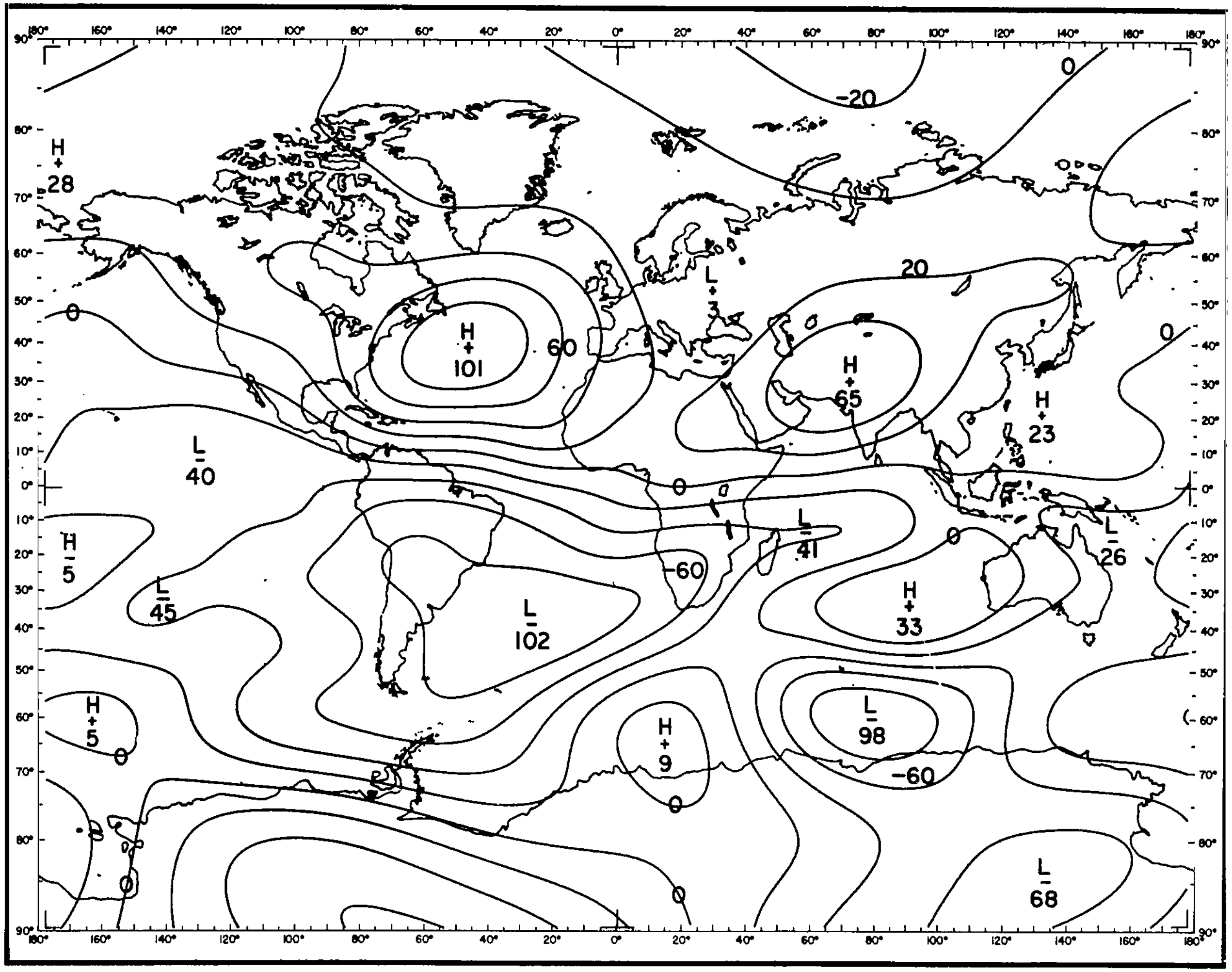

Figure C3—Geomagnetic secular change in gammas per year, north component, epoch 1965.0. GSFC (12/66).

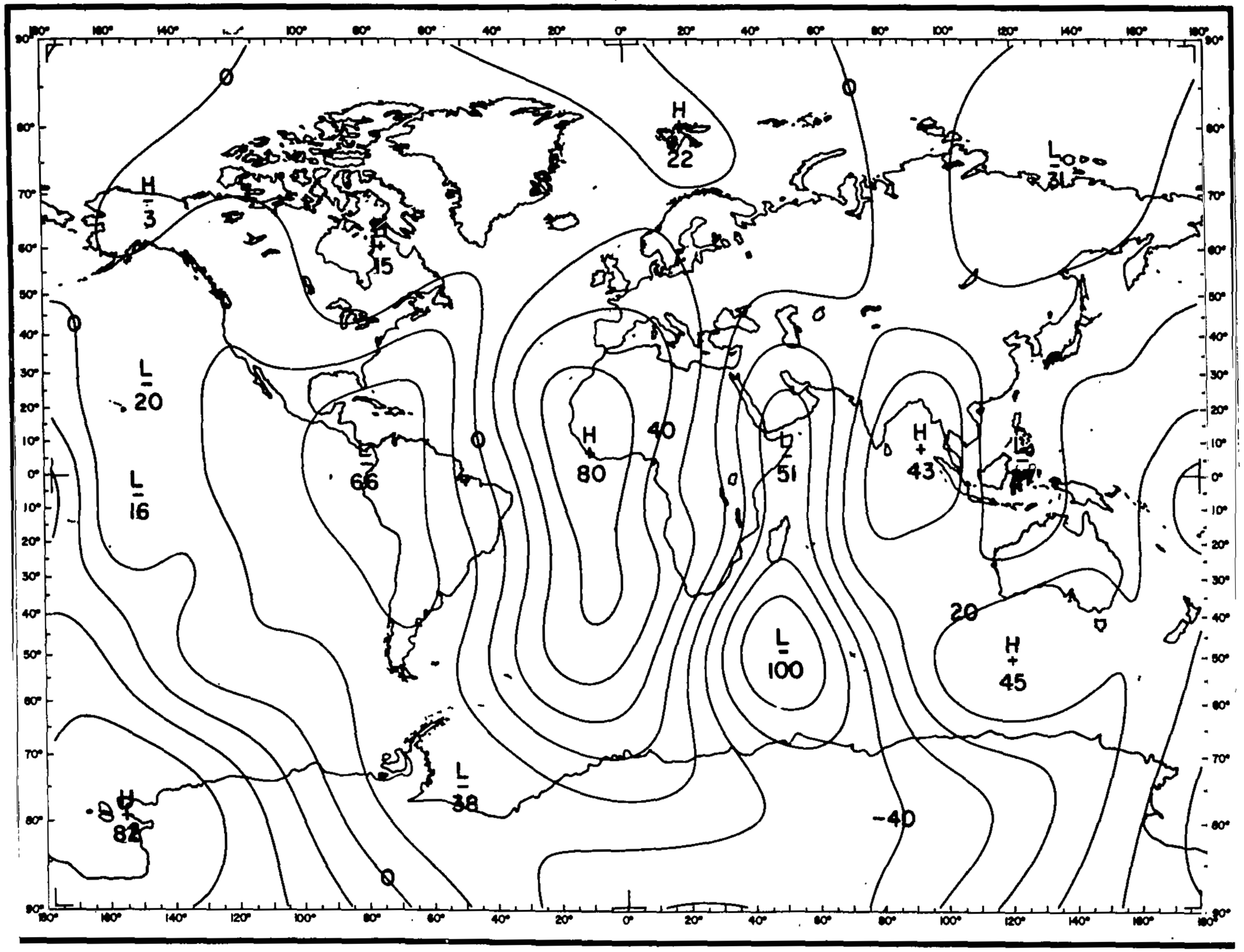

Figure C4—Geomagnetic secular change in gammas per year, east component, epoch 1965.0. GSFC (12/66).

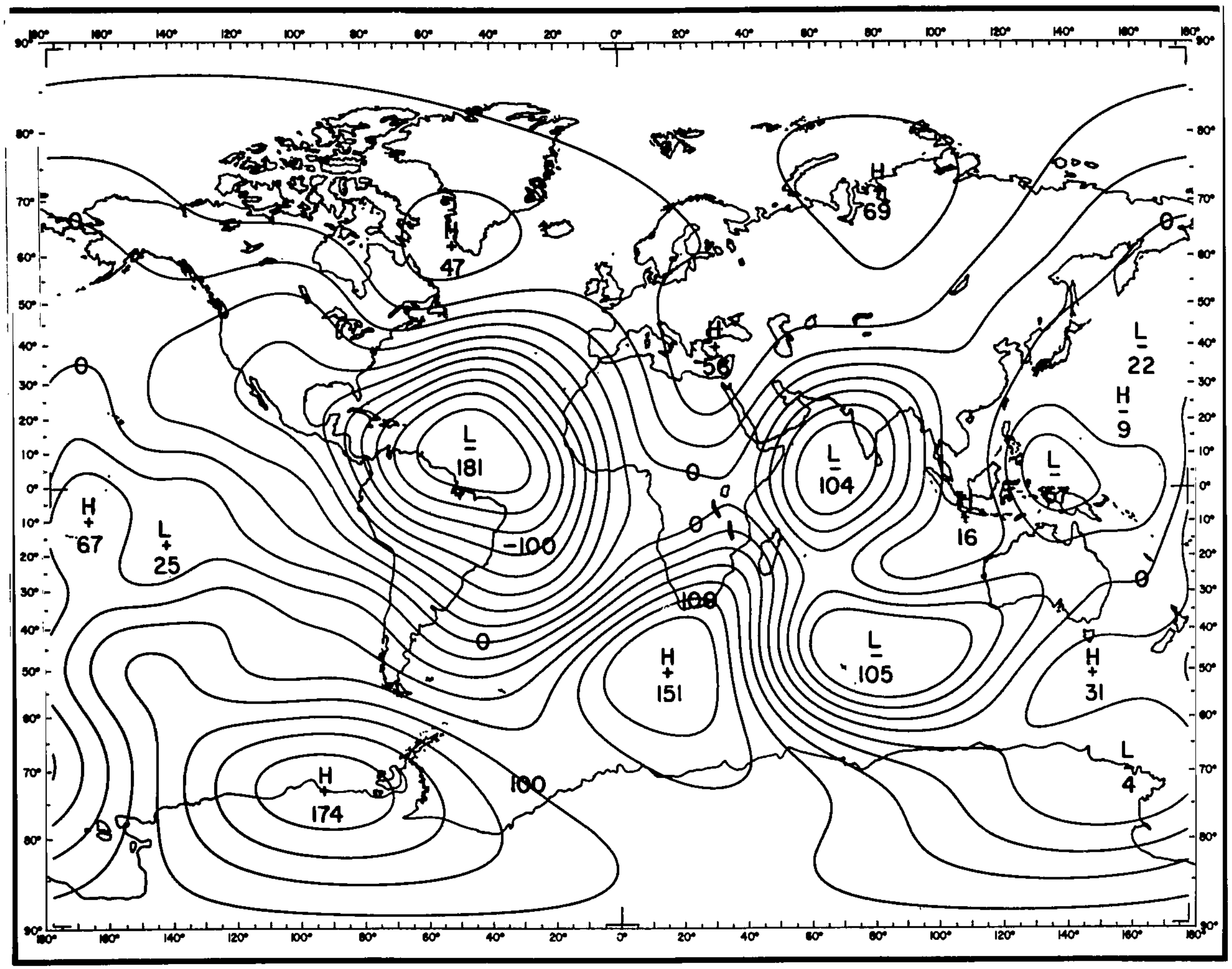

Figure C5—Geomagnetic secular change in gammas per year, vertical component, epoch 1965.0. GSFC (12/66).

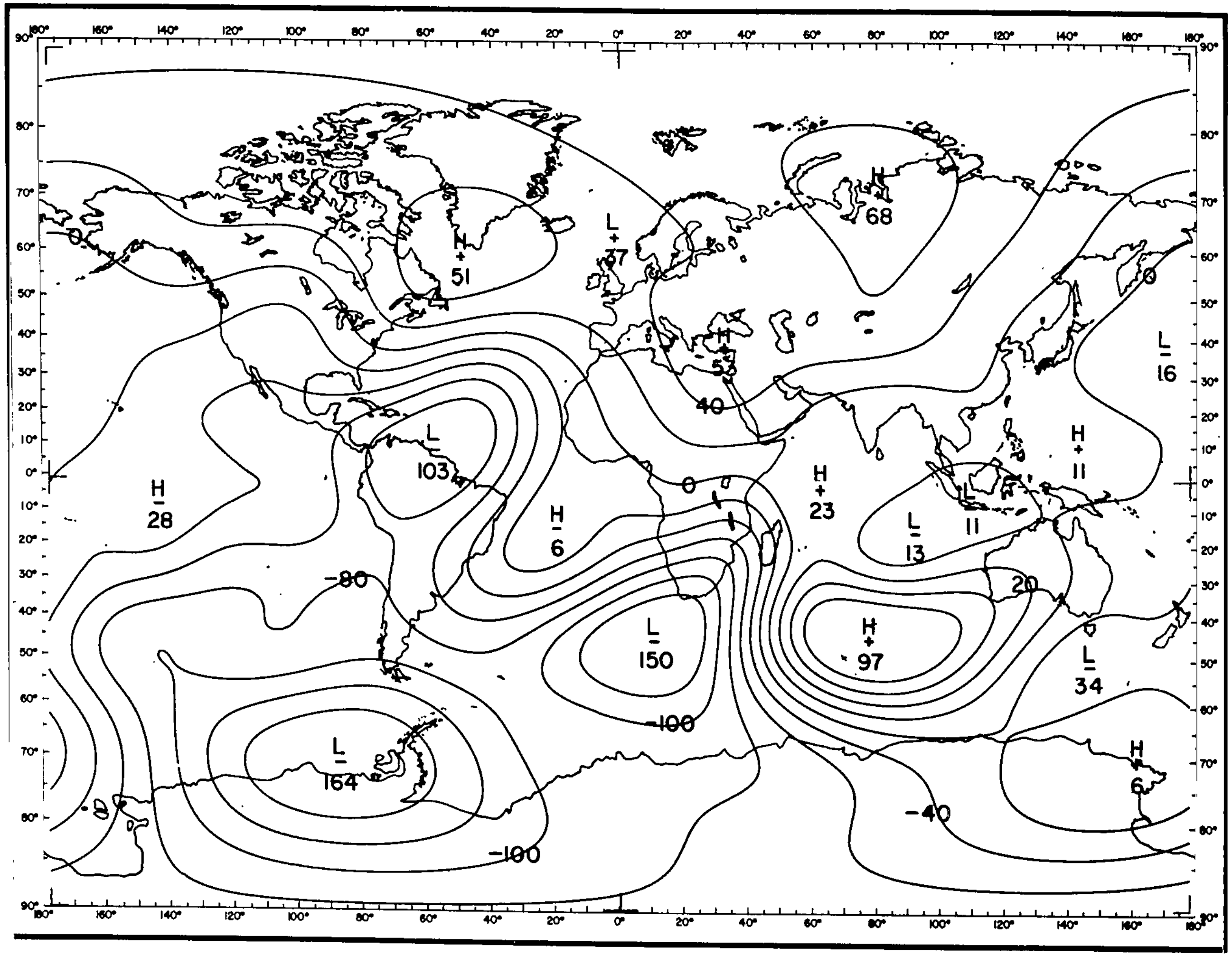

Figure C6–Geomagnetic secular change in gammas per year, total intensity, epoch 1965.0. GSFC (12/66).

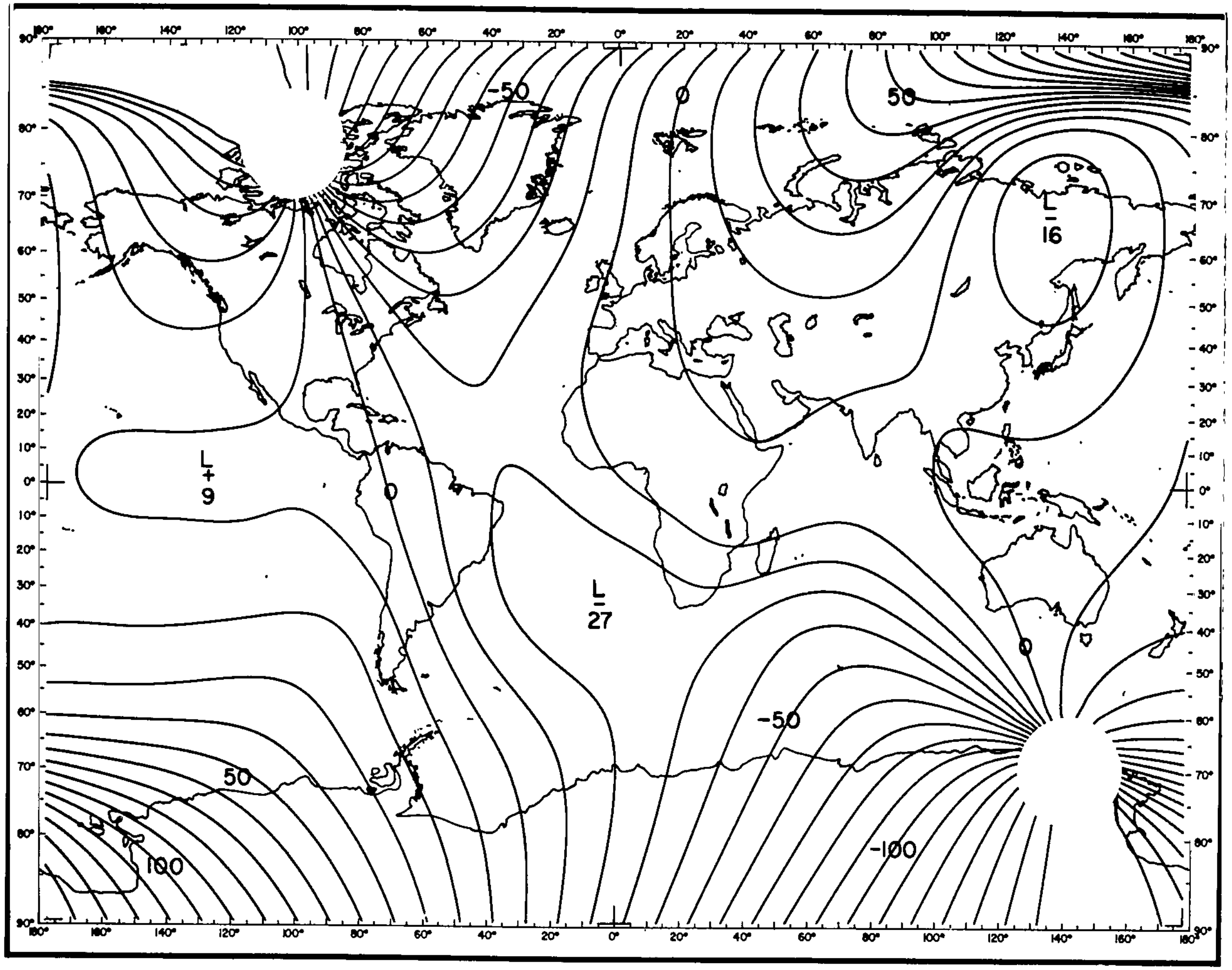

Figure C7–D in degrees, epoch 1965.0. GSFC (12/66).

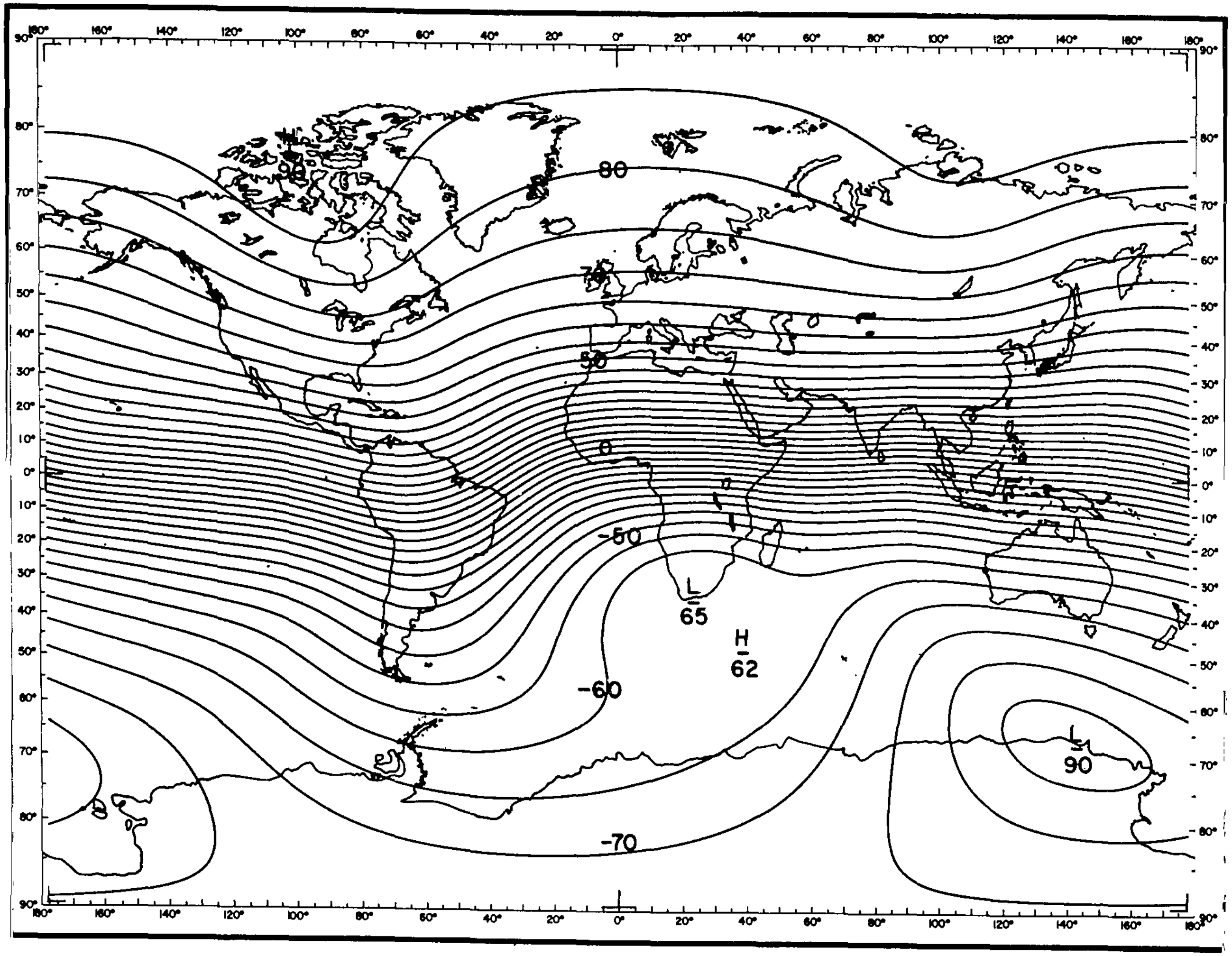

Figure C8–1 in degrees, epoch 1965.0. GSFC (12/66).

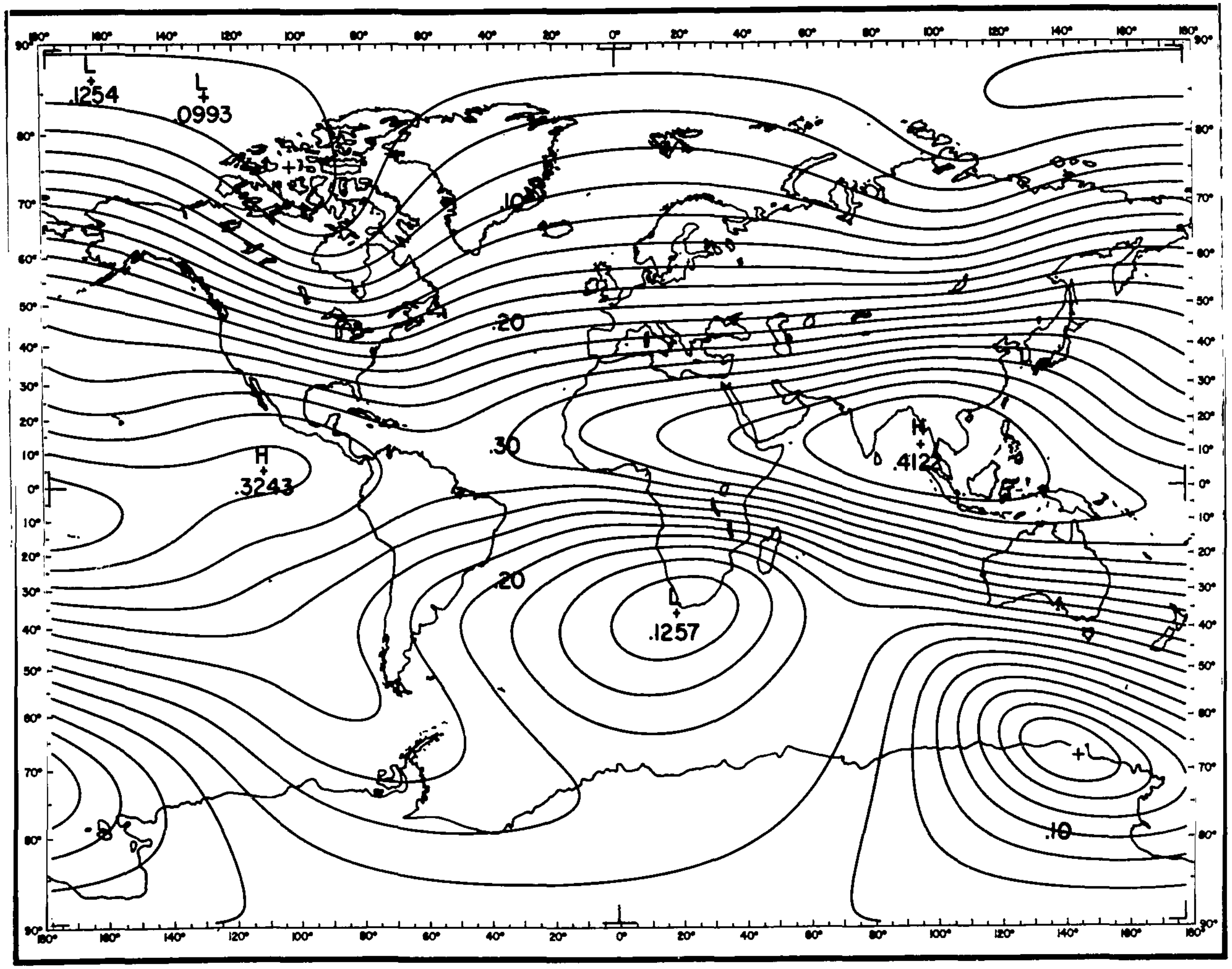

Figure C9—H in gauss, epoch 1965.0. GSFC (12/66).

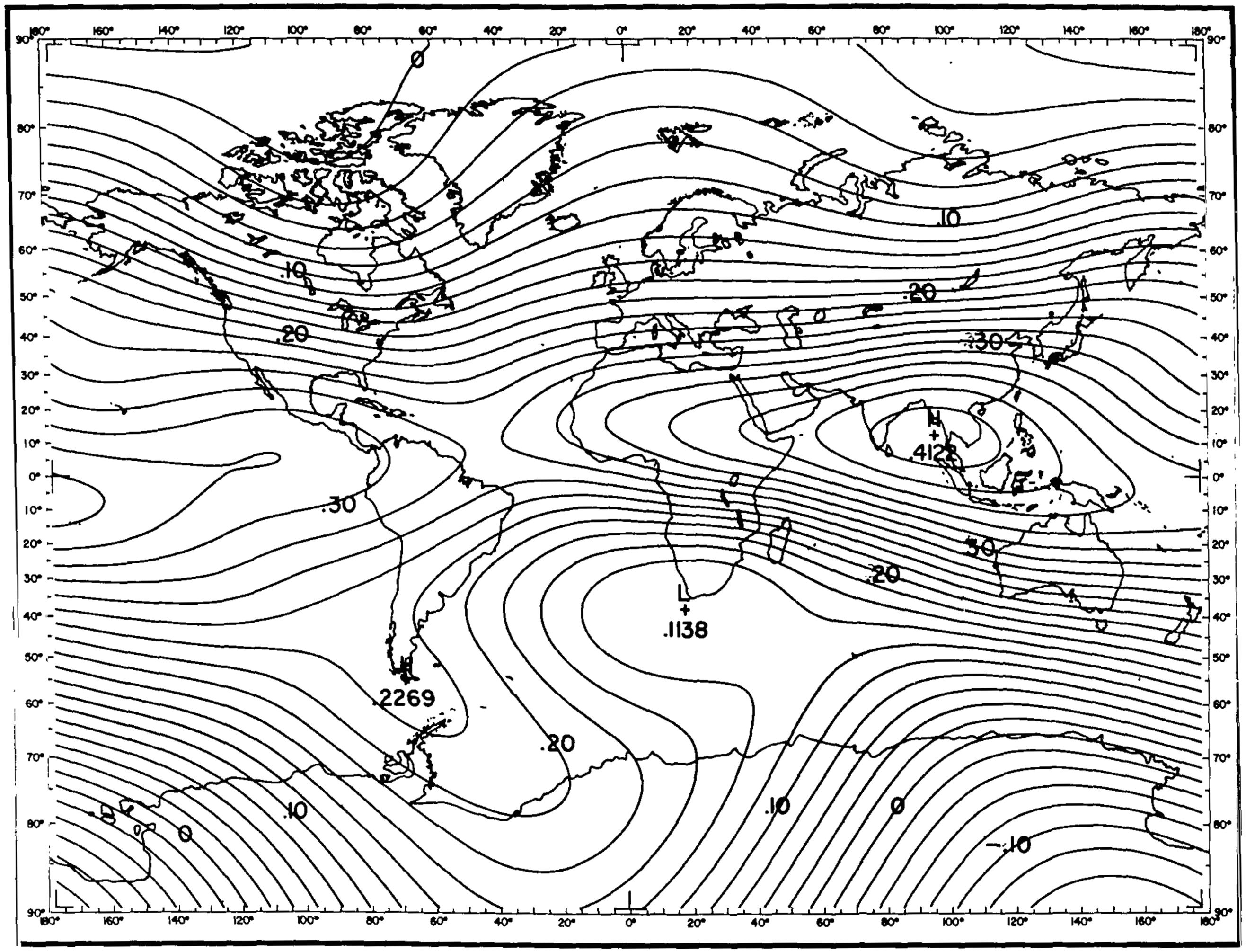

Figure C10–X in gauss, epoch 1965.0. GSFC (12/66).

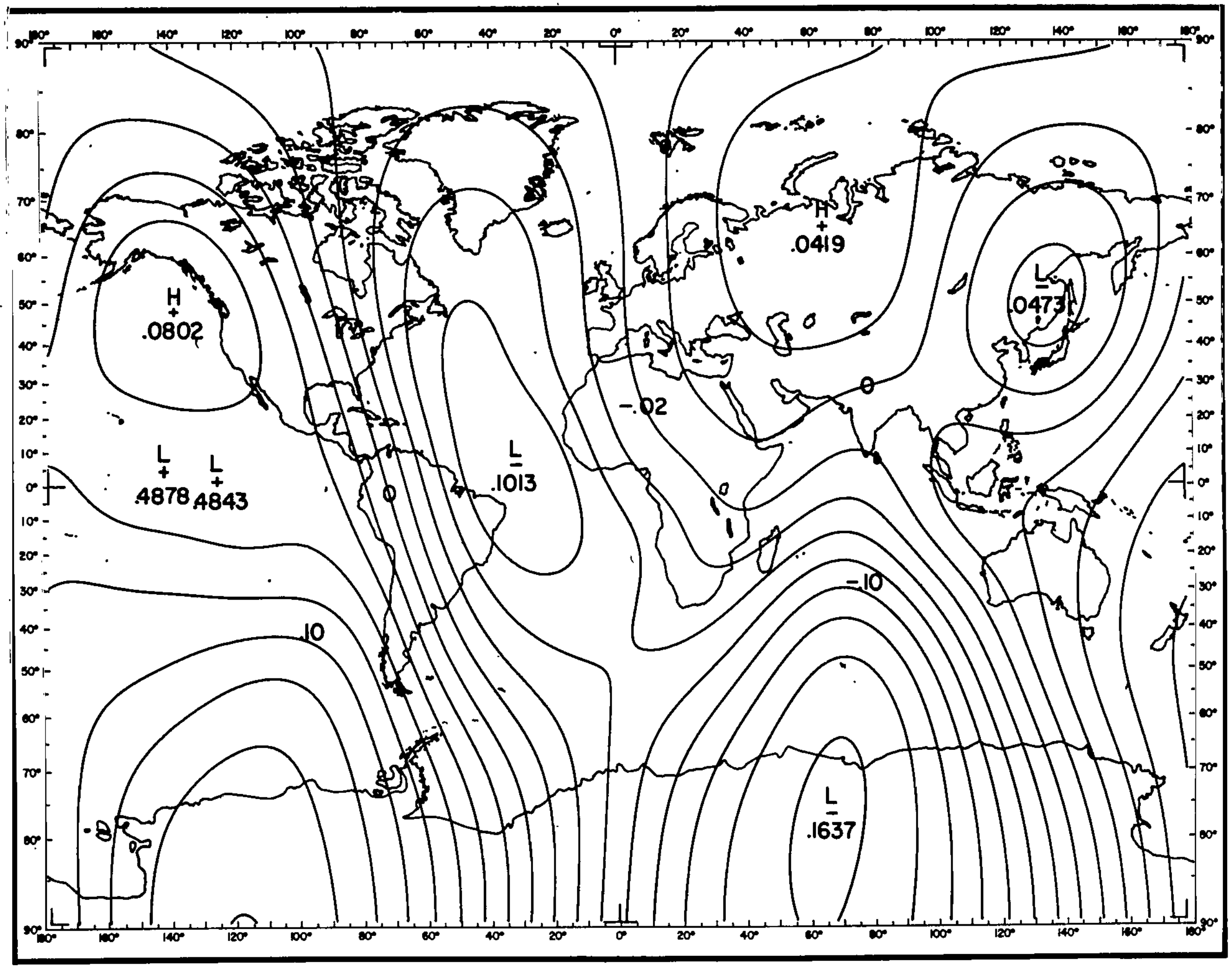

Figure C11–Y in gauss, epoch 1965.0. GSFC (12/66).

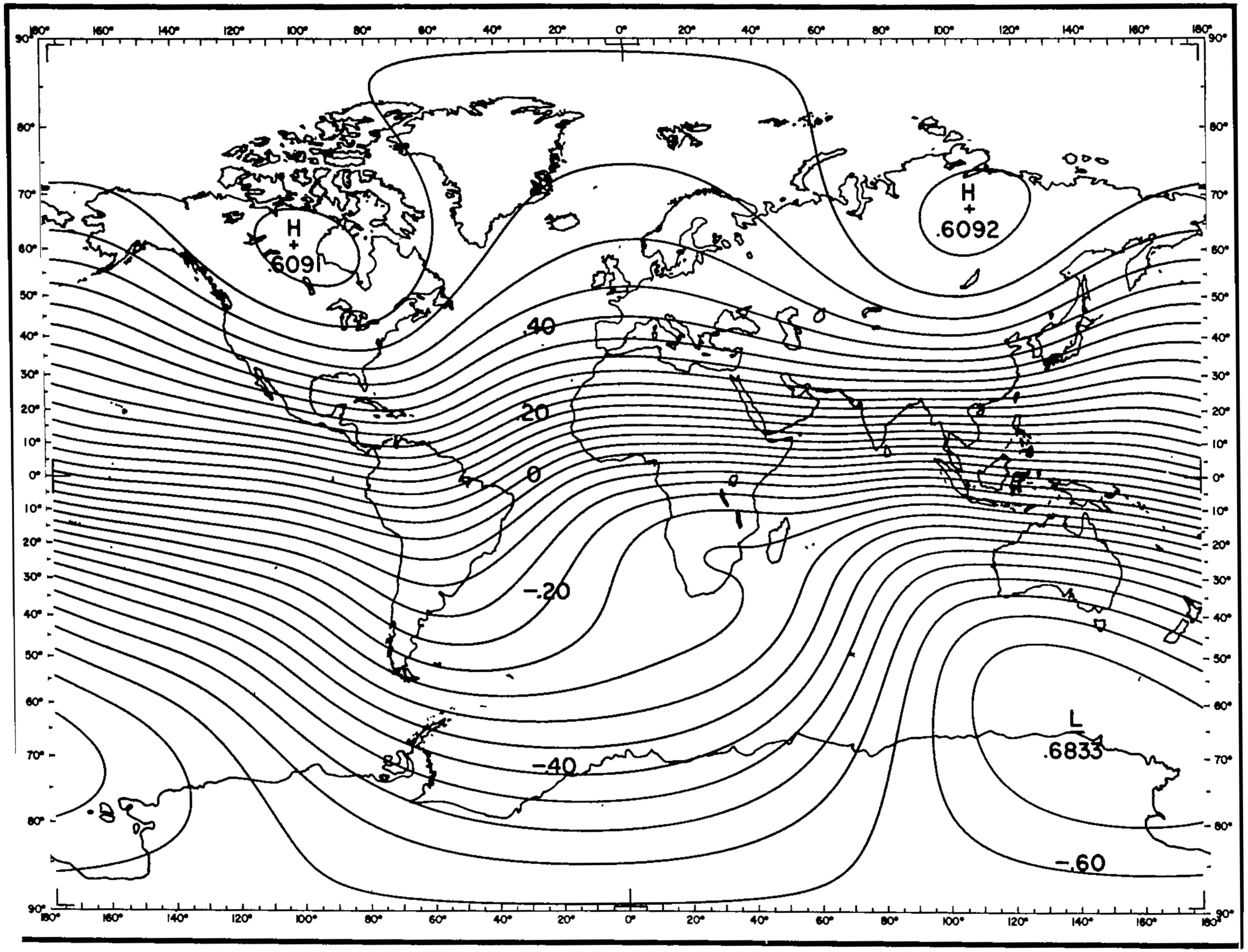

Figure C12—Z in gauss, epoch 1965.0. GSFC (12/66).

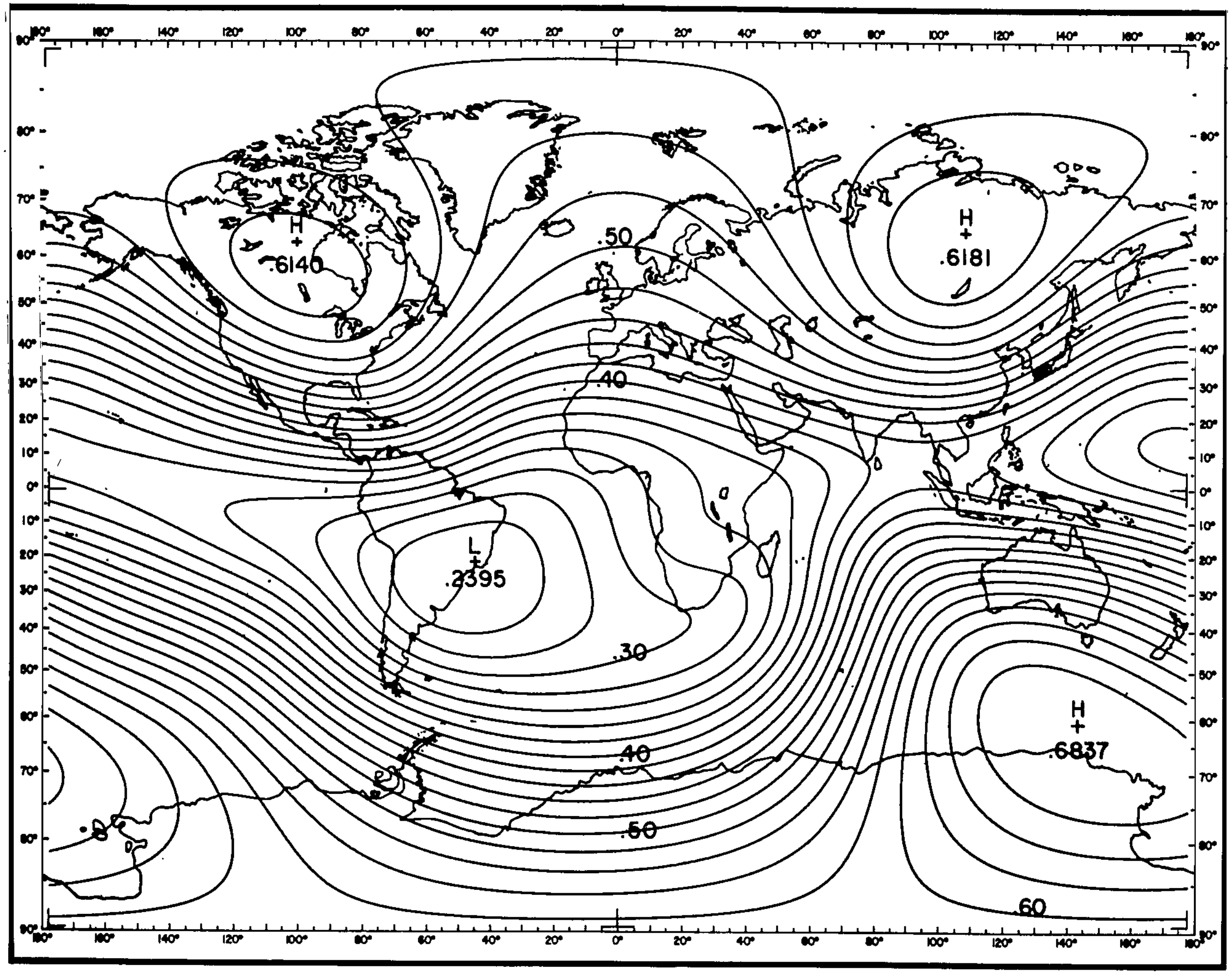

Figure C13–F in gauss, epoch 1965.0. GSFC (12/66).

National Aeronautics and Space Administration
WASHINGTON, D. C.

OFFICIAL BUSINESS

FIRST CLASS MAIL

POSTAGE AND FEES PAID
NATIONAL AERONAUTICS AND
SPACE ADMINISTRATION

010 001 38 51 30S 68074 00903
AIR FORCE WEAPONS LABORATORY/AFWL/
KIRTLAND AIR FORCE BASE, NEW MEXICO 8711

ATT MISS MADELINE F. CANOVA, CHIEF TECHN
LIBRARY /WLIL/

POSTMASTER: If Undeliverable (Section 158 Postal Manual) Do Not Return

"The aeronautical and space activities of the United States shall be conducted so as to contribute . . . to the expansion of human knowledge of phenomena in the atmosphere and space. The Administration shall provide for the widest practicable and appropriate dissemination of information concerning its activities and the results thereof."

—NATIONAL AERONAUTICS AND SPACE ACT OF 1958

NASA SCIENTIFIC AND TECHNICAL PUBLICATIONS

TECHNICAL REPORTS: Scientific and technical information considered important, complete, and a lasting contribution to existing knowledge.

TECHNICAL NOTES: Information less broad in scope but nevertheless of importance as a contribution to existing knowledge.

TECHNICAL MEMORANDUMS: Information receiving limited distribution because of preliminary data, security classification, or other reasons.

CONTRACTOR REPORTS: Scientific and technical information generated under a NASA contract or grant and considered an important contribution to existing knowledge.

TECHNICAL TRANSLATIONS: Information published in a foreign language considered to merit NASA distribution in English.

SPECIAL PUBLICATIONS: Information derived from or of value to NASA activities. Publications include conference proceedings, monographs, data compilations, handbooks, sourcebooks, and special bibliographies.

TECHNOLOGY UTILIZATION PUBLICATIONS: Information on technology used by NASA that may be of particular interest in commercial and other non-aerospace applications. Publications include Tech Briefs, Technology Utilization Reports and Notes, and Technology Surveys.

Details on the availability of these publications may be obtained from:

SCIENTIFIC AND TECHNICAL INFORMATION DIVISION

NATIONAL AERONAUTICS AND SPACE ADMINISTRATION

Washington, D.C. 20546